UNIVERSITY OF BELGRADE
FACULTY OF CIVIL ENGINEERING

Saad J. A. Al-Wazni

DAMAGE DETECTION AND LOCALIZATION FOR CIVIL STRUCTURAL HEALTH MONITORING

Doctoral Thesis

Belgrade, 2016

UNIVERZITET U BEOGRAD
GRADEVINSKI FAKULTET

Saad J. A. Al-Wazni

DETEKCIJA I LOKALIZACIJA OSTECENJA PRI MONITORINGU STANJA GRADEVINSKIH KONSTRUKCIJA

Doktorska Disertacija

Beograd, 2016

University of Belgrade
Faculty of Civil Engineering

Doctoral Thesis

DAMAGE DETECTION AND LOCALIZATION FOR CIVIL STRUCTURAL HEALTH MONITORING

Candidate:

Saad J. A. Al-Wazni

Supervisor:

Assoc. Prof. Dr. Zoran Mišković
University of Belgrade, Faculty of Civil Engineering

Members of the Commission for assessment and defense:

Prof. Dr. Milenko Stegić
University of Zagreb, Faculty of Mechanical Engineering and Naval Architecture
Assoc. Prof. Dr. Zoran Mišković
University of Belgrade, Faculty of Civil Engineering
Assoc. Prof. Dr. Ratko Salatić
University of Belgrade, Faculty of Civil Engineering
Assist. Prof. Dr. Nataša Prašč̆ević
University of Belgrade, Faculty of Civil Engineering

Belgrade, 2016

Univerzitet u Beograd
Gradevinski facultet

Doktorski disertacija:

DETEKCIJA I LOKALIZACIJA OSTECENJA PRI MONITORINGU STANJA GRADEVINSKIH KONSTRUKCIJA

Kandidat:

Saad J. A. Al-Wazni

Mentor:

V. Prof. dr. Zoran Misković

Univerzitet u Beograd, Gradevvinski Fakultet

Clanovi Komisije za ocenu i odbranu:

Prof. dr. Milenko Stegić

Sveuciliste u Zagrebu, Fakultet Strojarstvo i Brodogradnje

V. Prof. dr. Zoran Misković

Univerzitet u Beograd, Gradevvinski Fakultet

V. Prof. dr. Ratko Salatić

Univerzitet u Beograd, Gradevvinski Fakultet

V. Prof. dr. Nataša Praščević

Univerzitet u Beograd, Gradevvinski Fakultet

Beograd, 2016

ACKNOWLEDGEMENTS

I would like to express my grateful thanks to my supervisor Assoc. Prof. Dr. Zoran Mišković for his guidance, professional support, material support and patience during this study. I would like to thank a dean of the Faculty of Civil Engineering at University of Belgrade Prof. Dr. Branko Bozić and vice dean for scientific research Prof. Dr. Snežana Marinković, Assoc. Prof. Dr. Goran Mladenović and Assist. Prof. Dr. Milan Kilibarda for their kind support with the registration process and Administrative work and issuing official books. I also would like to thank to Prof. Dr. Milenko Stegić and Assoc. Prof Dr. Ratko Salatić for their helpful follow-up and support during the study and publishing the results and I am grateful for reviewers of the dissertation and one of them Assist. Prof. Dr. Nataša Praščević, for useful tips and suggestions that have been raised this thesis to a higher level. Also, I would like to thank the staff of the Faculty of Civil Engineering for the helping and support to complete my doctoral study particularly Professors who taught me eight courses, Prof. Dr. Branislav Pujević, Prof. Dr. Dragoslav Šumarac Prof. Dr. Dragica Jevtić and Assoc. Prof. Dr. Jasna Plavšić. Also, my thank for Mr. Mladen Jović from the staff of the construction laboratory in the faculty for helping with arrangements on instrumentation of experimental testing. In addition, the author expresses his gratitude to the Ministry of higher education and scientific research of the Republic of Iraq and Ministry of Education, Science and Technological Development of the Republic of Serbia for financial support for PhD scholarship within the project "World in Serbia". Finally, I wish to present my deepest thanks to my father, mother, wife and brothers for their invaluable support and their understanding and love, which prettifies my life.

DEDICATE

To my parents, wife, sons and brothers

ABSTRACT

The presented thesis studied proposed a novel procedures that was implemented to develop a Structural Health Monitoring (SHM) technique as non-destructive tests that can be applied to detect damage, localization and quantification of civil structures. This technique based on investigations of dynamic characteristics of the structures to detect the damages through their operational conditions of service life. The proposed procedure was built using Artificial Intelligence Technique (AIT) under concept of the methods of damage detection based on updating FE model using heuristic optimization methods. The proposed **SHM** procedure **U**sing **S**imulated **A**nnealing heuristic optimization methos was shortened to "SHMUSA-procedure". The SHMUSA-procedure was verified on four types of steel structural models; simply supported overhang beam; grid bridge, Verendeel bridge and Multi-storey building model to prove reliability, efficiency and robustness under various dynamic behaviours. The SHMUSA-procedure was adopted the changes in dynamic characteristics, natural frequency and normalized mode shape vector, which are extracted from experimental modal analysis and estimated from numerical modal analysis of the damage scenario for structural models. and their characteristics, location and severity,.

The experimental testing is implemented using simulation of ambient vibration measurements by exciting the structural models by shaker device using generated vibration signal. The dynamic response, output only, of the structural models are recorded using 8-accelerometers and 8-channel acquisition device. Experimentally, the modal properties of the structural models are extracted by ARTeMIS extractor software using Frequency Domain Decomposition (FDD) technique by peak picking method. The numerical simulation of structural models are modeled in Finite Element Model (FEM) using ANSYS package software by ANSYS Parametric Design Language (APDL). Numerically, the modal properties of structural models are estimated by ANSYS software using block Lanczos method of dynamic modal analysis for isotropic elastic linear structural models type. The Finite Element Analysis (FEA) is performed using three element types in the FE models, Beam4, Shell63 and Mass21, to analyze the four structural models.

The SHMUSA-procedure is created using high technical computing language of MATLAB environmental software for that purposes. In this procedure, the modified objective function is adopted in the SA optimization method to include the sensitive modal parameters to change in flexural stiffness of the structural model due to presence of damages. The proposed objective function in the SHMUSA-procedure consists combination of differences in modal frequencies and normalized mode shape vectors of the structural models.

The SHMUSA-procedure includes the calibration process, which is implemented on the initial FE model to tune the modal properties estimated numerically with those extracted experimentally of the structural models. The more significant parameters are selected to update the FE model during calibration process using the SHMUSA-procedure with specified objective function. The adopted objective function for calibration process include only the high sensitive modal parameter of natural frequencies of the structural models. The final results of the modal properties of the calibrated FE model have significant convergence corresponding to the modal properties of the experimental structural models.

The proposed SHM procedure is verified on the adopted four structural models by creating different damage scenarios, damage locations and damage ratios. The final results indicated that the performance of proposed SHM procedure has robustness and high efficiency to detect exactly or very close the damages, locations and extents of the implemented damage scenarios. The powerful of the proposed SHM procedure comes from the high effectiveness of the heuristic optimization SA method with its features which gives the global optimum value with quick convergence in small percentage of checked solutions of searching space.

The excellent results of the verification of the proposed SHM procedure using SA method means the capability of the procedure to identify damages for all types of simple and complex structural models. In addition, the proposed SHM procedure can be applied for real civil structures during operational condition in site with high reliability, and efficiency and effectiveness for damage detection as a non-destructive testing.

Keywords: structural health monitoring, dynamic characteristic, vibration of structures, ambient vibration testing, steel structures, simulated annealing, heuristic optimization
Science field: Civil Engineering - Structural Engineering
Narrow science field: Vibration of Steel Structures
UDK: 624.014.2(043.3)

REZIME

Prikazani teza studije je predložio nove procedure koje se sprovode da razvije Strukturno Zdravlje monitoring (SHM) tehniku kao bez razaranja testova koje se mogu primeniti za detekciju oštećenja, lokalizaciju i kvantitativno državnih struktura. Ova tehnika zasniva na istraživanjima dinamičkih karakteristika objekata da otkriju štetu kroz njihove operativne stanja radnog veka. Predloženi SHM Postupak se utvrdi na četiri vrste čeličnih strukturnih modela; jednostavno podržali ispust zraka; rešetka most, Verendeel most i model višespratnica. Predloženi SHM postupak je usvojila izmene u dinamičkih karakteristika, prirodnog učestalosti i načina oblika, strukturnih modela, koji su izvađeni iz eksperimentalne modalne analize i procenjene od numeričke analize modalni.

Eksperimentalno ispitivanje se sprovodi pomoću simulaciju ambijentalnih vibracija merenja od najuzbudljivijih strukturne modele šejker uređaja sa generiše vibracije signalom. Dinamički odgovor, samo izlaz, strukturnih modela su snimljeni korišćenjem 8-ubrzanja i 8-channle uređaj sticanje. Eksperimentalni modal osobine strukturnih modela su izdvojite pomoću Artemis odsisnog softvera pika metodom branje frekventnom domenu razlaganja (FDD) tehnikom. Numerička simulacija strukturnih modela su modelira konačnih elemenata Model (MKE) koristeći ANSIS paket Softvare bi ANSIS Parametric Design Jezik (APDL). Numeričke modal svojstva strukturnih modela se procenjuju pomoću ANSIS softver za blok algoritam metodom dinamičke analize modalne za izotropnoj elastične linearno tipa strukturni modeli. U analizi FE, dva tipa elementa se primenjuju na FEM da se analiziraju strukturne modele, Beam4 i Mass21 tip elementa.

Predloženi SHM Postupak se vrši pomoću vještačka inteligencija tehnika (AIT), koji se primenjuje u ovoj studiji pomoću funkcije na tzv metodu heuristike optimizaciju za otkrivanje oštećenja i njihove karakteristike, lokacije i ozbiljnost, u strukturnim modelima. Predloženi SHM postupak usvaja heurističkog optimizaciju simuliranog kaljenja (SA) metoda u AIT. Predloženi SHM procedura se kreira pomoću višu stručnu računara jezik MATLAB softvera životne sredine za te svrhe. U ovoj studiji, modifikovani cilj funkcija je usvojen u SA metode optimizacije uključiti osetljive modalni parametri za promenu u savijanja krutosti strukturnog modela usled prisustva štete. Predloženi cilj funkcija sastoji

kombinaciju razlika u modalnih frekvencija i modalne raseljavanja vektora strukturnih modela.

Predloženi SHM postupak obuhvata proces kalibracije, koji se realizuje za početnu FE modela za podešavanje numeričke ažuriran FE višenamenskih karakteristika strukturnih modela sa onima ekstrahuje eksperimentalno. Što više značajni parametri su odabrani da ažuriraju model FE tokom procesa kalibracije koristeći predlog SHM postupak sa naznakom funkcije cilja. Usvojeni cilj funkcija za proces kalibracije uključuju samo Visokoosetljivi modal parametar prirodnih frekvencija strukturnih modela. Konačni rezultati modalnih osobina kalibriranu FE modela imaju značajnu približavanja koji odgovara modalnih osobina eksperimentalnim strukturnih modela.

Predloženi SHM Postupak se utvrdi na usvojenim četiri strukturnih modela stvarajući drugačije oštećenja scenarija, šteta lokacije i odnosi oštećenja. Konačni rezultati su pokazali da su performanse predložene SHM postupku ima robustnost i visoku efikasnost za detekciju tačno ili veoma bliske štete, lokacije i prostiranje provedenih oštećenja scenarija. Snažan predloženog SHM postupka dolazi iz visoke efikasnosti u heurističkog metode optimizacija SA sa svojim karakteristikama koje daje globalnu optimalnu vrednost sa brzim konvergencije u malom procentu proverene rešenja u potrazi prostora.

Izuzetni rezultati verifikacije predloženog postupka SHM koristeći SA metod podrazumeva sposobnost postupka za identifikaciju štete za sve vrste jednostavnih i složenih strukturnih modela . Pored toga , predloženi SHM postupak se može primeniti za prave civilnim strukturama u operativnom stanju na sajtu sa visokom pouzdanošću , i efikasnosti i efektivnosti za detekciju oštećenja kao bez razaranja.

Ključne reči: praćenje stanja struktura, dinamički karakteristika, vibracija konstrukcija, ambijentalne vibracije, čelična konstrukcija , simulirano kaljenje, heuristička optimizacija

Naučna oblast: Građevinarstvo - Građevinarstvo - inženjerske konstrukcije

Uža naučna oblast: Vibracija čeličnih konstrukcija

UDK: 624.014.2(043.3)

CONTENTS

LIST OF FIGURES

LIST OF TABLES

SYMBOLS AND ABBREVIATIONS

Latin uppercase letters

M	mass matrix
D	damping matrix
K	stiffness matrix
F(t)	external applied force vectors with respect to the time (t)
A and B	constants of initial condition that initiate the motion
N	represents number
K_d	stiffness matrix of damaged structure
F	force amplitude vector
$H(\omega)$	frequency response function matrix of the system
U	structural displacement
G	flexibility matrix
C	output matrix
A_m	state matrix containing the dynamics of the system
$G_{xx}(j\omega)$	power spectral density matrix of the input
$G_{yy}(j\omega)$	power spectral density matrix of the response
R_k	residue
A_k	residue matrix of the output
U_i	unitary matrix holding the singular vectors
S_i	diagonal matrix holding the scalar singular values
L	total length of the strucutre
H	total height of the strucutre
X	x-xis of the structure represents longitudinal axis in plane xy
Y	y-axis of the structure represents transverse axis in plane xy
Z	z-axis of the structure represents vertical axis in plane zx or zy
E	energy of the system
T	temperature or time
T_o	initial temperature
N^T	number of checked solution in the configuration
K	number of included elements in the structural model
W_f	weighting factor of natural frequency
W_d	weighting factor of the mode shape
W_p	weighting factor of the position of damage
T	superscript represents transpose matrix

Obj_Fun	objective function of optimization problem
Obj_Fun_{comb}	objective function of optimization problem combined from two variables or more
D_{pj}^{exp}	experimental static displacement of the j^{th} component due to apply the p^{th} load
D_{pj}^{num}	numerical static displacement of the j^{th} component due to apply by the p^{th} load
Ps	number of applied static loads
$F(x_{initial})$	initial value of optimization problem objective function
$F(x_{current})$	current value of optimization problem objective function
$F(x_{new})$	new value of optimization problem objective function
D_e	damaged element number
D_r	damage ratio of damaged element
T_f	final temperature of the system
N_c	number of cooling cycle
T^c	previous cycle temerature
T^{c+1}	next cycle temerature
$Freq$	differences in the natural frequencies between experimentally extracted from damaged model and numerically estimated from updated FE model
$Disp$	differences in the normalized mode shape vectors between experimentally extracted from damaged model and numerically estimated from updated FE model
$E\_initial$	modulus of elasticity of initial model material
$M\_initial$	additional mass of initial model material
S_L, S_E and S_ρ	relevant scaling factor for the length, modulus of elasticity and mass density, respectively
$Mass\_Density^{equivalent}$	equivalent mass density in kg/mm^3 of the floor from both actual steel floor plate and additional mass in that floor
$Mass_{additional\_mass}^{actual}$	actual mass in kg of the additional mass distributed on each floor
$Mass_{floor\_plate}^{actual}$	actual mass in kgof the steel floor plate of the original structural model of each floor
$Volume_{floor\ plate}^{actual}$	actual volume of the steel floor plate in mm^3 of the original structural model of each floor
$R(p_k)$	output error residue based on (k) number of parameter (p)
S	sensitvity matrix
D_r	damage ratio
D_e	damaged element

Latin lowercase letters

$\ddot{x}(t)$	acceleration
$\dot{x}(t)$	velocity
$x(t)$	physical displacement
$q(t)$	time variation of the displacements
e_n	element deformation vector
h_d	distance between the measurement coordin
f	natural frequency
f_i	natural frequency for ith mode
n	number of modes
m	number of components included in the computations
i	mode number
j	component number
x_k	internal state vector
y_k	measurement vector
w_k	process noise
v_k	measurement noise
d_k	scalar constant
$f(x)$	function of variable x
x	variable
v_i^k	velocity of agent i at iteration k
c_j	weighting factor
s_i^k	current position of agent i at iteration k
s_i^{k+1}	new position of agent i at iteration $k+1$
$p-best_i$	best solution at the current agent i
$g-best$	global solution of the group of searching points
w	weighting function
$f_i^{num-undam}$	numerically estimated value of natural frequency for the intact model
$f_i^{exp-undam}$	experimentally extracted value of natural frequency for the intact model
$f_i^{num-dam}$	numerically estimated value of natural frequency for the damaged model
$f_i^{exp-dam}$	experimentally extracted value of natural frequency for the damaged model
$f_i^{num\text{-}updated\text{-}dam}$	numerically estimated value of natural frequency for the updated damaged model
k	element number
ps	applied static load number

$x_{initial}$	initial value of optimization problem solution
$x_{current}$	current value of optimization problem solution
x_{new}	new value of optimization problem solution
p	acceptance probability used in simulated annealing method
r	randomly generated nmuber in the range of [0, 1]
f^*	average increase in the objective function
p_o	initial acceptance probability
p_f	final acceptance probability
f^c	cooling factor
c_1 *and* c_2	constants
r_d	number of fundamental dimensions
g	gravitational acceleration
t_CS	thicness of cross section of FE overhang beam model
t_RHS	thickness of rectangular hollow section of FE grid bridge model
t_TS	thickness of T-section of FE grid or Vierendeel bridge model
w_RSHBS	width of rectangular solid hidden beam section of FE grid or Vierendeel bridge model
_initialt	represents the initial value of the parameters
_opt	represents the optimal value of the parameters
t_RHSB	thickness of rectangular hollow section for main longitudinal lower and upper beams of FE Vierendeel bridge model
h_RHSBS	equivalent hieght of rectangular hollow section for stiffener part of main longitudinal upper and lower beams of FE Vierendeel bridge model
t_RHSC	thickness of rectangular hollow section for columns of FE Vierendeel bridge model
h_RHSCS	equivalent hieght of rectangular hollow section for stiffener upper and lower part of columns of FE Vierendeel bridge model
t_SHS	thickness of square hollow section for main beams and columns of FE multi-storey building model
h_SHS	dimension of square hollow section for main beams and columns of FE multi-storey building model
h_SSS	dimension of square solid section for beam-column joint section of FE multi-storey building model
t_Plate	thickness of square steel floor plate of FE multi-storey building model
d	crack depth from the bottom side of the cross section
t	total depth of the cross section

Greece uppercase letters

Φ	eignvectors matrix or characteristic vectors matrix
Δ	Change in the variable
β_i	weighting factor from the accuracy of the computations of the natural

	frequencies
β	reduction factor of damage in the range of [0.01-1.00]

Greece lowercase letters

ϕ	mass-normalized mode shape vector
ω	circular frequency
λ	eignvalue matrix
ϕ_i	mass-normalized mode shape vector for ith mode
ω_i	circular frequency for ith mode
$\phi^d_{n,i}$	local change in the curvature between the undamaged and damaged structure
$\phi_{n,i}$	modal displacement for the i^{th} mode shape at the measurement coordinate n
ε_i	the error for the i^{th} experimentally and numerically estimated values of natural normalized displacement
$\phi^{exp}_{i,j}$	the i^{th} experimentally extracted values of normalized displacement of j^{th} component of the intact model
$\phi^{num}_{i,j}$	the i^{th} numerically estimated values of normalized displacement of j^{th} component of the intact model
$\phi^{num-updated-dam}_{ij}$	the i^{th} numerically estimated values of updated normalized displacement of j^{th} component of the damaged model
δ_p	variable represents the position of damage
$\lambda^{updated}_i$	the i^{th} numerically updated eigenvalues
$\lambda^{initial}_i$	the i^{th} numerically initial eigenvalues
λ^{dam}_i	the i^{th} experimentally eigenvalue of damaged structure
λ^{undam}_i	the i^{th} experimentally eigenvalue of intact structure
α	reduction factor of temerature of cooling schedule
ν	Poisson's ratio of material
ρ_initial	mass density of initial model material
π	terms of dimensionless products
δd_j	differences between the experimentally extracted and numerically estimated modal properties
δp_k	variation of the updated parameter
γ	weighting factor of stiffness of damaged element

Abbreviations

NDE/T	non-destructive ealuation/testing
VBDD	vibration-based damage detection

VBDI	vibration-based damage identification
SHM	structural health monitoring
AIT	artificial intelligent technique
DOFs	degree of freedom(s)
FEA	finite element analysis
FRFs	frequency response function(s)
EMA	experimental modal analysis
FE	finite element
MAC	modal assurance criterion
ODS	operational deflection shape
GSM	gapped-smoothing method
ERA	eigensystem realization algorithm
FEM	finite element model
GA	genetic algorithm
ANN	arteficial neural network
FDD	frequency domain decomposition
PCA	principle component analysis
SA	simulated annealing
PST	power series technique
SRF	stiffness reduction factor
TS	tabu search
PSO	particle swarm optimization
AVM	ambient vibration measurements
AVT	ambient vibration testing
OMA	operational modal analysis
PPM	peak picking method
BFD	basic frequency domain
EFDD	enhanced frequency domain decomposition
SDOF	single degree of freedom
SSI	stochastic subspace identification
SVD	singular value decomposition
PSD	power spectral density
NP	non-deterministic polynomial time
AIM	artificial intelligent method
SGA	simple genetic algorithm
FSA	fast simulated aannealing
SSA	standard simulated aannealing
CSA	classical simulated annealing
OSA	ordinary simulated annealing
DSA	direct search simulated annealing
DC-1	first damage scenario of the damaged model
DC-2	second damage scenario of the damaged model
GUI	graphical user interface
APDL	ANSYS parametric desigen language

1. INTRODUCTION

1.1. General

The cost and complexity of modern constructions make the demand of new investigation techniques of structural health becomes more important issue. In addition to the cost of maintenance for these constructions to preserve their intended function from inevitable ageing and degradation resulting from functional performance. The presence of damages in structures affects on their integrity and could reduce their performance or service life [1]. In some structures are generally inspected at period of two or more years and the main dependence on visual inspection [2]. So, the structures may be damaged during inspection period and becomes progressively in worst state. As the inspections rely heavily on the inspector's experience and knowledge, therefore the visual inspections alone are proven to be unreliable [3]. In recent years, the field of structural health inspection methods get on more attention from engineers and researchers to evolve the new approaches to the evaluation and maintenance of civil infrastructures [1], [4].

The Non-Destructive Evaluation/Testing (NDE/T) methods have been developed and successfully used to investigate the significant changes in the properties of simple and small structures in order to prevent unforeseen failure [1], [5], [6], [7], [8, [9], [10]. The conventional and local approaches of non-destructive testing and evaluation include; X-ray; gamma-ray; ultrasonic; magnetic particle induction; liquid (dye) penetrant; acoustic emissions; half-cell potential readings and eddy currents [10], [11]. The classical NDE/T techniques require measurements in the close vicinity of damage and commonly having the ability to estimate only for small area [11], [12]. Consequently, the inspection of a large and a complex structure (such as complicated bridge, multi-storey building, etc) using the NDE/T methods alone could be costly and time consuming. As well, the components under inspection have to be accessible and the structure needs to be taken out of service [5], [11], [13].

One of the modern NDE/T techniques depends on vibration-based damage detection (VBDD) techniques and sometimes referred to vibration-based damage identification

(VBDI) techniques which is defined in term called Structural Health Monitoring (SHM). The application of structural system identification technique is used as a black box models which concentrates on input/output relationships and is mainly directed to application of structural health monitoring [14]. The SHM technique is the process of implementing damage detection strategy for civil engineering structure [15]. In SHM technique the entire structure system can be evaluated simultaneously using relatively few sensors and instruments with the basis is that damage to a structure will alter its global dynamic characteristics when exposed to an environmental and an external excitation over time (such as ambient vibration, blast loading, earthquake, etc) [15], [16]. The SHM process includes two applied procedures for the civil structure system, the dynamic analysis and the statistical analysis. The dynamic analysis is represented by the observation of a civil structure system using periodically sampled dynamic response measurements and the extraction of the dynamic characteristics. Then the statistical analysis of the dynamic characteristics is made to determine the present state of structure system health. From SHM technique could obtain information about the existence, location, and extent of damage in the structure system which based on the assumption that the damage will change the structural system properties (stiffness and mass) which produces an alteration of dynamic characteristics (natural frequencies, mode shapes and damping ratios) [1], [4], [17], [18].

Finally, the damage identification using SHM of the structure system state could be specified in three questions:

1- Is there damage in the structure system (existence)?

2- Where is the damage in the structure system (location)?

3- How severe is the damage in the structure system (extent)?

4- How many years is remaining service life for the structure?

The first three questions participate to evaluate the fourth question of remaining service life for the current state of the structure system, which represents a diagnostic of the structure system.

To answer on the first question requires recording data of dynamic behavior of the structure system from intact and damaged case. While the answer of the second and third question should be through analyzing the simulated model of the structure system and

compare them with actual recording data to avoid pseudo identification of damage. Lastly, application of statistical test is made to update the structure model where could be after that specified the type of answers. As a result, those questions should be criteria for the success of any new procedures of damage identification [19].

On the other hand, there are also some difficulties and obstacles for the application of SHM technique. It could not constantly to get data recording of the intact case of the structure system. it is sometime impossible to conduct a complete set of measurements that allow a satisfactory extraction of mode shapes. The changes in dynamic characteristics are sometimes unrelated with the presence of damage.

In present study, the research focuses on the application of SHM technique based on VBDD method to four civil structural models which is the first study in Faculty of Civil Engineering-University of Belgrade. The significant reliable results of this study could allow the possibility of application this study for real civil infrastructures in the field. Those four structural models are designed in suitable scale according to a set of similitude requirements to the prototype structures.

The adopted structural models are classified from a simple to the complex structures:

1- Overhang steel beam model

2- Plane grid steel bridge model

3- Multi-story steel building model

4- Vierendeel steel bridge model

The four adopted structural models in this study are constructed in the Structural Laboratory, Faculty of Civil Engineering at University of Belgrade. The Vierendeel bridge model was scaled model with some changes based on a actual superstructure constructed in the south of Belgrade city located in Cacak city. This model was divided into two model, plane grid model without two fences in both side of the model and Vierendeel model with two fences. Other models were selected depend on what is available of structural models from previous researches in the faculty. The decision to adopt these structural models to include as possible as several types of superstructures in this research to study different actions of structural behaviors and to simulate the complicated structures in the proposal procedures of health evaluation of civil structures such as Vierendeel bridge.

In previous studies, no experimental and numerical verification was performed on complicated multi-story building and vierendeel bridge models. In addition, it is necessary to develop reliable methods that are capable of identifying damage for those more complex types. Also, the reliable estimations of dynamic characteristics for these structural models are essential for a successful implementation of VBDD methods. As a result, it is necessary to identify specific test procedures and numerical simulation that would produce the lowest levels of uncertainty, and therefore produce the great probability of detecting damage using VBDD methods. More specifically, in the present study, extensive well controlled dynamic tests, numerical simulations and damage detection trials were implemented on four structural models.

1.2. Scope of the research

The present research concentrate on the main three aspects of civil structural health monitoring. Those primarily aspects are Experimental Investigation (EI), Numerical Computation (NC) and Artificial Intelligent Technique (AIT) for statistical analysis and the relation among them to create a sophisticated system for monitoring a complex modern structural models. Figure 1.1 schematizes the general framework of the current research as a three cores which are dealt with in details through the next chapters.

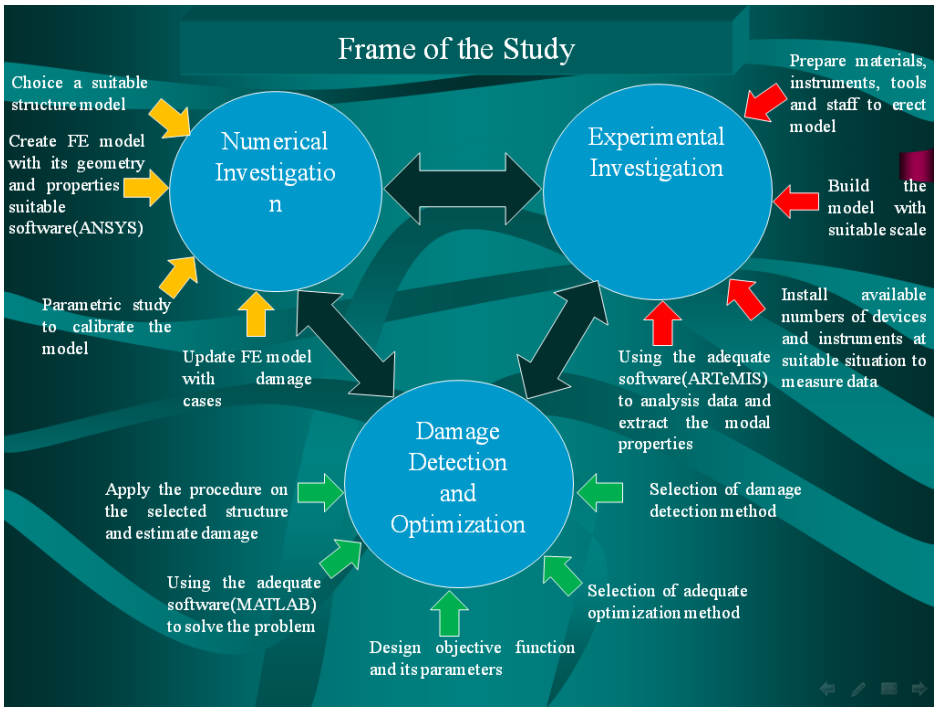

Figure 1.1: The general concept of SHM of the current research

The first core of the current research is the experimental investigation (EI) and all parts of this field, selection of the model, supplying the material and tools and devices to erect the models, preparing and installing the available instruments and devices for testing, selection of suitable positions of measurements points for data recording and finally extraction the results from the available extractor software by analyzing data from vibrating structural model using ambient vibration excitation. The experimental test was conducted using novel extractor software (ARTeMIS-Software) on the scaled models and the extraction of dynamic characteristics (natural frequencies and mode shapes) were made using eight transducers as the model was subjected to shaker device to simulate the ambient vibration excitation coming from environmental loads such as human activities, traffic, wind etc.

The second core focuses on the numerical computations (NC) and all parts of this theoretical side of the present research, creating finite element (FE) models of the selected scaled structures using commercial finite element software (ANSYS-Software) and all their geometry and material properties, extracting of the dynamic characteristics and comparing the numerical results with those were extracted from experimental investigation and

studying the influence of several structural models parameters on the numerical results to be close to the actual experimental results using updating process of the FE models to implement them in advance procedures.

While, the last core includes the sophisticated part of the structural health monitoring system. In this part the statistical analysis of the structural models results are made using the adequate heuristic optimization method (Simulated Annealing) with designing of proposed objective function and its variables and range of searching space for the proposed procedure of calibration process and the proposed procedure of damage detection method for the structural models. This proposed procedures were created by new advance subroutine in a high-level technical computing language (MATLAB-Software) that could properly handle all these things to monitor the structures system.

In this study the three main parts of SHM technique are applied for adopted structural models, experimental investigation, numerical computation and statistical process to detect damage, location and extent. The previous studies and details will present in next chapters.

1.3. Objective of the research

The author of dissertation starts during the years 2012-2015 in the field of structural health monitoring which is include three main axes; experimental test of structures; numerical simulation of structures and artificial intelligent techniques. The aims of this study are:

1- To gain experience and the procedure of experimental investigation of civil structures using Data acquisition system, which includes the process of sampling signals from the transducers (accelerometers) and converting the resulting samples into numerical values.

2- To gain experience and ability to extract dynamic characteristics of civil structures under ambient vibration excitation.

3- To gain experience through the analysis some experimental cases concerning aspects dynamic response of civil structures which are very important in the proposed damage identification procedure.

4- To gain experience and create procedure of numerical estimation using FE models and computing the modal properties of the civil structures using modal analysis. Then, create procedure to compare results and calibrate them with experimental results.

5- To gain experience concerning in statistical analyses for type of heuristic optimization algorithm and target functions with all factors affect to minimize differences in dynamic characteristics between experimental and numerical results which have significant effect in the proposed damage identification procedure.

6- To gain experience and create proposed procedure of damage identification to evaluate the health state of the structures as robust artificial system of SHM. The proposed procedure of damage identification should be able to detect the existence, location and severity of damage accurately.

1.4. Significance of the research

This dissertation deals developing proposed procedures of a vibration-based SHM which could be reliable and robust and applicable for detecting damage in several simple or complex real structures under ambient excitation.

A large number of previous researches were carried out either experimental or numerical work, while the present study tests the proposed procedures relies on extraction of experimental testing and verification of numerical simulation. The experimental vibration testing was carried out using shaker device to simulate ambient vibrations excitation. The ambient vibration measurements were conducted using a limited number of transducers (only 8-accelerometer) which are available in the lab of the Faculty of Civil Engineering. The dynamic responses of the structural models are measured under different additional mass cases have been used to evaluate the robustness of the proposed procedure.

Also, the most of researches dealt either simple structural model or few of them were conducted in a small space frame model, whereas in the current research and due to the rarity of using complex structures, four structural models are classified from simple to complicated are adopted: simple steel beam; plane grid steel bridge; multi-story steel building and Vierendeel steel bridge. As well, the previous studies adopted simple structural behaviors, such as, a beam action or a truss action or a plate bending action only,

while in this research, all structural behaviors were studied; a beam action, a plate bending action, a truss action, beam-column action and space frame action.

Also, a proposed procedure was developed using heuristic optimization for calibrating the dynamic responses of finite element simulation of the structural models to be closer to the experimental modal responses extracted from the measured vibration responses. Also, the new objective function used in heuristic optimization was proposed with its variables and weighting factors which are affect on the accuracy of diagnosis of damage in the structural models. Finally, developing proposed procedures of a vibration-based SHM which is reliable and robust was made and applicable for detecting damage in several simple or complex real structures under ambient vibration excitation.

1.5. Organization of the dissertation

The dissertation of damage detection and localization for civil structural health monitoring is organized in nine chapters:

In chapter 1, the general idea of structural health monitoring importance in civil structures and frame, aim, significance and layout of the dissertation are presented. In chapter 2, the overview of previous studies in the field of damage detection based on changing of dynamic characteristics of civil structures is presented. In chapter 3, is aimed at analysis method of identification of dynamic characteristics using ambient vibration measurements. In chapter 4, the concept of the optimization method analysis is extended to damage detection based on changing of dynamic characteristics.

In chapter 5, deals with the experimental analyses of the adopted structural models. In chapter 6, deals with the numerical modeling applications using finite element model (FEM) with parametric analysis in order to calibrate the numerical dynamic characteristics on the basis of the similar experimental dynamic characteristics. In chapter 7, the definitions and verifications of proposed optimization algorithms and proposed damage detection procedures are presented.

Finally, the chapter 8 deals with the conclusions and recommendations of the study, and chapter 9 includes references referred to in text and appendices.

2. OVERVIEW OF PREVIOUS STUDIES IN THE FIELD OF DAMAGE DETECTION BASES ON CHANGES OF DYNAMIC CHARACTERISTICS OF CIVIL STRUCTURES

2.1. General

One of the modern techniques of structural health monitoring (SHM) is the vibration-based damage detection methods. These techniques depend on that existence of damage in a structure leads to change of the dynamic characteristics or vibration modes or modal properties of that structural system [15], [20]. The natural frequency and mode shape are the dynamic characteristics of structure which can be used for structural health monitoring purposes [21], [4]. The main task during structural health monitoring is art to extract information about the existence, location, and extent of damage in the structure due to the change of dynamic characteristics. The SHM technique is to monitor and interpret these changes in structural dynamic characteristics, extracted from measurements during experimental modal analyses and signal-processing techniques. The extraction experimentally of the natural frequencies and mode shapes of a vibrating structure can be accomplished using modern vibration testing equipment and instrumentation. Also, the dynamic characteristics, natural frequency and mode shape, of structural components are often predicted numerically using Finite Element (F.E.) analysis and then later verified experimentally with dynamic analysis testing systems. The structural modal data can be utilized for cost-effective health monitoring and operational life assessment without requiring the structure to be dismantled [18].

In civil structures, damage is defined as changes introduced into a structural system, either intentional or unintentional, which adversely affect the current or future performance of that structural system [12]. The presence of damage may be due to changes in the material properties, consequence of aging, chemical-physical interaction with the environment and to the time varying applied loads [22]. Also, structural damage is defined

as a measurable increase in the incremental local flexibility of a critical region [23]. The damage in structure is usually local phenomenon and in order to take in account this local problem, a combination of local and global properties is required on the complex structures. These dynamic characteristics or modal parameters are global properties of the structure which are used in damage detection in the structures. The variations of physical properties of the structure change in the stiffness and mass properties of the structure that will cause alteration the dynamic characteristics of that structures [20], [24]. These changes in modal properties of the structure depend on location and extent of the damage, therefore the changes are not the same for each mode of the structure [20]. This concept of damage definition is relied on comparison between two cases of that structural system, original which is assumed initial/intact or undamaged case and current/present or may be damaged case.

2.2. Dynamic characteristics of a structure

To characterize the dynamic behaviour of a structure in tern of its modes of vibration, the dynamic characteristics for each mode are defined by modal frequency, modal damping and mode shape [25], [26], [27]. Also, they are called modal properties/parameters of a structure and they are associated with each other for each mode. The dynamic characteristics are computed from the principle of the equations of motion of the dynamics of a structure with N degrees of freedom and viscous damping coefficient can be expressed as:

$$[M]\{\ddot{x}(t)\}+[D]\{\dot{x}(t)\}+[K]\{x(t)\}=\{F(t)\} \quad 2.1$$

where are:

M , D and K - the $n\times n$ mass, damping and stiffness matrices, respectively,

$F(t)$ - the external applied force vectors with respect to the time t.

For initial vibration, the force vector can be defined as:

$$F(t)\}=\{0\} \quad 2.2$$

$\ddot{x}(t)$ - the acceleration,

$\dot{x}(t)$ - the velocity,

$x(t)$ - the physical displacements.

and it can described by:

$$x(t) = q(t)\phi \quad (2.3)$$

where are:

ϕ - the mode shape vector,

$q(t)$ - the time variation of the displacements.

and it is described by the simple harmonic function as:

$$q(t) = A\cos\omega t + B\sin\omega t \quad (2.4)$$

where are:

A and B - constants of initial condition that initiate the motion,

ω - the circular frequency.

Substituting Eqs. (2.2), (2.3) and (2.4) into Eq. (2.1) , where ω_i and ϕ_i are unknown, the response of system for undamped structure can be expressed as:

$$[(-\lambda[M]\Phi + [K]\Phi)]q(t) = 0 \quad (2.5)$$

The solution of this equation has two ways either trivial solution, $q(t) = 0$, that means there is no motion in the structure or nontrivial solution and that is useful, $q(t) \neq 0$, the expression of Eq. (2.5) can be written:

$$[K]\Phi = \lambda[M]\Phi \quad (2.6)$$

where are:

λ - the eignvalue matrix.

So, this algebraic problem is called the matrix real eignvalue problem if want to distinguish it from the complex eignvalue problem for system with damping.

Φ - the eignvectors matrix or characteristic vectors matrix.

and is also known modal matrix and, the Eq. (2.6) can be written for the i^{th} eignvalue equation for ambient vibration as well [64]:

$$[K]\{\phi_i\} - \omega_i^2[M]\{\phi_i\} = 0 \quad (2.7)$$

where the determinate of term is equal to zero, it implies the inverse of term is not exist.

$$\det([K] - \omega_i^2[M]) = 0 \quad (2.8)$$

This equation is known as the *characteristic equation* or *frequency equation* and has N real and positive roots for ω_i^2 because the structural mass and stiffness matrices, M and K, are symmetry and positive definite. The eignvalue matrix is diagonal matrix and each element value is a scalar and equal to square of frequency and is also known *characteristic values matrix* or *spectral matrix*. Where ω_i is the natural circular frequencies and it measures the number of repetition per unit of time [27] and also is defined in a natural cyclic frequency f_i of structural vibration [26]. The corresponding ϕ_i is eignvector which represents mode shape vector for i^{th} mode $i=1,2,...,N$, N is the number of modes of an N-DOFs of structural system, where mode shapes matrix can be written as:

$$\Phi = [\phi_1, \phi_2, ..., \phi_N] \quad 2.9$$

The mode shape is called *shape* because they are unique in shape, but not in value and that is, the mode shape vector for each mode does not have unique values [28], [29]. That means the mode shape describes a shape, not the absolute value of vibrating motion. Therefore, the amplitude ratios between all vector elements is fixed, but the length of the vector may be arbitrarily selected.

Finally, the vibrating structure with N-DOFs has N natural frequency which is arranged in sequence from smallest to largest corresponding mode shapes and the first mode is also known as *fundamental mode* [26]. The term *natural* is used to qualify each of these dynamic properties to emphasize the fact that these are natural properties of the structure in free vibration and they depend only on its mass and stiffness properties.

On the other hand, there are different ways to represent the dynamic characteristic of the structure [28], [29], such as: a set of linear second order differential equations, typically used in Finite Element Analysis (FEA); Frequency Response Functions (FRFs) matrix model, it is used in Experimental Modal Analysis (EMA) and a modal model, it is obtained from either FEA or EMA. All those dynamic characteristics are used in the damage detection methods, as discussed in the next section.

2.3. Structural crack theory

In fracture mechanics, the cracks are defined as the propagation and existence of defects in the material of a structure and methods of analytical solid mechanics are used to compute the driving force on a crack and characterize the material resistance of that structure [30]. The physics of stress and strain are applied by the theories of elasticity and plasticity to estimate mechanical failure due to the existed defects in real material of the structure.

In general, the reproduce of crack comes from applying the force in three ways, as showing in [30]:

1- Mode-I: tensile stress normal to the plane of the crack (opening mode).

2- Mode-II: shear stress acting parallel to the plane of the crack and perpendicular to the crack front (sliding mode).

3- Mode-III: shear stress acting parallel to the plane of the crack and parallel to the crack front (tearing mode).

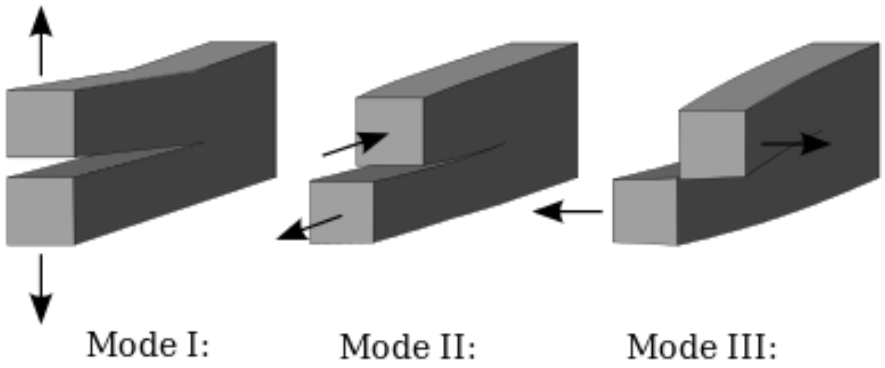

Figure 2.1: Concept of structural crack type [134]

There are two types of behaviours of material during operating conditions that include loads, linear elastic and nonlinear or inelastic [30]. In some particular material may the assumption of elastic behaviour not work particularly in composite material, therefore the inelastic behaviour is needed.

In this study, where the steel structural models are used, the linear elastic behaviour is adopted numerically during the linear elastic modal analysis for damaged models.

2.4. Structural Damage detection methods

The earlier studies in damage detection of structures were performed in the 1970's and 1980's by the offshore oil industry [12], however most of the proposed techniques were not efficient. Therefore, more attention from researchers in last few decades has been taken in this field to improve methods for detecting damage in structures.

Structural damage detection based on structural modal data, such as natural frequencies and mode shapes, is a rapidly developing field since the relation between natural frequencies and local defects has been reported. Over the last 30 years, several damage detection methods have been formulated. The parallel development of electronics and measurement equipment made it possible to implement damage detection theory in practice. The damage detection methods that make use of measured modal data are effective and safe for construction. Vibration measurements are usually carried out under natural conditions, without applying additional forces, so the process is fully non-destructive for the structure [31].

The main concept of these methods relies on the comparison between two cases, undamaged/intact and damaged response of the structure which are extracted experimentally and/or numerically, as shown in Figure 2.2.

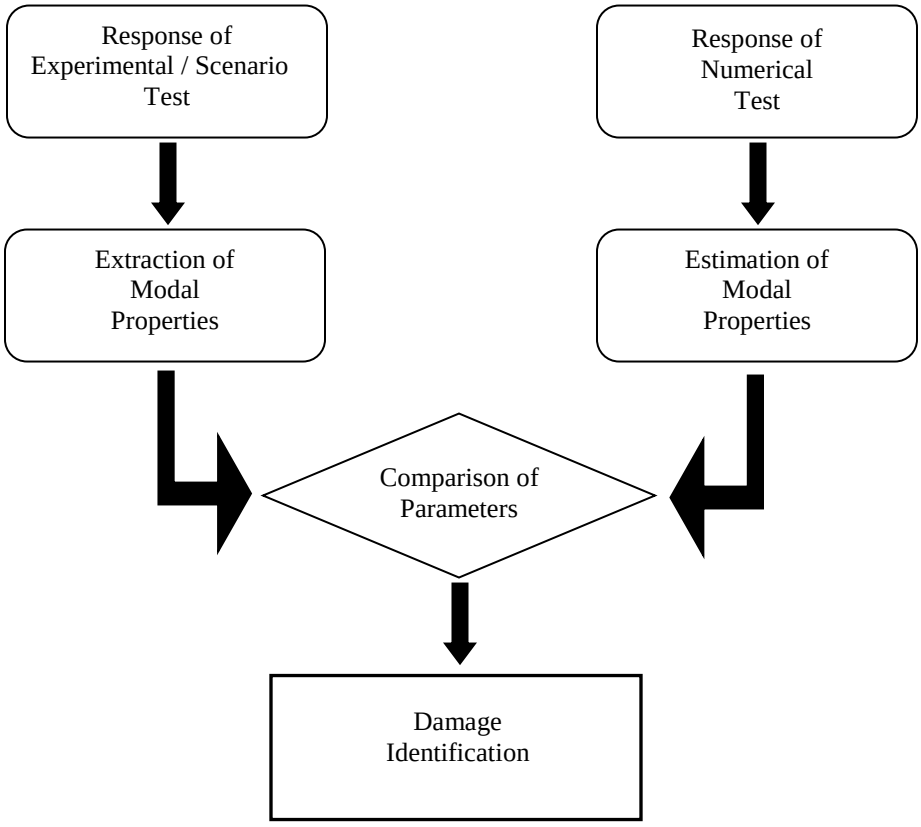

Figure 2.2: Concept of structural damage detection methods

The methods that deal with only numerical FE models used the simulation of experimental response, therefore the scenarios of those cases are assumed to simulate the actual response in real structures or structural models. On the other hand, the methods that deal with experimental and numerical responses of real structures or structural models are more reliable and efficient. In present study, the experimental and numerical investigations are applied. There are several methods of structural damage detection that will be discussed in next sections.

2.4.1. Damage detection methods based on natural frequency changes

The natural frequency of a structure is one of the fundamental dynamic characteristics of the structure. The natural frequency is a function of the physical properties, mass and stiffness, of a structure and can be extracted from the vibration signal measured from the structure and estimated from modal analysis from a FE model. The relative change or shift

of natural frequency of the structure can be used as an indicator of the presence of damage in structure. The assessment methods based on the observation of the changes of the structural natural frequencies compare the frequencies evaluated through experimental modal analysis respect to a known reference condition are discussed substantially. The parallel development of electronics and measurement techniques made possible implementation of damage detection theory in practice. Vibration measurements are usually carried out under natural conditions, so-called ambient vibration measurements, without applying additional forces, so the process is fully non-destructive [32].

Cawley and Adams in 1979 reported a procedure for detecting damage in composite material from the differences of modal frequency values [12]. They presented that an error between measured frequencies and computed using model based on a local stiffness reduction can be used to detect damage. Also, they included multi damage positions and a number of mode pairs in their work for each damage location. They concluded that the minimum value of an error indicates the location of damage.

Friswell et al. in 1994 presented approach to identify damage based on a assuming of damage scenarios in the structural model [12]. From the structural model, they computed the natural frequencies for first few modes for both the intact case and the damaged case which produced from scenarios. They estimated a ratios resulted from intact and assumed damage scenario cases of the structural model that can compare them with other ratios computed from a intact candidate and damaged structure. They concluded a relation of these two sets of numbers of ratios that can be used to detect damage in the structure if those ratios were equal and near 100.

Doebling et al in 1996 mentioned the differences in natural frequencies can be estimated by [33], [34]:

$$\Delta\omega_i^2 = \frac{(e_n(\phi_i))^T \Delta K_d (e_n(\phi_i))}{\phi_i^T M \phi_i} \qquad 2.10$$

where are:

$\Delta\omega$ - the change in the natural frequencies between the undamaged and damaged structures for the i^{th} mode,

ϕ_i - the i^{th} mode shape vector,

$e_n(\phi_i)$ - the element deformation vector that is computed from the mode shapes,

ΔK_d - the change in the matrix stiffness due to the existence of damage,

M - the mass matrix.

In the above expression assumes that the damage does not change mass matrix. Several researchers applied this expression to their work to detect the damage location only [34].

Salawu in 1997 presented an important review dealt with using the natural frequency only as a diagnostic parameter in structural evaluation procedures using vibration monitoring [20]. The author presented some of damage detection techniques based on frequency changes and sensitivity concept. Those techniques depend on the ratio of frequency changes as a function of corresponding physical parameter values, such as stiffness parameter, tension force, stress level and strain modal value, and could be used to detect the damage location. Several structural models were investigated such as: simply supported models, box girder bridges, high steel mast, two continuously supported plates model and prestressed concrete bridge models. The author mentioned that the procedures are based on the fact that the natural frequencies are sensitive indicators of structural health. Also, a cheap acquirement and quick and reliable implementation of frequency measurements made the analysis of periodical frequency measurements can be applied to monitor structural health and could provide an inexpensive evaluation technique.

Salawu mentioned that 5% of change in natural frequency is necessary to detect damage with confidence [20]. It is mentioned that the stress for a particular modal frequency is minimum at modal nodes which are points of zero modal displacements. He reported that the location of damage for a particular vibration mode affects on the percentage of reduction in natural frequency, since the significant reduction (up to 15%) occurred when damage is at regions of comparatively high stress in the structure. Theoretically, to simulate the existence of damage or crack and its severity in beam section, the reduction in second moment of area could be applied and that leads to reduce the local bending stiffness at that cross-section. Also, the significant reduction in frequency is

occurred when the damage is at regions of high curvature for a particular vibration mode. It is mentioned that the lower vibration modes would be sufficient for damage detection technique and when use the most sensitive modes to the damage, the technique is improved.

Salawu concluded that this approach of health evaluation of structure based on natural frequency is potentially useful [20]. Also, it is concluded that the natural frequency changes alone are not sufficient to identify the location of structural damage. Particularly, if structure has more than one crack and it could result the same frequency change which is caused from two different locations.

Doebling et al. in 1997 also presented a review dealt with damage detection methods which use the change in measured vibration response of structural system [12]. They mentioned that the damage detection methods based on vibration depend on concept that the modal properties are functions of the physical properties of the structure such as; mass, damping and stiffness. Therefore, changes in those physical properties such as reduction in stiffness resulting from presence of damage in the structure will cause noticeable change in modal properties.

Doebling et al. concluded that use of ambient or external load vibration measurements needs more investigation in the evaluation of structural health. Also, the authors reported that the use of measured vibration data is very promoted for damage detection using ambient signals. Finally, it is concluded for the development of health monitoring techniques needs more research to prove that the modal properties have enough sensitivity level for small damage in all types of structures.

The advantage of using natural frequencies as a parameter is that they have less statistical variation from random source as compared to other modal parameters [35]. The identification of a damage location and the severity of damage based on the change in the global properties derived from measurements at a limited number of sensor locations is a problem that has a non-unique solution. A large number of frequencies need to be measured for precise damage extent and location prediction. Measurement of multiple frequencies is generally not possible with good accuracy due to the presence of noise, coupling of the higher modes and the limitations of the measuring equipment etc. Also, global property like the natural frequency is not very sensitive to local damage in the structure [5]. Also changes

of natural frequencies give just an indication of damage existence, could conclude that a damage identification method using only change of natural frequencies is not sufficient to locate the damage [5]. However, locating the damage using just natural frequencies is difficult as modal frequencies are global properties of the structure, and hence cannot provide spatial information about structural changes. Therefore, mode shapes information are required to determine the location of the damage. In addition, multiple modes have to be considered for better estimation of severity and location of the damage, since the each natural frequency and corresponding mode shape are affected to different extents depending on the location of the damage.

2.4.2. Damage detection methods based on mode shapes changes

Damage in a structure also change its mode shapes and this change can be used to detect and locate damage in the structure. The mode shapes can be derived from the vibration signal and estimated by modal analysis from FE model. The essential condition to validate the experimental modal model is that each experimentally extracted mode of a structure should be normal to other mode vectors when weighed by the numerical mass or stiffness vector (derived from the FE model) and this process is called orthogonality. Unfortunately experimental modal vectors are not always orthogonal because of inaccuracies in measurement, incorrect mass matrix in the FE model and error introduced by the reduction algorithm used to modify the FE model mass matrix to match the dimensions corresponding to the number of measurement locations. So, The modal assurance criterion (MAC) is introduced which is a statistical measure of the consistency (degree of linearity) between estimates of a modal vector [29], [36], [37]. MAC and many of its variants have been used for the validation of experimental models, structural fault detection and optimal sensor placement among other applications.

Fox in 1992 used the mode shape information for the location of structural damage [38]. The author used the modal assurance criteria MAC to estimate the level of correlation between undamaged beam structure and damage beam structure with crack-like defect modes. He used numerical and experimental modal analysis in his work. Fox concluded

that the natural frequency and MAC value are reasonable indicators of the presence of damage. Also, it is concluded that the MAC value alone is a little insensitive.

Nahvi and Jabbari in 2005 also used numerical and experimental approach to detect crack in uniform cantilever beams using vibration analysis and the linear fracture mechanics theory [39]. The beam model is excited by a hummer and to avoid a non-linearity, the crack is assumed to be always open. They used mode shapes as well as the natural frequency in their proposed procedure. They concluded that the crack location and size have noticeable effects in the first and second mode. They observed decreasing natural frequencies of the cracked beam as crack becomes deeper. The fundamental frequencies are mostly affected in the case that crack is located near to the maximum moment zone. The reason is that the presence of a crack near the maximum moment zone significantly reduces the global stiffness of simply supported beam. It can be inferred that the changes of the frequencies of higher modes depend on how the crack is closed to the corresponding mode shape nodes. As a consequence, natural frequency of the cracked beam is less affected for a crack located at the node points (points of zero amplitude) of the corresponding mode shape [39].

Fayyadh and Abdul Razak in 2011 used the mode shapes for damage location detection from numerical simulation of a concrete reinforced beam [40]. The authors applied two cases load to simulate the damage case of a structure, 50 % and 70% of failure load. They proposed a residual value resulted from the curve fitting procedure on mode shape vectors as an indicator for damage location. They concluded that considered first six mode shapes using residual value as an indicator showed good sensitivity and ability to locate the damage.

On the other hand, the curvature of mode shapes was used widely as indicator to damage detection from derivatives of mode shape due to the changes in it to obtain spatial information about vibration changes [12], [33], [34]. The absolute change in mode shape curvatures using the central difference approximation can be formulated in general form:

$$\phi^{d}_{n,i} = \frac{\phi_{n-1,i} - 2\phi_{n,i} + \phi_{n+1,i}}{h_d{}^2} \qquad 2.11$$

where are:

$\phi^{d}_{n,i}$ - the local change in the curvature between the undamaged and damaged structures due to local reduction in stiffness which is caused by presence of damage,

$\phi_{n,i}$ - the modal displacement for the i^{th} mode shape at the measurement coordinate n,

$n\pm1$ - the measurement coordinate of points before and after the certain point,

h_d - the distance between the measurement coordinates.

Many studies were carried out using this method in literature [12], [33], [34]. Abdo in 2012 reported the application of using high-order mode shape derivatives, fourth derivative, in damage detection of plate-like structure [41]. He verified the reliability of his procedure on a simple supported and cantilever steel plate using numerical analysis of low and high-order mode shapes. The damage was simulated as reduction in modulus of elasticity of damaged element and he applied different scenarios. The author concluded that the damage detection procedure using fourth derivative of mode shapes gave a good result to localize the damage regardless if they are high or low-order mode shapes. Also, it was concluded that using fourth derivative procedure of mode shapes is better damage identification than those of using curvature of mode shapes. He concluded that important thing to apply this procedure for damage detection is the accuracy of vibration measurements.

Akinovic et al in 2013 used damage detection method based on mode shape for identifying the location of damage only [42]. They applied their method on a cantilevered steel beam model using numerical investigation. The author used a central difference approximation to compute slope and curvature of displacement node shapes differences between the intact and damaged structural models. Damage numerically was simulated by reducing the height of a cross beam of damaged element. They concluded that damage detection based only the displacement mode shapes of damaged structure is not suitable and efficient. Also, using the curvature is the best indicators of damage location than the slope. Finally, they concluded that the drawback of this method is difficult to extract experimentally modes with required necessary measurement accuracy and it needs a lot of sensors for mode shape measurements.

Some researches adopted the damping ratio as a one of the modal parameters, Ernest in 2012 represented a damage detection procedure based on change of damping ratio [43].

He used a simple supported steel beam with experimental testing using electromagnetic vibrator to excite structural model to get the dynamic response in vertical direction at different locations using accelerometers. The damage was simulated by cutting small part of the structural model with three different damage scenarios for undamaged and damage cases of model. The author concluded that damage on the structural model increase the ratio of critical damping value and increase the severity of damage increases the change ratio of damping ratio value.

2.4.3. Damage detection methods based on frequency response function (FRF) changes

The linear dynamic system could be presented by equivalent expression is called frequency response function (FRF) [10]. Therefore, the change in mass or stiffness of a structure will change the acquired FRF response of that structure. Description of the theoretical aspect of this method can be described in general by the following equation [18], [33], [44]:

$$M\ddot{x} + C\dot{x} + Kx = F(t) \tag{2.12}$$

where are:

x - the vector of nodal degree of freedom of the structure,

M , C and K - the mass, damping and stiffness matrices, respectively,

$F(t)$ - the external force vector with respect to the time t.

For the case of the harmonic excitation, the force vector can be defined as:

$$F(t) = Fe^{j\omega t} \tag{2.13}$$

where are:

ω - the forcing frequency,

F - the force amplitude vector.

Therefore, the response vector may be assumed as:

$$x(t) = Xe^{j\omega t} \tag{2.14}$$

then, Eq. (2.3) may be rewritten as:

$$(-\omega^2 M + j\omega C + K)X = F \tag{2.15}$$

the relation between the response $X(\omega)$ and the excitation $F(\omega)$ at each frequency ω is given by:

$$X(\omega)=H(\omega)F(\omega) \quad 2.16$$

where are:

$H(\omega)$ - the Frequency Response Function matrix of the system,

and it is given by:

$$H(\omega) = (-\omega^2 M + j\omega C + K)^{-1} \quad 2.17$$

The individual Frequency Response Function $H_{ij}(\omega)$ is defined by the relation between the response at the i^{th} coordinate with a single excitation applied at the j^{th} coordinate. This relation is given by:

$$H_{ij}(\omega)=\frac{X_i}{F_j} \quad 2.18$$

Thus, the column vector of the frequency response function matrix $H_j(\omega)$ may represents the normalized structure shape at each frequency ω, and this matrix is defined as Operational Deflection Shape (ODS).

Several studies dealt with this method such as, Owolabi et al. in 2003 conducted a research on the experimental investigations of the effects of cracks and damages on the integrity of structures, in order to detect, quantify, and determine their presence and locations [10]. They used two sets of aluminium beams, one set were fixed ends and the other were simply supported. Cracks are implemented in seven different locations along the length of beam for each set. Measurements of the accelerometers are recorded at seven different points on each beam model. The damage detection schemes used in their study depended on the measured changes in the first three natural frequencies and the corresponding magnitudes of the measured acceleration frequency response functions (FRFs). They identified that when cracks being located at position of maximum bending moments of the structure, changes of natural frequencies are the most significant. In other words, the fundamental frequency decreases significantly as the crack location moves towards the mid-point of the simply supported beam and in general, the higher the number of modes used, the greater the degree of accuracy and dependability of predicted results could expects [10]. They concluded that the vibration behaviour of the beams is very

sensitive to the crack location, crack depth and mode number. Also, it is concluded that the proposed procedure is feasible using natural frequency and FRF amplitudes.

Yoon et al in 2010 presented method using operating deflection shape (ODS) derived from experimental FRF data to detect the location and extent of damage in steel beams, composite beams, and plate like structure [45]. They used FRF data obtained from intact structure only. They concluded that their method successfully identified the location and extent of the notches on the selected models. Also, it is concluded to improve the reliability of detecting damage should the measurements of structural responses and positioning of excitation points be accurate and precise.

Baneen et al in 2012 used a noise suppression method as a vibration based damage detection method [46]. They validated their method based on simulated data and experimental measurements. They used FRFs to extract mode shapes form a uniform steel beam model with two narrow slots at different location. The proposed method uses a set of damage indices from each mode generated by the Gapped-Smoothing Method (GSM), and suppresses the noise by allowing only those peaks which show the location of the damage. The proposed improvement reduces and removes false peaks from result and allows only the peaks that give useful information about the damage location. They concluded that, if a spatial resolution of 1 mm is used, the method is able to detect more severe damage even by only considering the first two modes, but a higher spatial resolution is required to identify less severe damage from experimental results.

2.4.4. Damage detection methods based on measured flexibility matrix changes

In this method of damage detection uses the dynamically measured flexibility matrix to compute changes in the static behaviour of the structure. The flexibility matrix relates the applied static force and resulting structural displacement, so it is defined as the inverse of the stiffness matrix. Each column of the flexibility matrix represents the displacement pattern of the structure associated with a unit force applied at the corresponding DOF. The measured flexibility matrix is estimated from the mass-normalized measured frequencies and mode shape. In this method, the formulation of the flexibility matrix is approximate

and only first few modes of the structure are taken which is most sensitive to changes [12]. Damage detection using changes in flexibility matrix is implemented by comparing the differences between the flexibility matrix of intact and damaged case of a structure, as given below:

$$U = GF \tag{2.19}$$

where are:

U - the structural displacement,

G - the inverse of the stiffness matrix (flexibility matrix),

F - the applied force.

For the first few modes of the structure, the expression can be formulated as [32]:

$$G = \sum_{i=1}^{n} \frac{1}{f_i^2} \{\phi_i\} \{\phi_i\}^T \tag{2.20}$$

where are:

f_i - the natural frequency for the i^{th} mode of the structure,

ϕ_i - the i^{th} mass-normalized mode shape.

Then, the change in the flexibility matrixes ΔG in structure due to existence damage in structure can be obtained by:

$$\Delta G = G_{damage} - G_{undamage} \tag{2.21}$$

Several researchers dealt with this meaning of expression in their work [12], [31]. Aktan et al. in 1994 proposed a condition index to evaluate the integrity of two bridges and this index is defined using measured flexibility matrix [23]. They analyzed the accuracy of this method by comparing the measured flexibility to the static deflections induced by a set of truck-load tests. They concluded that the reliability in their method is not perfect but adequate to evaluate the damage in the structures.

Pandy and Biswas in 1994 presented a damage detection method based on change in the measured flexibility of the structure [47]. They applied the method to several numerical model and to actual beam. They concluded that could detect damage and its location from the first two measured modes of the structure.

2.4.5. Damage detection methods based on measured stiffness matrix changes

In this method of damage detection uses the dynamically measured stiffness matrix to compute changes in the behaviour of the structure. Also, the dynamically measured mass and damping matrices can be estimated with stiffness matrix to detect damage and its location.

Salawu and Williams in 1993 presented a damage detection method based on direct comparison of measured stiffness, mass and damping matrices to detect location of damage [48]. They applied their method to simply supported steel beam and it relies on experimental modal analysis. They concluded that the method is the best from the four tested methods, but it is incapable to detect location of damage in a low stress zone.

On the other side, there are some methods adopted different ways to detect damage in structures. Lam and Yin in 2011 proposed dynamic reduction-based structural damage detection of transmission towers method [49]. They verified their method experimentally using eigensystem realization algorithm (ERA) and numerically using FEM to extract modal properties, natural frequency and mode shape, of the scaled steel transmission tower model. They simulated damage numerically as a reduction in stiffness of the substructure of the model and there is no change in the mass distribution of the structural system. While, the damage experimentally was represented by removing the certain member completely from the structural model in different damage scenarios. The comparison between the healthy and damaged state of the model are applied to detect damage using the measurements of sets of vibration data to extract modal frequencies and mode shapes. The authors concluded that the proposed method is suitable for that adopted structure with fast estimation of the damage case but the accuracy is not high. Also, it was concluded that the simulation of damage experimentally by removing the substructure totally practically is not real.

2.4.6. Damage detection methods based on updating structural model using optimization methods

In these methods, the modification of structural model properties such as mass and stiffness are applied to reproduce as closely as possible the measured static or dynamic response from the data [12]. These methods solve for the updated matrices (or perturbations to the nominal model that produce the updated matrices) by forming a constrained optimization problem based on the structural equations of motion, the nominal model, and the measured data. Comparisons of the updated matrices to the original correlated matrices provide an indication of damage. Also, they can be used to quantify the location and extent of damage.

Those methods have differences in the applied various algorithms, which can summarized, as follow [33]:

1. Type of used objective function including parameters.
2. Type of applied constraints on the problem.
3. Type of implemented optimization method.

The various methods and their differences are discussed in the following section to describe each of the classification items in the previous researches. Kirkegaard and Rutter in 1995 presented a comparative study of three techniques to assess damage based on vibration data and one of them based on Artificial Neural Network (ANN) [50]. They verified the proposed procedure experimentally and numerically on a cantilever steel beam with two damage cases. They used the differences in the first few natural frequencies between intact and damaged structure as indicator for damage. The authors concluded that the procedure based optimization method gave better indication for damage location and more studies in civil structures are needed.

Ruotolo and Surace in 1997 reported damage assessment method based on optimization method, Genetic Algorithm (GA), using modal parameters of the lower modes [51]. They verified the method numerically and experimentally on a cantilever steel beam with different damage scenarios. The objective function includes the difference in natural frequencies and modal curvature between the undamaged and damaged structures. The damage was presented numerically by reducing the stiffness of damaged element and experimentally by wire erosion to produce notch. The modal properties were extracted experimentally from frequency response functions and to excite the model, broadband

random noise approximating to a white noise process was employed at free end. The calibration of the finite element model was implemented to match between the numerical and experimental natural frequencies. The authors concluded that the proposed method can detect damage, its location and its severity with satisfactory accuracy.

Friswell et al in 1998 presented proposed procedure based on a combined GA and eignsensitivity algorithm for the damage location in structure using vibration data [52]. Thy verified the procedure numerically on a cantilever steel beam and experimentally on a cantilever steel plate. The modal properties of the plate model were extracted experimentally using impact excitation of the structural model. The objective function includes the differences in the natural frequencies and mode shapes of the intact and damaged structural model. The damage was simulated numerically by reducing the stiffness of the damaged element and experimentally by saw cuts of the damaged element. The authors concluded that the use changes in frequencies could treat the errors in testing data or in modeling when comparing between the undamaged and damaged structural model or the numerical and experimental structural model. Also, it was concluded that the proposed procedure successfully detected the damage location in the structure.

Xia and Hao in 1998 reported damage detection procedure based optimization method, GA, using vibration data [53]. They verified the proposed procedure numerically and experimentally on a cantilever steel beam and a frame steel beam. The damage represented in the structural model experimentally by saw cut of the damaged element and numerically by reducing the stiffness of the damaged element with different damage scenarios. To match the finite element model modal frequencies with those extracted from experimental, updating process was implemented only for the first model. The objective function includes the direct comparison between the changes in the measured numerically and extracted experimentally modal properties, natural frequencies and mode shapes, of the intact and damaged structural models. The authors concluded that the frequency changes only are not sensitive to damage detection particularly to local damage. In addition, it was concluded that the proposed procedure detected the damage location accurately with studied weighting factors of two parts of objective function.

Au et al in 2003 presented proposed damage detection procedure based on optimization method, GA, using incomplete and noisy modal test data [54]. They verified the procedure numerically on a single-span simply supported steel beam and a three-span continuous steel beam with different noise levels. To simulate the limited number of sensors experimentally which are small when compared with the degree of freedom of the finite element model, the numerical simulation was applied to extract modal properties of the structure. The damage was simulated by reducing the bending stiffness of damaged elements with different damage scenarios. The authors concluded that the incomplete and noisy modal data have adverse effect on the accuracy of damage detection. Also, the use of the natural frequencies and mode shapes together on the damage detection is more efficient and accuracy.

Sahin and Shenoi in 2003 presented damage detection method based on optimization method, Arteficial Neural Network (ANN), global and local vibration-based analysis data [55]. The global properties were changes in natural frequencies and the locale were curvature mode shapes. The verified the proposed method numerically and experimentally on a cantilever steel beam with different damage scenarios. The damage was simulated numerically and experimentally by reducing the thickness of cross section of damaged elements. To extract modal properties of the structural model experimentally, two different type of excitation were applied using an elector-dynamic vibration generator with. The authors concluded that the reduction in frequencies provides necessary information for the damage location and severity but the change in curvature mode shapes gives better indicator for damage detection. It was concluded the experimental procedure has an important effect and gives reliability in the damage detection. In addition, the proposed method has robustness and accuracy.

Rao etal in 2004 presented proposed damage detection procedure based on optimization method, GA, using the concept of residual force method [56]. They verified the procedure numerically on three simple steel structural models: a plane truss, a cantilever beam and portal truss. The objective function includes the residual value of eignvalue and eignvector between the undamaged and damaged structural model. The damaged was simulated in the model by reducing the stiffness of the damaged element with different

damage scenarios and two cases of noise. The authors concluded that the proposed procedure has excellent agreement even with use the few modes in objective function.

Lee et al in 2005 reported damage detection procedure based optimization method, ANN, using only the ratios of modes shapes between the intact and damaged case instead of the mode shapes themselves [57]. They verified the procedure only numerically on a simply supported steel beam and together with experimentally on a simply supported bridge model in the laboratory and a simply supported composite bridge with multiple girders in the field. The modal properties of both bridge models were extracted experimentally in the laboratory and the field by frequency domain decomposition (FDD) using ambient vibration data caused by traffic loading. The damage was simulated numerically by reducing the bending rigidity of the damaged element with different damage scenarios and two cases of noise to simulate the modeling errors. While, the damage represented experimentally for the model in the laboratory by cutting out parts in the damaged girder segments and for the model in the field by torch cuts on the main girder. The authors concluded that, for the complex structures, using only modal frequency is not effective and difficult to detect the damage because of the environmental effects as well as the significant effect of support condition. In addition, it was concluded that the use of updated model in damage detection procedure gives more accurate results and better representing of real behavior of the structure. Also, including the first few modes in the computations of damage detection shows good accuracy. Finally, the concluded that the proposed procedure detected the damage location with good accuracy, whereas the damage severities has small errors at different scenarios.

Park et al in 2006 presented proposed method of damage detection based on optimization method, GA, using frequency and modal strain-energy [58]. They verified the procedure on free-free aluminum beam model using numerical and experimental analysis. The modal properties were extracted experimentally using frequency domain decomposition (FDD) of measured acceleration signals by exciting model with impact hammer. The damage was simulated numerically by reducing the flexural stiffness of damaged element and experimentally by creating cracks in the structural model with different scenarios. They adopted objective function including differences, in natural

frequencies and modal strain-energy using modal curvature of the structural model, between the intact and damaged cases. The authors concluded that the proposed procedure has good accuracy for detecting the damage in all implemented scenarios.

Bandara et al in 2007 reported a damage identification method using frequency response function (FRF) based damage index and ANN method with data reduction technique of Principle Component Analysis (PCA) [59]. They verified the method on a pin-pin supported steel beam with different damage locations and sizes. The experimental testing was done by applying an impact fore from hammer as excitation force. at certain point on the model to compute FRF functions for undamaged and different damaged cases. The numerical estimation of the model was implemented for intact and different damaged cases to compute the FRF functions for measured points on the beam model with using damage simulation as a reduction in the second moment of area. The authors concluded that the data size using PCA could be reduced significantly without affecting the data and the proposed method has excellent ability to detect damage location and severity. In addition, the procedure using FRFs measurements even from one sensor enables to detect damage for simple structure.

He and Hwang in 2006 and 2007 presented a proposed procedure of damage detection based on an hybrid algorithm combining an adaptive real-parameter GA with Simulated Annealing (SA) method using dynamic response of a structure [4], [60]. They verified the procedure on four simple steel structural models; a cantilever curved beam , a cantilever beam, a clamped beam and a simply supported equal-sided sector of a composite spherical laminate shell. The adopted objective function includes the differences in natural frequencies, mode shapes and displacements of static response of the structural models with different scenarios including either a single damage or multi damages cases. The damage was simulated numerically by reducing the modulus of elasticity (the stiffness) of damaged element and in one case only they used the stiffness and mass reduction together. Three errors cases were considered in measured natural frequency and mode shape to simulate the error of the experimental testing data. The authors concluded that the procedure is effective and precise in damage detection with different boundary condition in damaged elements by reducing the stiffness or even with use mass reduction. In addition, they concluded that the

results are affected with errors coming from experimental testing to be close but not in the exact location and extent of damage.

Gomes and Silva in 2008 presented a comparison between damage detection procedure based on optimization method, GA, and sensitivity method using modal frequencies shifts [61]. They verified the proposed procedure numerically on a siply supported concrete beam and a concrete portal frame model. The damage was simulated by reducing the static moment of inertia about one axis of damaged element and used one position in the first model and different positions in the second model. They concluded that the GA-based damage detection procedure and sensitivity method have robust to identify damage location and extent but not exactly. In addition, method sensitivity was not able to detect multi damage in the structure because its simplification, contrarily, GA procedure, which is depended on complete finite element analysis, enables to deal with more than one crack.

Meruane et al in 2008 reported damage detection method based on optimization method, GA, applied on a multi-cracked simply supported reinforced concrete beam [62]. They verified their work experimentally using suspended model by soft springs to simulate free-free boundary condition. They used non-symmetrical increasing static load to introduce cracks in the model and from each step, the modal properties were extracted to represent experimentally the different damage scenarios using an impact hammer for excitation. While, numerical representation of damage was simulated by reducing the stiffness of damaged elements in the model. The objective function includes the differences in modal parameters, natural frequency and mode shape as an index MAC, between undamaged and damaged model cases with adopting first four bending modes. They concluded that the proposed method has fast and efficient to reach the global minimum even with noise and error in experimental and numerical analysis respectively.

Panigrahi et al in 2008 presented comparison between analytical solution and numerical optimization solution using GA method-based damage detection procedure by the meaning of the residual force method for indentifying macroscopic structural damage [63]. The verification of the proposed procedure was implemented on a cantilever steel beam with homogenous and non-homogenous material in the sense of modulus of

elasticity. They used objective function includes modal properties of a structure with comparison between the intact and damaged model with different assumed damage scenarios. The damage was simulated by reducing the stiffness of damaged element with reduction factor and then recalculate the stiffness and mass matrices theoretically. The authors concluded that the GA based-damage detection procedure show excellent agreement with theoretical procedure of damage detection for adopted structural model.

Rosales et al in 2009 presented a comparison between two damage detection approaches, the first used ANN method and the other by applying the inverse problem with a Power Series Technique (PST) [64]. They verified the first approach on a cantilever steel beam-like structure and the second on a simple supported spinning steel beam with numerical estimation. The damage was simulated by introducing springs to represent the stiffness reduction of damaged elements in the first approach. In addition, for second approach the damage was simulated by reducing the depth of cross section of damaged element. The objective function included the change of natural frequency between the intact and damaged cases for the first three modes of the structural model in different damage scenarios. The authors concluded that the first algorithm using PST is simple procedure with very low cost to detect damage but it is for simple structures with small error. While the second procedure ANN-based damage detection handle more complex structures with smaller errors.

Panigrahi et al in 2009 reported damage detection procedure based optimization method, ANN, using the residual force method for indentifying macroscopic structural damage [65]. They verified the procedures on a uniform strength two steel structural models as study of a real leaf spring, the first is a triangular plate and another is a beam with variation in both width and depth. The modal parameters were estimated from numerical analysis of the models before and after applying damage scenarios. They used residual force vector to provide objective function for to be minimized for achieving the dynamic balance between intact and damaged case of the models in the sense of damage factor. The authors concluded that the results show excellent agreement between the damage factors of scenarios and those detected from proposed procedure.

Bakhary et al in 2006 and 2010 presented damage detection approach based on optimization method, ANN, using a structural model and a substructure technique [66], [67]. They verified the procedure numerically by applying on a two-span continuous concrete slab structure and a three-story concrete portal frame with different damage scenarios. The damage was simulated by reducing modulus of elasticity, in the term of stiffness reduction factor (SRF), of damaged elements. The authors concluded that the approach has ability to detect all damage in the structure and has efficiency and reliability compared with classical technique even with small damage.

Meruane and Helyen in 2010 reported damage detection procedure based on optimization method, an hybrid real-GA, using dynamic response [68]. They verified their procedure on a free-free tridimensional space aluminum frame model with different damage scenarios. Experimental test using Driving Point Residues (DPR) and numerical estimation were implemented to extract modal properties, natural frequency and mode shape, of structural model. Different objective functions were applied including the difference in modal frequencies, mode shapes, an index MAC, strain energy residual and modal flexibility matrices between the experimental and numerical results. The damage experimentally was represented by replace steel bar with another from plastic or by completely removing the damaged bar from the structural model, while numerically was by reducing the stiffness of the damaged element. The author concluded that the proposed procedure based genetic algorithm reaches a more precise solution than conventional method even with incompleteness in the measured of degree of freedom.

Arafa et al. in 2010 presented damage detection procedure based on hybrid optimization from combined two methods, Tabu Search (TS) method and Genetic algorithm, [69]. They compared between FE model and experimental model estimated natural frequencies to minimize the error value computed by objective function. Two damage locations assumed to verify their procedure and applied on simple beam models. The experimental tests are implemented for those beam models in addition to the numerical analysis. Experimentally, the damage induced using wire-cutting and then the test is conducted for the damaged model. They concluded that the proposed damage detection

method using adaptive two optimization methods has ability to explore damage in simple beam models.

Aghabarati and Tehranizadeh in 2011 presented the application of damage detection procedure based on optimization method, ANN, with three networks on a plane six-span steel truss bridge model [70]. They used static response of displacement of measured points as parameter of objective function during applied external force in truss model. Numerical simulation were implemented to estimate the results of simulated damage case by reducing the stiffness of damaged member with different damage scenarios. The comparison between the analytical and numerical results was included in objective function to identify the damage in the structural model. The author concluded that the procedure has the ability to detect damage in the structural model.

Liu et al in 2011 represented damage detection procedure based on optimization method, GA, using dynamic response of the structural model [71]. They verified the procedure on a simply supported concrete beam and used numerical analysis to simulate the experimental dynamic response for three damage scenarios. They redefined the including of two or more of modal parameters in the objective function as so-called "multi-objective function". Also, it was studied the effect of weighting factors for each parts of objective function on the accuracy and convergence speed of damage identification. Their work adopted objective function includes two modal properties, natural frequency and mode shape in an index of MAC, as a multi-objective function. The damage was simulated by reducing the modulus of elasticity of damaged element in different levels and using comparison between the healthy and damaged case of the structural model for detecting damage. The authors concluded that the damage detection procedure based on genetic algorithm using the multi-objective function has prominent and more closely performance.

Hadi and Abdulkareem in 2012 proposed damage detection method based on optimization method, GA, using stiffness and mass matrices, which are formulated using Hamilton's principle [72]. They used a simply supported curved steel beam for verifying their method using numerical simulation only. The author adopted two objective functions, only natural frequency and the other includes MAC as an index for mode shapes. The Damage was simulated by reducing the modulus of elasticity of damaged elements with

different levels of damage scenarios. They concluded that the proposed procedure with objective function including the natural frequency was effective and more accurate to detect damage position and extent with different damage cases.

Nejad et al in 2012 proposed damage detection method based on optimization algorithm, Particle Swarm Optimization (PSO), using incomplete dynamic data with a different level of noise [73]. They verified their method on three simple structural models: a cantilever steel beam, a four bay plane steel truss and a two-span-story plane steel frame. The author used objective function includes the comparative frequency change vectors, which represent the change in frequencies before and after damage element. Their work was verified using numerical simulation only and the damage was simulated by reducing the elastic modulus of damaged elements for different damage locations. They concluded that the proposed method has capability to detect damage location and severity even with small noise.

Kang et al in 2013 proposed damage detection method based on optimization method, PSO, using combined data of static and modal tests [1]. They used a clamped steel beam model to test the efficiency of their proposed method and by comparing the results with other optimization methods using numerical tests only. The authors used objective functions including displacements of nodes and natural frequencies for detecting damage in the structural model with different level of noise with two damage cases. Damage numerically was simulated by reducing the modulus of elasticity of damaged elements. They concluded that the proposed procedure is accurate and quick to detect damage for both damage cases.

Kourehli et al in 2013 proposed damage detection procedure based optimization, SA method, using incomplete modal data and incomplete static response of damaged structures [74]. They used a simply supported concrete beam and a three-story steel plane frame in their work for numerical investigation. The performance of their proposed procedure has been verified by experimental testing using modal data of a mass-stiffness system. They used two types of objective function, the first including natural frequencies and mode shapes and the other includes static displacement of selected nodes. Damage numerically was simulated by reducing the elasticity modulus of the damaged elements. The authors

concluded that the proposed method using different objective functions is a promising procedure for damage detection although incomplete modal data and static response even with noise.

Zhang and Yu in 2014 presented procedure using TS optimization method to find the optimal solution of damage detection in plane truss model in the sense of sensor location [75]. They concluded from their numerical simulation that the proposed procedure by TS method has reliable results with high accuracy.

Finally, from previous studies can conclude that the efficiency, accuracy and robustness of the damage detection methods based on optimization method are preferred to use in SHM. Some of the studies reported that the low-frequency global modal properties, natural frequency and mode shape, have been noted to be sensitive to change of operational conditions and still can be used as damage indicators. However, other studies presented that there is drawbacks of used modal property alone in damage detection, because of the disparity in decision about the ability of the global modal properties, natural frequency and mode shape, to detect damage in the structure even with presence of noise or with small local damage particularly in large or complex structures, more studies with combination of both modal properties are needed. In addition, most of mentioned researches above verified their procedures on small simple structure such as beam or plane truss-like structure and they avoided the large or complex structures because the cost and complexity of the large models due to the large number of local measurements and the type of instrumentations required for local measurement on the structure as well as the complexity in the computations. The damage detection method based on optimization methods such as GA and ANN were extensively discussed in the literature, while some of optimization methods such as simulated annealing (SA) are rare. In addition, the most of the previous studies implemented either numerical simulation of the structural models only or with experimental verification but for simple models to avoid complexity of the problems caused by data error and modeling error. It was noted that some studies implemented damage by removing totally the selected damaged member of damaged structural model to represent the damage experimentally and that is unrealistic. Also, for the small levels of damages, the previous proposed method cannot usually detect them or with different errors percentage. In the

experimental testing, the first challenge for researchers is the appropriate extraction of the modal properties of the structures due to the measurement noise in the vibration data. As well, the incomplete data of the structural model from selected measurement points because of the limited number of available sensors could give inadequate or instable modal mode and add more complication to the problem. It was observed that using few first modes of the structures are enough and effective to detect damages. To match the results between the experimental and numerical analysis, calibration process is required even with the difficulty for large and complex structure with many variable components.

2.5. Proposed damage detection procedure for structural health monitoring (SHM) based on changes of dynamic characteristics of the structure using Simulated Annealing (SA) optimization Method

In this thesis, a procedure to detect damage based on heuristic optimization method, Simulated Annealing (SA), using ambient vibration measurements, is proposed. The proposed procedure for damage detection is used as structural health monitoring (SHM) technique for structures under operational conditions. The name of the proposed procedure is shortened to call "**SHMUSA**" propsed **S**tractural **H**ealth **M**onitoring procedure **U**sing **S**imulated **A**nnealing optimization method.

The proposed procedure is verified on all four adopted steel structural models, one is a simple beam and three are complex models such as grid bridge, vierendeel bridge and 10-storey building. To prove the reliability and robustness of the method, the verification of the proposed procedure is implemented using numerical and experimental testing for all four structural models with different damage scenarios. To create the damage experimentally, in the different damage scenarios, cutter machine are used to carry out the scenarios by cutting small part of the selected damaged elements. While, numerically the damage is simulated by reducing the flexural stiffness of selected damaged element through apply reduction factor to the depth of that damaged element. The experimental modal analysis is implemented using ambient vibration measurements by simulated excitation using shaker device. The proposed method of damage detection tests the change in modal

properties, natural frequency and mode shape, under ambient vibration measurements due to the presence of damage in the structures to detect damage characteristics in the all four structural models. Those damage characteristics represent three levels of damage identification which are:

1- The first level is defined by the presence of damage in the structural models,

2- The second level is the detection the location of damage in the structural model,

3- The third level quantifies the severity of that damage.

4- The remaining time of the structure during service life.

Herein, the forth level of the damage identification which is the evaluation of the remaining healthy state of the structure after presence of damage is excluded. In addition, the effect of environment conditions influence on modal properties of the structures is not investigated.

In presented study, the adopted damage detection procedure based on the changes in the dynamic characteristics of the structure, in the process of Structural Health Monitoring (SHM) using ambient vibration measurements, includes multiple phases to be carried out before, during and after the observation of structures that are subject to structural monitoring. The proposed procedure is improved from the procedure are included in the published paper deals with the methods of damage detection of structures based on change of dynamic characteristics [76]. The flow chart of the proposed SHMUSA procedure is shown in *Figure 2.3*., and could be summarized in the following steps:

1- Modeling by FE model and application of modal analysis of the structure without damage (the initial reference state), as shown in *Figure 2.3* (a).

2- Experimental extraction of modal characteristics of the structure without damage (the reference state) measuring ambient vibrations to identify the modal characteristics from the measurement data, as shown in *Figure 2.3* (a).

3- Calibation process of the initial FE model based on the model modal characteristics extracted experimentally of the structures in the reference state in order to achieve adequate consistency of modal properties, natural frequencies and mode shapes, as shown in *Figure 2.3* (a).

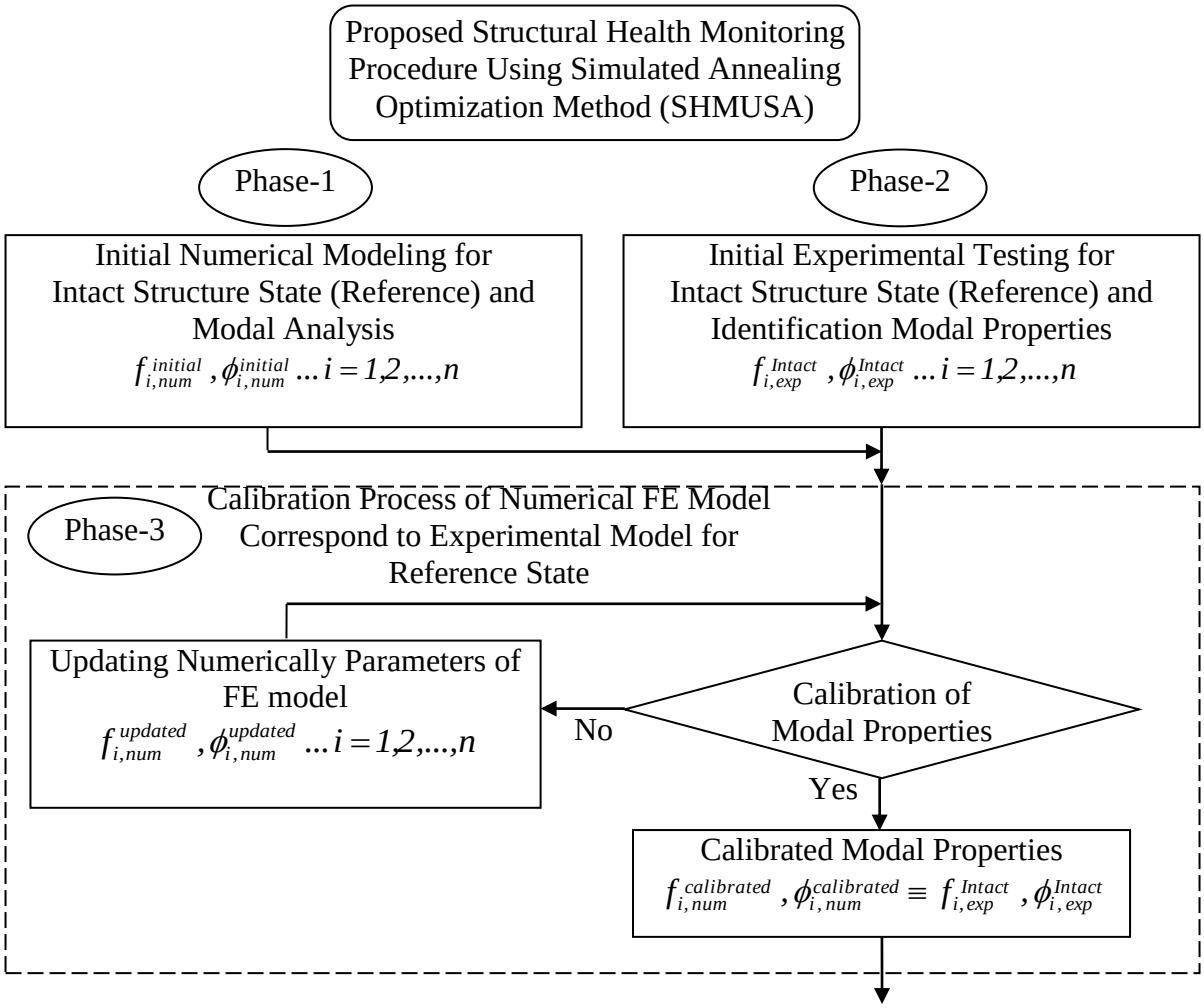

Figure 2.3 (a): Flow chart of the the initial stage of proposed SHM damage detection procedure (SHMUSA) based on vibration during structural health monitoring

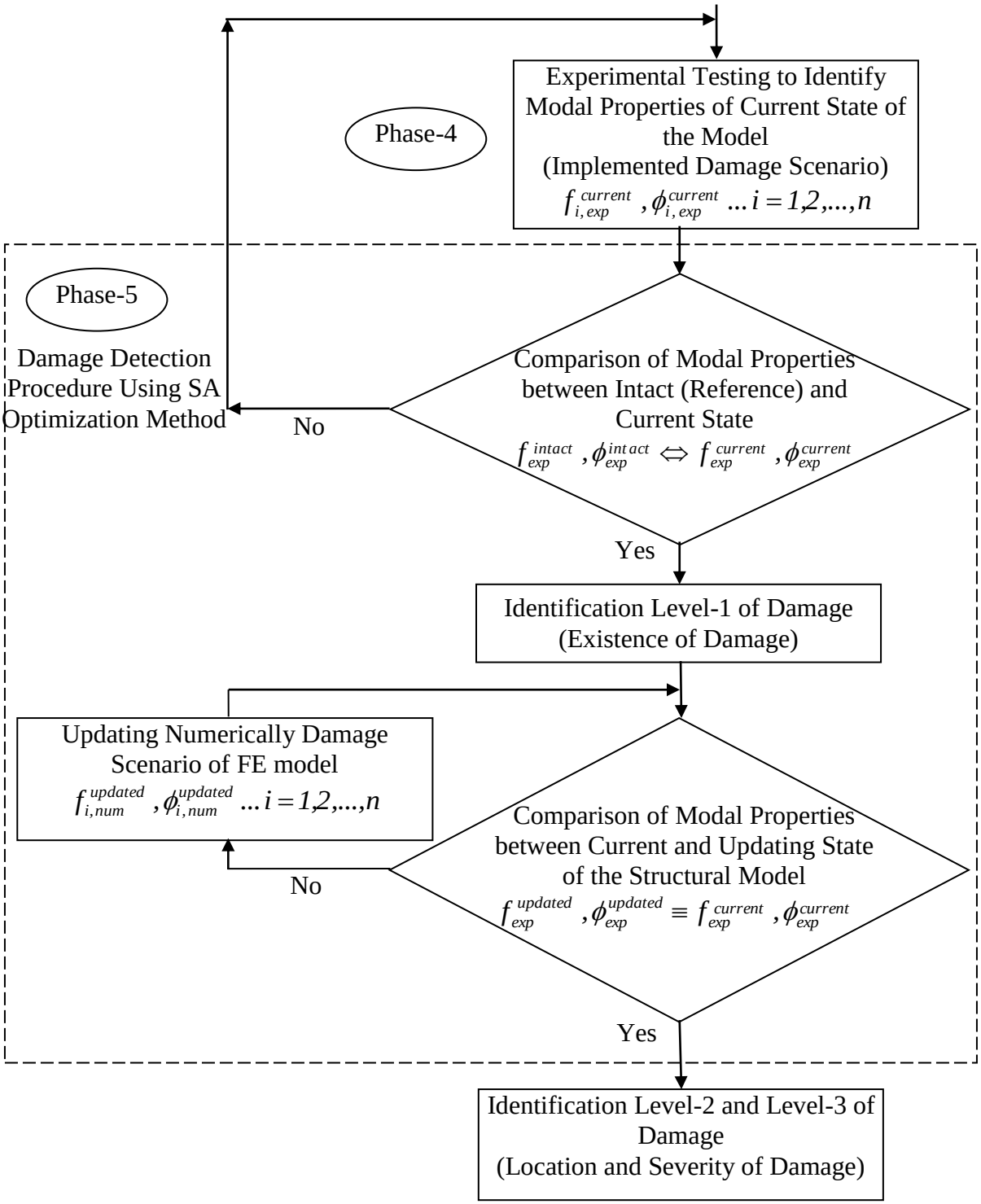

Figure 2.3 (b): Flow chart of the final stage of proposed SHM damage detection procedure (SHMUSA) based on vibration during structural health monitoring

4- Experimental testing on the potentially damaged structures (the current state) by measuring ambient vibrations to identify the modal characteristics of implemented damage scenario from measurement data, as shown in *Figure 2.3* (b).

5- Application of proposed optimization method in order to detect damage characteristics, location and severity for that actual damage scenario which is created in the structural model, as shown in *Figure 2.3* (b).

The first three phases can be defined as the initial stage, because they match the state of the structure without damaging it (the reference). The third and fourth stages are the final phase to be executed during the service life of potentially damaged during structural health monitoring, as shown in *Figure 2.3* (a) and (b).

2.5.1. Initially numerical modelling and estimation of modal properties of structures

Numerical modeling of structures using of the ANSYS package software for structural analysis based on FEM, Phase-1, it is necessary in order to create a numerical model of the structure without damaging it, and to determine the modal characteristics of the structure intact, so-called. reference structure. This model structure represents the initial step in the formation of an adequate numerical model of the structure for further analysis in the detection and localization of structural damage. This modal characteristics of the model, higher or lower extent, deviate from the real characteristics of the reasons the impossibility of adequate modeling of mass and stiffness, as well as due to the presence of suitable non-structural elements (the presence of fences on bridges, walls in buildings facilities, ... etc.), Which is usually not modeled in the numerical model.

2.5.2. Experimental implementation of ambient vibration measurements and extraction of real modal properties of structure

In order to create a numerical model of the structure corresponding to the real geometrical parameters in the reference undamaged or current condition, it is necessary to implement the phase-2, in order to identify the real structural modal parameters, natural

frequencies and mode shapes of the first few own the most relevant stable modes. Using developed measuring equipments, primarily highly sensitive accelerometers, enabled the implementation of the so-called ambient vibration measurement of the structure. The application of high-resolution data acquisition systems, with appropriate acquisition parameters, it is possible to obtain high quality records of the acceleration in limited sets of representative points in field conditions.

After carrying out the measurements of ambient vibration in the phase-2, it is followed by the so-called identification of modal characteristics of recorded data of acceleration of the structure. For that purpose, a very reliable available identification method is needed such as Frequency Domain Decomposition (FDD) method using known software for the identification of system parameters based on measurements of ambient vibrations ARTeMIS extractor software [77].

For the implementation of the experimental analysis of measurement data, it is necessary to establish the appropriate arrangement of the sensor on the structural model and measuring points. The present phase illustrates the possibility of identification of modal characteristics of the structure which is extremely important stage in the detection of damages. The same process is carried out in the so-called the reference state (state structures without damaging) and the damaged state of the structure (current state of the structure), as well as during construction monitoring to detect possible damage as shown in Phase-4 in the *Figure 2.3*.

2.5.3. Calibration of the numerical FE model with experimental results of the structural model

In order to form an adequate numerical model for the detection of damage, it is necessary to implement numerical model calibration/correlation with the results of the experimental analysis of the structure. In this regard, it is necessary to conduct the procedure for adjusting the initial FEM model formed in phase-1 according to the experimentally extracted modal frequencies in a certain phase-2. This procedure is known as Finite Element Model Updating - FEM Updating, [78], [79], [80] and can be carried out on the basis of dynamic experimental analysis. The proposed damage detection procedure

on the basis of vibrations apply this process on the results of experimental studies of structural model response based on measurements of ambient vibrations, in phase-3, as shown in *Figure 2.3*.

Calibration process initially formed FEM model involves a change in the structure lower/higher unreliable parameters which are assumed in the numerical initial FE model. By this, it means:

- The differences in the stiffness of relevant structural elements.
- Differences in elasticity modules of materials of the structure.
- Discrepancies between actual and theoretical range of construction and structural elements.
- Differences between real and theoretical boundary conditions, and ...etc.

Calibration procedure of initial FEM model can be performed "by hand/manualy" using appropriate parametric analysis with the variation adopted relevant parameters at specific intervals, or automatically, using appropriate software packages for this purpose, such as FEMtools [79], where algorithms are implemented properly optimization, in order to find combinations with the smallest changes in the initial FEM model construction that results in the best agreement with the observed modal characteristics.

In this thesis, calibration procedure executed automatically process using optimization method, SA, is proposed and written subroutine in MATLAB package software [81]. To measure the correlated modal characteristics of the numerical model correspond to experimentally extracted modal characteristics, are adopting modal frequencies forms.

2.5.4. Damage detection procedure to detect damage characteristics, location and extent of damage scenario

During the operation of structure, in order to detect possible damage permanently or in appropriate time intervals, monitoring of modal characteristics, phase - 4 and phase - 5 monitoring of structure, as shown in *Figure 2.3*. In these stages, in addition to the experimental ambient vibration recording, the identification of the presence of possible damage with appropriate identification modal characteristics is conducted. The damage

detection procedure is carried out by comparing the modal characteristics of the current situation with the corresponding values identified in the reference condition during the phase-2. The damage detection process on the basis of implemented damage scenario as a current state compares the changes of the dynamic characteristics of the structure during updating process of damaging the FE model to detect location and extent.

The verification of the adopted proposed procedure on the different structural models and more details about all steps of the procedure will discuss in the chapter seven.

3. IDENTIFICATION METHODS BASED ON AMBIENT VIBRATION MEASUREMENTS

3.1. General

In experimental investigations, to estimate and identify dynamic characteristics of civil structures, modal analysis of structure under specified excitation is required. The excitation conditions can be classified into three types: initial excitation, known artificial excitation and unknown excitation. The first one is free vibration measurements after initial conditions are assumed on the structure [82]. The second type is defined by applying controlled external dynamic excitation on the structure using mechanical devices such as a linear or eccentric mass shaker. The last one is implementation of a broadband random vibrations produced from the natural and service live loads acting on the structure (such as traffic, pedestrians, machines, wind, etc.) [15], [83], [84], [85].

A forced vibration testing is applied to the tested structure and the record of the response is continuously monitored. This type has the advantage of being able to control the nature of the test excitation input like frequency content, intensity and sweep rate and the results are relatively more accurate and complete. However, the disadvantage of the forced excitation is more complex and costly.

For free vibration testing, response measurements are made on free decay of the test object following an initial excitation. The excitation can be produced using either initial velocity (impulsive excitation) or initial displacement and the required time of testing is small relatively in comparison to forced vibration testing. Therefore, the preliminary testing is conducted by free vibration tests before the performance of main tests.

In the third type of vibration test, random vibration produced from random natural and service live loads acting on a structure is the most practical and commonly used method for identifying the modal properties of structures [82]. In this method, the external excited forces are not measured but are supposed as broadband random, however, suitable modal identification requires that the measured dynamic response has spectral

characteristics reflect the modes properties of the structure [86], [87]. This approach of data measurements for dynamic response is defined as *Ambient Vibration Measurements* (AVM) and the test includes applying this type of excitation is called *Ambient Vibration Testing* (AVT). This field of use ambient vibration for the evaluation of structural health is important and deserves more studies [12]. In ambient vibration measurements, all parameter estimation are based on response signals therefore it is also called *Output Only Modal Analysis* and the analysis based on the operating condition of ambient vibration data recorded of the structure is also called *Operational Modal Analysis* (OMA) [83], [86], [88].

3.2. Ambient vibration measurements (AVM)

The ambient excitation is defined as the excitation experienced by a structure under its normal operating conditions [85]. The aim of ambient vibration measurements is to use dynamic behaviour of a structure for the evaluation of its capacity and condition from recording a large numbers of points [87], [89]. Particularly, for large structure is difficult and costly to apply external controlled force to provide levels of excitation for structures significantly higher than those provided by ambient vibration [87]. For large civil structure, the ambient excitation is the only practical way to excite the global dynamic response [15]. Due to significant increment of interest has been noted during the last decade for structural health monitoring, many research used ambient vibration in their studies [22], [90]-[93]. In ambient vibration measurements, a structure can be adequately excited by wind, traffic and human activities. These vibrations are hardly felt by human senses and highly sensitive instruments are required to read these measurements since its amplitudes are very small and careful data analysis also is needed.

3.2.1. Advantages of AVM

The main advantage of ambient vibration tests is implementation economy where only the output vibration of the structure is measured [86], [89], [93]. Particularly attractive for large civil structure, such as building bridge, can be expensive and difficult to carry out artificial vibration or free vibration. Identifying modal properties using ambient vibration measurements is easiness of execution. The AVM is applicable to urban environment and

provide valuable information with little data and certain number of measured points. The AVM has ability simultaneous assessment of motion in different directions and provides excitation with long duration. In bridge structure is noted there is no disturbance to traffic loads during the measurements of test and AVM supplies suitable rang of modal frequencies [83], [93].

On the other hand, the data recorded from ambient vibration test and the extracted modal properties could be used for implementing calibration with those numerical investigations. Also, the experimental results using AVM could be applied to develop and update the FE models of structures. Where, the numerical estimations provide information to experimental databases from which the new or similar structures can be improved or evaluated. The correlations of the data recorded by AVM and numerical simulation assist in the evaluation of structural integrity after the occurrence of damage. Therefore, the accurate estimation of structural modal properties can be computed to specify the level of safety and reliability and consequently, the final decision if the structural performance within expectations could be taken.

3.2.2. Limitations of AVM

There are some limitations for using ambient vibration test to extract the modal properties of structures. (1)The identification methods are more sophisticated [86]. As the loading is not measured, in the development of identification method it needs to be modeled (by some stochastic process) or its dynamic effects on the measured response have to be removed. Otherwise it is not possible to explain the characteristics in the data based solely on the modal properties. (2)Without loading information the identified modal properties can have significant identification uncertainties. In particular, the results are as good as the broadband assumption applied. (3)The identified modal properties only reflect the properties at the ambient vibration level, which is usually lower than the serviceability level or other design cases of interest. Therefore, the use of ambient vibration as excitation applying on the structure frequently limits the range of natural frequencies [94]. This is especially relevant for the damping ratio which is commonly perceived to be amplitude-dependent.

In addition, if use traffic loadings to generate ambient vibration for bridge structures, some important issues concerning this type of test are considered [95]: (1)Vehicles used as a source of vibration excitation affect the modal properties of the tested structure by their moving additional mass, (2)The moving live load acts mainly in vertical direction; in case of existence an important horizontal mode this kind of excitation can be insufficient, (3)Reasonable resolution in the frequency domain is difficult to obtain because of short time of bridge excitation. (4)Recording of long time series of data to increase resolution of the data in frequency domain can diminish the content of valuable signal in comparison with noise by low intensity of traffic, (5)Location of vehicles on the bridge is limited to the roadway and some parts of the structure cannot be excited up to appropriate level.

3.3. Ambient identification methods

The ambient vibration/operational modal methods can be generally classified into two aspect: frequency or time domain and bayesian or non-bayesian where the non-bayesian method were developed earlier than Bayesian ones [86]. Those methods implement some statistical estimation for identification such as correlation function and spectral density of measured vibration data. These methods are applied to pre-process recording data of structural dynamic response due to ambient vibration excitation, such as frequency domain decomposition (FDD)/Peak Picking Method (PPM), Stochastic Subspace Identification (SSI) and Eigen Realization Algorithm (ERA) etc. [82], [86].

3.3.1. Frequency Domain Decomposition (FDD) method

In this method, the modal properties of a structure are extracted from output response only when the structure is excited by a broad-band vibration [96]. It is developed of the classical frequency domain approach as defined Basic Frequency Domain (BFD) technique. It is classified as frequency domain and non-Bayesian type and it is based on simple signal processing using discrete Fourier transform. This method uses the power spectral density matrix at the peak to estimate modal properties directly and other implementations of the method benefits of the coherence between channels [97]. The FDD method overcomes the disadvantages of BFD method which requires well separation of the modes to give

reasonable estimation of the modal properties and the estimations become heavily biased if the close modes are detected and the frequency resolution of the spectral density estimate limits the extracted frequency [96]. The FDD has high accuracy even if the modes are close and it is not sensitive to noise and also it is called the peak picking technique [97].

3.3.2. Enhanced Frequency Domain Decomposition (EFDD) method

The EFDD technique is similar to FDD technique in theory except additional step is added to EFDD by identifying the single-Degree-of-freedom spectral Bell functions from using FDD identified mode shapes [96]. Then, all modal properties are estimated from these single degree of freedom (SDOF) Spectral Bells functions.

The FDD identified mode shape used as reference vector in a correlation analysis based on the modal assurance criterion MAC to implement the identification of the SDOF Spectral Bell. To certain frequency, it estimates the MAC vector between the reference vector and the singular vectors on both sides of the FDD picked frequency. The corresponding singular value is included in the description of the SDOF Spectral Bell if the largest MAC value of this vector is above a user-specified MAC Rejection Level. Therefore, the user could control the level of rejection of MAC to include singular value in SDOF Spectral Bell and use of initial MAC rejection level of 0.8 is recommended [97].

This EFDD method estimates is good if correlation function decays to a sufficiently small level of correlation and that needs having significant frequency resolution to be the bias of the natural frequency small [96].

3.3.3. Stochastic Subspace Identification (SSI) method

In this SSI method, the recorded time signals are required to identify modal properties under assumption of excitation using white noise [97], [98]. This method is classified as time domain and non-Bayesian type. The dynamic behavior of s structure can be described by a stochastic state space model, as:

$$x_{k+1} = A_m x_k - w_k \qquad 3.1$$

$$y_k = Cx_k - v_k \quad 3.2$$

where are:

x_k - the internal state vector,

y_k - the measurement vector,

w_k , v_k - white noise terms representing process noise and measurement noise, respectively,

A_m - the state matrix containing the dynamics of the system.

C is the output matrix.

Then, using numerical techniques such as QR-factorization, Singular Value Decomposition (SVD) and least squares on the measurements, the subspace method identifies the state space matrices. The SVD is used to reject the noise, while QR results in a significant data reduction. Consequently, identification of the modal properties (by an eignvalue decomposition), natural frequencies and damping ratios and mode shapes, depend on the mathematical description of the structure (the state space model) [97].

3.3.4. Eigen Realization Algorithm (ERA)

This method can be classified as time domain modal analysis method and can be used to identify the modal properties of a structure during realizing the state-space system which is created based on the recorded vibration measurements [99]. The state-space system represents a physical system during a set of first-order differential equations with variables consisting input (measured or assumed excitation forces) and output (recorded displacement or acceleration response) information. The modal properties (natural frequencies and mode shapes) are estimated from the realized state-space matrices using processing the equations in the time domain.

3.4. Structural health monitoring techniques using ambient vibration measurements

Ambient vibration measurements are used in damage detection methods to monitor integrity of structures under serviceability live. The advantages of this method, made

experimentally widely applying in many studies and projects of damage detection methods. However, not all methods are proper to identify modal properties using ambient vibration (e.i. from only output modal analysis) such as the method based the FRFs [62]. Several researchers used ambient vibration in their works such as, Lee et al. in 2002 presented health monitoring approach for bridge structure under ambient vibration data induced by unmeasured traffic loadings [57], [100]. The vertical accelerations of the structure are measured when vehicles are running. The modal properties were identified from the free-decay signals estimated using the random decrement method. The authors concluded that the modal properties extracted from AVM are reasonably identified. Also, it was concluded that implemented scenarios of damage were detected very successfully for different load conditions. In addition, they concluded that the accuracy of damage location is more important than damage severity in practical applications.

Andersen et al. in 1999 presented comparison of four identification methods including BFD using ambient vibration data on highway bridge structure in Swiss [97]. They concluded that all four methods have reasonable estimations of the modal properties, natural frequency and mode shape, and they have fast estimations, high accuracy and simplicity.

Ventura and Horyna in 2000 reported a series of ambient vibration tests were applied to the reinforced concrete 48-storey One Wall Centre at Vancouver in Canada [101], [102]. They used a 16-channel data acquisition system with time record for period of 12 minutes per set-up at 2000 samples per second with different set-up configurations. They applied FDD and SSI for data analysis to identify modal properties of the structure. They concluded that there are differences in the modal properties between the FE model estimation and experimental results by 15% lower, however, even with those different values the ambient vibration tests significantly identify the modal properties.

Reynolds et al. in 2003 reported a remote monitoring system using ambient vibration measurement tests on stadium structure at Bradford in UK [103]. The aim of the study is to understand the effect of a crowd on changes of modal properties of the structure compared with empty case. The analysis methods of ERA, FDD, EFDD and SSI are applied for ambient vibration to extract the modal properties of the structure. The positions of

transducers were in vertical and horizontal direction and they studied different cases of crowd. They concluded that the crowd has significant effect on the modal properties compared with empty case of the structure by decrease the natural frequencies and increase the damping ratios. Also, it was concluded that the ambient vibration measurements has reliability to identify the modal properties of the structure.

Wenzel and Furtner in 2006 presented damage detection method using ambient vibration measurements on two stay cable bridges structures [82]. Yin et al. in 2009 presented damage detection procedure using ambient vibration measurements applied on a large-scaled three dimensional electricity transmission tower [88].

Lamarche et al. in 2007 represented a comparison between ambient vibration and forced-vibration tests on a full-scale two-storey reinforced concrete building structure [104]. They used FDD technique to extract modal properties natural frequency and mode shape, of the structure from ambient vibration measurements. An eccentric-mass shaker was used to generate a sinusoidal horizontal harmonic load applied on the structure to record acceleration responses of the structure. The position of the shaker was placed to excite both flexural and torsional modes of vibration and low-frequency forced-balanced accelerometers were installed to measure vibration data of the structure at 100 Hz for 10-20 min. They concluded that the modal properties extracted by ambient vibration test using FDD technique have good agreement with those extracted by forced-vibration test. Also, it was concluded that the MAC value close to 1 which means the high level of correlation between both tested methods.

Ali et al. in 2012 presented modal identification and FE model updating of a full-scale lively staircase structure using ambient vibration testing [95]. They measured only the vertical response of empty case of the structure due to ambient vibration with 4 accelerometers and 4-channel data acquisition. They applied FDD method to extract modal properties, natural frequency and mode shape, of the structure.

Su et al. in 2012 reported approach to detect damage in a 6-storey shear building structural model under excitation of simulated ambient vibration based on its sub-structural natural frequencies [105]. They used wavelet transform to evaluate the modal properties of the structure with different level of noise for period of ambient vibration measurements is

five minutes and sampled at 200Hz. They extracted the modal properties of structural model with excellent agreement and it was concluded that with ambient vibration response, the damage cases easily and accurately could be identified.

Finally, the ambient vibration excitation is simple and cheaper way to identify modal properties with acceptable representation of modal properties of the structure.

3.5. Adopted Ambient Identification method for SHM

In this study, the Frequency Domain Decomposition (FDD) technique is adopted to extract experimentally the modal properties natural frequency and mode shape, of the structural models from ambient vibration measurements. The FDD method is applied on the ambient vibration data using ARTeMIS extractor software [77] which is provided at Faculty of Civil Engineering.

In addition, the simulated of ambient vibration excitation is implemented using shaker device and by generating random signal. The detail of experimental tests will discuss in the chapter five.

3.5.1. Theoretical background of FDD method

The FDD performs an approximate decomposition of the system response into a set of independent single degree of freedom (SDOF) systems, one for each [96]. The decomposition is performed simply by decomposing each of the estimated power spectral density (PSD) matrices. In this method, the singular values are estimates of the auto spectral density of the SDOF systems, and the singular vectors are estimates of the mode shape. The excitation is assumed as pure Gaussian white noise and all natural modes are lightly damped.

The relationship between the unknown input $x(t)$ and the measured response $y(t)$ can be expressed as [89]:

$$G_{yy}(\mathrm{j}\omega) = \overline{H}(\mathrm{j}\omega) G_{xx}(\mathrm{j}\omega) H(\mathrm{j}\omega)^T \qquad 3.3$$

where are:

$G_{xx}(\mathrm{j}\omega)$ - the $r \times r$ Power Spectral Density (PSD) matrix of the input,

r - the number of inputs,

$G_{yy}(\mathrm{j}\omega)$ - the $m \times m$ PSD matrix of the responses,

m - the number of responses,

$H(\mathrm{j}\omega)$ - the $m \times r$ Frequency Response Function (FRF) matrix,

"—" and superscript T - denote complex conjugate and transpose, respectively.

The FRF can be written in partial fraction, i.e. pole/residue form:

$$H(\mathrm{j}\omega) = \sum_{k=1}^{n} \frac{R_k}{j\omega - \lambda_k} + \frac{\overline{R}_k}{j\omega - \overline{\lambda}_k} \tag{3.4}$$

where are:

n - the number of modes,

λ_k - the pole,

R_k - the residue,

it is given as:

$$R_k = \phi_k \lambda_k^T \tag{3.5}$$

where are:

ϕ_k, λ_k - the mode shape vector and modal participation vector, respectively.

In this method, suppose the input is white noise, i.e. its PSD is a constant matrix, i.e. $G_{xx}(\mathrm{j}\omega) = C$, then Eq. (3-3) becomes:

$$G_{yy}(\mathrm{j}\omega) = \sum_{k=1}^{n} \sum_{s=1}^{n} \left[\frac{R_k}{j\omega - \lambda_k} + \frac{\overline{R}_k}{j\omega - \overline{\lambda}_k} \right] C \left[\frac{R_s}{j\omega - \lambda_s} + \frac{\overline{R}_s}{j\omega - \overline{\lambda}_s} \right]^H \tag{3.6}$$

where are:

superscript H - denotes complex conjugate and transpose.

Multiplying the two partial fraction factors and making use of the Heaviside partial fraction theorem, after some mathematical manipulations, the output PSD can be reduced to a pole/residue form as follows:

$$G_{yy}(\mathrm{j}\omega) = \sum_{k=1}^{n} \frac{A_k}{j\omega - \lambda_k} + \frac{\overline{A}_k}{j\omega - \overline{\lambda}_k} + \frac{B_k}{-j\omega - \lambda_k} + \frac{\overline{B}_k}{-j\omega - \overline{\lambda}_k} \quad 3.7$$

where are:

A_k - the k^{th} residue matrix of the output PSD.

As the output PSD itself the residue matrix is an $m \times m$ hermitian matrix and is given by:

$$A_k = R_k C \left(\sum_{s=1}^{n} \frac{\overline{R}_s^T}{-\lambda_k - \overline{\lambda}_s} + \frac{R_s^T}{-\lambda_k - \lambda_s} \right) \quad 3.8$$

The contribution to the residue from the k^{th} mode is given by:

$$A_k = \frac{R_k C \overline{R}_k^T}{2\alpha_k} \quad 3.9$$

where are:

α_k - minus the real part of the pole $\lambda_k = -\alpha_k + \mathrm{j}\omega_k$.

As it appears, this term becomes dominating when the damping is light, and thus, is case of light damping, the residue becomes proportional to the mode shape vector:

$$A_k \propto R_k C \overline{R}_k = \phi_k \gamma_k^T C \gamma_k \phi_k^T = d_k \phi_k \phi_k^T \quad 3.10$$

where d_k is a scalar constant. At a certain frequency ω only a limited number of modes will contribute significantly, typically one or two modes. Let this set of modes be denoted by $Sub(\omega)$. Thus, in the case of a lightly damped structure, the response spectral density can always be written:

$$G_{yy}(\mathrm{j}\omega) = \sum_{k \in Sub(\omega)} \frac{d_k \phi_k \phi_k^T}{j\omega - \lambda_k} + \frac{\overline{d}_k \overline{\phi}_k \overline{\phi}_k^T}{j\omega - \overline{\lambda}_k} \quad 3.11$$

3.5.2. Identification FDD technique

In the FDD method there are some steps to perform the modal analysis for any structural system using ARTeMIS extractor software [96]:

1- Estimate power spectral density matrix from the raw time series data. The estimate of the output $\hat{G}_{yy}(j\omega)$ known at discrete frequencies $\omega = \omega_i$ is then decomposed.

2- Perform singular value decomposition (SVD) of the spectral density matrices:

$$\hat{G}_{yy}(j\omega_i) = U_i S_i U_i^H \quad 3.12$$

where are:

$U_i = [u_{i1}, u_{i2}, ..., u_{im}]$ - a unitary matrix holding the singular vectors u_{ij},

S_i - a diagonal matrix holding the scalar singular values s_{ij}.

Near a peak corresponding to the k^{th} mode in the spectrum this mode or may be a possible close mode will be dominating. If only k^{th} mode is dominating there will only be one term in Eq. (3.11). Thus, in the case that the first singular vector u_{ij} is an estimate of the mode shape:

$$\hat{\phi} = u_{i1} \quad 3.13$$

and the corresponding singular value is the auto power spectral density function of the corresponding single degree of freedom system, Eq. (3.11). This power spectral density function is identified around the peak by comparing the mode shape estimate $\hat{\phi}$ with the singular vectors for the frequency lines around the peak. As long as a singular vector is found that has high MAC value with $\hat{\phi}$ the corresponding singular value belongs to the SDOF density function.

3- If multiple data sets are available, then average the first singular value of all data sets and average the second etc.

4- Peak picking on the average singular values. For well-separated modes always pick on the first singular value. In case of close or repeated modes, pick on the second singular value, the third singular value etc. as well.

5- Optionally, If multiple data sets are available, inspect the singular values of each data set and edit the peak picking position if necessary.

The first three steps are performed automatically during data processing and the others require the user is doing them using the editor. The technique is completely non-parametric technique where the modes are estimated purely by signal processing and the detail of the applications on the structural models will discuss in chapter five.

3.5.3. Data measuring devices in structural health monitoring (SHM)

In the field of SHM, the sensing and data acquisition technology is developing during years and the specialist engineers should search always to new technology which is applicable to the SHM to obtain the structural dynamic response on widely varying length and time scale [15]. Therefore, the gain of accurate measurements of dynamic response of a structural system is very important and depends on the used data recording system technology.

There are several different sensor systems applied on the SHM field which are employed for one of the following [15]:

1- Identification and tracking problem in the structural problem.

2- Improvement and validation and uncertainty quantification of the structural model.

3- Monitoring of structural systems.

So, the main objective of sensors system device used in the SHM system is to precisely detect the problem by having high sensitivity for any damage in the structural system.

The data acquisition is the portion of SHM deals with data collecting process and related with the sensors system. The economic aspect plays the main base in making decisions regarding the data acquisition device to be used in the SHM system. The data acquisition process includes the following stages [15]:

1- The selecting of excitation device to gain the real structural response.

2- The adopted sensors types which have efficiency to sense any change due to damages.

3- The numbers of the sensors that being enough to capture the structural dynamic response.

4- The locations of the sensors to extract the real structural modal properties.

5- The data storage hardware which is able to process recording data.

In addition, the duration or interval of data recording at which the data is collected, should be considered in this portion and has significant effect on the operational evaluation of the system.

In this study, the use of the high quality data measuring devices are used which are available in the laboratory of the Faculty of Civil Engineering at University of Belgrade, as

will discussed in the next subsections. In addition, all structural models testing to obtain the dynamic response using the SHM system is carried out by the author and staff of the laboratory for structures of Faculty of Civil Engineering at the University of Belgrade. The testing process include the following devices, shaker, data acquisition, accelerometers, voltage regulator and PC computer.

3.5.3.1. Shaker device used in excitation method

In present study, the shaker device is used to simulate the ambient vibration excitation for the adopted structural models. The device is supplied to conduct the experimental test and obtain the real dynamic response of the models. The shaker is type of a music device, bass shaker, which produce low vibrations in the range from 5 Hz to 200 Hz, as shown in *Figure 3.1*. The device is installed in the suitable positions close to the structural models during the testing to obtain the better representation of the dynamic response. The device produced from ButtKicker LFE Kit company includes the BKA1000-N power amplifier, ButtKicker LFE transducer, and all the cables needed for fast and easy setup.

Figure 3.1: Shaker device used in the simulation of ambient vibration testing

3.5.3.2. Accelerometers

A set of eight Silicon Design Model-2400 accelerometers with the range of DC-600 Hz are used which are produced from Silicon Designs (SDI), Inc, company. In addition, the high quality cables or a transmission system are used, as shown in *Figure 3.2* . All 8-accelerometers (transducers) are connected up to a high quality data acquisition system. The accelerometers record the acceleration of the measurement points.

Figure 3.2: Accelerometers used in the ambient vibration testing

3.5.3.3. Data acquisition device

The data acquisition device type is a Hottinger Baldwin Messtechnik - QuantumX HBM data acquisition device. The device has 8 channels, battery powered, connected with storage PC device by high quality cables, as shown in *Figure 3.3*. The device is used for recording the measurements of acceleration of the selected points on the structural models. It has the unique capability to acquire signals from any analog sensor.

Figure 3.3: Data acquisition device used in the ambient vibration testing

3.5.3.4. Distribution of accelerometers positions on the structural models

The position of accelerometers on the structural model is one of the important aspects in designing an appropriate sensors system during SHM procedure to measure the dynamic

response of the structure. Also, due to the economic limitations, it is usually used limited number of sensors in the experimental testing depend on the availability of sensors in the Laboratory. In the same time, it is not desirable to lose information about the response of the structural model due to using a limited number of sensors. In the case of small structural models, just up to 10 points are sufficient, while in the case of large structures up to 60, or more, test points is required for representation relevant mode shapes [77]. However, there are no clear guidelines of number of measurement points, and it depends on structural model type, design, and other factors [77]. Therefore, the structural models are prepared to distribute the points of measurements in suitable positions to reflect the actual behavior through real mode shapes of the model under vibration and the available number of accelerometers. The measurements points are divided to either individual transducer for simple model or as a set of transducers for complex models.

Also, it should mentioned that the main objective of this study is to identify the damage location and severity in the adopted structural models and the validating of distribution of the accelerometer positions is out of scope of this study.

3.5.3.5. Data storage system PC

The data storage system used is Dell laptop with installed software for data recording CAT-MAN software which supplied with the data acquisition device, as shown in *Figure 3.4*. Each measurement requires 20 minutes for completing recording, which produce a data file contains rows and 8 columns of acceleration values which represents acceleration time history. The measure parameters which are used in the test, sampling frequency, cut-off frequency and intensity level were 600 Hz, 200 Hz and 7, respectively.

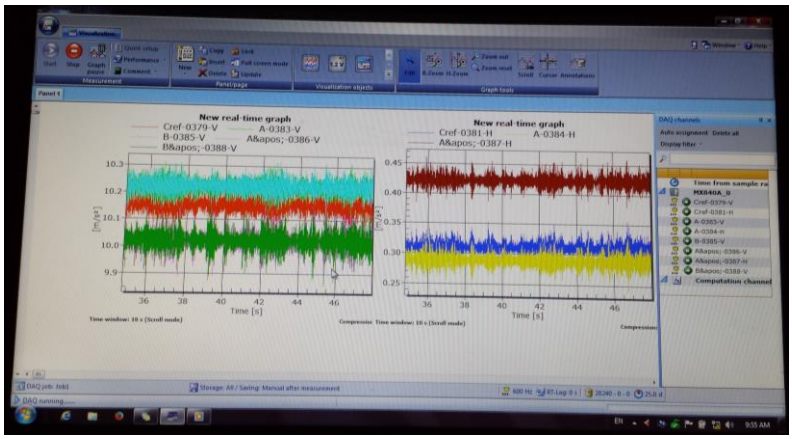

Figure 3.4: PC storage system used in the ambient vibration testing

3.5.3.6. Complementary equipments

In addition to the previous mentioned devices above, there are additional equipments such as: cables, voltage stabilizer, connectors and Battery 12 V for acquisition device, as shown in *Figure 3.5*.

*Figure 3.5: Additional e*quipments *used in the system of structural health monitoring (SHM)*

3.5.4. Verification of ARTeMIS extractor software on the civil structures

There are several extractor software are used in the field of SHM, in this study, the ARTeMIS extractor software is adopted to extract the modal properties of structural models because it is available at Faculty [77]. ARTeMIS means Ambient Response Analysis and Modal Identification Software with small change to be like name of a one of the Greek deities "Artemis". The ARTeMIS is a tool to identify the modal properties of structures in the cases of the only response is known. The features of the ARTeMIS extractor are [106]:

1- The extractor software can conduct modal analysis accurately under operational conditions or ambient vibration without need to excite the structure by external force.

2- The modal identification depends only on the output only.

3- Multiple data sets could handle with multiple reference points and processed number of channels and there is no limitation for used file data.

4- The extractor has two frequency domain and one time domain identification techniques to extract modal properties.

5- The animation and comparison of different mode shape estimates from different project can perform in the software by computing MAC matrix.

6- The software run under Window system and easily use with other software such as MATLAB or excel to call them from his own application.

All these features with its graphical user interface make the ARTeMIS extractor very user-friendly software, accurate and understandable.

For the purposes of verification of the author's experience in the performance of the ARTeMIS extractor software on the application of civil structures, two paper were published in the fifth international conference (GNP) in Montenegro. The first one presented the application of the ARTeMIS extractor software to extract the modal properties of the one approach of Gazela Bridge structure in Belgrade [107]. While, the second studied the comparison between frequency (FDD) and time (SSI) domain technique which are included in the ARTeMIS extractor software for the same part of the bridge structure [108].

3.5.4.1. Extraction of modal properties of Gazela bridge structure using ARTeMIS extractor software

In this study, the verification of the ARTeMIS extractor software was conducted by testing and analyzing of the experimental recorded response from ambient vibration measurements of one approach of Gazela bridge structure, as shown in *Figure 3.6* [107]. The modal properties, natural frequency and mode shape, of the structure were extracted under operational excitation using FDD technique.

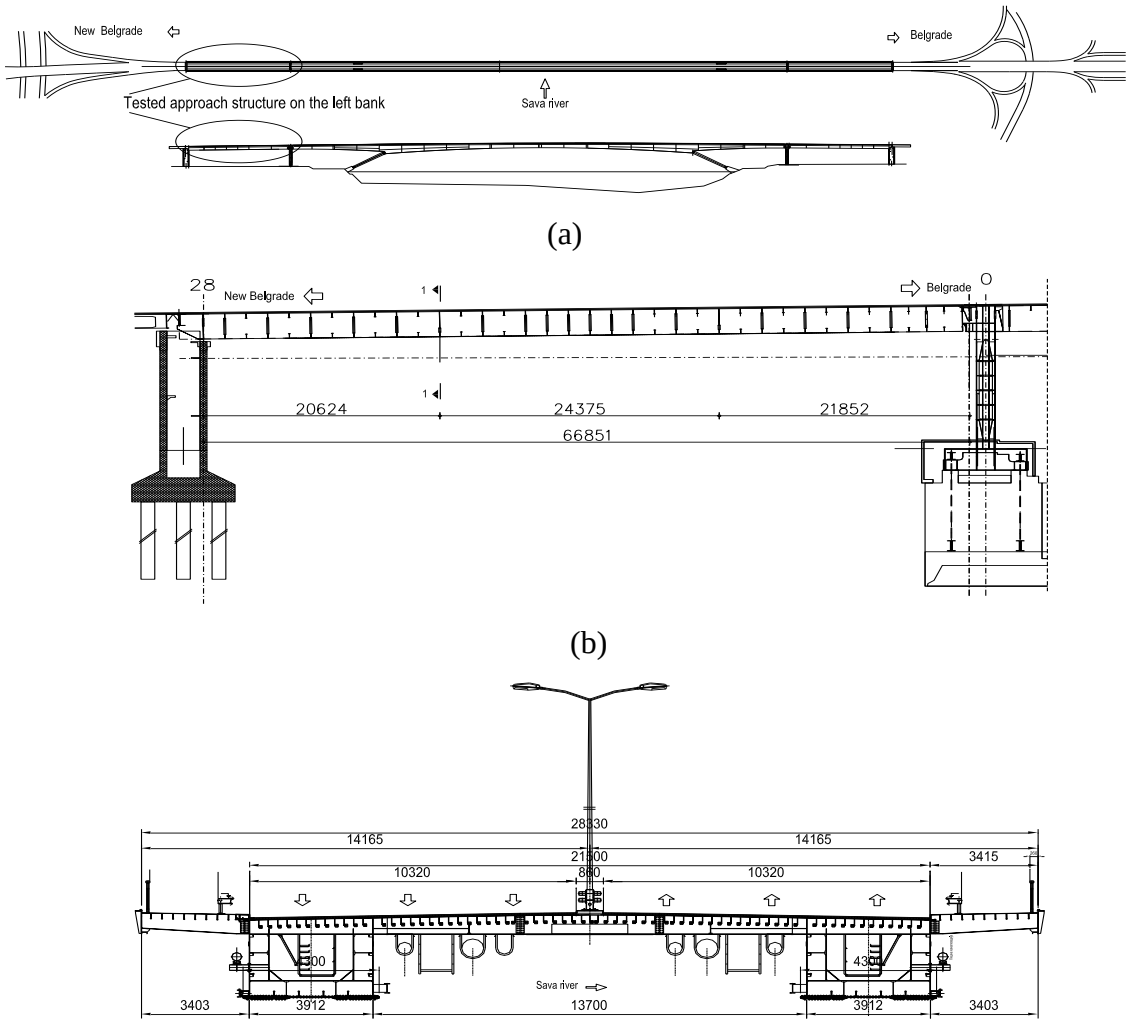

Figure 3.6: Layout of GAZELA bridge structure: (a) position of tested part (b) Longitudinal section (side view) and (c) cross section (front view) [107]

Gazela bridge is important bridge in Belgrade across the Sava river and it is a part of the expressway European route E75 connecting north with south by Novi Sad - Belgrade - Niš cities. The total length of the bridge structure, *Figure 3.6*, composed of three structures of total length of L = 66.85 + 332.0 + 66.85 = 465.7 m. The main span of the bridge is length of 332 m, while the approach structures are length of 66.85 m. All structures are 28.3 m wide, with three traffic lanes in each direction. Main and approach structures are composed of two main steel beam girders connected with cross beams incorporated into the orthotropic slab, as shown in *Figure 3.7*. Main longitudinal beams of approach structures on left and right bank of the Sava river, in thirds of the span are connected with strong beams. Total height of cross section of approach structures beams is H=2.99 m.

Figure 3.7: Tested GAZELA bridge approach structure on the left bank of Sava river [107]

Ambient vibration measurements of left bank approach structure of Gazela bridge carried out by a staff of the Laboratory for structures of the University of Belgrade on 9 July, 2013. The 8-channel, battery powered, Hottinger Baldwin Messtechnik - HBM data acquisition system was used for recording response of SiliconDesign Model-2240 accelerometers during the measurement, as shown in gure 4. The limited number of accelerometers only eight was used with appropriate reference points. Total test consists of 6 independent measuring swaps, with duration of 45 minutes of recording time each.

Figure 3.8: Accelerometers inside of left bank approach structure of GAZELA bridge [107]

Adequate test plan required choice of limited number and position of test points for sufficient representation of the most significant structural mode shapes, in order to complete the test during limited time of one day. For the presented study is estimated that 29 test points will be sufficient for representation the most significant mode shapes with the lowest frequencies, as shown in *Figure 3.9.* Test points longitudinally were positioned at the position of main cross-beam of the structure at thirds of the span and at mid-points of the span between main cross beams. In longitudinal direction were 7 points in the row. Along the cross direction, test points were located close to up-stream and down-stream cross section web of up-stream and down-stream box girder of the structure, in total four points in the column. Additional point No.-155, close to the test point No.-15, introduced because of size consistency of all measurement data sets.

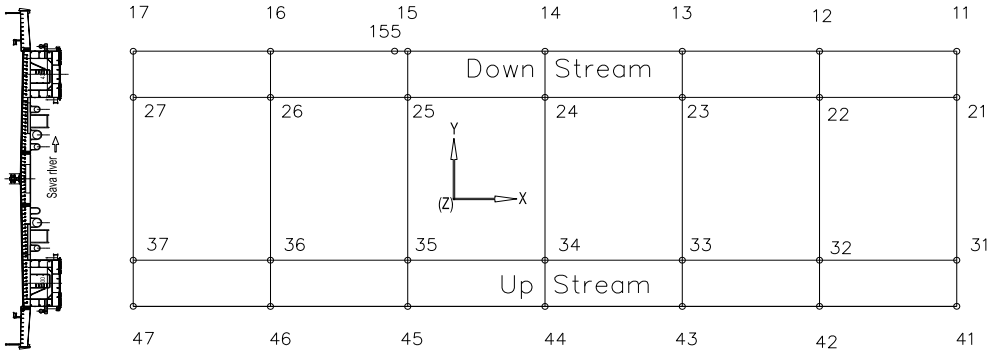

Figure 3.9: Layout of measurement points during ambient vibration test of the approach structure of GAZELA bridge [107]

Tested data that extracted from the site were recorded according to the locations and directions taking into account the upstream and downstream way of the Sava River, also, the method of testing which was started and finished toward directions of Centre of city and New Belgrade, as listed in the Table 3.1.

Table 3.1: Locations of accelerometers and directions of measurement during site test [107]

Down - Stream	D1	11 Z	11 Y	21 Z	15 Z*	15 Y*	16 Z	16 Y	26 Z
	D2	12 Z	12 Y	22 Y	15 Z*	15 Y*	155 Z	155 Y	25 Z
	D3	13 Z	13 Y	23 Z	15 Z*	15 Y*	14 Z	14 Y	24 Z
Up - Stream	U1	31 Z	31 Y	41 Z	15 Z*	15 Y*	36 Z	36 Y	46 Z
	U2	32 Z	32 Y	42 Z	15 Z*	15 Y*	35 Z	35 Y	45 Z
	U3	33 Z	33 Y	43 Z	15 Z*	15 Y*	34 Z	34 Y	44 Z
* Reference points, Y-lateral, Z-vertical direction of acceleration measurement									

Typically, a small set of accelerometers and recording channels is available, as it is in this study used just eight sensors. Positions of sensors during one set of measurement, in ARTeMIS software structural measurement model is shown in *Figure 3.10*. Two reference accelerometers, one in vertical and one in horizontal direction kept at the same location during all sets of measurement, 15Z and 15Y respectively. The rest of six sensors were placed on different locations during each measurement on up-stream (U1, U2 and U3 measuring set) and down-stream (D1, D2 and D3 measuring set) box girder of the structure. It has been recorded six data sets during the ambient vibration test of the structure. Using reference points accelerometers vibration responses recorded during all measurement sets are related and comprehensive global structural response could be extract through analyzes of measuring sets together. The main rule is that reference points/accelerometers were placed in such a way, that all modes contribute well to the response signal at the reference points. If close modes are expected, we paid some extra attention to these modes having them well represented in the reference signals. The accelerometer positions during each measuring set is listed in Table 3.1.

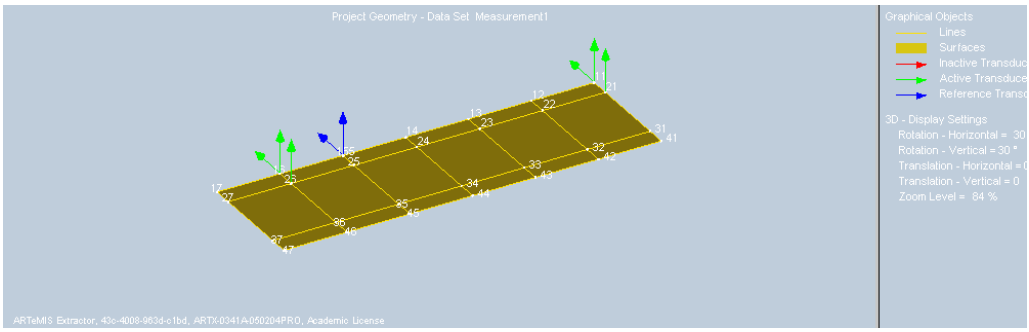

Figure 3.10: Locations and directions of accelerometers during one of measurement presented in ARTeMIS extractor software [107]

During data acquisition, accelerometer signals were filtered with cut-off frequency of 40 Hz, while the sampling frequency was assumed of 600 Hz. Theoretically, assumed sampling and cut-off frequencies were sufficient to record responses up to 40 Hz. The good rule is to sample a little higher than it is really necessary and then decimate the signal afterwards. However, a good rule of thumb is to say, that we need at least points corresponding to 500 cycles of the lowest natural frequency that it is expected. This is estimation for the case when data are totally noise-free and without close modes. In most cases it is necessary to take records of time series corresponding about 1000 cycles of the lowest natural period which could be expected, or more. Initially, for estimated the lowest frequency of without previous computation, and has been assumed duration of each record of 45 minutes.

Then, the experimental modal analysis was conducted using ARTeMIS extractor by FDD technique and the singular values are estimates of the auto spectral density of the SDOF systems. In the case of GAZELA approaching bridge structure, the FDD estimation procedure computed singular values of the spectral density matrices just after the signal processing of data is completed, as shown in *Figure 3.11*.

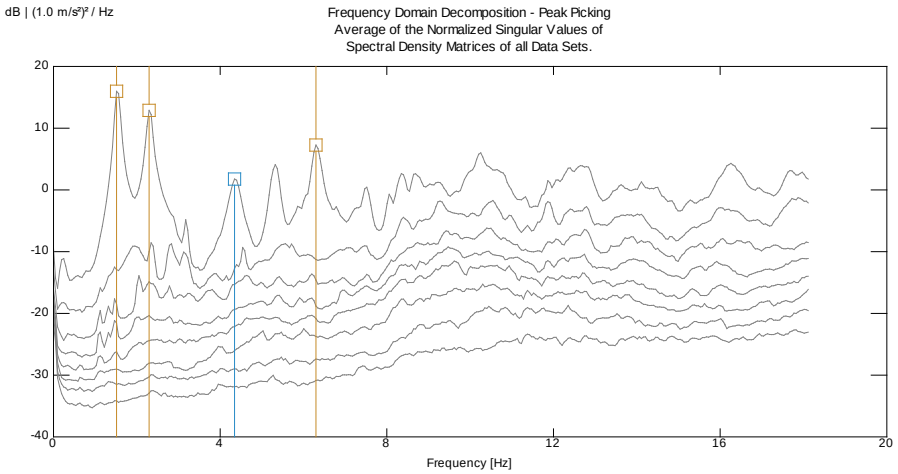

Figure 3.11: Spectral Density Matrices of all data sets using ARTeMIS software [107]

For well-separated modes always exists pick on the first singular value. In the case of close or repeated modes, pick on the second singular value, the third singular value etc. If multiple data sets are available, inspection of the singular values of each data set and edit the peak picking position is necessary [77], [109]. These singular values have been normalized with respect to the area under the first singular value curve. The six data sets present normalized singular values computed for each data set have been averaged to obtain the displayed curves, each set with two accelerometers, in order to obtain the presented six curves the following operations have been performed: 6x6 dimensional spectral density matrices of data sets 1 up to 6 have been estimated. Hence, to estimate the new well-separated mode that lying at the peak corresponds to any mode in the spectral density matrix, may be a possible structural mode and could be dominating. In the case that two modes are dominating, the first singular vector is always being a good estimate of the mode shape of the strongest mode [96] as shown in *Figure 3.11*. Vertical lines indicate that singular value of the modes have been picked on. In this case, it was still possible to pick the modes on the first singular values. Therefore, by this control computation, cross-validation of the results and thereby make a quality control of the modal results.

After applying FDD technique, the results of the extracted modal properties, natural frequencies and mode shapes, of the Gazela bridge structure is shown in the *Figure 3.12*. All estimated frequencies were in the range of (1.514 - 6.299) Hz, which seems to be

logical results and expected real structural behavior, according to previous design computation. First four modes have been identified by the applied method and their character of the bending modes; they correspond to first and second bending modes of simply supported structure. Also, two composed torsion-bending modes which correspond to clear-bending modes, are estimated, and they have been expected as well because composition of bridge structural system.

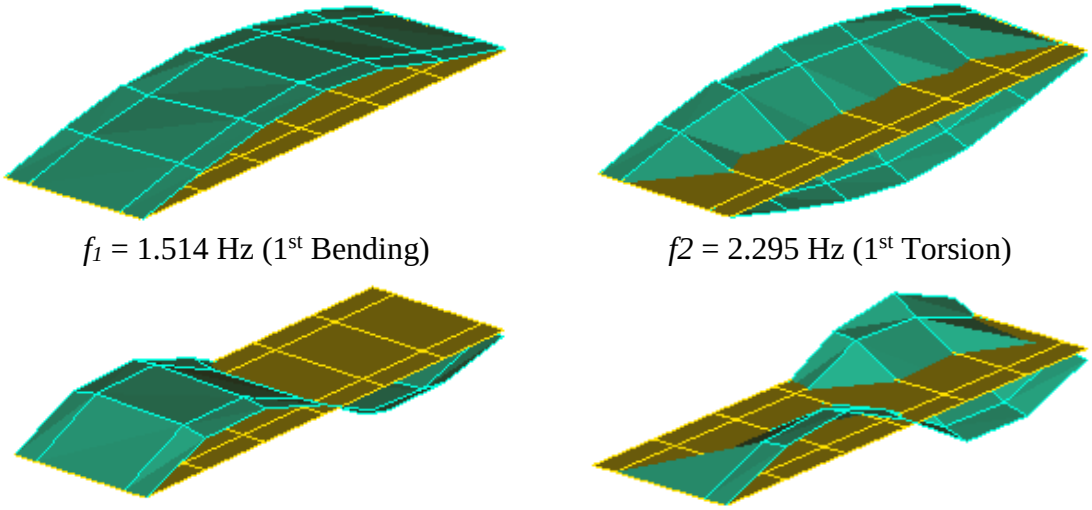

f_1 = 1.514 Hz (1st Bending) $f2$ = 2.295 Hz (1st Torsion)

$f3$ = 4.346 Hz (2nd Bending) $f4$ = 6.299 Hz (Bend+Tors)

Figure 3.12: Extracted Modal properties using FDD technique byARTeMIS extractor software [107]

Consequently, the performance of Peak-Picking identification method (FDD technique) has been successfully and quickly extracting the vibration properties and it seems to agree very well on the natural frequency estimates of the first four modes. The results exhibit good representations of the FDD estimation and the features of the ARTeMIS extractor software allow obtaining and displaying these results easily and accurately. Also, ambient vibration test, as quick and economical test, could be very useful excitation method to extract the modal properties of the civil structure as SHM technique by periodical checking of structural behavior in the sense of possible damages of important infrastructural structures under operational condition such as high intensity of traffic.

3.5.4.2. Comparison of FDD and SSI modal identification technique of Gazela bridge structure using ARTeMIS extractor software

In this study, the verification of the FDD technique including in ARTeMIS extractor software was conducted by comparing with SSI technique of the experimental extracted modal properties from ambient vibration measurements of the same one approach of Gazela bridge structure [108]. The modal properties, natural frequency and mode shape, of the structure were extracted under operational excitation using FDD technique.

As mentioned previously, the frequency domain decomposition (FDD) technique estimate the power spectral density matrix of the structural system, *Figure 3.11*, while time domain stochastic subspace identification (SSI) directly processes the recorded time signals data and estimates the stabilization diagram. In this study and for Gazele bridge structure, the power spectral matrices and the stabilization diagram of the response only were conducted, as shown in *Figure 3.13*. The results of the FDD technique are the same of the previous study, [107], however, the SSI results were conducted for the same recorded data of the bridge structure [108].

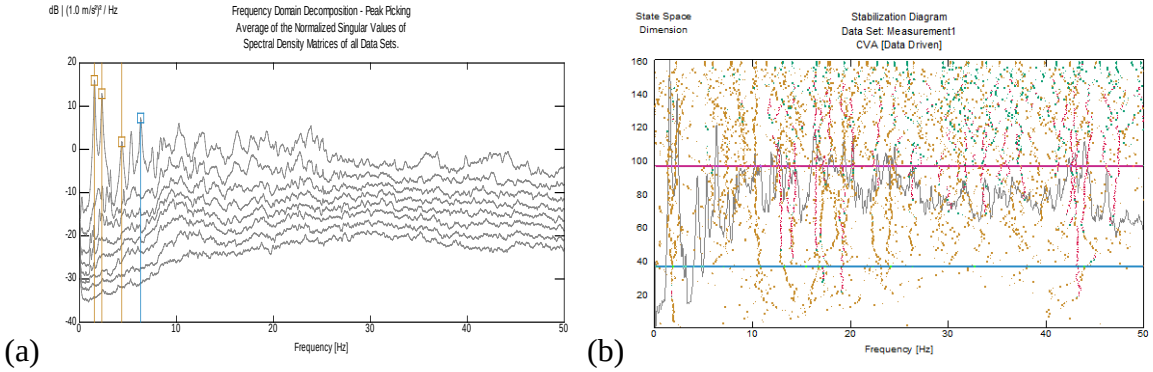

(a) (b)

Figure 3.13: Experimental analysis using ARTeMIS extractor (a) spectral density matrices of all data sets (b) stabilization diagram of measured data set [108]

The figures are drawn between the frequency (horizontal axis in the range between zero and Nyquist frequency) and vertical axis which is the amplitude in FDD technique

with range upper and lower than zero state and the state space dimension (model order) in SSI technique with range between one to the maximum state space dimension specified earlier. Also, the figures present the natural frequencies of all the estimated eigenvalues.

The comparison of modal properties results, frequencies and mode shapes, between the two applied FDD and SSI techniques of the Gazela bridge structure are listed in the Table 3.2. In this way, the results are cross-validation and thereby make a quality control of the modal results. The characters of extracted mode shapes of the structure using SSI technique were the same extracted by FDD technique, as shown in *Figure 3.12*.

Table 3.2: Extracted modal frequencies using ARTeMIS extractor by FDD and SSI technique [108]

Mode Shape No.	Frequency (Hz)		Differences (Hz)	Mode Shape Character
	By FDD method	By SSI method		
1	1.514	1.652	-0.138	1st Bending
2	2.295	2.330	-0.035	1stTorsion
3	4.346	4.875	-0.529	2nd Bending
4	6.299	6.400	-0.101	Bend. and Tors.

Also, the comparison among the modes was accomplished using the tool for the quantitative comparison of modal vectors MAC. The MAC-value represents the degree of correlation between two mode shapes for both applied estimation procedures, which is in the range of $[0, 1]$, if MAC value equal to a unity denotes perfectly correlated mode shapes, while if a MAC value equal to zero would suggest a complete lack of correlation (i.e. orthogonally of mode shapes) [110].

For verification purposes, the values of MAC between both FDD and SSI technique were computed according to the Eq. (4.10) and the results are listed in Table 3.3. In addition, the values of MAC give an indication for the relationship between each extracted two modes. The values of MAC from the table show the correlation between each two extracted modes using FDD and SSI technique for the modal shapes of the structure.

Table 3.3: Comparison of MAC values between extracted mode shapes by FDD and SSI technique using ARTeMIS extractor software [108]

Frequency (Hz)		SSI Technique			
		1.652 Hz	2.330 Hz	4.875 Hz	6.400 Hz
FDD Technique	1.514 Hz	0.9188	0.1443	0.3541	0.05094
	2.295 Hz	0.1485	0.8802	0.3184	0.2806
	4.346 Hz	0.08002	0.08255	0.7292	0.1498
	6.299 Hz	0.195	0.2039	0.2693	0.8633

The results of MAC values verify the validity of the extracted modes with the respect to their stability and due to their approximate values that being near unity, which is listed Table 3.3, the results exhibit a good compatible between the two techniques FDD and SSI including the extractor software ARTeMIS.

Finally, the performance of two different systems identification methods, the frequency-domain based Peak-Picking (FDD) and the time-domain based on estimation of state space system (SSI), have been compared and discussed. The comparison shows that both methods give reasonable estimation of the natural frequencies and mode shapes, with MAC-values close to one. While, the advantage of FDD method is its simplicity and ability to provide fast and accurate estimate of the modal properties for complex Gazela bridge structure. Also, ARTeMIS extractor software is a good tool to facilitate extraction of modal properties accurately and rapidly with high understandable results. Therefore, in this thesis the ARTeMIS extractor software using FDD technique are adopted to extract the modal properties of all adopted structural models from ambient vibration measurements.

4. METHODS OF OPTIMIZATION IN STRUCTURAL DAMAGE DETECTION BASED ON CHANGES OF DYNAMIC CHARACTERISTICS

4.1. General

The optimization methods used in structural health monitoring system based on dynamic properties are an important part of the whole system. These methods represent the sophisticated part which explores existence and severity of structural damage. Like other real world optimization problems, it involves complexities such as discrete, continuous or mixed variables, multiple conflicting objectives, non-linearity, discontinuity and non-convex search region. The search space (design space) may be so large with more local minima and the global optimum cannot be found in a reasonable time. The existing linear or nonlinear optimization methods such as classical method may not be efficient or they are computationally expensive for solving such problems [111]. In general, mathematical model is often complex, and the objective function which have to be minimized may be non-convex and have several local minima. Therefore, the global optimization methods are required to prevent the stagnation to a local minimum. In the recent years, there has been a great deal of interest in developing methods for solving global optimization problems [112].

Numerical optimization procedures involved in damage detection usually include a set of variables, which have to be updated in order to obtain the minimum difference between the numerical and experimental results for damage state. Existence of damage has to be uncovered trough the comparison between the undamaged and damage state. Usually, it models by stiffness reduction of a structural element. Numerical optimization procedures require construction the so-called objective function that has to include all representative parameters that have to correlate. The selection of the objective function not only affects

the interpretation of the best correlation, but also influences the convergence of the optimization procedure [62], [113].

4.2. Background of optimization

A mathematical optimization is the selection of a best element from set of available alternatives with regard to some criteria. An optimization problem consists of maximizing or minimizing a real function by systematically choosing input values from within an allowed set and computing the value of the function [114].

Due to cost and complexity of problems nowadays, it is needed to optimization process to solve that problem with simple way and low cost to preserve time and money. There are many type of optimization problem simulate the engineering problems such as structural design and shape design. In addition, damage detection method based on updating modal properties using optimization method was added to those engineering problems. Many type of optimization method are also applied to solve those engineering problems such as; **Optimization algorithm**s, **iterative methods** and **heuristics methods**. This classification of optimization methods depends on type of variables (i,e, discrete or continuous), selection of variable from search space (i.e. randomly or systematically), what type of optimum are searching (i.e. local or global), type of problem (i.e. linear or nonlinear problem), exist of problem limitations (i.e. constrained or unconstrained), Accuracy of the optimum (i.e. exact or approximate), termination criteria and the rate of convergence and size of search space (i.e, small, large or huge) [114]. Also, optimization problem can be classified into **Deterministic** and **Nondeterministic** (stochastic or probabilistic).

Deterministic methods are most often used whenever the cost function presents certain numerical characteristics that allow us to explore known theoretical results so as to find optimal points. The gradient based optimization methods is a one type of classical deterministic numerical optimization methods to find local optimum with first-order optimization. In the optimization problems including more local minima, *Figure 4.1*, this type of optimization methods is easily trapped by local optimal solutions and this is one of the drawbacks [11] [115]. In addition, the extensively computations are spent in this

methods during searching the optimal solution which makes such methods inefficient for complex optimization problems.

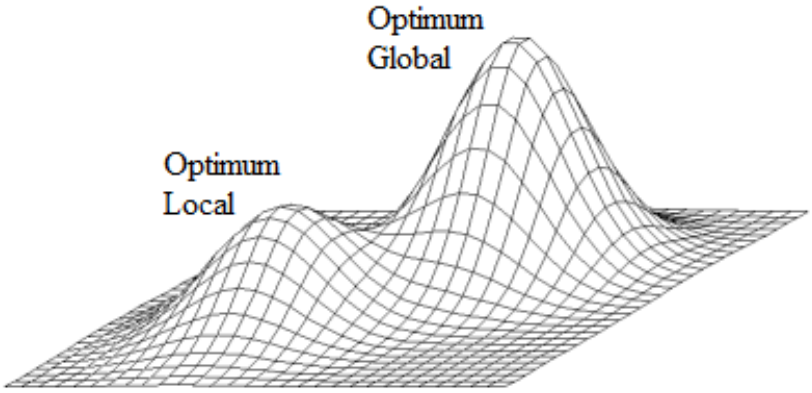

Figure 4.1: Local and global minima optimization problem [115]

Stochastic or **Probabilistic** optimization methods are nondeterministic optimization methods that generate and use random variables [114], [115]. For stochastic problems, that employs a degree of randomness as part of its logic, which involves random constraints for example. Those algorithms typically use uniformly random steps as an assistant input to guide its behavior, in the hope of achieving good performance in the "average case" over all possible choices of random steps. The stochastic optimization methods use random iterates to solve stochastic problems, which means many iterative steps are required to explore the global optimal solution. Those types of iterative methods use the rate of convergence of objective functions to specify the termination of the optimization procedure.

One of those methods is **Hill Climbing** method which is a mathematical optimization technique belongs to the family of local search [115]. It is an iterative algorithm that attempts to minimize or maximize an objective function $f(x)$, where x is a vector of discrete or continuous variables. At each iteration, hill climbing adjusts a single element in x and determine whether the change improves the value of $f(x)$.With hill climbing, any change that improves $f(x)$ is accepted, and the process continues until no change can be found to improve the value of $f(x)$. Also, the drawback of this method is no guarantee to find global optimum when there are more local minima in the search space [115]. Some optimization methods have been improved to solve this problem by considering a

neighboring configuration, repeated local search and more complex schemes. Those methods are called Heuristics optimization methods.

Heuristic optimization methods are a higher-level procedure which aims to find, generate, or select a partial search algorithm that may provide a sufficiently good solution to an optimization problem, particularly with incomplete or imperfect information or limited computation capacity [114], [115]. Heuristics search space a set of solutions which is too large to be completely covered during iterations. Heuristics may make few assumptions about the optimization problem being solved, and so they may be usable for a variety of problems. Compared to optimization algorithms and iterative methods, heuristics do not guarantee that a globally optimal solution can be found on some class of problems. Many heuristics implement some form of stochastic optimization, so that the solution found is dependent on the set of random variables generated. In combinatorial optimization, by searching over a large set of feasible solutions, heuristics can often find good solutions with less computational effort than optimization algorithms or iterative methods. Those methods with some improvement also they are called metaheuristic method.

In general there is no known method that could prevent premature convergence in optimization problems. In optimization process could gets caught in a local optimum and that depends on some reasons such as; type of objective function, configuration of solution during iterations and features of optimization algorithm etc. [114]. Increasing the degree of exploration may reduce the chance of premature convergence.

4.3. Types of Heuristic Optimization Methods

As mentioned previously, optimization of damage detection of structures is one of complex, hard and nonlinear problem, particularly when there are many variables and limitations. Those problems are called combinatorial problems, because consists of a set of parameters [116]. Also, exist of limitations or constraints in problem, and there are two types of constrained problems, equality and inequality constrained. The optimization methods solve such problems is classified as NP-Complete problems which means non-deterministic polynomial time complete problems. Those methods can exhibit different behaviors on different runs and amount of time taken by an algorithm to run as a function

of length of the string representing the input and whose solutions can be verified in polynomial time. For this reasons, needs one of the methods are rather problem-specific: there is no guarantee for finding optimal solution for one NP-complete problem. In this regard, heuristic optimization methods should be used to solve these problems.

Innumerable numbers of heuristic optimization methods or techniques have been developed for the optimum structural damage detection in the last decades. Those heuristic methods such as Genetic Algorithms (GA), Simulated Annealing (SA), Artificial Neural Network (ANN), Particle Swarm Optimization (PSO) and Tabu Search (TS) have been improved and applied to solve structural optimization problems [111]. The techniques which adopt in their procedure those methods are so-called **Artificial Intelligence Methods** (AIM). Those heuristic methods consist a set of variables including in the objective function need to be updated in order to obtain the minimum difference between two states of the structural model.

4.3.1. Genetic Algorithm (GA)

Genetic algorithms, one of the optimization tools based on artificial intelligence, have been extensively applying in structural damage detection applications. These algorithms have much stronger global optimization performance than traditional mathematical closed form gradient based algorithms. In comparison to traditional algorithms, genetic algorithms can find out optimal value of objective function without the continuity requirements of the objective function and the gradient information are not required. Also, parallel clues in some searching process results, not only to avoid falling into local minima, but also that GAs are more efficient and effective, [117]. GAs are stochastic search technique based on the mechanism of natural selection and natural genetics. They combine the principle of survival of the fittest among string structures with a structured yet randomized information exchange to form a search algorithm with some of innovative flair of human search. Actually, GAs have extensive application in structural damage detection [54].

The GA operation usually consists of three operations: reproduction (selection), crossover (recombination) and mutation (rarely random change). The genetic algorithm starts with an initial population, which may, for example, corresponds to initial numerical

values of a variable set. The size of this population may vary, and generally relates to the problem under consideration. The members of population are either strings of zeros and ones, i.e. binary strings, or strings of real parameters (real numbers). Each string of population corresponds to a chromosome and each binary (or real [53]) element of the string to a gene. Population size refers to the number of individuals (chromosomes) consisting that population during one generation. The term chromosome refers to a possible solution of the problem and it consists of number of genes, while the each gene represents a problem variable. A new population must be developed from initial population. For each specific problem implementation must be developed analogue from the described fundamental genetic processes, [52], [118].

The reproduction stage means that the selection of a set of chromosomes, based on natural selection, to be as parents. Thus, members of the population chosen for reproduction, based on their fitness, are defined according to some specified criteria. Crossover is a genetic operator that combines (mates) two chromosomes (parents) to produce a new chromosome (offspring). Behind the crossover, lies the main idea that the new chromosome may be better than both of the parents, because it takes the best characteristics from the parents. The final process is mutation. Mutation randomly changes a particular gene in a particular chromosome. Thus, 0 may be changed to 1, or vice versa. The process of mutation in a genetic algorithm occurs very rarely and hence probability of a change in a string should be kept very low [118].

4.3.2. Artificial neural network (ANN)

An Artificial Neural Network is an assembly (network) of a large number of highly connected processing units, the so-called nodes or neurons [5], [50]. Unidirectional communication channels, so-called connections connect neurons. The strength of the connections between the nodes are represented by numerical values, so-called weights. Knowledge is stored in the form of a collection of weights. Each node has an activation value, which is a function of the sum of inputs received from other nodes through the weighted connections. The neural networks are capable of self-organization and knowledge acquisition, i.e. learning. Most neural networks have some sort of "training" rule whereby

the weights of connections are adjusted based on presented patterns. In other words, neural networks "learn" from examples and exhibit some structural capability for generalization. Training provides a set of known input-output pairs, patterns, to the network. The network iteratively adjusts the weights of each node to obtain the desired output (for each input set) within a desired level of accuracy. Error is defined as a measure of the difference between the computed pattern and the expected output pattern. This technique is known as multilayer perception network [66], [70].

4.3.3. Particle Swarm Optimization (PSO)

Particle Swarm Optimization (PSO) is a technique with many similarities with genetic algorithms, except that the standard PSO does not use all genetic algorithm operators, such as crossover and mutation. It was developed in 1995 by James Kennedy (social-psychologist) and Russell Eberhart (electrical engineer) [119], [120], [121].

Main properties of PSO algorithm could be summarized as follow:

1- PSO is a robust stochastic optimization technique based on the movement and intelligence of swarms.

2- PSO applies the concept of social interaction to problem solving.

3- It uses a number of agents (particles) that constitute a swarm moving around in the search space and looking for the best solution.

4- Each particle is treated as a point in a N-dimensional space which adjusts its “flying” according to its own flying experience as well as the flying experience of other particles.

5- Each particle keeps track of its coordinates in the solution space which are associated with the best solution (fitness) that has achieved so far by that particle. This value is called personal best, P^{best}.

6- Another best value that is tracked by the PSO is the best value obtained so far by any particle in the neighborhood of that particle. This value is called global best, g^{best}.

7- The basic concept of PSO lies in accelerating each particle toward its P^{best} and the g^{best} locations, with a random weighted acceleration at each time step.

Each particle tries to modify its position using the following information; current positions, current velocities, distance between the current position and P^{best}, and distance between the current position and g^{best}. The modification of the particle's position can be mathematically modeled according to the following Eq. (4.1):

$$v_i^{k+1} = w \times v_i^k + c_1 \times rand_1(...) \times (p_{best} - s_i^k) + c_2 \times rand_2(...) \times (g_{best} - s_i^k) \quad 4.1$$

where are:

v_i^k - the velocity of agent i at iteration k,

c_j - the weighting factor, $j = 1,2$,

$rand_i$ - the uniformly distributed random number between 0 and 1, $i = 1,2$,

s_i^k - the current position of agent i at iteration k,

s_i^{k+1} - the new position of agent i at iteration $k+1$,

$p-best_i$ and $g-best$ - the best solution at the current agent i and global solution of the group of searching points, respectively,

w - the weighting function, which usually utilize in Eq. (4.1) as following:

$$w = w_{Max} - [(w_{Max} - w_{Min}) \times iter] / iter_{Max} \quad 4.2$$

There are some features of PSO method could improve its performance during iteration process such as immune mechanisms, selection, receptor editing, and vaccination and these mechanisms are incorporated into method procedure [118].

4.3.4. Tabu Search Method (TS)

Word Tabu (Taboo) comes from Polynesian Tongan language, where aborigines of Tonga island used by to indicate things that cannot be touched because they are sacred [122], [123]. As practical optimization tool, Tabu Search (TS) method is a meta-heuristic iterative procedure, which starts from some initial feasible solution and attempts to determine a better solution. TS procedure initially starts from several neighborhood hyper-points (position), and selects the new point (move) producing the best solution among all candidate points (moves) for current iteration. The best candidate solution may not improve the current solution. Selection of the best move (which may or may not improve the current

solution) based on the supposition that good moves are more likely to reach the optimal or near-optimal solutions. The set of admissible solutions attempted at a particular iteration, forms a candidate list. TS selects the best solution from the candidate list. Candidate list size is a trade-off between accuracy and performance.

The TS could be understood as an improvement of hill-climbing optimization method with short-term memories. The most important basic steps of any TS heuristic are the definition of search space and neighborhood around the trials [123].

4.3.5. Simulated Annealing Method (SA)

Simulated Annealing (SA) is the simulation of annealing of a physical many particle system to find the global optimum solutions of a large combinatorial optimization problem [74], [116]. It uses a temperature parameter that controls the search. At each step the temperature is slowly lowered, system is "cooled", and a new point is generated using an annealing function. At each step, distance of the new points from the current point is proportional to the temperature. If the energy (cost) of this new point is lower than that of the old point, the n`ew point is accepted. If the new energy is higher, the point is accepted probabilistically, with probability dependent on a "temperature" parameter. This unintuitive step sometime helps identify a new search region in hope of finding a better minimum.

Annealing function that takes random steps with size proportional to temperature and generates a point based on the current point and the current temperature is used. Also, the Boltzmann acceptance probability is used which is based on the chances of obtaining a new state E_{K+1}, relative to a previous state E_K, as given in Eq. (1) [116]:

$$p = \begin{Bmatrix} 1 & case \Delta E \le 0 \quad E-energy \\ e^{\frac{-\Delta E}{T}} & case \Delta E > 0 \quad E-energy \end{Bmatrix} \tag{4.3}$$

Acceptance probability depends on internal energy level change $\Delta E = E_{K+1} - E_K$. Thus, if E_{K+1} results $\Delta E \le 0$, it will be always accepted, whereas if E_{K+1} results in $\Delta E > 0$, its acceptance depends on acceptance probability. According to acceptance probability, there is a high probability that the change of variable(s) will be accepted, while the annealing temperature T is high, and vice versa. Thus, SA algorithm accepts changes

of variable(s) in the case that it increases objective function value, which is helpful to avoid that solution become trapped in local minima. Important issue of SA algorithm is an initial temperature T_o, from which the algorithm starts and decrement of temperature during optimization procedure. There are different approaches for determination of current temperature from initial temperature and this process is so-called cooling-schedule (decreasing of temperature) [116].

The Simulated annealing optimization algorithm terminates when one or more of following situations occur: the limited number of iterations or a certain run-time is reached, the maximum/minimum value of objective function with a certain level of convergence is achieved and alteration in the improvement of objective function is less than the function tolerance.

4.4. Applications of heuristic optimization methods in structural health monitoring

The optimization methods used in SHM apply to analysis the dynamic responses of the structures under service life to evaluate their integrity. The analysis of the response includes the comparison between the intact and assumed damaged state of the real structure. This process is done through the updating of the dynamic properties of the structure and then analyzes it to get the responses for that change. Also, in researches the comparison between the numerical and experimental scaled structural models is made to study changes in the behavior of the structures and develop and solve arising problems of such procedures.

The main part in those damage detection procedures using heuristic methods is objective function. The design of objective function is very important to include all parameters that sensitive for the change in the dynamic behavior of the structure. Damage detection procedures based on dynamics properties have been developed through the comparison between the undamaged and damaged state of the structural model using designed objective function. As mentioned previously in chapter two, the change in modal properties, natural frequency and mode shape, due to presence of damage in the structure have high sensitivity and effect on the dynamic behavior of that structure.

Applications of heuristic optimization methods and types of objective functions in damage detection methods will be discussed below.

4.4.1. Heuristic methods-based damage detection method

4.4.1.1. Genetic Algorithm (GA)

Several studies adopted GA heuristic optimization and it has been extensively applied for damage detection method such as Ruotolo and Surace in 1997 reported damage assessment method based on optimization method GA [51]. They verified the method numerically and experimentally on a cantilever steel beam with different damage scenarios. They implemented systematic numerical investigation to design the parameters of GA such as population size of 50 individuals, crossover probability of 0.8 and mutation probability of 0.8. They repeated the run of calculation program 20 times in order to get assurance about the results. The objective function includes the difference in natural frequencies and modal curvature between the undamaged and damaged structures. The authors concluded that the proposed method can detect damage, its location and its severity with satisfactory accuracy.

Friswell et al in 1998 presented proposed procedure based on a combined GA and eignsensitivity algorithm for the damage location in structure using vibration data [52]. Thy verified the procedure numerically on a 1 m long cantilever steel beam with cross section of (25x50) mm and experimentally on a 3 mm cantilever steel plate of (305x357) mm clamped along one edge. They used meaning of elitism to ensure that the best solution is maintained during optimization process without mating or mutation. They used 10 generations only for each optimization problem and implemented only one run for each optimization program. The objective function includes the differences in the natural frequencies and mode shapes of the intact and damaged structural model. They concluded that the proposed procedure successfully detected the damage location in the structure.

In addition, Xia and Hao in 1998 [53], Au et al in 2003 [54], Rao etal in 2004 [56], Park et al in 2006 [58], Gomes and Silva in 2008 [61], Meruane et al in 2008 [62], Panigrahi et al in 2008 [63], Meruane and Helyen in 2010 [68] and Liu et al in 2011 [71],

they applied GA to their proposed damage detection procedure with different parameters or combined with another optimization method as hybrid optimization.

He and Hwang in 2006 and 2007 presented proposed procedure combined between simulated annealing and genetic algorithm as an adaptive real-parameter to detect damage in simple structural models [4], [60]. In their work, they used SA method to generate randomly a new point from the neighborhood of the current point which is generated by mutation process of real genetic algorithm. Also, they applied Boltzmann machine to control the accepted solution with logarithm relation to reduce temperature during optimization process. They make use of the features of SA to modify the GA process. They verify their proposed adaptive procedure only numerically on simple structural models, such as a curved cantilever aluminum beam with 45º and 1 m radius, a 3.045 m cantilever aluminum beam, a 0.6 m clamped aluminum beam and a simply supported composite (glass/epoxy) spherical shell. They concluded that the proposed adaptive procedure by using SA features modified the ability of GA to detect damage in the structural models by increasing its precision and efficiency.

Also, Hadi and Abdulkareem in 2012 proposed damage detection method based on GA [72]. They used a 10 m long simply supported curved steel beam with cross section of $9.3x10^{-3}$ m^2 for verifying their method using numerical simulation only. They adopted two objective functions, only natural frequency and the other includes MAC as an index for mode shapes. They adopted 80 generations as maximum number for termination criteria. They concluded that the proposed procedure with objective function including the natural frequency was effective and more accurate to detect damage position and extent with different damage cases.

4.4.1.2. Artificial neural network (ANN)

Numerous studies also were implemented using ANN optimization method in the field of damage detection in the structures such as Sahin and Shenoi in 2003 presented damage detection method based on ANN [55]. The global properties were changes in natural frequencies and the locale were curvature mode shapes. The verified the proposed method numerically and experimentally on a 450 mm long cantilever steel beam with

40 mm width and 3 mm thickness.. They concluded that the experimental procedure has an important effect and gives reliability for the proposed damage detection procedure. In addition, the proposed procedure using ANN has robustness and accuracy to detect damage in the structure. Also, many studies applied ANN optimization method for damage detection based vibration. Lee et al in 2005 [57], Bandara et al in 2007 [59], Rosales et al in 2009 [64], Panigrahi et al in 2009 [65] and Bakhary et al in 2006 and 2010 [65], [66].

In addition, Aghabarati and Tehranizadeh in 2011 presented the application of damage detection procedure based on ANN with three networks on a plane six-span steel truss bridge model [70]. They used static response of displacement of measured points as parameter of objective function during applied external force in truss model. The comparison between the analytical and numerical results was included in objective function to identify the damage in the structural model. They concluded that the procedure has the ability to detect damage in the structural model.

4.4.1.3. Tabu Search Method (TS)

Arafa et al. in 2010 presented damage detection procedure based on hybrid optimization from combined two methods, TS method and GA, [69]. The adaptive optimization procedure consists of two steps; the main step is using TS method to explore several local solutions in the search space. The second step is using real coded GA as a global optimizer to find the global solution from explored local solutions by TS method with minor generated solutions. Their objective function minimizes the error value between updated FE and damaged experimental model estimated natural frequencies. They verified the procedure on simple beam models with two damage scenarios. They concluded that the TS method improved the ability of optimization procedure using GA to explore damage in the models.

Zhang and Yu in 2014 presented procedure using TS optimization method to find the optimum solution in the field of damage detection for plane truss structural model in the sense of optimal sensor position [75]. They used the mean value of off-diagonal elements in the MAC indicator as objective function. They concluded from their numerical work that the proposed procedure using TAsmethod has accurate results.

4.4.1.4. Particle Swarm Optimization (PSO)

In recent years, there are a few of studies proposed damage detection procedure based on PSO method such as Nejad et al in 2012 proposed damage detection method based on optimization algorithm, PSO, using incomplete dynamic data with a different level of noise [73]. Their procedure adopted passive congregation which means as an attraction of an individual to other group members in search space but without social behavior. In this way, the procedure could be avoided trapping in local minima. Their objective function includes the comparative frequency change vectors, which represent the change in frequencies before and after damage element. They verified their method on three simple structural models and they concluded that the proposed method has ability to find optimal damage location and severity.

Kang et al. in 2013 applied PSO technique to solve structural damage detection problem [1]. They proposed, to improve the convergence speed and accuracy, some immune mechanisms, such as selection, receptor editing, and vaccination. These mechanisms are incorporated into PSO and propose an Immunity Enhanced PSO (IEPSO). The algorithm was applied to the benchmark optimization function and damage detection problems using combined data. Their results show that the performances of original PSO are improved; the convergence speed is accelerated and easily getting entrapped in a local optimum in the case of complex multimodal problems. Compared with Differential Evolution (DE), PSO and an Adaptive Real-parameter using SA and GA (ARSAGA), IEPSO is the most efficient optimization method for damage identification.

4.4.1.5. Simulated Annealing Method (SA)

Ng et al. in 2009 introduced a probabilistic optimization approach to detect and characterize laminar damage in beams using combination of simplex search method as main and simulated annealing method as minor [11]. In their proposed methodology, the simulated annealing is employed to identify a solution, as initial trial for a simplex search method, which is close to the global optimum. They proposed approach which consists two steps to accurately explore global optimal solution. The first step of approach starts using

SA method by generating a set of configuration N^T, assumed $N^T = 20$ solutions, from random initial solution. This set of configuration has a random small change, in uncertain parameters, close to the current solution. They adopted Boltzmann acceptance probability to control the process using linear relation for reducing temperature with reduction factor of 0.5. They adopted two termination criteria for their proposed approach; either a specified level of convergence of uncertain parameters is reached or a specified run-time is achieved. Then, the simplex search method is implemented to find the global solution by treating the candidate solution from SA first trial. They verified their method numerically only on a 2 m long aluminum beam with a width, height, Young's modulus and density of 12 mm, 6 mm, 72 GPa and 2750 kg/m^3, respectively. They concluded that a two-stage optimization process consisting of simulated annealing is implemented to guarantee that the solution finds the global optimum, followed by a standard simplex search method that maximizes the probability density function of the damage scenario conditional on a set of measurements. Also, it was concluded that the results show the potential and robustness of the proposed approach.

Kourehli et al. in 2013 proposed approach by simulated annealing optimization method to detect damage using incomplete modal data and incomplete static response of a structure [74]. They verified their approach numerically on two models, the first is a 4 m long concrete simply supported beam with cross-section, Young's modulus and mass density of 0.12 m^2, 25 GPa and 2500 kg/m^3, respectively. The second model is a steel three-storey plane frame with total height and width of 10.8 m and 6 m, respectively. Also, their approach is tested experimentally using 8 DOFs spring-mass system with eight translating masses connected by springs. They used a package exist in MATLAB software to perform simulated annealing process in random steps and generated new solution based on current solution. They adopted Boltzmann acceptance probability to control the acceptance of new solutions and linear relation for cooling schedule to decrease temperature. In addition, reannealing process after a specified number of accepted solutions was adopted to improve the approach. They used termination criteria such as the maximum number of iteration or objective function value is reached, alteration in the improvement of objective function is less than the function tolerance and the maximum time runs of approach is achieved. They

concluded that their proposed approach using simulated annealing is a promising approach [74].

The drawback of those previous proposed procedure in the researches using simulated annealing method for damage detection procedures is the use of existed package in MATLAB software instead of writing speared subroutine in the software to be more flexible to control all parameters and features of simulated annealing algorithm and connect them with the structural problems. In addition, they used numerical testing only or with experimental testing on simple structural models in their works to verify the proposed procedures. Also, application of SA method in damage detection procedure together with another optimization method may be improved the solution in some sense, however, the computations and run time of procedure could be more extensive and complex. In addition, the SA method could lose its features to explore the global solution due to the restrictions in the process.

So, new procedures for damage detection using simulated annealing method by controlling all parameters and features of the method are needed. Also, these procedures should be written in advance language software such as MATLAB and verified on 3D-Space complex structural models to study the reliability and robustness of such procedure.

In this thesis, new damage detection procedure using simulated annealing method written by subroutine in MATLAB language software is proposed. The proposed procedure could control all parameters of simulated annealing algorithm and connect it with structural damage problem analyzed by ANSYS language. The proposed procedure applied on four structural models to verify its efficiency and ability to detect damage location and severity. Those structural models include two 3D-space complex structures as well as simple structures. Also, the experimental testing of all adopted structural model are performed using simulation of ambient vibration excitation to verify the proposed procedure.

4.4.2. Objective functions used in heuristic optimization for damage detection method

The aim of any optimization method is to maximize or minimize the objective (fitness) function. In the case of vibration based damage detection task, an objective

function represents the difference between the measured and numerical modal data. Fundamental objective functions, related with the damage detection process, usually correspond, as it is defined in [68], to frequency differences, modal displacements differences, Modal Assurance Criterion (MAC) values, strain energy residuals and difference between flexibility matrices. Different researches contain a part or combination of all these fundamental objectives. The selection of the objective function not only affects the interpretation of the best correlation, but also influences the convergence of the optimization procedure [62]. Therefore, the details of including dynamic properties into objective functions will discuss in next subsections.

4.4.2.1. Differences in modal frequencies

Kirkegaard and Rutter in 1995 adopted objective function was formulated in terms of fractional changes of natural frequencies of the structure before and after damage in order to reduce the effect of modeling errors [52]. Their objective function is following:

$$\text{Obj\_Fun} = \log\left(W_f \cdot \sum_{i=1}^{n} \left(\frac{f_i^{\exp-dam} / f_i^{\exp-undam}}{f_i^{num-dam} / f_i^{num-undam}} - 1\right)^2\right) \quad 4.4$$

where are:

$f_i^{num-dam}$ and $f_i^{exp-dam}$ - the i^{th} numerically and experimentally estimated values of natural frequencies for the damaged model, respectively,

$f_i^{num-undam}$ and $f_i^{num-undam}$ - the i^{th} numerically and experimentally estimated values of natural frequencies of the i^{th} mode for the undamaged/intact model, respectively,

i - the modal frequency number $i = 1,2,....,n$,

n - the included number of modal frequencies in the computations,

W_f - the weighting factor of the estimations of the natural frequencies.

To avoid the solution from trapping in local minima they applied the following constrain:

$$\left| \frac{f_i^{num-dam}}{f_i^{num-undam}} - \frac{f_i^{exp-dam}}{f_i^{exp-undam}} \right| \le \beta_i \quad 4.5$$

where are:

β_i - the weighting factor from the accuracy of the computations of the natural frequencies.

They concluded that the differences in values of natural frequencies between intact and damaged model could be adequate to explore damage in the simple structural models.

Ruotolo and Surace in 1997 adopted three objective functions; one which includes the difference in natural frequencies between the undamaged and damaged structures [51]. Their objective function is following:

$$\text{obj\_Fun} = \sum_{i=1}^{n} (1 - \frac{f_i^{\exp-dam} / f_i^{\exp-undam}}{f_i^{num-dam} / f_i^{num-undam}})^2 \quad 4.6$$

They included only the first three modal frequencies in their study. They concluded that the differences in natural frequency values between intact and damaged model could detect damage in the model with satisfactory accuracy.

Also, Hadi and Abdulkareem in 2012 adopted two objective functions; one of them is relied on the direct change in the values of natural frequencies between the numerical and the experimental damaged structural model [72], as following.

$$\text{obj\_Fun} = \sum_{i=1}^{n} (f_i^{\exp} - f_i^{num})^2 \quad 4.7$$

They simulated the experimental damaged values of natural frequency from assumed numerical study. They concluded that the objective function has good ability to detect damage in a structural model.

It could be concluded that the change in natural frequencies has significant sense to presence of damage in the simple structural models. In addition, using of this type of objective function should be previously well implemented calibration process for initial intact FE model.

4.4.2.2. Differences in modal mode shape

Ruotolo and Surace in 1997 studied objective function including the difference in normalized mode shapes between the undamaged and damaged structures [51]. Their objective function is given as following:

$$\text{obj\_Fun} = \sum_{i=1}^{n} \sum_{j=1}^{m} \left(\phi_{i,j}^{num-dam} - \phi_{i,j}^{\exp-dam} \right)^2 \quad 4.8$$

They included only the first three modal frequencies in their study. They concluded that the differences in natural frequency values between intact and damaged model could detect damage in the model with satisfactory accuracy.

Nahvi and Jabbari in 2005 adopted the comparison between the experimentally extracted and numerically estimated mode shapes to detect the damaged element [39]. They used the meaning of error to describe the difference in mode shapes, as given in the following equation:

$$\text{obj\_Fun} = \sum_{i=1}^{n} (\varepsilon_i)^{\frac{1}{2}} = \sum_{i=1}^{n} \left(\sum_{j=1}^{m} (\phi_{i,j}^{\exp} - \phi_{i,j}^{num})^2 \right)^{\frac{1}{2}} \quad 4.9$$

where are:

ε_i - the error for the i^{th} experimentally and numerically estimated values of natural normalized displacement

$\phi_{i,j}^{exp}$ and $\phi_{i,j}^{num}$ - the i^{th} experimentally and numerically estimated values of natural normalized displacement of j^{th} component, respectively,

i - the modal frequency number $i = 1,2,....,n$,

n - the included number of modal frequencies in the computations,

j - the component number $j = 1,2,....,m$,

m - the included number of components in the computations.

They adopted only the first two modes in their work and they concluded that higher modes should be included to increase the ability to detect damage accurately.

4.4.2.3. Modal Assurance Criterion (MAC)

An alternative method that does not require the mode shape scaling between two sets of mode shapes is to use the modal assurance criterion (MAC) which is indicator for quantitative comparison of modal vector [124]. It is also used in the objective function to reflect the change of mode shape vectors due to the presence of damage in the structure.

Hadi and Abdulkareem in 2012 adopted two objective function was relied on the MAC between the experimental and numerical mode shape vectors [72]. The MAC is given

as second objective function compared with one depends on the change of the natural frequency, the equation as followed:

$$MAC(\phi_{\exp}, \phi_{num}) = \frac{(\phi_{\exp}^{T} \cdot \phi_{num})^2}{(\phi_{\exp}^{T} \cdot \phi_{\exp})(\phi_{num}^{T} \cdot \phi_{num})} \quad 4.10$$

where are:

ϕ_{exp} and ϕ_{num} - the experimentally and numerically estimated normalized mode shapes vector, respectively,

T - superscript represents transpose matrix of mode shape vector.

They concluded that the MAC alone has less sensitivity compared with the change of natural frequency to detect damage in structure.

4.4.2.4. Combination of modal properties

Friswell et al. in 1998 presented proposed objective function includes the three terms; the differences in the natural frequencies, the difference in the mode shapes and the weight against position of damages of the damaged structural model [52]. Their objective function is followed:

$$\text{obj\_Fun}_{\text{comb}} = W_f \cdot \sum_{i=1}^{n} \left(\frac{f_i^{\exp} - f_i^{num}}{f_i^{\exp}} \right)^2 + W_d \cdot \sum_{i=1}^{n} (\phi_i^{\exp} - \phi_i^{num})^T (\phi_i^{\exp} - \phi_i^{num}) + W_p \cdot \delta_p \quad 4.11$$

where are:

W_f, W_d and W_p - the weighting factors of the natural frequencies, mode shape and position of damage, respectively,

δ_p - the variable represents the position of damage equal to zero if one site is damaged and equal to 1 if more than one site is damaged,

They concluded that the mode shape can give valuable information but mode shape alone in objective function is less accuracy than natural frequencies and insensitive. Therefore, they used in their work only first and second part in their objective function with values of weighting factors are $W_f^i = 100$ and $W_p = 0.25$ for one structural model case and $W_f^i = 1000$ and $W_p = 0.25$ for another structural model case and only the first five modal frequencies are included.

Xia and Hao in 1998 adopted objective function includes the relative difference between the changes in the measured numerically and extracted experimentally modal properties, natural frequencies and mode shapes, of the damaged structural model [53]. Their objective function is followed:

$$\text{obj\_Fun}_{\text{comb}} = W_f^2.Fun_f + W_d^2.Fun_d \quad 4.12$$

$$\text{Fun}_{\text{f}} = \sum_{i=1}^{n} W_{f,i}^2 . \left(\left[\frac{\lambda_i^{updated} - \lambda_i^{initial}}{\lambda_i^{initial}} \right]^{num} - \left[\frac{\lambda_i^{dam} - \lambda_i^{undam}}{\lambda_i^{undam}} \right]^{\exp} \right)^2 \quad 4.13$$

where are:

$\lambda_i^{updated}$, and $\lambda_i^{initial}$ - the i^{th} numerically updated and initial eigenvalues, respectively,

λ_i^{dam}, and λ_i^{undam} - the i^{th} experimentally eigenvalues of the damaged and undamaged strucutre, respectively.

$$\text{Fun}_{\text{d}} = \sum_{i=1}^{n} W_{d,i}^2 . \sum_{j=1}^{m} \left(\left[\phi_{ij}^{updated} - \phi_{ij}^{initial} \right]^{num} - \left[\phi_{ij}^{dam} - \phi_{ij}^{undam} \right]^{\exp} \right)^2 \quad 4.14$$

where are:

$\{\phi_{ij}\}$, - the j^{th} component of the i^{th} normalized mode shape for selected experimentally degrees of freedom,

j - the component number $j = 1,2,....,m$,

m - the included number of components in the computations.

They used the first 12 modes in their computations and the weighting factor $W_f^2 = 1$ and $W_d^2 = 10,1,0.1,0.001$ respectively . They concluded that the change in frequencies or mode shape alone are not satisfactory particularly, local damage for frequency and large errors in mode shape. Therefore, the combination of natural frequencies and mode shapes change together should be included.

Park et al in 2006 presented proposed objective function includes differences, in natural frequencies and modal strain-energy using modal curvature of the structural model, between the intact and damaged cases [58].

$$\text{obj\_Fun}_{\text{comb}} = W_f.Fun_f + W_s.Fun_s \quad 4.15$$

$$\text{Fun}_{\text{f}} = \sum_{i=1}^{n}.\left(\left(\frac{f_i^{undam} - f_i^{dam}}{f_i^{undam}}\right)^{\exp} - \left(\frac{f_i^{undam} - f_i^{updated}}{f_i^{undam}}\right)^{num}\right)^2 \quad 4.16$$

$$\text{Fun}_{\text{s}} = \sum_{i=1}^{n}\sum_{k=1}^{K}\left(\left[\theta_{ik}^{undam} - \theta_{ik}^{updated}\right]^{num} - \left[\theta_{ik}^{undam} - \theta_{ik}^{dam}\right]^{\exp}\right)^2 \quad 4.17$$

where are:

θ_{ij}^{undam} and θ_{ij}^{dam} - the i^{th} mode numerical and experimental intact and damaged modal strain energy, respectively, for k^{th} element of the intact state of the structural model for selected experimentally degrees of freedom,

k - the element number $k = 1,2,....,K$,

K - the included number of elements in the structural model,

$\theta_{ij}^{updated}$ - i^{th} numerical updated modal strain energy for k^{th} element of the intact state of the structural model.

They adopted only the first four modes in their computations with weighting factors of $W_s = 1$ and $W_f = 1, 0.1, 0.01$, respectively. They concluded that the combined objective function is better to detect accurately damage in the structure with $W_f = 0.1$.

He and Hwang in 2006 and 2007 adopted objective function including three parts, the differences in natural frequencies, the difference in mode shapes and the difference in the displacements of static response of the structural models [4] , [60]. In the first study of He and Hwang in 2006 [4], they adopted only the difference in natural frequencies and static displacements, as given in equation:

$$\text{Obj\_Fun}_{\text{comb}} = W_f.\sum_{i=1}^{n}.\left(f_i^{\exp} - f_i^{num}\right)^2 + W_p.\sum_{ps=1}^{Ps}\sum_{j=1}^{m}\left(D_{psj}^{\exp} - D_{psj}^{num}\right)^2 \quad 4.18$$

where are:

D_{psj}^{exp} and D_{psj}^{num} - experimental and numerical static displacement of the j^{th} component due to apply the ps^{th} load, respectively,

ps - the applied static load number $ps = 1,2,....,Ps$,

Ps - the number of applied static loads.

They adopted only the first 10 modes in their computations with weighting factors of $W_f = 1$ and $W_p = 1000$, respectively. They concluded that the combined objective function has significant effect to detect assumed damage in the structural model precisely.

In the second study of He and Hwang in 2007 [60], they adopted only the difference i natural frequencies and mode shapes, as given in equation:

$$\text{obj\_Fun}_{\text{comb}} = W_f . \sum_{i=1}^{n} . \left(f_i^{\exp} - f_i^{num} \right)^2 + W_d . \sum_{i=1}^{n} \sum_{j=1}^{m} \left(\frac{\phi_{ij}^{\exp} - \phi_{ij}^{num}}{\phi_{ij}^{\exp}} \right)^2 \quad 4.19$$

where are:

ϕ_{ij}^{exp} and ϕ_{ij}^{num} - experimental and numerical radial displacement of the j^{th} component of the i^{th} mode shape, respectively.

They adopted weighting factors of $W_f = 1$ and $W_d = 100$, respectively. They concluded that the combined objective function has significant effect to detect assumed damage in the structural model precisely.

In addition, Kang et al. in 2013 [1] adopted the same formula of objective function used by He and Hwang in 2006 [4], but only the adopted the relative normalized difference in the natural frequencies and static displacements instead of the direct difference. They adopted weighting factors of $W_f = 1000$ and $W_p = 1000$ in their research.

Finally, it is concluded that the combination formula of objective function is more adopted for detecting damage accurately of location and severity of damage. In addition, the change in natural frequencies and mode shapes has significant sensitivity to presence of damage in the structures and can overcome the drawbacks of the change in each modal property alone. Also, using of change in normalized mode shapes vectors is better than use MAC as indicator because of the mode shape could be detected local change in the displacement of nodes instead of the global indicator as MAC. On the other hand, the weighting factors used of combined objective function have significant effect on the final results of detecting damage precisely. The values of the weighting factor depends on the type of structural model if it is simple or complex, the number of measurement points or elements/nodes adopted in the computations and the sensitivity of the modal property to the presence of damage in the structure.

4.5. Adopted heuristic optimization Simulated Annealing (SA) method

In the latest research, Kang et al.(2013) indicated that the disadvantage of GA is it exhibits a distinguished drop in efficiency as the number of unknown parameters to be identified is more than two and premature convergence is likely to happen [1]. He et al. in 2006 indicated that either too much iteration or not accurate results were found in either Genetic Algorithm (GA) or Simple Genetic Algorithm (SGA) or by combined SGA with eigensensitivity approaches [4]. They attributed to that SGA spends much computation time in the encoding as well as decoding processes and the space of the parameters to be found is continuous not discrete. Furthermore, the bits of the parameters will be large if high precision of the parameter values is desired and the lack of hill-climbing ability, an inherent shortage of GA, was still not tackled. For this reasons, they proposed a novel hybrid algorithm to overcome these problems, a real-parameter GA was used and adopt the advantage of SA for damage detection, because it is good at hill climbing for optimum solutions, but its convergence speed is very slow [4].

On the other hand, Simulated Annealing (SA), which is known to be one of the most reliable search algorithms in locating the globally optimal point [125]. The SA is a popular local search meta-heuristic used to address discrete and continuous optimization problems. the main feature of SA is to escape local optima by allowing hill-climbing moves (i.e. some time towards the worst solution) in hopes of finding a global optimum. In addition, the SA has, a quick convergence, easy to implement in hard and nonlinear problems [126]. So, in this study Simulated Annealing is adopted.

4.5.1. Methodology of SA method

Simulated annealing (SA) is a probabilistic technique for approximating the global optimum of a given function [116]. Specifically, it is a metaheuristic to approximate global optimization in a large search space. It is often used when the search space is discrete and for problems where finding the precise global optimum is less important than finding an acceptable local optimum in a fixed amount of time or computations.

The name of simulated annealing is mimicry from the principle of annealing from materials science. It is based on the fact that certain material alloys have multiple stable states with different molecular distributions and energy levels. In the annealing process, an alloy is initially heated up to a temperature at which all particles are randomly distributed in the liquid phase. The temperature is then slowly decreased until the material solidifies. Then, if the temperature is reduced at a sufficiently slow rate, the annealing process always guarantees that the alloy reaches its global minimum energy state [11], [116].

Kirkpatrick et al. in 1983 depended on statistical mechanics, which means only the most probable behavior of the system in thermal equilibrium at a given temperature is observed in experiments [116]. This can be characterized by the average and small fluctuations about the average behavior of the system, when the average is taken over the ensemble of identical systems. In this ensemble, each configuration, defined by the set of atomic positions, $\{ r_i \}$, of the system is weighted by its Boltzmann probability factor.

Kirkpatrick et al. in 1983 reported to implement SA in combinatorial optimization problem, five ingredients are needed; a description of configuration of the system, a random generator of moves or rearrangements of the elements in a configuration, a quantitative objective function containing parameters that have to be made, an annealing schedule of the temperature and length of times which the system is to be evolved [116].

Tsallis and Stariolo(1995) indicated that in SA technique, one or more artificial temperatures are introduced and gradually cooled, in complete analogy with the well known annealing technique frequently used in Metallurgy for making a molten metal to reach its crystalline state (global minimum of the thermodynamical energy) [127]. They indicated that the SA was extended in 1986 by Ceperley and Alder for quantum systems. The system “tries” to visit, according to a visiting distribution assumed to be Gaussian (i.e., a local search distribution) in the neighborhood of its actual state ~x. The jump is always accepted if it is down hill (of the energy/cost function); if it is hill climbing, it might be accepted according to an acceptance probability assumed to be the canonical-ensemble Boltzmann-Gibbs one. So, they represented that Geman and Geman showed, for the classical case, that a necessary and sufficient condition for having probability one of ending in a global minimum is that the temperature decreases logarithmically with time and this

algorithm is sometimes referred to as Classical Simulated Annealing (CSA) or Boltzmann machine. It easily recognize that, if instead of decreasing, the temperature was maintained fixed, this procedure precisely is the well known Metropolis et al [11], [29] one for simulating thermostatistical equilibrium. The next interesting step along the present line was Szu's 1987 proposal of using a Cauchy-Lorentz visiting distribution, instead of the Gaussian one [127]. This is a semi-local search distribution: the jumps are frequently local, but can occasionally be quite long (in fact, this is a L´evy-flight-like distribution). Also, They referred that Szu and Hartley showed, the cooling can now be much faster (the temperature is now allowed to decrease like the inverse of time), which makes the entire procedure quite more efficient and this algorithm is referred to as Fast Simulated Aannealing (FSA) or Cauchy Machine [127].

4.5.2. Optimization procedure using SA method

Simulated Annealing heuristic optimization procedure starts initializing value of objective function $F(x_{initial})$, which corresponds to a randomly selected initial point in the searching space, $x_{initial}$. The initial solution depends on one or more of initial values of variable(s) or parameter(s), depends on the structure of problem, which have to be chosen randomly too. Then, initially have to be proposed the total number of iterations, according to the all possible solutions in the searching space. Hence, the initial solution $x_{initial}$ have to be assumed as a current solution $x_{current}$ and $F(x_{current}) = F(x_{initial})$.Searching for the better solution begins in the neighborhood of the current solution, during so-called Cooling Schedule. The neighborhood configuration is design relying on the structure of the problem and number and range of variable(s) including in the problem. A set of new variable(s) are generated randomly from searching space in the j^{th} iteration, and define the so-called new solution, $x_{new} = x_i$. The new value of the objective function $F_i = (x_{new})$, comes from the vector of the new parameter values, x_{new} in i^{th} iterations. The new solution x_{new} will be or accepted, depends on the acceptance probability p, defined by Eq. (4.20), [116].

$$p = \begin{Bmatrix} 1 & case \Delta F \le 0 \quad \min of \ function\ (\Delta E \le 0 \quad E-energy) \\ e^{\frac{-\Delta F}{T}} & case \Delta F > 0 \quad \min of \ function\ (\Delta E > 0 \quad E-energy \end{Bmatrix} \qquad 4.20$$

Acceptance probability or **Boltzmman Mechine** depends on internal energy level difference, defined by the objective function values, $\Delta F = F(x_{new}) - F(x_{current}) = \Delta E$. If $F(x_{new})$ results $\Delta F \le 0$, the new state, which corresponds to x_{new} vector of variable(s), will be always accepted current solution, $x_{new} = x_{current}$. Whereas, if $F(x_{new})$ results in $\Delta F > 0$, acceptance of the x_{new} state depends on acceptance probability defined by $p = e^{-\Delta F / T}$ at particular annealing temperature T in comparison with randomly generated parameter r in the range $[0,1]$. If $p > r$, will be accepted and the $x_{current} = x_{new}$, otherwise the new state, defined by x_{new}, will be rejected and this mechanism is called **Metropolis Test** [116]. According to acceptance probability, there is a high probability that the change of variable(s) will be accepted, if the annealing temperature T is high, and vice versa. Thus, SA algorithm accepts some changes of state without of improvement of the solution, in order to avoid that solution become and be trapped in local minima. In the case that the new state is accepted, x_{new} becomes $x_{current}$ in a new iteration, $F(x_{current}) = F(x_{new})$. In the next iteration, the annealing temperature T is going to be reduced, according to proposed so-called Cooling Schedule during the iterations, which decreases the acceptance probability p. until the system "freezes" and no further change occur. Due to the important of cooling schedule on the process of simulated annealing optimization, there were many studies dealt with this issue.

Finally, to implement the SA algorithm, a number of decisions have been made, mainly concerned with controlling the temperature, the number of iterations and the condition under which the system is declared 'frozen'. In this regard, *Figure 4.2* shows the flowchart of general steps of proposed SA algorithm procedure in current study with adopting the above strategy of SA algorithm. The detail of proposed SA procedure depends on the type of structural model problem and all parameters related with it. So, the proposed procedure are applied for two type of problem, the first is calibration of the model using

updating process and the other is damage detection problem by updating model modal properties.

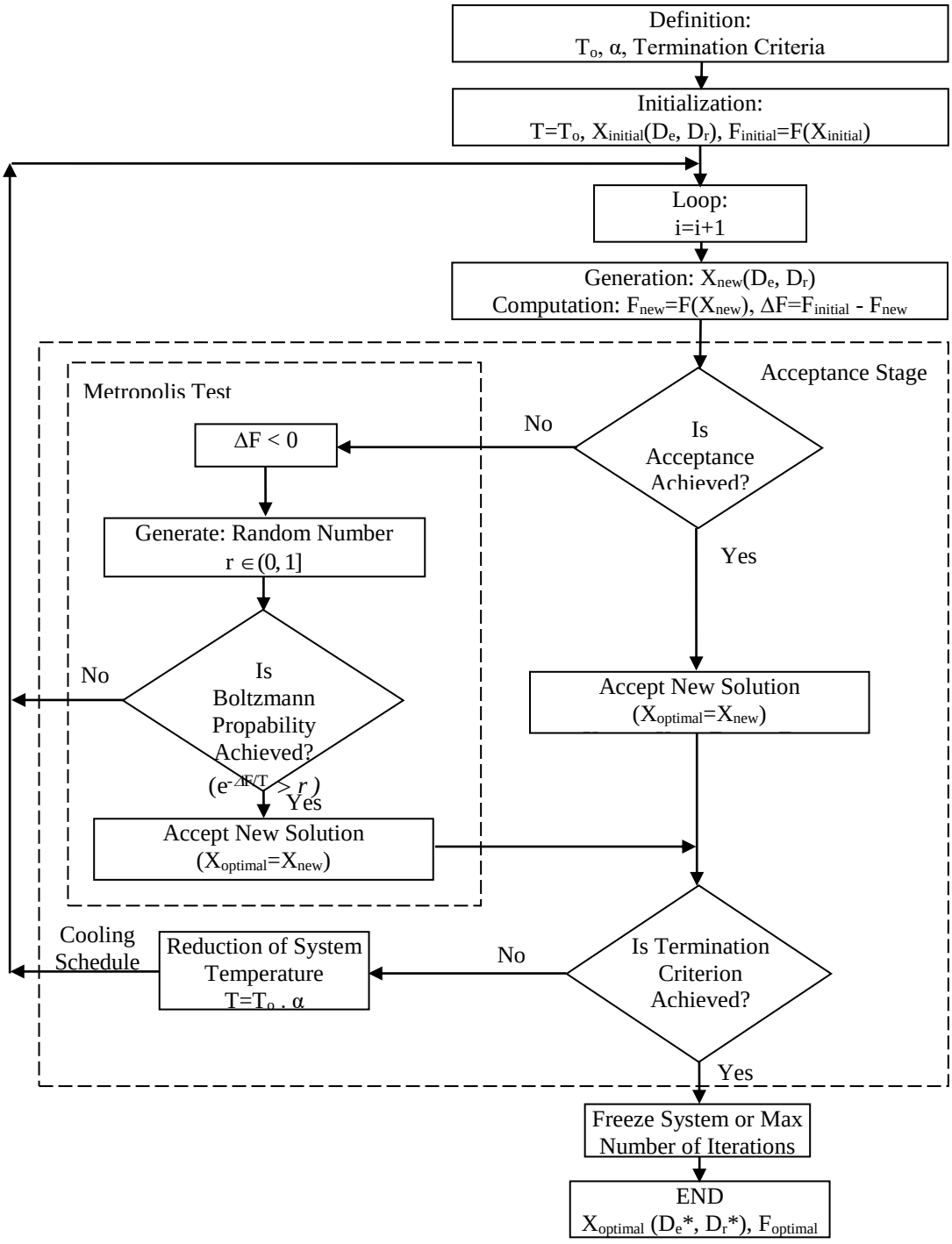

Figure 4.2. Flow chart of adopted simulated annealing (SA) optimization algorithm for proposed SHM damage detection procedure (SHMUSA)

4.5.3. Initial temperature and cooling schedule adopted in SA method

Important issue of SA algorithm is an initial temperature T_o, as start parameter of the algorithm and cooling schedule during iterations which defines decreasing of the temperature and reduction of the acceptance probability. Some authors [116], [125], suggested different approaches for determination of initial temperature and so called cooling-schedule.(decreasing of temperature) Those approaches could be defined either by linear, exponential or logarithm relation.

Kirkpatrick et al. 1983 reported that the annealing schedule can be developed by trial and error for a certain problem [116]. They used linear relation between initial and current temperature of 0.95 reduction factor.

Miskovic in 2000 used the equation of accepted probability and converted it to determine the initial temperature [128]. In his work assumed that $F(x_{initial}) = p = [0.8 - 0.95]$, then $F(x_{initial})$ is given in Eq. (4.21):

$$F(x_{initial}) = e^{\frac{-\Delta F}{T_o}} \tag{4.21}$$

where are:

$F(x_{initial})$ - an initial value of objective function,

ΔF - a changing in the objective value,

T_o - an initial temperature.

Then, can be calculating the initial temperature by converting the above equation, as given in Eq. (4.22):

$$T_o = \frac{-\Delta F}{\ln(\frac{1}{F(x_{initial})})} \tag{4.22}$$

Ceranic et al. in 2001 indicated that the initial temperature can be estimated automatically by conducting a random pilot survey of the solution space, in which all increases in the objective function are accepted [125]. Their work adopted that the suitable initial temperature is determined given acceptance probability, according to following Eq. (4.23):

$$T_o = \frac{-f^*}{\ln(p)} \qquad 4.23$$

where are:

p - the acceptance probability $p = 0.8$,

f^* - the average increase in the objective function and equal to all function increases divided by number of increases.

Hasancebi and Erbatur in 2002 referred that cooling schedule requires of an initial temperature, a final temperature and cooling factor, which is introduced to adjust the reduction of the temperature in the consequent cooling cycles [129]. They proposed equations to formulate the cooling schedule parameters based on assumed acceptance probabilities and thus allow them to be chosen automatically irrespective of problem type. Otherwise, an arbitrary choice of these parameters exhibits problem dependency and entails an extensive numerical experimentation

$$T_o = -\frac{1}{\ln(p_o)}, \quad T_f = -\frac{1}{\ln(p_f)}, \qquad 4.24$$

where are

T_o and T_f - an initial and final temperature of the system,

p_o and p_f - an initial and final acceptance probability.

In equation (4.24) and before calculating the initial temperature, a value has to be assumed for the initial acceptance probability p_o. This means that the initial temperature is assigned in such a way that the poor candidate designed at the beginning is treated with an average p_o probability of acceptance. Note that the initial temperature will be high for higher values of the initial acceptance probability, p_o. Therefore, it is generally chosen in the range of $p_o = [0.5 - 0.9]$. Similarly, the algorithm is forced to terminate at a temperature given in second part in Eq. (4.24) with respect to an assumed final acceptance probability p_f. To accomplish this, they proposed that the final acceptance probability is assumed to small values, such as $p_f = 1 \times 10^{-7}$ *or* 1×10^{-8}. They proposed cooling factor as given in Eq. (4.25):

$$f^c = \left[\frac{\ln(p_o)}{\ln(p_f)} \right]^{\frac{1}{(N_c - 1)}} \quad 4.25$$

The equation (4.25) shows the cooling factor $0 < f^c < 1$ which serves to reduce the temperature gradually between successive cooling cycles. For this purpose, firstly the number of cooling cycles, N_c, is assigned, then the temperature of the next cycle temerature T^{c+1} ,with reference to that of previous cycle temerature T^c, is calculated as in Eq. (4.26):

$$T^{c+1} = f^c \times T^c \quad 4.26$$

The manner the temperature decrease is determined, thus to develop an efficient annealing algorithm, is very sensitive to the number of cooling cycles, N_c. A small value of cooling factor, f^c, obtained with the low values for N_c might cause a rapid cooling schedule, which may end up with the stagnation of the algorithm in a local optimum [129]. On the other hand, a large value of N_c will eliminate this situation by careful annealing, however, it will cause a prohibitively heavy computational burden. In their paper indicated, it has been experienced that for $N_c = 100$ a premature local optimum is found, and they concluded that $N_c = 200$ and $N_c = 300$ are appropriate values [129].

In the presented study, the linear relation is used to produce the new temperature after improve the solution in SA optimization process, as given in Eq. (4.27):

$$T = \alpha \times T_o \quad 4.27$$

where are:

α - the reduction factor in the range of $\alpha = [0.7 - 0.9]$ between two subsequent iterations depend on the type of structural model problem.

T_o - the initial temperature parameter,

To avoid the complexity of the problem and extensively computations, is adopted by the trial and error approach which proposed by Kirkpatrick et al. [116] for each type of the structural model problem. It is fixed to be $T_o = 20$ for all structural model problems.

4.5.4. Configuration of initial and neighboring solution in searching space used in SA method

There is an analogy between a physical annealing process and an optimization process of damage detection. Different positions and values of damage of the structural problem correspond to different arrangements of the atoms. The minimum value of objective function corresponds to energy of the system. The optimal solution with exact damage location and severity corresponds to the lowest energy state. In the same manner the atoms find their way to build a perfect crystal structure through random movements, the global optimum is reached through a search within randomly generated damaged models

It is worth mentioning, Akbulut and Sonmez in 2011 indicated that there are three type of simulated annealing method have been developed depend on solution(s) belong to the search space which represents a neighborhood of the initial solution as well as the initial solution [130]. Those types of configuration are randomly generated from search space. The randomly selection of the neighborhood are designed depend on the structure of combinatorial problem. The types of those methods are following:

4.5.4.1. Standard Simulated Annealing (SSA)

This SA method initialize with only one solution or point which belongs to search space [116], [130], [131]. Then, the neighborhood of initial solution is generated randomly within the search space. This method of SSA is used for small search space with simple optimization problem including small range and number of variables in the problem structure. This method some time is called Classical Simulated Annealing (CSA) [130].

In this study, the standard simulated annealing is applied for proposed procedure for damage detection on the simple structural model. In addition, this method is adopted for proposed procedure for calibration process of all structural models.

4.5.4.2. Ordinary Simulated Annealing (OSA)

The ordinary SA method (OSA) starts with one configuration which belongs to search space and represents the initial solution, also, the neighborhood of the initial solution

is as one configuration selected randomly within search space [130], [131]. This configuration consists from number of points belong to the search space. The shape and number of solution in the search space is design depend on the structure of optimization problem. In this method, search becomes restricted to a small portion of the feasible domain because the new configuration is generated in the neighborhood of the current ones. The ordinary SA optimization method is used for large or huge search space problems.

Herein, the ordinary SA method also applied for proposed procedure for complex structural models to get faster convergence with small number of iterations during optimization process.

4.5.4.3. Direct search Simulated Annealing (DSA)

The direct search simulated annealing (DSA) method differs from ordinary SA in two issues; firstly it adopts a set of current configurations rather than just one configuration and secondly it keeps the best configuration [131]. That means in the direct search SA, there is a memory to save the best set of configurations, which includes the near global solution and return to that set to search more precisely for the best solution.

The drawbacks of this method that it replaces the worst current configuration if it accepts a configuration generated during iterations and that appears when a large number of variables is adopted in the optimization problem [130]. Therefore, this methods is not adopted in the presented study.

4.5.5. Termination criteria adopted in SA method

In this thesis, the proposed SA optimization algorithm terminates when one of the following situations occur:

1-The limited maximum number of iterations (adopted in the range [200 - 1000] depend on the type of structural model problem) is reached.

2-The minimum value of objective function (optimum) (adopted here is zero) or near optimum value with a suitable certain level of convergence between two subsequent iterations is achieved.

3-The alteration in the improvement of objective function is less than the function tolerance (adopted as 0.001).

4-The system of the problem becomes freezing, which is mean that the temperature of the system less than one.

4.6. Application of adopted SA algorithm in some optimization problems

For the purposes of verification of the adopted SA algorithm, exploration of the optimum value in mathematical function, as optimization problem, is studied. This function used as benchmark problem to check the results of the adopted SA algorithm to detect the optimum value and compare it with the mathematical exact minimum value.

The benchmark problem with continuous variable is defined in Eq. (4.28) and tested in [128]:

$$f(x) = c_1 . \left[\frac{(c_2 . x)^4}{4} - \frac{(c_2 . x)^3}{3} - (c_2 . x)^2 \right] + 3 . c_1 \qquad 4.28$$

where are:

x - a continuous variable,

c_1, c_2 - a constant parameters.

The mathematical solutions of the benchmark for defined constant parameters are:

1- The global minimum of the function f_{min}^{globa} when $x = 2 / c_2$.

2- The local minimum of the function f_{min}^{local} when $x = -1 / c_2$.

For the determination of the exact value of the benchmark function, the values of constant parameters is adopted as $c_1 = 2$ and $c_2 = 3$. Therefore, the diagram of the values of the benchmark function is shown in *Figure 4.3*:

1- The global minimum of the function $f_{min}^{globa} = f(x = 0.666) = 0.666$.

2- The local minimum of the function $f_{min}^{local} = f(x = -0.333) = 5.166$.

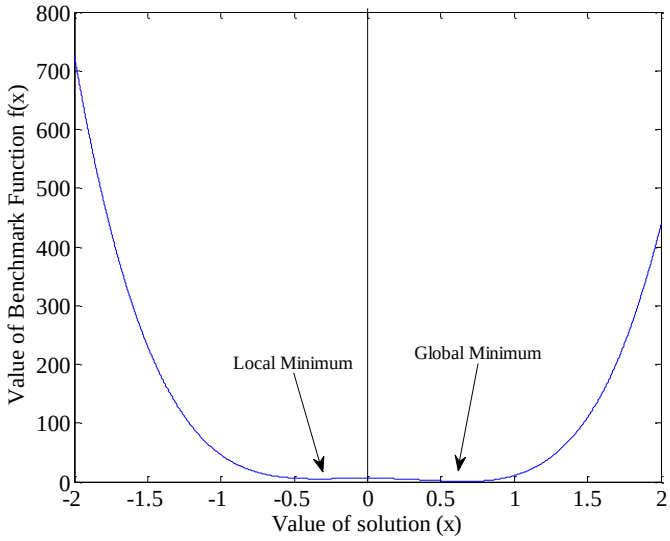

*Figure 4.3. Diagram of benchmark function(Eq. (*4.28*)) for the adopted constant parameters values* $c_1 = 2$ and $c_2 = 3$

For this test, the adopted parameters of SA algorithm are $T_o = 5000$, $\alpha = 0.95$ and the initial solution of benchmark is assumed at $x_{initial} = 0$ and the value of benchmark function is $f_{initial} = f(x_{initial}) = 6$. The adopted SA algorithm procedure is written as subroutine in MATLAB software. The subroutine of SA algorithm detected the numerical value of the benchmark of $f_{min}^{optimal} = 0.6667$ at $x = 0.6655$ after 76 iterations with accuracy of -0.0007 and maximum number of iteration of 168, as shown in *Figure 4.4*.

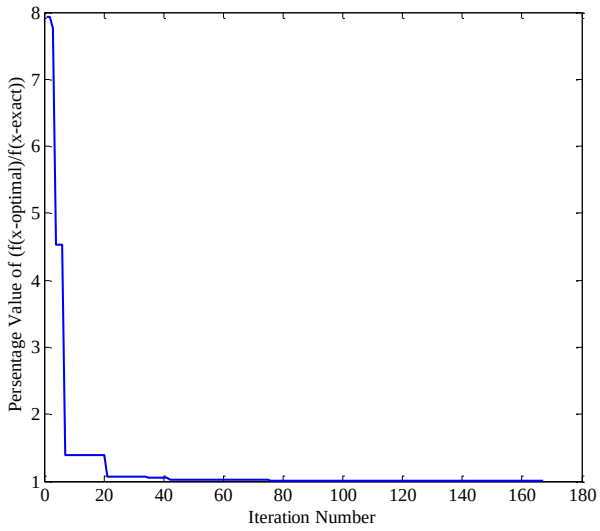

*Figure 4.4. Improvement of optimal value of benchmark function (Eq. (*4.28*)) for the adopted constant parameters values* $c_1 = 2$ and $c_2 = 3$ *according to exact value during SA algorithm process*

The results of the test adopted SA algorithm exhibit the high accuracy and reliability of the procedure that will be adopted for the proposed structural damage detection procedure in the next chapters.

4.7. Adopted objective function for SA method

In this thesis, the presented form of objective function, which is adopted in all parts of the study for the application of proposed SA optimization procedure for damage detection. The proposed objective function includes two parameters: the difference in modal natural frequencies between the experimental damaged and the numerical updated model. The second part is the differences in normalized scaled mode shape vectors for experimentally selected measurement points between the experimental damaged and numerically updated model. Those parameters are chosen due to their significant influence on the observed task. The proposed form of objective function includes some modifications of the previously used forms of objective function, while, the adopted form of objective function is defined by Eq. (4.29):

$$\text{Obj\_Fun}_{\text{proposed}} = W_f \,.\, \text{Freq} + W_d \,.\, \text{Disp} \qquad 4.29$$

where are:

W_f and W_d - weighting factors of two parts of the proposed objective function, difference in natural frequencies and difference normalized mode shape vectors, respectively,

Freq and Disp - the differences in the natural frequencies and normalized mode shape vectors between experimentally extracted from damaged model and numerically estimated from updated FE model, respectively.

The values of weighting factors depend on the type of structural model which is adopted herein to verify the proposed damage detection procedure. The first part of proposed objective function represents the summation of relative difference (error) square in the natural frequencies between experimentally extracted from damaged model and numerically estimated from updated FE model, as given in Eq. (4.30):

$$\text{Fun}_{\text{f}} = \sum_{i=1}^{n} \left(\frac{f_i^{\,exp\text{-}dam} - f_i^{\,num\text{-}updated\text{-}dam}}{f_i^{\,exp\text{-}dam}} \right)^2 \qquad 4.30$$

where are:

$f_i^{\,exp\text{-}dam}$ and $f_i^{\,num\text{-}updated\text{-}dam}$ - represent modal natural frequencies extracted from experimental testing for damaged structural model and estimated from numerical computation for the updated damaged FE model, respectively,

n - the number of included modes in the computations.

In order to reach the targets in damage detection procedures, namely, detection of the damage location and extent, the precise mathematically defined norm is adopted as a measure of difference between mode shape vectors in the second part of the proposed objective function. The differences in normalized mode shape vectors, with components corresponding to measuring points and directions, are taken into account by representing the difference between the values of normalized scaled displacement components of all observed modal vectors, as given in Eq. (4.31).

$$\text{Disp} = \sum_{i=1}^{n} \left[\sqrt{\sum_{j=1}^{m} \left(\phi_{ij}^{\exp - dam} - \phi_{ij}^{num-updated-dam} \right)^2} \right] \qquad 4.31$$

where are:

$\phi_{ij}^{exp-dam}$ and $\phi_{ij}^{num-updated-dam}$ - the normalized mode shape vector components in vertical and horizontal directions at measurement points, extracted experimentally from damaged model and estimated numerically from updated damaged FE model, respectively.

m - the total number of components of experimentally selected measurement points (accelerometers), located at particular nodes of the structural model.

So, the final form of proposed objective function with its weighting factors is given in Eq. (4.32):

$$\text{Obj\_Fun}_{\text{proposed}} = W_f \cdot \sum_{i=1}^{n}\left(\frac{f_i^{exp\text{-}dam} - f_i^{num\text{-}updated\text{-}dam}}{f_i^{exp\text{-}dam}}\right)^2 + W_d \cdot \sum_{i=1}^{n}\left[\sqrt{\sum_{j=1}^{m}\left(\phi_{ij}^{\exp-dam} - \phi_{ij}^{num-updated-dam}\right)^2}\right] \quad 4.32$$

In general, the application of one form of objective function for different structural damage detection procedures is very rare in the previous researches even with the structure is simple or complex. Herein, this meaning takes into account to preserve the same objective function for all adopted structural models regardless if simple or complex structure.

5. EXPERIMENTAL TESTING OF THE ADOPTED STRUCTURAL MODELS

5.1. General

This chapter describes the experimental process that is performed to extract the dynamic characteristics of the adopted four structural models in this study. This part of the study represents a first part of the main three parts included in the proposed SHM procedure in presented thesis to detect damages in structural models, as shown in Figure 1.1. The experimental test is conducted for all adopted structural models; overhang beam, grid bridge, Vierendeel bridge and 10-story building model.

The structural models are set up in the available space of laboratory with suitable designed scale differs from model to another. The scaled structures are designed depend on the geometry, wide, length and high of the each real structure. In addition, some changes in the scaled structures are made to idealize the structural models to facilitate the erection and experimental test process.

As mentioned previously in chapter three, the excitation method adopted in present study is by simulating the ambient vibration measurements using shaker device installed directly neighbouring to the structural models to record dynamic response (output response only). The ARTeMIS extractor software is used to extract dynamic characteristics/modal properties, natural frequencies and mode shapes, of the structural models.

The main objective of this chapter is outlying a set of laboratory testing that is implemented to measure vibration response of adopted structural models at different states of loading for intact case of the models. The states of the loading are conducted in two states of adding masses; the first is without additional masses (original state of the models e.g. self weight) and the second state is implemented by adding additional masses over the structural model in selected positions. The additional masses state of the models is studied to increase the range of the modal properties values of the structural models to predict the real behaviour of the structures. Only two structural models are tested for the additional

masses state; grid bridge and Vierendeel bridge model while the simple overhang beam and 10-story building model are tested by only the original self weight.

Also, the experimental test is implemented for the damaged structural models after performing the adopted damage scenarios for all adopted structural models to extract the modal properties. Different locations of damage with different extents are implemented on the structural models to verify the proposed damage detection procedure. The experimental test of the damaged state of the models in one damage location are performed after testing of the intact state of the models and then repairs that damage to create the new damage location.

In this study, the experimental modal analysis of the adopted structural models is performed in the construction laboratory of the Faculty of Civil Engineering at University of Belgrade. All devices, equipments and tools are prepared by the author and staff of the laboratory to implement the experimental test which are available in the laboratory of the faculty. The erect of the structural models is conducted by formers staff imported from special company for the building of the steel structure in Belgrade. The steel materials and tools are bought from the market in Belgrade city provided by special company.

5.2. Experimental modal analysis of the simply supported overhang beam model

In this study, the first tested structural model is a simply supported steel overhang beam. The selection of this beam model is as simple case to implement the experimental testing and extracting the modal properties. The present study adopted this model as a simple beam structure has only the flexural behavior. This beam model has only movement in one direction, vertical displacement, and the transverse and longitudinal displacements are very small and neglected. The verification of proposed damage detection procedure could start with the simple model and later with more complex structures.

5.2.1. Description of the overhang beam model

The simply supported steel overhang beam has the total length of 1500 mm with rectangular cross section of dimensions of 5x50 mm. The overhang of 20 mm was made on the left-hand side to provide support, while the overhang of 380 mm was made on the right-hand side to make the structure unsymmetrical. The mid-span length between the supports was 1100 mm. Initial material properties adopted by modulus of elasticity of $E_{\_initial}$=2x10^5 N/mm^2, Poisson's ratio ν=0.3 and mass density $\rho_{\_initial}$=7.860x10^3 kg/m^3. The schematic view of the beam setup is shown in *Figure 5.1*.

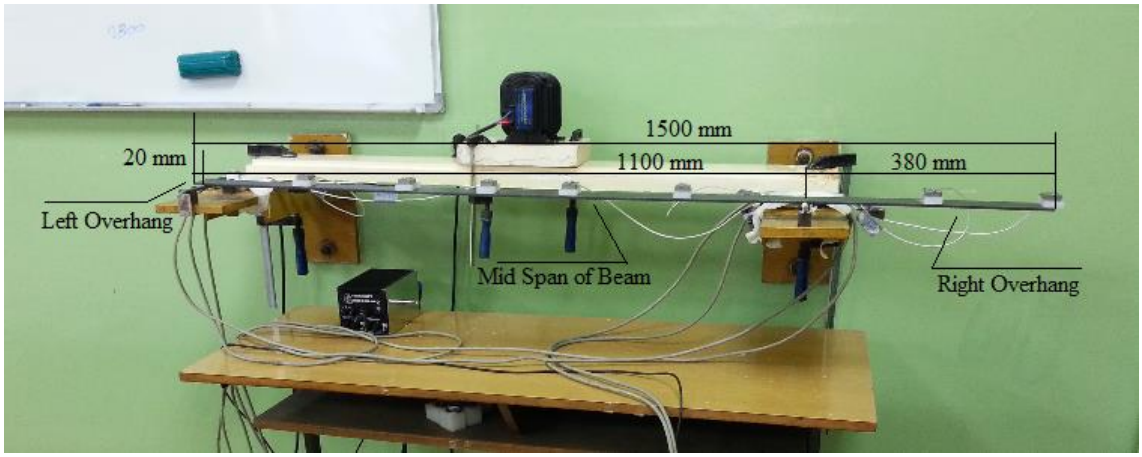

Figure 5.1. Overhang steel beam model

The overhang beam model is supported by two types of supports; the hinge support used at left hand side of the beam model, *Figure 5.2* (a), and roller support used at right hand side of the beam model, *Figure 5.2* (b),. The supports are designed to act as hinge and roller boundary conditions in two support locations along the length of the beam.

(a)  (b) 

Figure 5.2. Simple supports of overhang steel beam model (a) left hinge support and (b) right roller support

Those supports are designed to prevent movements in the direction parallel to the vertical axis of the beam cross section. In addition, the hinge support at the left side, *Figure 5.2* (a), is designed to prevent one more movement in the direction of longitudinal axis of the length of the beam model. The two supports are created by setup beam cross section on the circular section of two steel rods used as roller supports. Those two steel rods are based on two grooved cubic steel parts which are screwed by bolts on the thick base plate installed on the wall, as shown in *Figure 5.1*. The hinge support is created using glue the beam cross section on the circular section of steel rod, as shown in *Figure 5.2* (a).

The way of fixed the supports is necessary in the experimental testing to prevent any undesirable movement in the supports during the excitation of the structural model by simulated ambient vibration using shaker device. Also, the vibration response of the beam model could include contributions from more modes of vibration. This is helpful in damage detection process to have a diverse range of modal modes in the vibration response of the beam model and important to not miss the response from a vibration mode which may be affected by the damages in the structural model.

5.2.2. Positions of the accelerometers on the overhang beam model

As mention previously in the paragraph 3.5.3.4, the location of accelerometers on the structural model is one of the important issues in the experimental testing to gain the real structural behavior of the structure.

In this study and for overhang beam model, some trials is designed and applied to fix the appropriate distribution of accelerometers positions using seven accelerometers. Also, during fixing the distribution of accelerometer positions, the more important point takes in the account which is not putting the sensors on the stationary nodes of major vibration modes of the beam mode. The stationary point means the point have zero displacement vector in the mode shape vectors. Due to the simple geometry of the beam model, these stationary nodes are identified and designed positions of seven accelerometers along the length of beam model are shown in *Figure 5.3*. It is clear from figure that the length of the beam model divided into 10 nodes and nine elements with unequal lengths. The unequally of element length is due to distribution of accelerometers and supports position and overhang lengths.

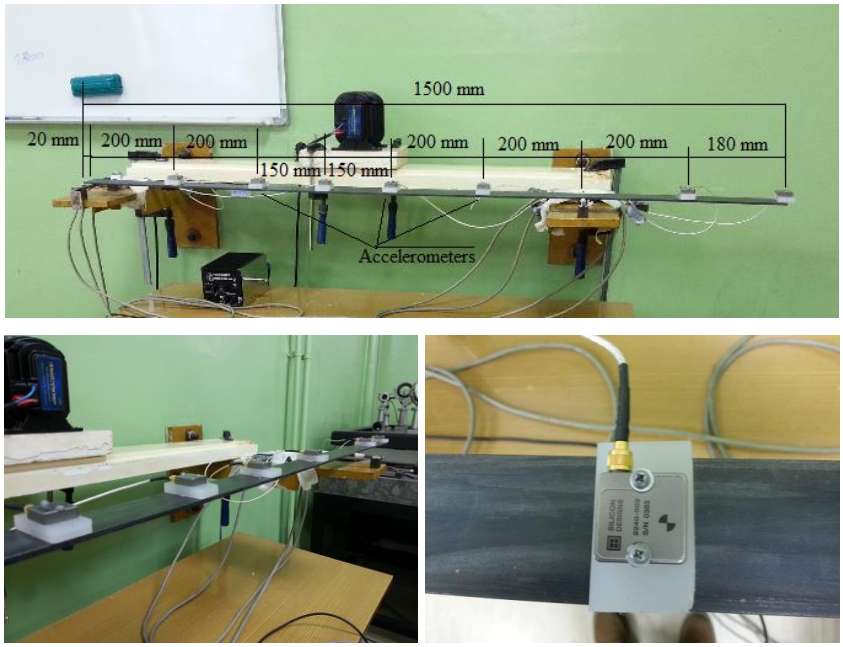

Figure 5.3. Distribution of accelerometer positions along the length of overhang beam model and installation on the silicon cubic part

5.2.3. Data acquisition system and signal processing using simulated ambient vibration of the overhang beam model

Ambient vibration simulation is carried out using a music device, bass shaker, which produces low vibrations in the range from 5 Hz to 200 Hz. It was installed on the independent wood beam connected with both supports of the beam model. Seven accelerometers of low noise, high sensitivity and low frequency accelerometers, Silicon Designs Model 2400 with the range of DC-600 Hz, are used for vibration measurements and installed and placed on cubes glued on the beam.model. Data acquisition was conducted by 24-bits 8 channel HBM - Hottinger Baldwin Messtechnik, QuantumX measuring amplifier, as shown in *Figure 5.4*.

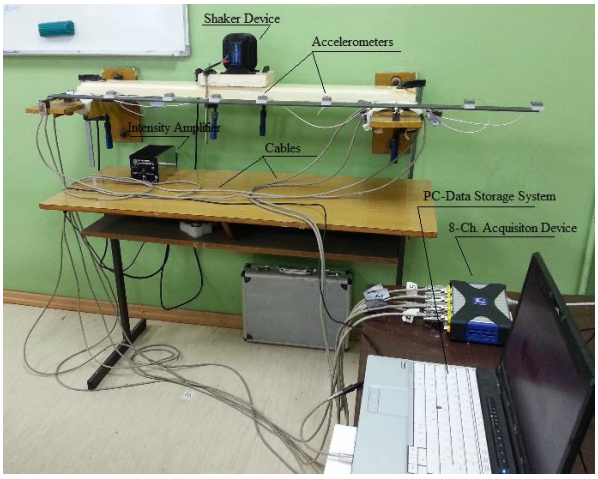

Figure 5.4. Data acquisition system of overhang beam model

The process of experimental testing is started by holding the shaker device with specified intensity and recording the acceleration response of the overhang beam model from seven specified accelerometers. The excitation vibration using shaker device is random vibration signals generated by MATALB software from some music file. The increase of intensity is required to decrease the undesirable noise during recording data and many trials are implemented to fix the suitable value of intensity of 2, 3 and 5 to be more confidence and intensity value of 5 is used.

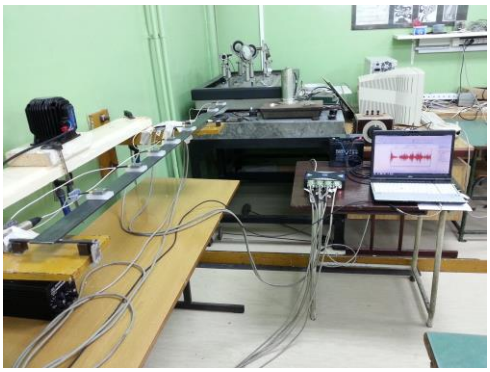

Figure 5.5. Recorded data during simulated ambient vibration measurements of overhang beam model

The program CAT-MAN software provided with acquisition device is installed in a Dell Inspiron laptop to record vibration response of the structural model, as shown in *Figure 5.5*. The frequency range of the vibration response of the overhang beam has been investigated using numerical model. Also, several trials of testing are performed on the model in order to select the appropriate sampling frequency of the vibration response and those trials are necessary to better understand the frequency content of the vibration response of the beam model under random vibration signals applied by the shaker device. The time recording is 20 min with sampling frequency of 600 Hz and filtering frequency of 200 Hz.

Herein and for this model, the recorded data of accelerometers include only the vertical movement at each measurement point of the seventh measurement points. The sample of acceleration history of the one accelerometer recording data of the overhang beam model for the first 100 seconds of the recording is shown in *Figure 5.6* and the others are shown in Appendix - A1.

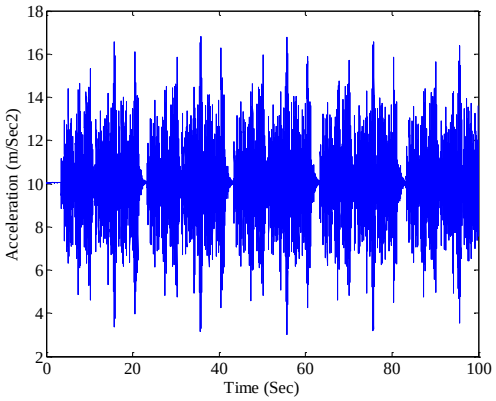

Figure 5.6. Acceleration history time for one accelerometer during simulated ambient vibration measurements using shaker of intact overhang beam model

There are some steps to define the geometry of structure and parameters of experimental analysis in the ARTeMIS software in specified file to start data processing of the recorded data. Those steps are:

1- The geometry of the structural model in coordinate system is written in CFG file defined in ARTeMIS software. In this file also the title of the project, the sampling frequency, name of recorded data file and description of the accelerometers and their direction of movements during excitation are written, as listed in Appendix -B. The geometry of the overhang defined in ARTeMIS software and distribution of accelerometers along the length of beam model are shown in *Figure 5.7*. In this case of measurement, there is no need to specify the reference point (reference accelerometer) because it is only one set of measurement points.

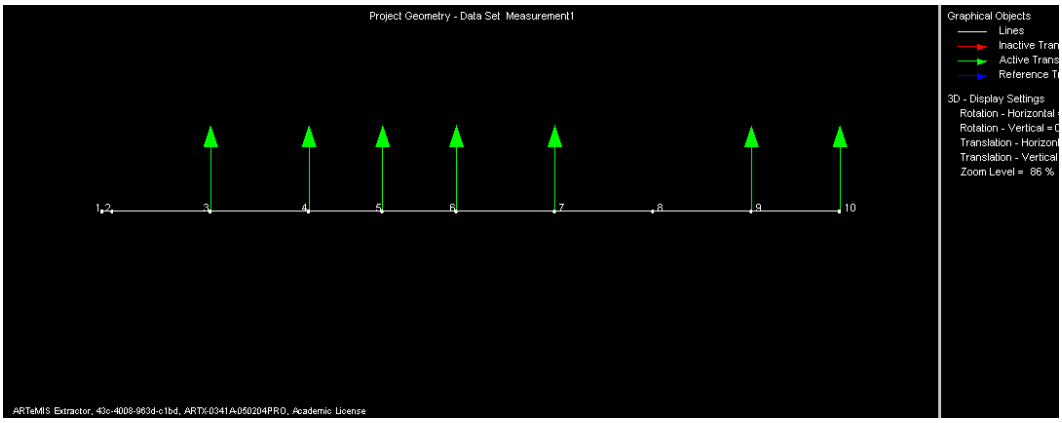

Figure 5.7. Geometry of overhang beam model and distribution of accelerometers along the length of intact overhang beam model

2- The parameters of data processing in ARTeMIS software is adopted to process the recorded data. Those parameters are such as; sampling frequency (600 Hz), number of channels (7), number of frequency line (1024), frequency line spacing (0.293 Hz), overlap (66.67 %), filtering (Butterworth) and window function (Hanning).

Then, the data processing is conducted to estimate the average of the normalized singular value of spectral density matrices of data set and from which the peak picking procedure is applied to extract the modal properties of the overhang beam model.

5.2.4. Extraction of modal properties of the intact overhang beam model using ARTeMIS extractor software

The modal frequencies and mode shapes of the intact overhang beam model are extracted using ARTeMIS - extractor software which is the state-of-the art of ambient vibration analysis. Frequency domain decomposition (FDD) technique is implemented by peak picking procedure with several measurement trials. Those trials are done to provide more confidence (5 trials for intact case) with the corresponding estimation of modal properties, according to the spectral density matrices, estimated using the recorded ambient vibration data.

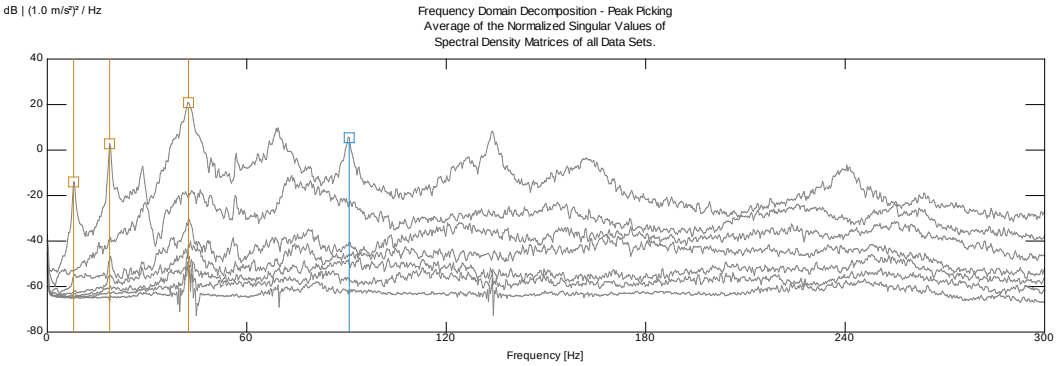

Figure 5.8. Spectral density matrices with selected modes using FDD estimation procedure in ARTeMIS extractor software of intact overhang beam model

The spectral density matrices of all measurement data of the overhang beam model are shown in *Figure 5.8*. The structural modes are estimated using the peak-picking procedure, according to FDD estimation technique explanation in paragraph 3.5.4. The vertical lines in figure represent the peak picking modal modes in FDD method which mean only the real structural modes are selected. The final results of the first four modal frequencies and the modes characters of the overhang beam model are listed in Table 5.1.

Table 5.1: Experimental extracted modal frequencies using ARTeMIS extractor for intact overhang beam model

Mode No.	Frequency Value of Intact Model (Hz)	Mode Character
1	7.910	1st Bending
2	18.750	2nd Bending
3	42.480	3rd Bending
4	90.820	4th Bending

Also, the first four mode shapes results and their characters corresponding to the natural frequencies of the overhang model are shown in *Figure 5.9*. The values of the first four mode shape vectors of the overhang beam model are provided as output SVS system file from the ARTeMIS software, as shown in Appendix -C.

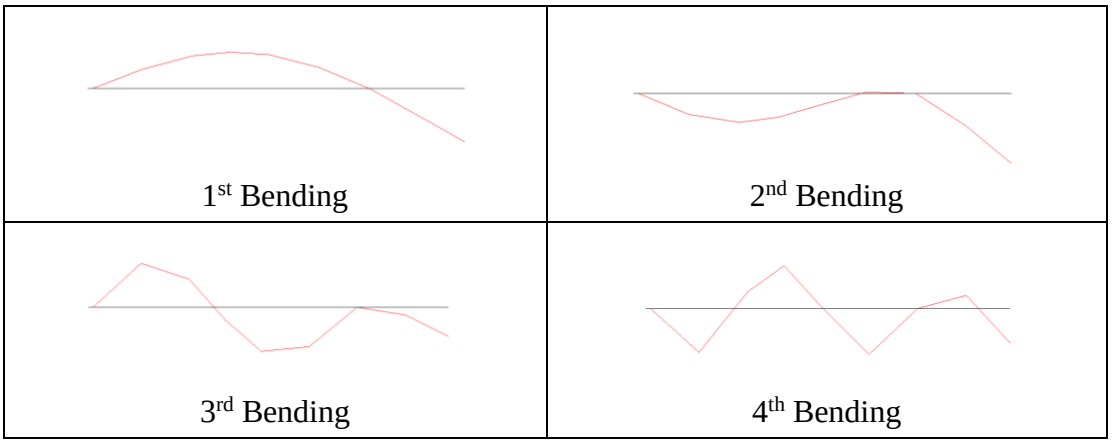

Figure 5.9. Experimental modal properties of the intact overhang beam model by FDD technique procedure using ARTeMIS extractor software

The values of the first mode shape vectors for the 10 nodes are listed in Table 5.2 for three axes, where in this model only the Z-axis is included for the vertical movement of the measurement points. The maximum value of displacement vector is at node number 10 and equal of 1. Those vector values are normalized depend on the maximum vector value, therefore all other points vectors are less than the maximum vector value of 1, as listed in Table 5.2.

Table 5.2: Experimental extracted mode shape vectors using ARTeMIS extractor for intact overhang beam model

Node No.	Displacement Vector-X	Displacement Vector-Y	Displacement Vector-Z
1	0.000	0.000	0.000
2	0.000	0.000	0.000
3	0.000	0.000	0.365
4	0.000	0.000	0.614
5	0.000	0.000	0.683
6	0.000	0.000	0.637
7	0.000	0.000	0.395
8	0.000	0.000	0.000
9	0.000	0.000	0.522
10	0.000	0.000	1.000

The exported output file from ARTeMIS software provide vector values with positive signs for all measurement points, therefore for the purposes of computations, the vectors values signs are assumed and taken as in the numerical results. In addition, to verify the final results of the extracted modal properties, the MAC values for the overhang beam model are calculated by Eq. (4.10) to obtain an indication for the relationship between each two modes, as listed in Table 5.3. The table shows the correlation between each two extracted modes of the model where the MAC values for each different modes are very small close to zero and equal 1 for each equal modes. Those MAC values verify the validity of the extracted modes with respect to their stability and the modes represent the real structural modes.

Table 5.3: MAC values of extracted mode shapes corresponding to natural frequencies using ARTeMIS extractor for intact overhang beam model

Frequency Value (Hz)	7.910	18.750	42.480	90.820
7.910	1	0.2488	0.0996	0.242
18.750	0.2488	1	0.1851	0.1722
42.480	0.0996	0.1851	1	0.09281
90.820	0.242	0.1722	0.09281	1

Also, the MAC values could be presented as a bar charts which is provided in ARTeMIS software, as shown in *Figure 5.10*.

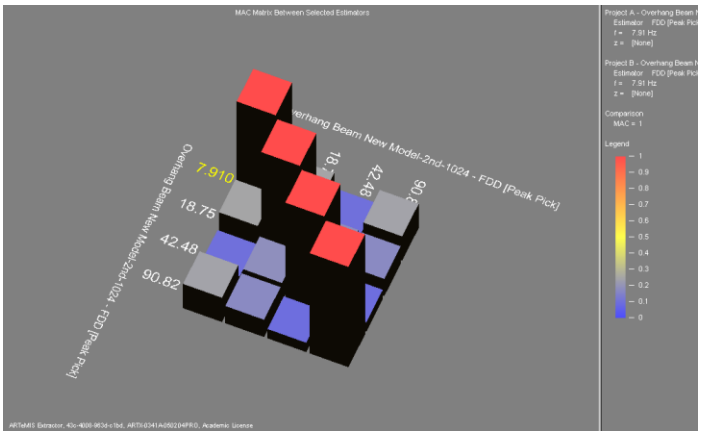

Figure 5.10. Bar charts of MAC values of experimental modal properties of the intact overhang beam model using ARTeMIS extractor software

5.2.5. Implemented damage scenarios in the overhang beam model

For the overhang beam model, two different damage extent scenarios are implemented to investigate the behavior of structural model and efficiency of the proposed procedure for detecting small and large extent of crack/notch. The location of damage is selected in position has significant impact on modal frequency changes. Damage is located at the distance of 397.5 mm c/c from the left edge of the beam, close to the second accelerometer, while the studied damage scenarios have different extents. The damage is created by cutter machine from the bottom side of the cross section

The first damage scenario, DC-1, consists of crack of 1.9 mm depth and 25 mm width on the cross section of overhang beam model at a distance of 387.5 mm from the left support, as shown in *Figure 5.11*. The first one is a small damage relatively, which afterwards extended and become more serious in the second one.

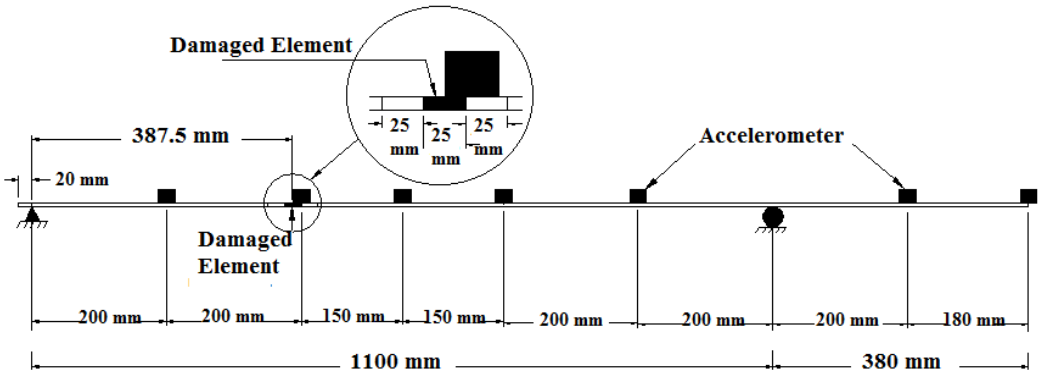

Figure 5.11. Location of damage scenarios on the overhang beam model with Accelerometers positions

Further extension of the entire damage produced the second scenario of damage, DC-2, by increasing crack depth from 1.9 mm to 2.75 mm of entire damage width of 25 mm at the same position, as shown in *Figure 5.12*.

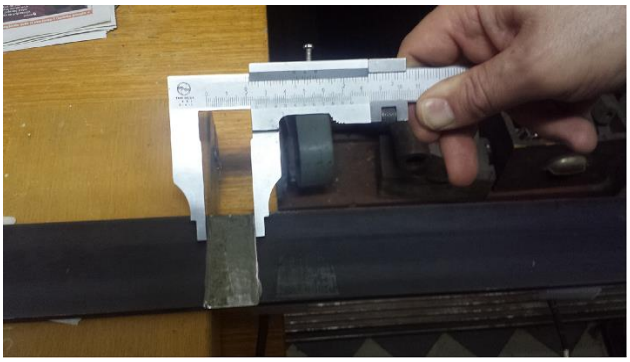

Figure 5.12. Extent of second damage scenario DC-2 on the overhang beam model

5.2.6. Extraction of modal properties of the damaged overhang beam model using ARTeMIS extractor software

After implementation of damage scenarios, three trials of ambient vibration measurements are carried out for each of the two damage scenarios in order to improve reliability in the extracted modal properties. The modal properties, natural frequencies and

mode shapes, of the damaged overhang beam model are extracted using ARTeMIS software with the same mentioned procedures of the intact model.

Table 5.4: Experimental extracted modal frequencies using ARTeMIS extractor for both damaged and intact overhang beam model

Mode No.	Frequency Value of Intact Model (Hz)	Frequency Value of Damaged Model (Hz)			
		DC-1	Reduction (%)	DC-2	Reduction (%)
1	7.910	7.910	0	7.031	11.11
2	18.750	18.160	3.15	17.58	6.24
3	42.480	41.310	2.75	39.84	6.21
4	90.820	90.530	0.32	90.53	0.32

The same values of parameters of data processing and experimental analysis are used for the damaged model. The first four values of modal frequencies for both damaged, both damage scenarios, and intact model are listed in Table 5.4. Respect to the intact model, in the case of DC-1, different frequency values are extracted for the second, third and fourth modes from experimentally recorded data, while in case of DC-2 different frequency values are extracted for all four first modes with more significant differences.

5.3. Scale of the large structural model

Any structural model must be designed, loaded, and interpreted according to a set of similitude requirements that relate the model to the prototype structure. These similitude requirements are based upon the theory of modelling, which can be derived from a dimensional analysis of the physical phenomena involved in the behaviour of the structure. Accordingly, this section discusses two distinct topics [132]:

1- Dimensional analysis and similitude theory.

2- Actual similitude requirements for different type of structural models, aimed at studying their response under elastic load conditions as well as under dynamic loading.

Particular emphasis is given to models of structures undergoing dynamic loading effects because this is an area where physical scale model testing can be of significant help to the structural engineer.

The qualitative characteristic enable physical phenomena to be expressed inserting fundamental measures of nature. The three general classes of the physical problems, namely mechanical (static and dynamic), thermodynamic and electrical, are conveniently described qualitatively in terms of the following fundamental measures [132]:

1- Length

2- Force (or mass)

3- Time

4- Temperature

5- Electric charge

these fundamental measures are commonly referred to as dimensions. Most structural modeling problems are mechanical, thus, the measures of length, force, and time are most important in structural modeling works.

The quantitative characteristic is made up of both a number and a standard of comparison. The standard of comparison, also called the standard unit, was often established rather arbitrarily from traditional usage (such as the inch). Each of the fundamental measures, or dimensions, thus has its associated standard units in the several different unit systems in use today (U.S. customary, SI , metrics, etc). Dimensions and units are such logical quantities that they are now taking completely for granted. It is difficult to realize that the present state of the physical descriptions of occurrences did not always exist.

The theory of dimensions can be summarized in two essential facts [132]:

1- Any mathematical description (i.e., equation) that describes some aspect of nature must be in a dimensional homogeneous form. That is, the governing equation must be valid regardless of the choice of dimensional units in which the physical variables are measured. As an example, the equation for bending stress, $\sigma = M.c/I$, is correct regardless of whether force and length are measured in Newton and meters, pounds, and inches, or other consistent units.

2- As a consequence of the fact that all governing equations must be dimensionally homogenous, it can be shown that any equation of the form:

$$F(X_1, X_2, ..., X_n) = 0 \quad (5.1)$$

can be expressed in the form

$$G(\pi_1, \pi_2, ..., \pi_m) = 0 \quad (5.2)$$

where are:

π - (pi) the terms of dimensionless products of the n physical variables $(X_1, X_2, ..., X_n)$,

$m = n - r_d$,

r_d - the number of fundamental dimensions that are involved in the physical variables.

The dimensional homogeneity among the physical parameters of the length L, modulus of elasticity E, gravitational acceleration g, and mass density ρ cannot be satisfied simultaneously when the bridge is scaled, because there are only three independent basic quantities (fundamental dimensions) which can be chosen arbitrarily. In the vibration based damage detection method, the primary variables are natural frequencies and mode shapes. Gravitational force has little influence on the values of natural frequencies and mode shapes, suggesting that the influence of the gravitational force can be neglected in the scaling process. The length L, modulus of elasticity E, and mass density ρ can then be chosen as the independent basic quantities. In that case, there are the following equations:

$$S_L = L_p / L_m \quad (5.3)$$

$$S_E = E_p / E_m \quad (5.4)$$

$$S_\rho = \rho_p / \rho_m \quad (5.5)$$

where are:

p and m - subscripts refer to prototype and model, respectively,

S_L, S_E and S_ρ - denote the relevant scaling factor for the length, modulus of elasticity and mass density, respectively, relating the prototype and model values. The scaling factors for

all other quantities associated with the model can be calculated from equations of S_L, S_E and S_ρ.

Dynamics of Structural model, time-dependant loadings, is one of the hard problem because of their complex nature and effect of structures, have placed small-scale structural model techniques on a par with an analytical techniques [132]. The dynamic loadings of interest to the structural engineer range from wind or traffic induced elastic vibrations to blast and impact loadings that can cause considerable structural damage. Vibration problems of elastic structures are very common in civil engineering practice. Prior to constructing the laboratory model, a preliminary numerical study is carried out to investigate the appropriate scaling model method to ensure that the dynamic behaviour of the laboratory mode could reproduce that of the scaled model. Therefore, it was necessary to investigate a scaling model method to properly scale the laboratory model from the prototype. In this study, the adopted four structures used for verification of the proposed SHM procedure are scaled as a one-third scale model of full scale real bridge in site for grid and Vierendeel bridge. For multi-storey (MS) building, the scale is a one tithe of the full scale real building based on the available space in the structural laboratory of the University of Belgrade.

Some scaling relationships for important standard physical parameters [132] with adopted parameters in this study are listed in the Table 5.5.

Table 5.5: Similitude requirements for the scaled models

Scaling Parameters	Dimension	Scaling Factors	Values of Scaling Factors According to [132]	Values Scaling Factors of Bridge Models	Scaling Factors Values of MSBuilding
Length	L	S_L	3	3	10
Displacement	L	S_L	3	3	10
Force	F	$S_E S_L^2$	9	9	100
Time	T	S_l	3	1	1
Frequency	T^{-1}	S_l^{-1}	1/3	1/3	1/10

Velocity	LT^{-1}				
Gravitational Acceleration	LT^{-2}			Neglected	Neglected
Acceleration	LT^{-2}				
Mass Density	$FL^{-4}T^{2}$				
Strain					
Stress	FL^{-2}	S_E	1	1	1
Modulus of Elasticity	FL^{-2}	S_E	1	1	1
Poisson's Ratio		1	1	1	1

Modeling with gravitational force neglected is convenient because the same mass density and strength values for the structural steel could be used for the scaling model as that of the prototype bridge. The same materials as that of the prototype were used, so the scale, relating to the Young's modulus and density of the materials used, assumed a unitary value.

5.4. Experimental modal analysis of the simply supported grid bridge model

The second tested structural model is a simply supported steel grid bridge as a first part of a prototype real superstructure had been constructed in site on the highway located in Cacak city in the south of Serbia. The scaled grid bridge model is constructed in the lab based on the selected scale factor, which is discussed before. The selection of this structural model is as an advanced case of structure to implement the experimental testing and extracting the modal properties. The present study adopted this model as a plane structure has torsion behavior as well as to the flexural behavior. In addition, this plane structural model has movements and rotations in two directions, vertical and transverse displacement as well as rotation about x and y-axis, and the longitudinal displacement and rotation about z-axis is neglected. In regarding to verification of proposed SHM procedure to detect

damage, this structural model is as common civil structural applications and moderate structure from simple to more complex structures.

5.4.1. Description of the grid bridge model

The simply supported steel grid bridge has 6800 mm long and 830 mm wide with 10 grids length of 672 mm. The main longitudinal edge and cross steel beams are rectangular hollow section dimensions of (30 x 50 x 2.8) mm. The deck of the bridge model is formed as a thin orthotropic plate made of steel, with thickness of 1.5 mm and with 7 longitudinal stiffeners spaced on 100 mm, *Figure 5.13*.

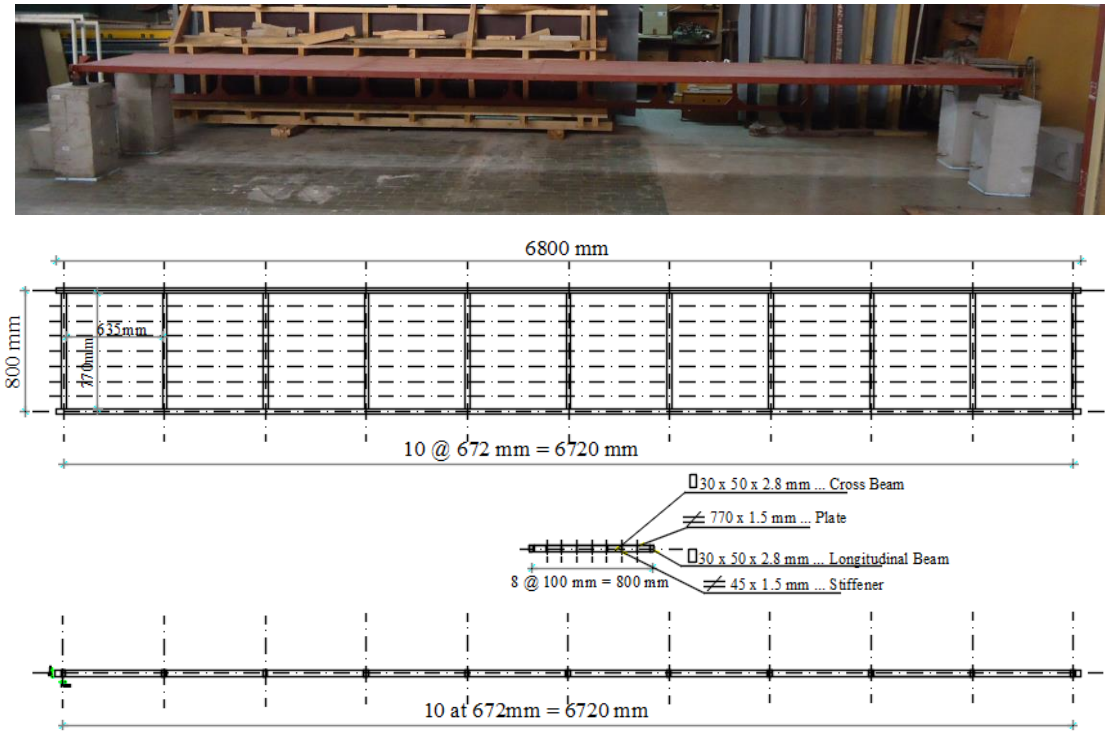

Figure 5.13. Layout of steel grid bridge structural model

The total width of the model is 800 mm c/c, containing 8-grid of 100 mm c/c. The grid bridge model is fabricated from two main longitudinal steel beams have rectangular hollow section of (30x50x2.8) mm located at the edges of the model. For the main transverse beams, eleven beams have the same section of (30x50x2.8) mm are used by

welding with the main two longitudinal beams to formulate the whole model. Additional longitudinal beams act as stiffeners for the model welded with the main transverse beams. The distribution of the stiffeners is equal over the total width of the model at 100 mm c/c. Each stiffener has a plate section of (45x1.5) mm, which is welded also with the top plate placed orthogonally. The plate of the deck is welded over the grid frame at 50 mm welding at 150 mm spacing, as shown in *Figure 5.14*.

All parts of the model are welded along the whole contact areas by the company staff and author. Firstly, the main longitudinal and transverse beams are welded then the stiffener beams with the thin plate and after that the grid plates are welded with the main parts of the structure, as shown in *Figure 5.14*.

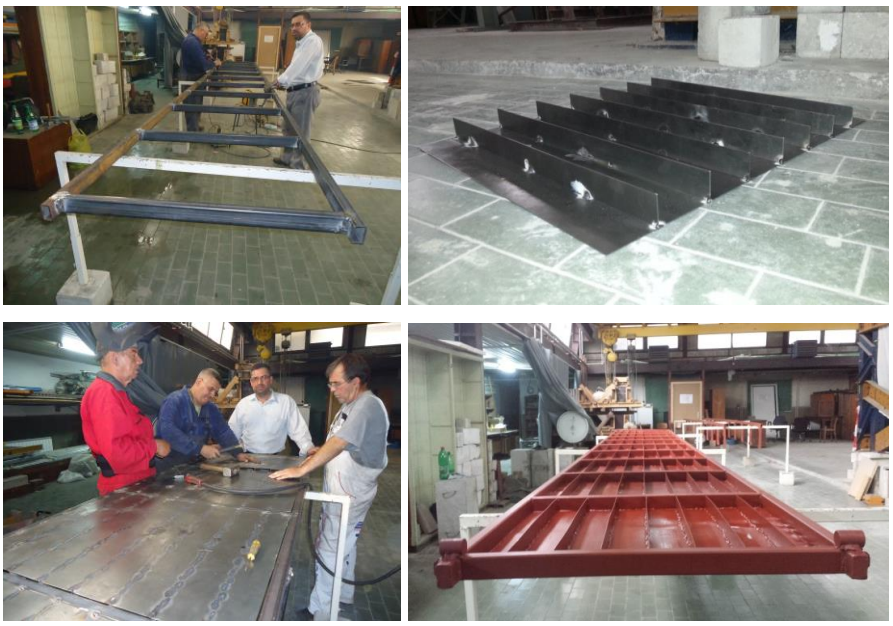

Figure 5.14. The grid bridge structural model during the erection stages

The grid bridge model is supported by four supports; two of them are hinge supports at left hand side of the model, as shown *Figure 5.15* (a) and (b). The other two supports at right hand side of the beam model are roller supports, as shown *Figure 5.15* (c) and (d). The fourth supports are set up to act as hinge and roller boundary conditions in two support locations along the length of the bridge model. All those supports are designed to prevent

movements in the direction parallel to the vertical axis of the beams cross sections. In addition, the hinge supports at the left side are erected to prevent two more movements in the direction of transverse and longitudinal axis of the length of the bridge model, as shown in *Figure 5.15* (a) and (b).

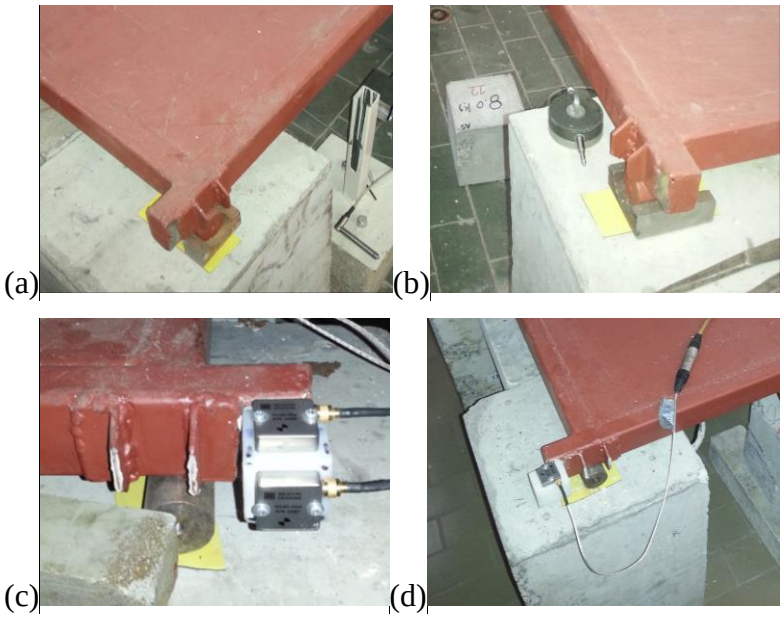

Figure 5.15. Simple supports of grid steel bridge model (a) first left hinge support, (b) second left hinge support, (c) first right hinge support and (d) second right roller support

Those four supports are erected by set up grid bridge beams cross sections on the circular section of four steel rods used as roller supports. For both hinge supports, the steel rods are based on thick base plate installed on a thin rubber pad, which are set up over cubic concrete parts, as shown in *Figure 5.15*. Each two concrete parts are connected together by two small cubic concrete parts using strong glue from upper and lower side. The hinge support is created by welding the circular section of steel rod from upper side with beams cross sections, as shown in *Figure 5.15* (a) and (b). The way of fixed the supports is necessary in the experimental testing to prevent any undesirable movement in the supports during the excitation of the structural model by simulated ambient vibration using shaker device.

In order to study modal frequencies in different frequency ranges, the grid bridge model is adopted in two loading states: without additional masses and with additional

masses, as shown in *Figure 5.16*. The model state with additional masses included 10-mass of concrete cubes placed at 50 mm joints of the main longitudinal and cross beams inside the span and the concrete masses have average mass of 7.925 kg, as shown in *Figure 5.16*.

(a)  (b) 

Figure 5.16. Grid bridge model of two loading states during testing (a) without additional masses (b) with additional masses

5.4.2. Positions of the accelerometers on the grid bridge model

For grid bridge model, several trials are implemented to fix the appropriate distribution of accelerometers positions using only eight accelerometers which are available. Due to the geometry of the grid bridge model, the accelerometers positions (measurement points) are selected in five sets along the length of model to cover as possible as the large number of degrees of freedom with limited numbers of accelerometers. Each set contains four measurement points with six degrees of freedom using six accelerometers. In each set, two points from right hand side have four degrees of freedom, two vertical and two transverse movements, and the other two points from left hand side have only two degrees of freedom of vertical movement, as shown in *Figure 5.17*. The other two accelerometers are used in specified measurement point with two degrees of freedom and this point is called "Reference Point", as shown in. This reference point is required to be in the same position for all sets during recording ambient vibration measurements to extract the modal properties of the grid bridge model using ARTeMIS software. All six accelerometers are set up on cubes glued on the intersecting nodes of the main and transverse beams of the bridge model except reference point is located at 84 mm from intersecting node, as shown in *Figure 5.17*.

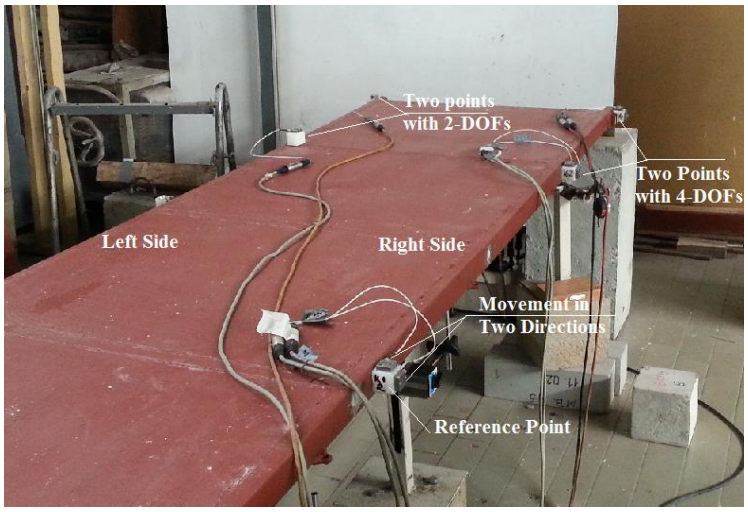

Figure 5.17. Distribution of eight accelerometers in the measurement points and movement directions in the first set of grid bridge model

The distribution of measurement points is adopted in five sets to present and reflect the real structural behavior, flexural and torsion, of the grid bridge model from ambient vibration measurements. The first, third and fourth set with distribution of accelerometers positions and directions are shown in *Figure 5.18*. Each set cover 2-grids from the 10-grids of the model, as shown in *Figure 5.13*.

(a)  (b)  (c) 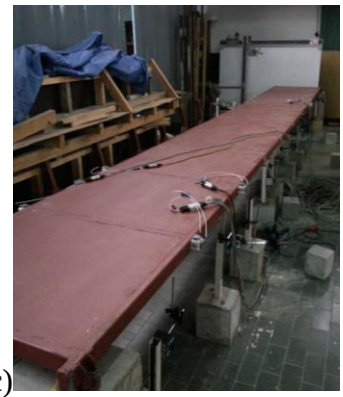

Figure 5.18. Distribution of sets of accelerometer positions along the length of grid bridge model with reference point (a) first set, (b) third set and (c) fourth set

The same distribution of measurement points is adopted for the model state with additional masses as five sets to present the real structural behavior of the grid bridge model from ambient vibration measurements. The first, third and fourth set with distribution of accelerometers positions and their directions are shown in *Figure 5.19*.

(a)  (b)  (c) 

Figure 5.19. Distribution of sets of accelerometer positions along the length of grid bridge model with additional masses (a) first set, (b) third set and (c) fourth set

5.4.3. Data acquisition system and signal processing using simulated ambient vibration of the grid bridge model

Simulation of ambient vibration measurements of the both grid bridge model states is carried out using the shaker device, acquisition device of 24-bits 8 channel and PC-storage system, as shown in *Figure 5.20*. The shaker device is installed on the lower connected concrete part between two concrete supports at right hand side of the model.

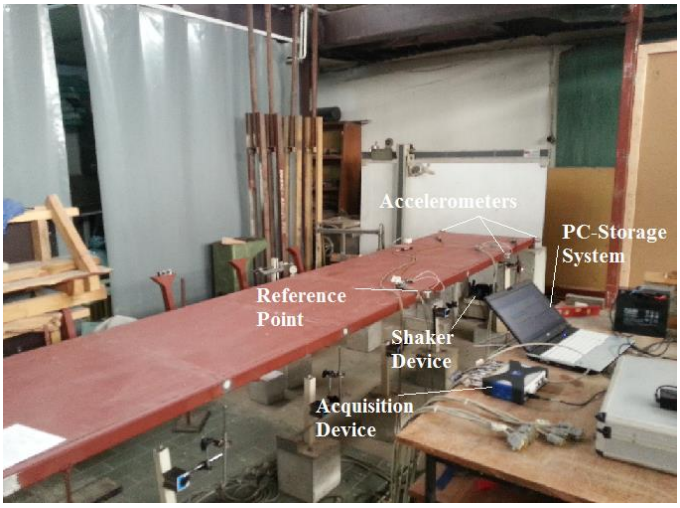

Figure 5.20. Data acquisition system of grid bridge model and the shaker device position

The process of experimental testing is started by holding the shaker device with specified intensity value of 5 using the same random vibration signals generated by MATALB software. The recording the acceleration time history of each specified accelerometers installed on the grid bridge model is stored in the PC as data file. The frequency range of the vibration response of the grid bridge model has been investigated using numerical model. Also, several trials of testing are performed on the bridge model in order to select the appropriate sampling frequency of the vibration response and the value of sampling frequency of 600 Hz and filtering frequency of 50 Hz are enough. The time of data recording is 30 min for each set. The same experimental testing process is conducted for the model state with additional masses, where it is the second stage after conducting the first testing for model state without additional masses.

For the grid bridge model, the recorded data of each set of accelerometers consist 5-vertical and 3-transverse movements including the reference point. The sample of acceleration history time of the first vertical accelerometers of the both grid bridge model states for the first 100 seconds of the recording are shown in *Figure 5.21* and the figures of acceleration time history of other accelerometers only for model state without additional masses are shown in Appendix - A2.

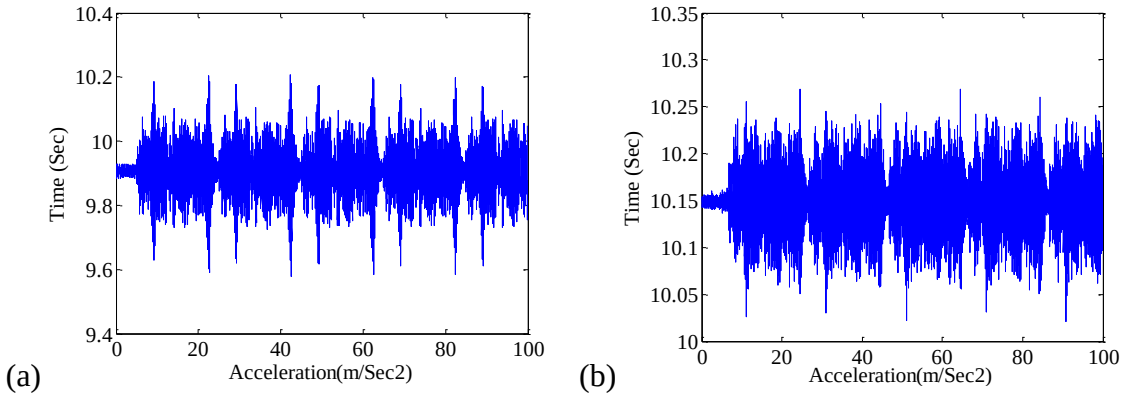

Figure 5.21. Acceleration history time for one accelerometer during simulated ambient vibration measurements using shaker of intact grid bridge model (a) without additional masses and (b) with additional masses

The geometry of the structural model in coordinate system, the title of the project, the sampling frequency, the names of recorded data file of all five sets and description of the accelerometers and their direction of movements during excitation are written in CFG file defined in ARTeMIS software. The geometry of the grid bridge model and distribution of accelerometers in each set of the five sets along the length of bridge model are presented in ARTeMIS software, as shown in *Figure 5.22*.

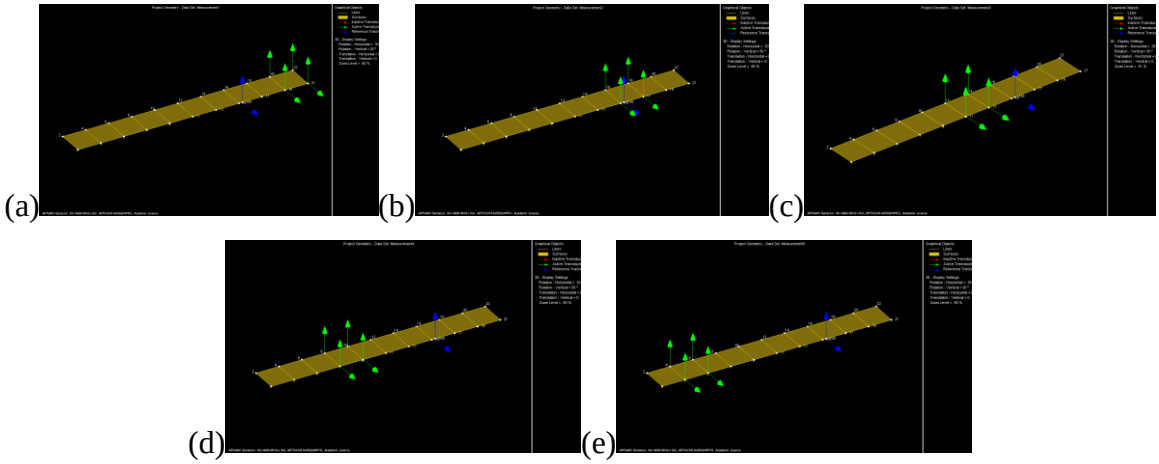

Figure 5.22. Geometry and distribution of accelerometers with reference point for (a) first set, (b) second set, (c) third set, (d) fourth set and (e) fifth set of measurements of intact grid bridge model

Figure 5.22 shows all five sets of measurements, in each set the blue arrows are the two movements (accelerometers) of the reference point, while the green arrows are six movements of the set measurements. Then, the data processing is conducted to estimate the average of the normalized singular value of spectral density matrices of all five data sets and from which the peak picking procedure is applied to extract the modal properties of the grid bridge model. Here, there is no effect of the model state with additional masses on representation in the ARTeMIS software and it is the same.

5.4.4. Extraction of modal properties of the intact grid bridge model using ARTeMIS extractor software

The modal frequencies and mode shapes of the intact grid bridge model are extracted using ARTeMIS - extractor software by the FDD technique. The peak picking procedure of FDD technique is implemented with number of frequency line of 8192 to get the appropriate frequency resolution and overlap of 66.67 %, filtering (Butterworth) and window function (Hanning). Several trials of measurements are conducted to provide more confidence of the extracted modal properties, according to the spectral density matrices estimated based on the recorded ambient vibration data. This procedure is implemented for both states of the model without additional masses and with additional masses. The diagram of the spectral density matrices of all data sets for both states of the grid bridge model are shown in *Figure 5.23*.

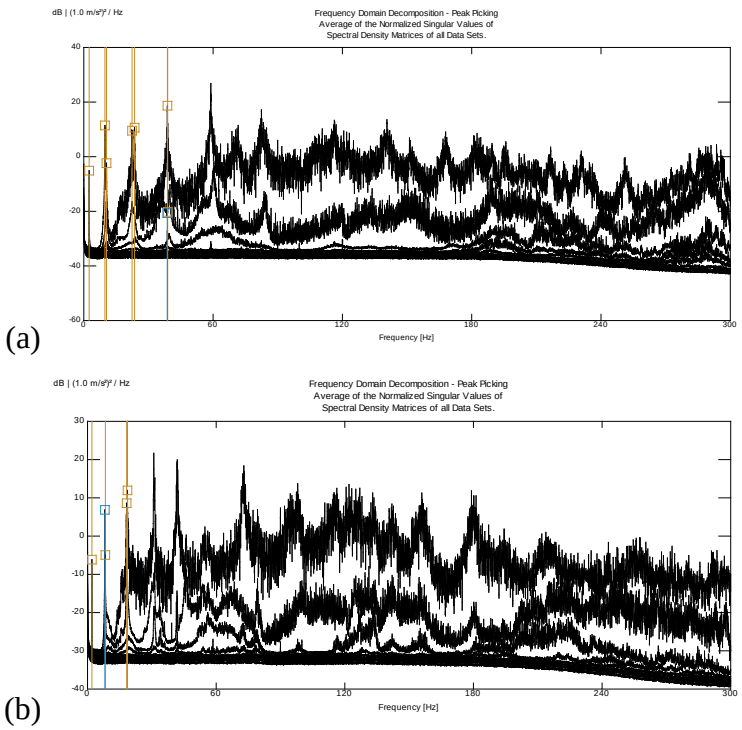

Figure 5.23. Spectral density matrices with selected modes using FDD estimation procedure in ARTeMIS extractor software of intact grid bridge model (a) without additional masses and (b) with additional masses

The structural modes are estimated using the peak-picking procedure, according to FDD estimation technique explanation in paragraph 3.5.4. The vertical lines in the figures represent the peak picking modal modes in FDD method, which means only the real structural modes are selected from the peaks. The results of the first five modal frequencies and the modes characters of the both grid bridge model states are listed in Table 5.6.

Table 5.6: Experimental extracted modal frequencies using ARTeMIS extractor for both intact grid bridge model states, without and with additional masses

Mode No.	Frequency Value of Intact grid bridge Model (Hz)		Reduction in Frequency		Mode Character
	Model State without Additional Masses	Model State with Additional Masses	(Hz)	Relative (%)	
1	2.490	2.051	0.439	17.63	1st Bending
2	9.814	8.093	1.721	17.54	2nd Bending
3	10.550	8.313	2.237	21.20	1st Torsion
4	22.410	18.240	4.170	18.61	3rd Bending
5	23.580	18.640	4.940	20.95	2nd Torsion

It is evident from table, that significant effect of the additional masses on the values of natural frequencies of loading state model with. The larger reduction is in the torsion modes than bending modes about 3-4 % and the minimum reduction is in the first mode and the maximum reduction is in the third mode.

On the other hand, the first five mode shapes results and their characters corresponding to the natural frequencies of the grid bridge model state without additional masses are shown in *Figure 5.24*. The values of the first five mode shape vectors of the grid bridge model state without additional mass are provided as output SVS system file from the ARTeMIS software. The extracted mode shape character for the model state with additional masses are same for the model state without additional masses, as shown in *Figure 5.24*.

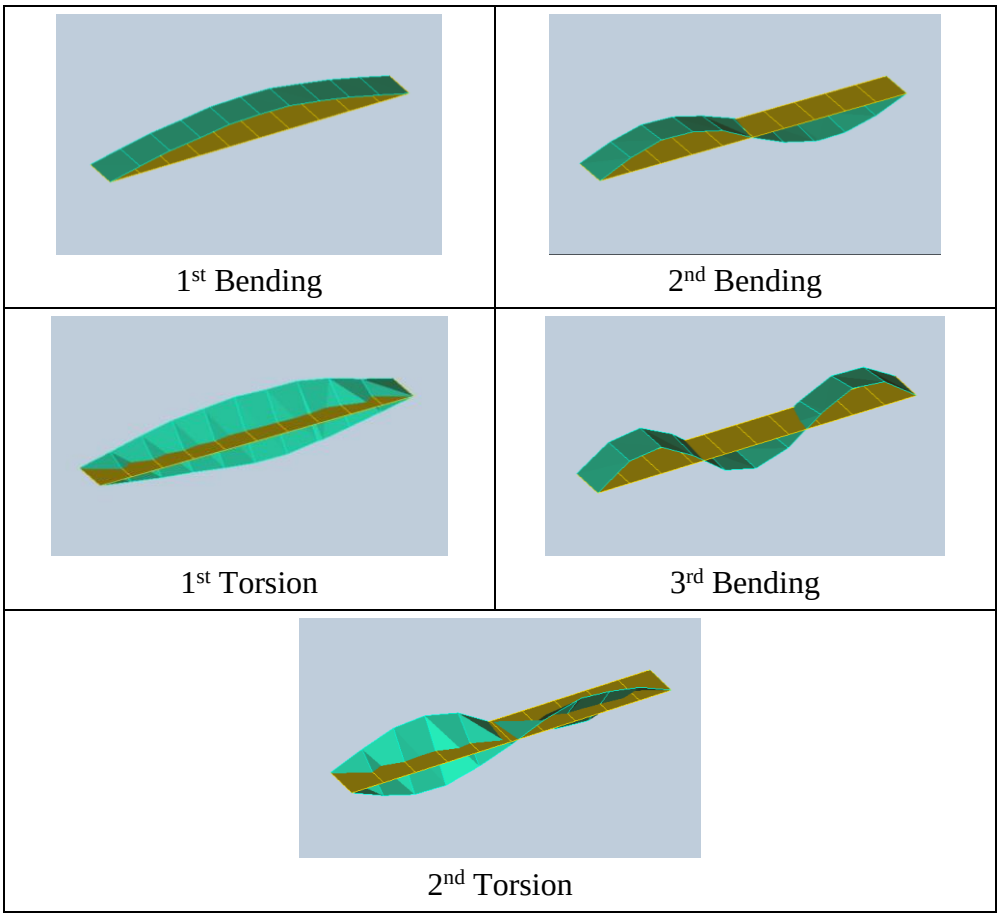

Figure 5.24. Experimental mode shapes of the intact grid bridge model by FDD technique procedure using ARTeMIS extractor software

The values of the first mode shape vectors of the both states of the grid bridge model without and with additional masses for the 23 nodes including reference point are listed in Table 5.7. The mode shape vectors in table are for three movement directions, where in this model the Y and Z-axis are included for the transverse and vertical movements, respectively, of the measurement points. The third movement in the longitudinal axis is very small and neglected. It is clear from Table 5.7 that the transverse displacements are small compared with the vertical displacements. The maximum value of displacement vector is at node number 11 and 12 equal of 1.00 or very close for both model states. For the first mode shape, first bending, the maximum displacement is in the middle and this

verifying the results. Also, the mode shape vectors of the model state with additional masses have little higher values than model state without additional masses.

Table 5.7: Experimental extracted mode shape vectors using ARTeMIS extractor for both intact grid brigde model states without and with additional masses

Node No.	Grid Bridge Model State Without Additional Masses			Grid Bridge Model State With Additional Masses		
	Disp. Vector-X (Long.)	Disp. Vector-Y (Trans.)	Disp. Vector-Z (Vert.)	Disp. Vector-X (Long.)	Disp. Vector-Y (Trans.)	Disp. Vector-Z (Vert.)
1	0.000	0.000	0.000	0.000	0.000	0.000
2	0.000	0.000	0.000	0.000	0.000	0.000
3	0.000	0.0117	0.303	0.000	0.0125	0.313
4	0.000	0.0117	0.294	0.000	0.0125	0.314
5	0.000	0.0115	0.575	0.000	0.0349	0.594
6	0.000	0.0115	0.567	0.000	0.0349	0.600
7	0.000	0.0536	0.776	0.000	0.0446	0.820
8	0.000	0.0536	0.766	0.000	0.0446	0.807
9	0.000	0.0079	0.928	0.000	0.0113	0.983
10	0.000	0.0079	0.915	0.000	0.0113	0.980
11	0.000	0.0349	1.000	0.000	0.0177	1.000
12	0.000	0.0349	0.986	0.000	0.0177	0.988
13	0.000	0.0119	0.961	0.000	0.0244	0.966
14	0.000	0.0119	0.953	0.000	0.0244	0.959
15	0.000	0.0315	0.812	0.000	0.0486	0.819
155	0.000	0.0140	0.777	0.000	0.0138	0.806
16	0.000	0.0315	0.792	0.000	0.0486	0.837
17	0.000	0.0139	0.587	0.000	0.0108	0.601
18	0.000	0.0139	0.585	0.000	0.0108	0.604
19	0.000	0.01520	0.306	0.000	0.0135	0.322
20	0.000	0.01520	0.310	0.000	0.0135	0.323
21	0.000	0.000	0.000	0.000	0.000	0.000
22	0.000	0.000	0.000	0.000	0.000	0.000

Those vector values are normalized depend on the maximum vector value, therefore all other points vectors are less than the maximum vector value of 1, as listed in Table 5.7. The exported output file from ARTeMIS software provide vector values with positive signs

for all measurement points, therefore for the purposes of computations, the vectors values signs are assumed and taken as in the numerical results.

In addition, to verify the final results of the extracted modal properties, the MAC values for the grid bridge model state without additional masses are calculated by Eq. (4.10) to obtain an indication for the relationship between each two modes, as listed in Table 5.8. The table shows the correlation between each two extracted modes of the model where the MAC values for each different modes are very small close to zero and equal 1 for each equal modes. Those MAC values verify the validity of the extracted modes with respect to their stability and the modes represent the real structural modes.

Table 5.8: MAC values of extracted mode shapes corresponding to natural frequencies using ARTeMIS extractor for intact grid bridge model state without additional masses

Frequency Value (Hz)	2.490	9.814	10.550	22.410	23.580
2.490	1	0.04931	0.02943	0.03803	0.05935
9.814	0.04931	1	0.1029	0.07769	0.09949
10.550	0.02943	0.1029	1	0.058	0.1397
22.410	0.03803	0.07769	0.058	1	0.2115
23.580	0.05935	0.09949	0.1397	0.2115	1

Also, the MAC values could be presented as a bar charts which is provided in ARTeMIS software, as shown in *Figure 5.25* for the both model states without and with additional masses. It is clear from figure, the validity of the extracted modes with respect to the same mode of value equal to 1 and different mode of value close to zero.

(a) 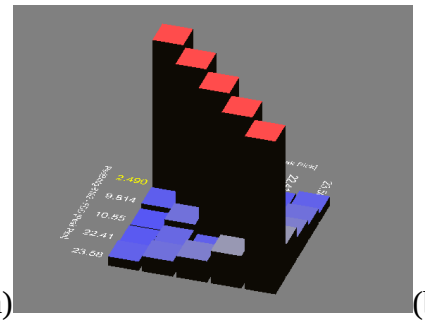 (b) 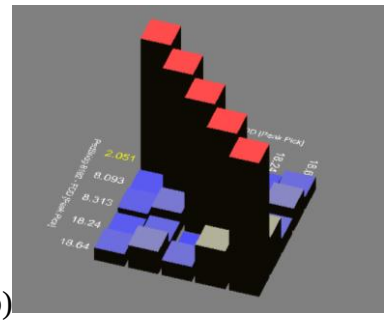

Figure 5.25. Bar charts of MAC values of experimental modal properties using ARTeMIS extractor software of the both intact grid bridge model states (a) without additional masses and (b) with additional masses

5.4.5. Implemented damage scenarios in the grid bridge model

For the both grid bridge model states, without and with additional masses, two different damage scenarios are implemented to investigate the behavior of structural model and efficiency of the proposed procedure for detecting damage location and severity in different positions on the model. The damages are created by cutter machine from the bottom side of the cross section of the main beams.

The first damage scenario, DC-1, is located at the distance of 2247 mm c/c from the left supports of the grid bridge model, as shown in *Figure 5.26*. The damage location in DC-1 is close to the first third of the entire length of the model on the left side of the model. The implemented damage scenario in DC-1 has crack length of 42 mm and crack depth of 20 mm of the total depth of 50 mm which represents 40 % of the total height of the beam cross section (i.e. damage ratio of 0.4), as shown in *Figure 5.27*.

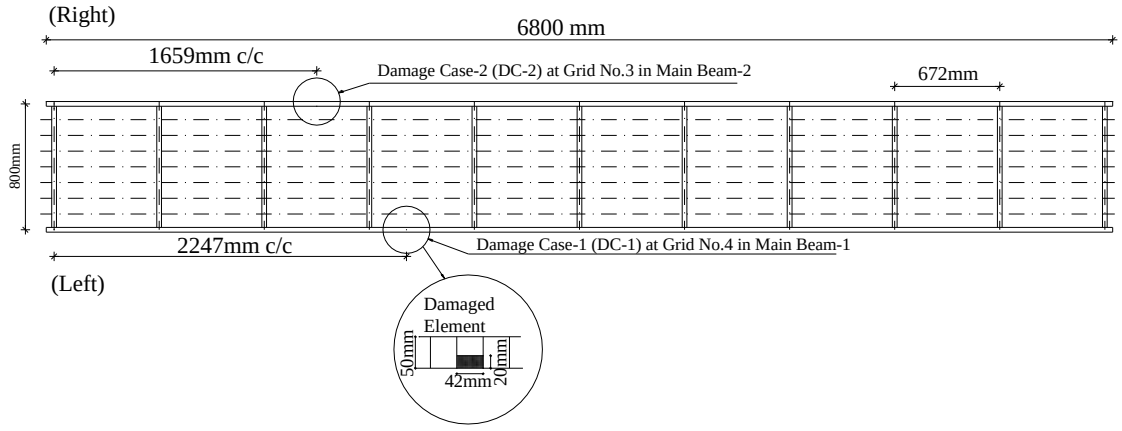

Figure 5.26. Location of damage scenarios on the grid bridge model

The second implemented damage scenario, DC-2, is located at a distance of 1659 mm c/c from left supports the grid bridge model, as shown in *Figure 5.26*. The second damage location is close to the first quarter of the entire length of the model on the right side of the

model. The implemented damage scenario in DC-2 has the same dimension of the first damage scenario DC-1 of crack length of 42 mm and crack depth of 20 mm.

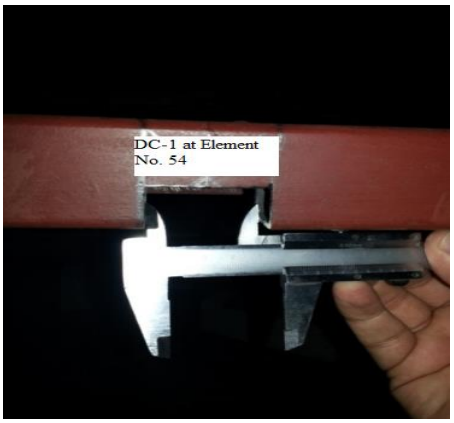

Figure 5.27. Severity of damage scenario in DC-1 on the grid bridge model

For each damage scenario, the model state without additional mass is first tested and then the second tested of the model state with additional mass. Also, the first DC-1 scenario is first examined and repaired, after which the second DC-2 scenario is implemented. The ambient vibration testing and estimation procedure for the intact case of the structural model is repeated after repairing the damage created in DC-1. In this way, the same modal properties were ensured as in the intact case.

5.4.6. Extraction of modal properties of the damaged grid bridge model using ARTeMIS extractor software

After implementation of damage scenarios, two trials of ambient vibration measurements are carried out for each of the two damage scenarios in order to improve reliability in the extracted modal properties of the damaged grid bridge model. The first five values of modal properties, natural frequencies and mode shapes, of the damaged model state without additional masses for both damage scenarios are extracted using ARTeMIS software. The results of natural frequency values of the damaged and intact model state without additional masses with percentage of reduction are listed in Table 5.9.

Table 5.9: Experimental extracted modal frequencies using ARTeMIS extractor for both damaged and intact grid bridge model state without additional masses

Mode No.	Frequency Value of Intact Model without additional masses (Hz)	Frequency Value of Damaged Model state without additional masses (Hz)			
		DC-1	Relative Reduction (%)	DC-2	Relative Reduction (%)
1	2.490	2.454	1.45	2.490	0.00
2	9.814	9.705	1.11	9.631	1.86
3	10.550	10.360	1.80	10.360	1.80
4	22.410	22.230	0.80	22.120	1.29
5	23.580	23.400	0.76	23.400	0.76

Respect to the intact model state without additional masses, in the case of DC-1, the maximum reduction in frequency value are extracted in the third modes (torsion mode), while in the case of DC-2, the maximum reduction in frequency value are extracted in the second mode (bending mode) with no reduction in the first mode.

On the other hand, for the damaged model state with additional masses, the first five values of modal properties, natural frequencies and mode shapes, for both damage scenarios are extracted using ARTeMIS software. The values of natural frequencies of the damaged and intact model state with additional masses with reduction values are listed in Table 5.10.

Table 5.10: Experimental extracted modal frequencies using ARTeMIS extractor for both damaged and intact grid bridge model state with additional masses

Mode No.	Frequency Value of Intact Model with additional masses (Hz)	Frequency Value of Damaged Model state with additional masses (Hz)			
		DC-1	Relative Reduction (%)	DC-2	Relative Reduction (%)
1	2.051	2.051	0	2.010	1.99
2	8.093	7.940	1.89	7.910	2.26
3	8.313	8.240	0.88	8.200	1.36
4	18.240	18.090	0.82	18.050	1.04
5	18.640	18.420	1.18	18.530	0.59

It is obvious from table that the DC-2 (located at first quarter of the entire length) is more significant reduction in natural frequency values than DC-1 (first third of the entire length). In addition, the maximum value of reduction in the DC-1, respect to the intact model state with additional masses, is in the second mode (bending mode) and it is the same mode for the case in DC-2, while there is no effect on the first mode in DC-1.

As a comparison between two states of grid bridge model, that the maximum reduction value is in the second bending mode for both states of the model and for both damage scenarios. Consequently, the different reduction values and positions could be concluded the loading state of the model has significant effect on the structural dynamic behavior.

5.5. Experimental modal analysis of the simply supported Vierendeel bridge model

The third adopted tested structural model is a simply supported steel Vierendeel bridge a prototype real superstructure had been built in site on the highway located near Cacak city in the south of Republic of Serbia. The scaled Vierendeel bridge model is installed in the lab based on the selected scale factor, which is discussed in paragraph 5.3, with adquate change to be suitable with the space of the lab of the faculty. The selection of this structural model is as a complex structure to implement the experimental testing and extracting the modal properties. The present study adopted this model as a 3D-space structure has the torsion behavior, the flexural behavior as well as to truss-bending action comes from fences of two sides of the model. In addition, this 3D-space structural model has movements in three directions, vertical, transverse and longitudinal displacement. As, the longitudinal movement is very small, therefore, it is neglected in this study. For the purposes of verification of proposed SHM procedure to detect damage in the structure, this structural model is as special complex civil structural applications and it is state-of-the-art of this study.

5.5.1. Description of the Vierendeel bridge model

The adopted model is a complex 3D-space, welded steel structure, has three structural actions, flexural, torsion and truss. The model consists of a grid floor and two fences with 11-column in each side. Total length of the model is 6720 mm that consists of 10-bay at 672 mm c/c for each, as shown in *Figure 5.28*, The total width of the model is 800 mm c/c, containing 8-grid of 100 mm c/c. This model consists of two main parts, the first is the grid floor. The grid floor has the same geometry description for the second adopted model of the grid bridge model, as discussed in paragraph 5.4.1.

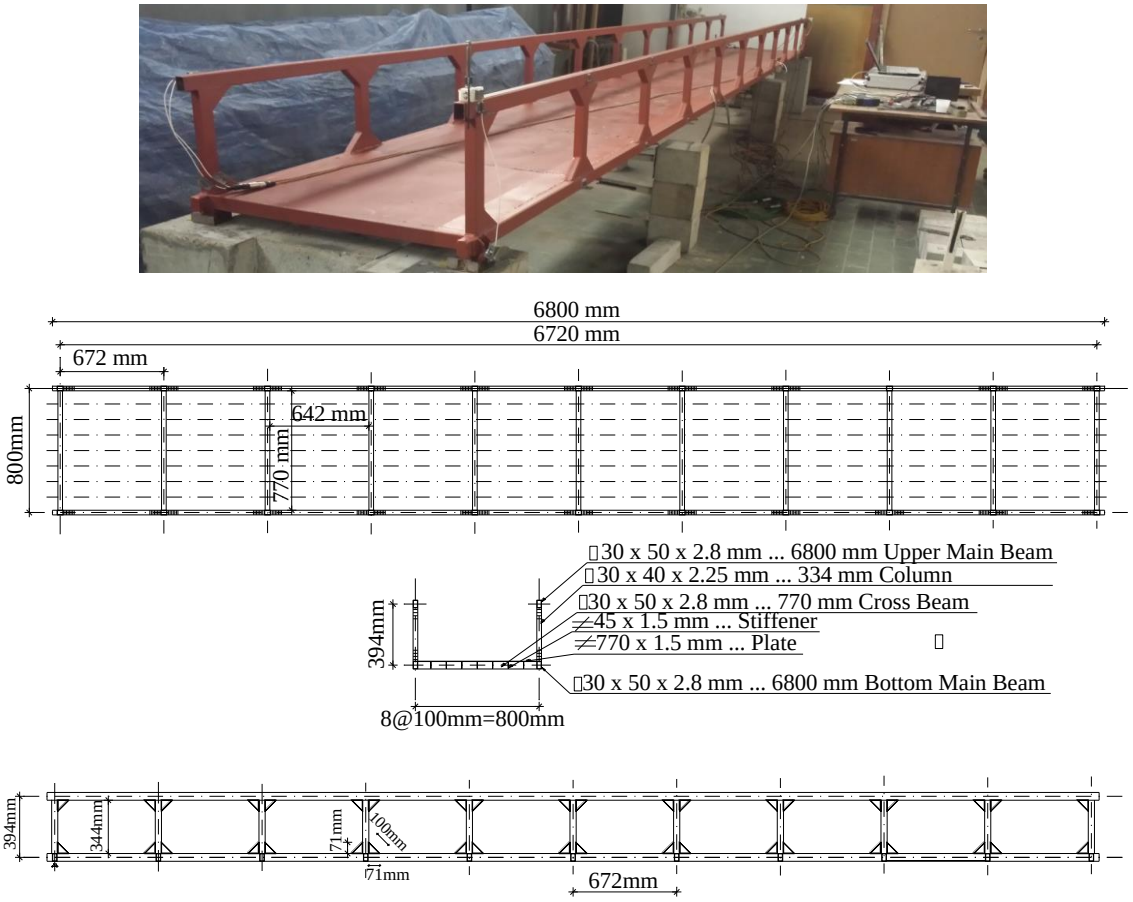

Figure 5.28. Layout of steel Vierendeel bridge structural model

As previously mentioned, the grid floor is fabricated from two main longitudinal steel beams have rectangular hollow section of (30x50x2.8) mm located at the edges of the floor.

For the main transverse beams, eleven beams have the same section of (30x50x2.8) mm are used by welding with the main two longitudinal beams to formulate the whole floor. Additional longitudinal beams act as stiffeners for the floor welded with the main transverse beams. The distribution of the stiffeners is equal over the total width of the model at 100 mm c/c. Each stiffener has a plate section of (45x1.5) mm, which is welded also with the top plate placed orthogonally. The plate of the deck is welded over the grid frame at 50 mm welding at 150 mm spacing, as shown in *Figure 5.13*.

The second part of this model is the columns and beams sections of the two fences located at both sides of the model left and right hand, as shown in *Figure 5.28*. The columns sections of the fences have (30x40x2.25) mm dimensions and the columns connect the two main longitudinal beams in the grid floor with main longitudinal upper beams. The main longitudinal upper beams have the same cross section as in the main longitudinal lower beams of grid floor. Each column is stiffened by two triangular steel parts have dimensions of (71x71x100x2.8) mm on the top and bottom, as shown in *Figure 5.28*.

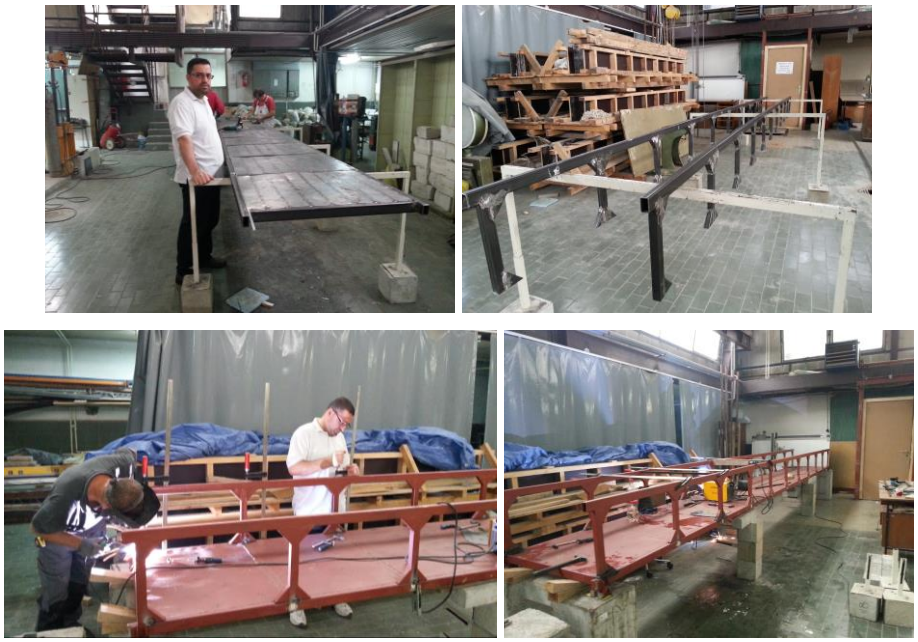

Figure 5.29. The Vierendeel bridge structural model during the erection stages

All parts of the model are welded by the company staff and author. Firstly, the grid floor are welded then the second part of the two fences in both sides of the model are welded with the main part of the structure, as shown in *Figure 5.29*.

The supports are on the two edges of the model over four concrete blocks. Each two concrete blocks are glued together by two concrete struts to stiffen the supports from the side movement. Two of the supports are hinge supports at left hand side of the model, as shown *Figure 5.30* (a) and (b). The other two supports at right hand side of the beam model are roller supports, as shown *Figure 5.30* (c). The fourth supports are set up to act as hinge and roller boundary conditions in two support locations along the length of the bridge model. Those four supports are designed as; one support is hinged in 3-direction, two supports are hinged in 2-direction and one support is roller. All those supports are designed to prevent movements in the direction parallel to the vertical axis of the beams cross sections. In addition, the hinge supports at the left side are set up to prevent two more movements in the direction of transverse and longitudinal axis of the length of the bridge model, as shown in *Figure 5.30* (a) and (b).

(a)  (b) 

(c) 

Figure 5.30. Simple supports of Vierendeel steel bridge model (a) first left hinge support, (b) second left hinge support, (c) both right supports

Those four supports are setup by installing Vierendeel bridge beams cross sections on the circular section of four steel rods used as roller supports. For both hinge supports, the steel rods are based on thick base plate installed on a thin rubber pad, which are set up over cubic concrete parts, as shown in *Figure 5.30*. The hinge support is created by welding the circular section of steel rod from upper side with beams cross sections, as shown in *Figure 5.30* (a) and (b). The way of fixed the supports is necessary in the experimental testing to prevent any undesirable movement in the supports during the excitation of the structural model by simulated ambient vibration using shaker device.

In order to study modal frequencies in different frequency ranges, the Vierendeel bridge model is also adopted in two loading states: without additional masses and with additional masses, as shown in *Figure 5.31*. The model state with additional masses included 10-mass of concrete cubes placed at 50 mm joints of the main longitudinal and cross beams inside the span and the concrete masses have average mass of 7.925 kg, as shown in *Figure 5.31*.

(a)  (b) 

Figure 5.31. Vierendeel bridge model of two loading states during testing (a) without additional masses (b) with additional masses

5.5.2. Positions of the accelerometers on the Vierendeel bridge model

For Vierendeel bridge model, several trials also are implemented to fix the appropriate distribution of accelerometers positions using only eight accelerometers which are available. Due to the geometry of the Vierendeel bridge model, the accelerometers positions (measurement points) are selected in ten sets along the length of model to cover

the large number of degrees of freedom of the grid floor part and the both fences part with limited numbers of accelerometers. Nine sets have the same distribution of the accelerometers positions on the measurement point for all nine internal columns as shown in *Figure 5.32*. Whereas, the tenth set has different distribution of accelerometers positions included the both supports edges points.

(a) 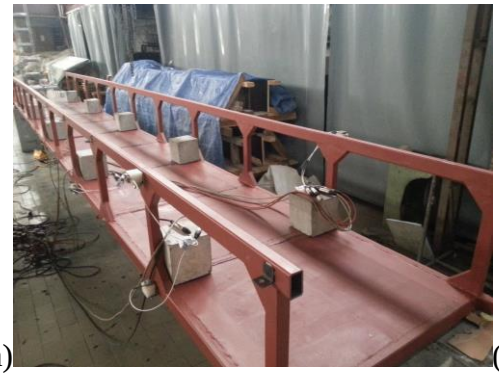 (b) 

Figure 5.32. Distribution of eight accelerometers of the measurement points and reference point with movement directions in the second set of Vierendeel bridge model state with additional mass

Each set of the nine sets contains four measurement points, two points in the lower beam and two points in the upper beam, with six degrees of freedom using six accelerometers. In each set, two points from right hand side have two degrees of freedom, one vertical movement in the lower point and one transverse movement in the upper point, as shown in *Figure 5.32* (a). The other two points from left hand side have four degrees of freedom each point has two movement, one vertical and other transverse movement, as shown in *Figure 5.32* (b).Whereas, the tenth set contains four measurement points with six degrees of freedom distributed on the upper points of both supports of the bridge model. The both upper right side points have only movement in transverse direction, while the both upper left side points have two movements in vertical and transverse direction, as shown in *Figure 5.33* and *Figure 5.35* (c).

The other two accelerometers are used in reference measurement point with two degrees of freedom, as shown in *Figure 5.33*. This reference point is required to be in the

same position for all ten sets during recording ambient vibration measurements to extract the modal properties of the Vierendeel bridge model using ARTeMIS software. The reference point is located at 84 mm from lower intersecting node close to the fourth column line, as shown in *Figure 5.33*.

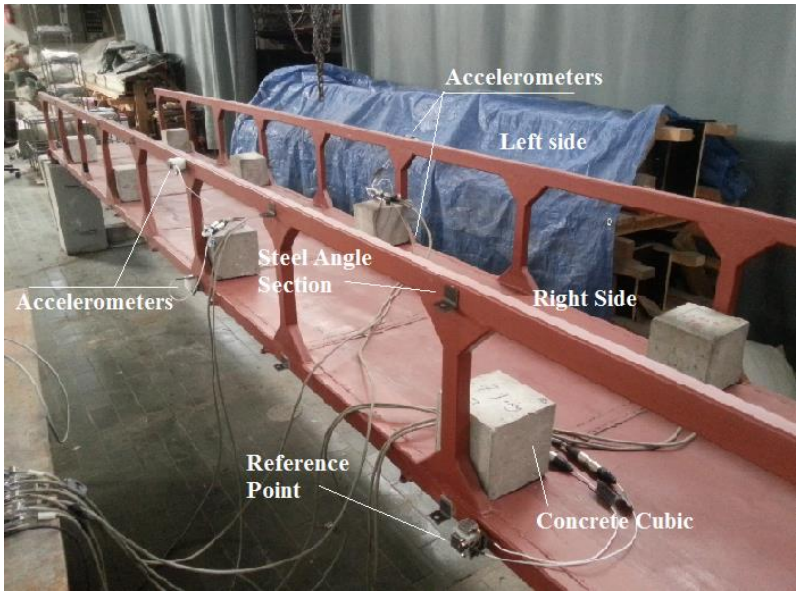

Figure 5.33. Positions of accelerometers of reference point and measurement points of fifth set and movement directions of Vierendeel bridge model state with additional mass

All accelerometers are set up on cubes and those cubes are installed by screws on steel angle section welded on the specified measurement points on the model, as shown in *Figure 5.33*. This way of connection helps to carry out the experimental testing fast by facilitating move the accelerometers through the ten sets during ambient vibration measurements. All accelerometers are set up on the intersecting nodes of the lower main and transverse beams and on the intersecting nodes of the upper main longitudinal beam and columns of the bridge model.

The distribution of measurement points is adopted in ten sets to present and reflect the real structural behavior, flexural and torsion, of the Vierendeel bridge model from ambient vibration measurements. The fourth, sixth and eighth set with distribution of accelerometers positions and directions are shown in *Figure 5.18*. Each set cover one line

of corresponding columns from the 9-line of columns of the model, as shown in *Figure 5.34*.

(a)  (b)  (c) 

Figure 5.34. Distribution of sets of accelerometer positions along the length of Vierendeel bridge model state without additional masses (a) fourth set, (b) sixth set and (c) eighth set

The same distribution of measurement points is adopted for the model state with additional masses of ten sets to present the real structural behavior of the Vierendeel bridge model from ambient vibration measurements. The second, fifth and tenth set with distribution of accelerometers positions and their directions are shown in *Figure 5.19*.

(a)  (b)  c) 

Figure 5.35. Distribution of sets of accelerometer positions along the length of Vierendeel bridge model state with additional masses with additional masses (a) second set, (b) fifth set and (c) tenth set

5.5.3. Data acquisition system and signal processing using simulated ambient vibration of the Vierendeel bridge model

Simulation of ambient vibration measurements of the both Vierendeel bridge model states without and with additional masses is carried out using the shaker device, acquisition device of 24-bits 8 channel and PC-storage system, as shown in *Figure 5.35*. The shaker

device is installed on the lower connected concrete part between two concrete supports at right hand side of the model.

(a)  (b) 

Figure 5.36. Data acquisition system of the both Vierendeel bridge model state (a) without additional masses and (b) with additional masses

The process of experimental testing is started by holding the shaker device with specified intensity value of 5 using the same random vibration signals generated by MATALB software. The recording the acceleration time history of each specified accelerometers installed on the Vierendeel bridge model is stored in the PC as data file. The frequency range of the vibration response of the Vierendeel bridge model has been investigated using numerical model. The selected of appropriate sampling frequency of the vibration response and the value of filtering frequency are adopted of 600 Hz and 50 Hz, respectively. The time of data recording is 30 min for each set and the same experimental testing procedure is conducted for the model state with additional masses, where it is the second stage after conducting the first testing for model state without additional masses.

For the Vierendeel bridge model, the recorded data of each set of accelerometers consist 4- vertical and 4-transverse movements including the reference point. The sample of acceleration history time of the first vertical movement accelerometers of the both Vierendeel bridge model states for the first 100 seconds of the recording are shown in *Figure 5.37*. The figures of acceleration time history of other accelerometers only for model state without additional masses are shown in Appendix - A3.

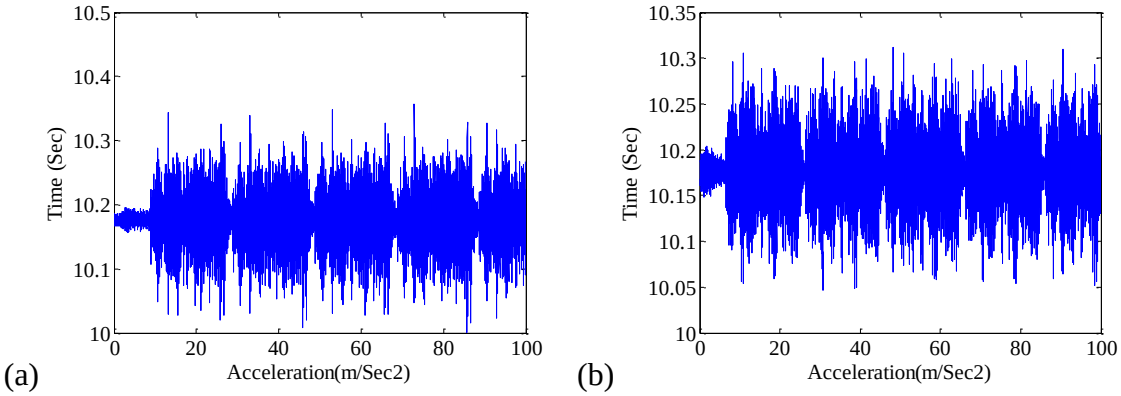

Figure 5.37. Acceleration history time for one accelerometer during simulated ambient vibration measurements using shaker of intact Vierendeel bridge model (a) without additional masses and (b) with additional masses

The geometry of the structural model in coordinate system, the title of the project, the sampling frequency, the names of recorded data file of all ten sets and description of the accelerometers and their direction of movements during excitation are written in CFG file defined in ARTeMIS software. The geometry of the Vierendeel bridge model and distribution of accelerometers in each set of the ten sets along the length of bridge model are presented in ARTeMIS software, as shown in *Figure 5.38.*

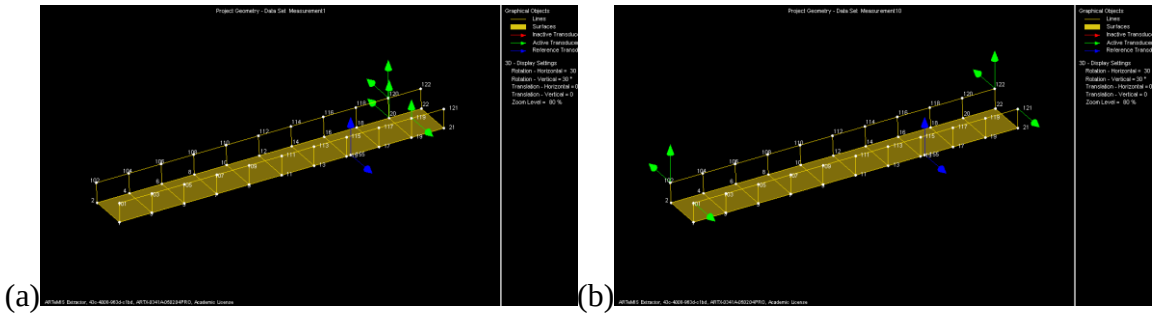

Figure 5.38. Geometry and distribution of accelerometers with reference point for (a) first set and (b) tenth set of measurements of intact Vierendeel bridge model

Figure 5.38 (a) shows one sample of set of measurement of the nine sets, in each set the blue arrows are the two movements (accelerometers) of the reference point, while the green arrows are six movements of the set measurements. Whereas, the Figure 5.38 (b) shows the set number ten and the distribution of the accelerometers positions and directions in both sides of supports of the bridge model.

Then, the data processing is conducted to estimate the average of the normalized singular value of spectral density matrices of all ten data sets and from which the peak picking procedure is applied to extract the modal properties of the Vierendeel bridge model. Here, there is no effect of the model state with additional masses on representation in the ARTeMIS software and it is the same.

5.5.4. Extraction of modal properties of the intact Vierendeel bridge model using ARTeMIS extractor software

The modal frequencies and mode shapes of the intact Vierendeel bridge model are extracted using ARTeMIS - extractor software by the FDD technique. The peak picking procedure of FDD technique is implemented with number of frequency line of 8192 to get the appropriate frequency resolution and overlap of 66.67 %, filtering (Butterworth) and window function (Hanning). Several trials of measurements are conducted to provide more confidence of the extracted modal properties, according to the spectral density matrices estimated based on the recorded ambient vibration data. This procedure is implemented for both states of the model without and with additional masses. The diagram of the spectral density matrices of all data sets for both states of the Vierendeel bridge model are shown in *Figure 5.39*.

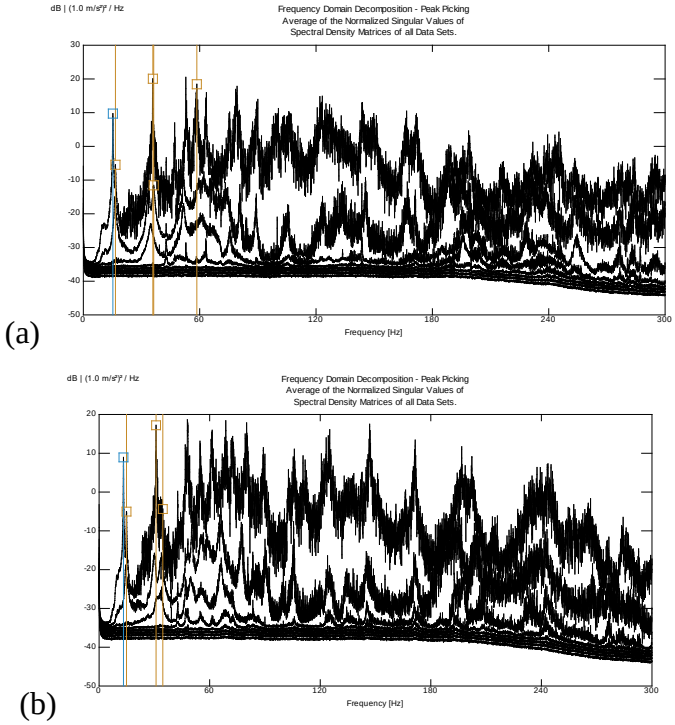

Figure 5.39. Spectral density matrices with selected modes using FDD estimation procedure in ARTeMIS extractor software of intact Vierendeel bridge model (a) without additional masses and (b) with additional masses

The structural modes are estimated using the peak-picking procedure, according to FDD estimation technique explanation in paragraph 3.5.4. The vertical lines in the figures represent the peak picking modal modes in FDD method, which means only the real structural modes are selected from the peaks. The results of the first four modal frequencies and the modes characters of the both Vierendeel bridge model states are listed in Table 5.11.

It is evident from table, that significant effect of the additional masses on the values of natural frequencies of loading state model. The larger reduction is in the bending modes than torsion modes about 5-9 % and the maximum reduction is in the third mode and the minimum reduction is in the fourth mode.

Table 5.11: Experimental extracted modal frequencies using ARTeMIS extractor for both intact Vierendeel bridge model states, without and with additional masses

Mode No.	Frequency Value of Intact Vierendeel bridge Model (Hz)		Reduction in Frequency		Mode Character
	Model State without Additional Masses	Model State with Additional Masses	(Hz)	Relative (%)	
1	15.234	13.220	2.014	13.22	1st Bending
2	16.552	15.197	1.355	8.19	1st Torsion
3	35.852	30.908	4.944	13.79	2nd Bending
4	36.291	34.570	1.721	4.74	2nd Torsion

On the other hand, the first four mode shapes results and their characters corresponding to the natural frequencies of the Vierendeel bridge model state without additional masses are shown in *Figure 5.24*. The values of the first four mode shape vectors of the Vierendeel bridge model state without additional mass are provided as output SVS system file from the ARTeMIS software. The extracted mode shape character for the model state with additional masses are same for the model state without additional masses, as shown in *Figure 5.40*.

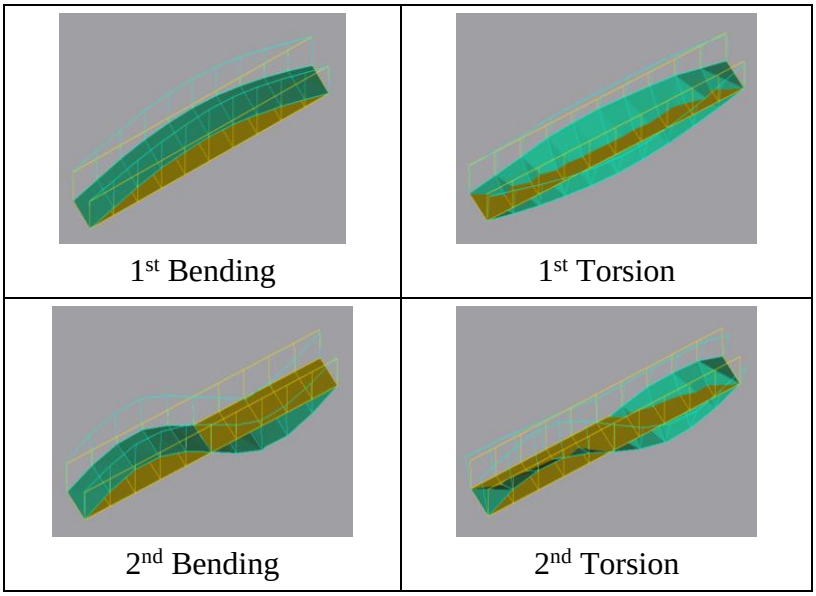

Figure 5.40. Experimental modal properties of the intact Vierendeel bridge model by FDD technique procedure using ARTeMIS extractor software

The values of the first mode shape vectors of the both states of the Vierendeel bridge model without and with additional masses for the 45 nodes, numbered as shown in *Figure 5.38*, including reference point are listed in Table 5.12. The mode shape vectors in table are for three movement directions, where in this model the Y and Z-axis are included for the transverse and vertical movements, respectively, of the measurement points. The third movement in the longitudinal axis is very small and neglected. It is clear from Table 5.12 that the transverse displacements are small compared with the vertical displacements. The maximum value of displacement vector is at node number 11 and 111 for the model state without additional masses and at node number 12 and 112 for the model state with additional masses and equal of 1.00 or very close, as listed in Table 5.12. For the first mode shape, first bending, the maximum displacement is in the middle and this verifying the results. Also, the mode shape vectors of the model state with additional masses have little smaller values than model state without additional masses.

Table 5.12: Experimental extracted mode shape vectors using ARTeMIS extractor for both intact Vierendeel brigde model states without and with additional masses

Node No.	Vierendeel Bridge Model State Without Additional Masses			Vierendeel Bridge Model State With Additional Masses		
	Disp. Vector-X (Long.)	Disp. Vector-Y (Trans.)	Disp. Vector-Z (Vert.)	Disp. Vector-X (Long.)	Disp. Vector-Y (Trans.)	Disp. Vector-Z (Vert.)
1	0.000	0.0000	0.0000	0.000	0.0000	0.0000
2	0.000	0.0000	0.0000	0.000	0.0000	0.0000
3	0.000	0.0062	0.3045	0.000	0.0110	0.2931
4	0.000	0.0062	0.2991	0.000	0.0110	0.2999
5	0.000	0.0182	0.5819	0.000	0.0367	0.5699
6	0.000	0.0182	0.5585	0.000	0.0367	0.5800
7	0.000	0.0056	0.8059	0.000	0.0305	0.7904
8	0.000	0.0056	0.7731	0.000	0.0305	0.8029
9	0.000	0.0032	0.9449	0.000	0.0117	0.9212
10	0.000	0.0032	0.9527	0.000	0.0117	0.9473
11	0.000	0.0022	1.0000	0.000	0.0151	0.9740

12	0.000	0.0022	0.9824	0.000	0.0151	1.0000
13	0.000	0.0092	0.9506	0.000	0.0134	0.9227
14	0.000	0.0092	0.9185	0.000	0.0134	0.9496
15	0.000	0.0076	0.8073	0.000	0.0045	0.7869
155	0.000	0.0095	0.7891	0.000	0.0356	0.7617
16	0.000	0.0076	0.7865	0.000	0.0045	0.8053
17	0.000	0.0190	0.5885	0.000	0.0150	0.5650
18	0.000	0.0190	0.5690	0.000	0.0150	0.5841
19	0.000	0.0023	0.3088	0.000	0.0138	0.2903
20	0.000	0.0023	0.2966	0.000	0.0138	0.3067
21	0.000	0.0000	0.0000	0.000	0.0000	0.0000
22	0.000	0.0000	0.0000	0.000	0.0000	0.0000
101	0.000	0.0143	0.0000	0.000	0.0148	0.0000
102	0.000	0.0181	0.0200	0.000	0.0220	0.0076
103	0.000	0.0153	0.3045	0.000	0.0142	0.2931
104	0.000	0.0252	0.3015	0.000	0.0168	0.3013
105	0.000	0.0099	0.5819	0.000	0.0278	0.5699
106	0.000	0.0380	0.5568	0.000	0.0190	0.5773
107	0.000	0.0333	0.8059	0.000	0.0566	0.7904
108	0.000	0.0724	0.7680	0.000	0.0502	0.8019
109	0.000	0.0473	0.9449	0.000	0.0559	0.9212
110	0.000	0.0489	0.9493	0.000	0.0424	0.9451
111	0.000	0.0178	1.0000	0.000	0.0176	0.9740
112	0.000	0.0441	0.9775	0.000	0.0234	0.9968
113	0.000	0.0384	0.9506	0.000	0.0194	0.9227
114	0.000	0.0590	0.9149	0.000	0.0361	0.9421
115	0.000	0.0059	0.8073	0.000	0.0228	0.7869
116	0.000	0.0532	0.7813	0.000	0.0361	0.7962
117	0.000	0.0176	0.5885	0.000	0.0402	0.5650
118	0.000	0.0360	0.5648	0.000	0.0209	0.5739
119	0.000	0.0133	0.3088	0.000	0.0405	0.2903
120	0.000	0.0205	0.2952	0.000	0.0103	0.3002
121	0.000	0.0178	0.0000	0.000	0.0468	0.0000
122	0.000	0.0132	0.0178	0.000	0.0060	0.0127

Those vector values are normalized depend on the maximum vector value, therefore all other points vectors are less than the maximum vector value of 1, as listed in Table 5.12. The exported output file from ARTeMIS software provide vector values with positive signs for all measurement points, therefore for the purposes of computations, the vectors values signs are assumed and taken as in the numerical results.

In addition, to verify the results of the extracted modal properties, the MAC values for the Vierendeel bridge model state without additional masses are calculated by Eq. (4.10) to obtain an indication for the relationship between each two modes, as listed in Table 5.13. The table shows the correlation between each two extracted modes of the model where the MAC values for each different modes are very small close to zero and equal 1 for each equal modes. Those MAC values verify the validity of the extracted modes with respect to their stability and the modes represent the real structural modes.

Table 5.13: MAC values of extracted mode shapes corresponding to natural frequencies using ARTeMIS extractor for intact Vierendeel bridge model state without additional masses

Frequency Value (Hz)	15.230	16.550	35.850	36.290
15.230	1	0.1048	0.05224	0.02707
16.550	0.1048	1	0.01854	0.04466
35.850	0.05224	0.01854	1	0.05638
36.290	0.02707	0.04466	0.05638	1

Also, the MAC values could be presented as a bar charts which is provided in ARTeMIS software, as shown in *Figure 5.25* for the both model states without and with additional masses.

(a) 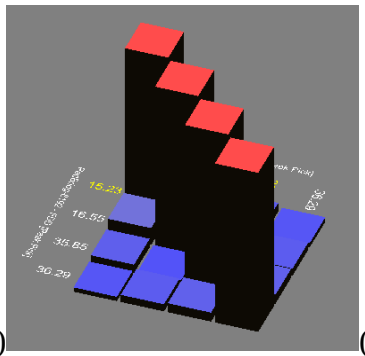 (b) 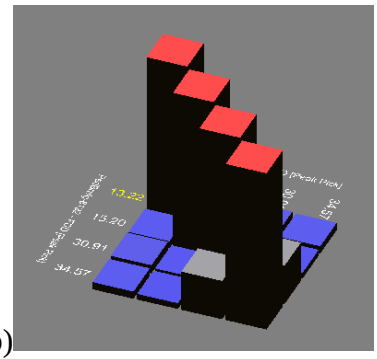

Figure 5.41. Bar charts of MAC values of experimental modal properties using ARTeMIS extractor software of the both intact Vierendeel bridge model states (a) without additional masses and (b) with additional masses

It is clear from figure, the validity of the extracted modes with respect to the same mode of value equal to 1 and different mode of value close to zero.

5.5.5. Implemented damage scenarios in the Vierendeel bridge model

For the both Vierendeel bridge model states, without and with additional masses, two different damage scenarios are implemented to investigate the behavior of structural model and efficiency of the proposed procedure for detecting damage location and severity in different positions on the model. The first damage scenario is at the upper main longitudinal beam and the second damage scenario is at the bottom side of the third column, as shown in *Figure 5.42*.

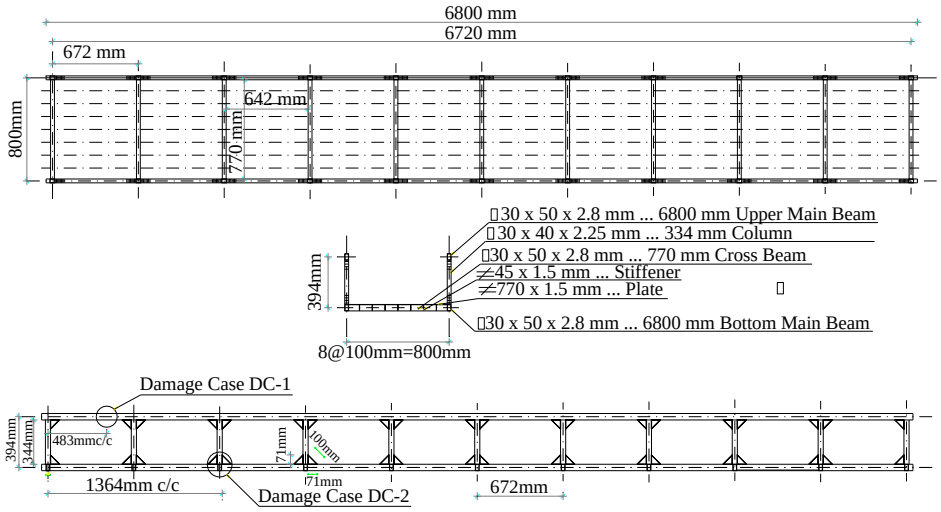

Figure 5.42. Location of damage scenarios on the damaged Vierendeel bridge model

The first damage scenario, DC-1, is located at the upper main beam on the first bay at the distance of 483 mm c/c from the left supports of the bridge model, as shown in *Figure 5.42*. The implemented damage scenario in DC-1 has crack length of 42 mm and crack depth of 20 mm of the total depth of 50 mm which represents 40 % of the total height of the beam cross section (i.e. damage ratio of 0.4), as shown in *Figure 5.43* (a).

The second implemented damage scenario, DC-2, is located at the lower part of the third column at distance of 1364 mm c/c from left supports of the Vierendeel bridge model,

as shown in *Figure 5.42*. The implemented damage scenario in DC-2 has tapered section with dimension of (54.8x5) mm from upper small side and (54.8x57) mm from lower large side, as shown in *Figure 5.43* (b).

(a)  (b) 

Figure 5.43. Extent of damage scenarios in DC-1 and DC-2 of the damaged Vierendeel bridge model

The second damage scenario is located at the lower stiffener part of the column with non-prismatic cross section, therefore the equivalent cross section have to be considered in the numerical investigation for this part of columns and for damage simulation. The dimension of damage scenario in this case has 5 mm width from upper side and 57 mm from lower side and height of crack is 54.8 mm, as shown in *Figure 5.43* (b).

For each damage scenario, the model state without additional mass is first tested and then the second tested of the model state with additional mass. Also, the first DC-1 scenario is first examined and repaired, after which the second DC-2 scenario is implemented. The ambient vibration testing and estimation procedure for the intact case of the structural model is repeated after repairing the damage created in DC-1. In this way, the same modal properties were ensured as in the intact case.

5.5.6. Extraction of modal properties of the damaged Vierendeel bridge model using ARTeMIS extractor software

After implementation of damage scenarios, two trials of ambient vibration measurements are carried out for each of the two damage scenarios in order to improve reliability in the extracted modal properties of the damaged Vierendeel bridge model. The first four values of modal properties, natural frequencies and mode shapes, of the damaged model state without additional masses for both damage scenarios are extracted using ARTeMIS software. The results of natural frequency values of the damaged and intact model state without additional masses with percentage of reduction are listed in Table 5.14.

Table 5.14: Experimental extracted modal frequencies using ARTeMIS extractor for both damaged and intact Vierendeel bridge model state without additional masses

Mode No.	Frequency Value of Intact Model without additional masses (Hz)	Frequency Value of Damaged Model state without additional masses (Hz)			
		DC-1	Relative Reduction (%)	DC-2	Relarive Reduction (%)
1	15.230	15.197	0.22	15.124	0.69
2	16.550	16.550	0	16.550	0
3	35.850	35.778	0.20	35.778	0.20
4	36.290	36.181	0.30	36.291	0

Respect to the intact model state without additional masses, in the case of DC-1, the maximum reduction in frequency value are extracted in the fourth modes (torsion mode). While in the case of DC-2, the maximum reduction in frequency value are extracted in the first mode (bending mode) with no reduction in the second mode for both damage scenarios as well as in fourth mode in the DC-2.

On the other hand, for the damaged model state with additional masses, the first four values of modal properties, natural frequencies and mode shapes, for both damage scenarios are extracted using ARTeMIS software. The values of natural frequencies of the damaged and intact model state with additional masses with reduction values are listed in Table 5.15.

Table 5.15: Experimental extracted modal frequencies using ARTeMIS extractor for both damaged and intact Vierendeel bridge model state with additional masses

Mode No.	Frequency Value of Intact Model with additional masses (Hz)	Frequency Value of Damaged Model state with additional masses (Hz)			
		DC-1	Relative Reduction (%)	DC-2	Relative Reduction (%)
1	13.220	13.220	0	13.110	0.83
2	15.197	14.978	1.44	14.978	1.44
3	30.908	30.908	0	30.908	0
4	34.570	34.167	1.16	34.167	1.16

It is obvious from table that the DC-2 (located at lower part of the third column) is more significant reduction in natural frequency values than DC-1 (located at the main upper beam). In addition, the maximum value of reduction in the DC-1, respect to the intact model state with additional masses, is in the second mode (torsion mode) and it is the same mode for the case in DC-2, while there is no effect in the third mode in both damage scenarios as well as in the first mode for DC-1.

As a comparison between two states of Vierendeel bridge model, that the maximum reduction value is in the second bending mode for model state with additional masses while it is different for the model state without additional masses for both damage scenarios. Consequently, the different reduction values and positions could be concluded the loading state of the model has significant effect on the structural dynamic behavior.

5.6. Experimental modal analysis of the multi-storey building model

The fourth adopted tested structural model is a steel multi-storey building a prototype real superstructure had been built in site in Belgrade city in the Republic of Serbia. The scaled multi-storey building model is installed in the lab based on the selected scale factor, which is discussed in paragraph 5.3, to be suitable with the space of the lab of the faculty. The selection of this structural model is as a complex space structure to implement the experimental testing and extracting the modal properties. The present study adopted this

model as a 3D-space frame tall building structure has the torsion behavior, the flexural behavior as well as to plate-bending and beam-column action comes from 10-storey model consist from beams, floors and columns. In addition, this 3D-space structural building model has movements in three directions, transverse in two directions. As, the vertical movement is very small, therefore, it is neglected in this study. For the purposes of verification of proposed SHM procedure to detect damage in the structure, this structural building model is as common complex civil structural applications and it is state-of-the-art of this study.

5.6.1. Description of the multi-storey building model

The multi-storey building model consists of 10 storeys (11 levels from 0 to 10) have 300 mm height for each one and the total height is 3000 mm, as shown in *Figure 5.44*. For simulation of actual behavior of the model, different types of masses are applied in order to simulate its modal properties of natural frequencies and mode shapes values. The building frame model consists of 25 floors, for each floor has (300x300) mm span length c/c. The model consists in the first floor 9-bay, second floor 6-bay, third and fourth 2-bay and from fifth to tenth are one bay, as shown in *Figure 5.44*.

In multi-storey building model, the zero level of the model contains rigid steel base that acts as a fixed supports for the columns, which are connected with the base plate by welding. In the level-1, level-9 and level-10, there are no plates as floors connecting the beams. The other levels have steel plates are provided as floors from level-2 to level-8 and each steel plate has 3 mm thick and connected by eight bolts with the beams in both x and y-direction of the model, as shown in *Figure 5.44*. Each floor in the level-2,3 and 4 carries concrete block of 4.5 kg as additional masses, which is connected by four bolts with the steel plate. As the level-2 has six floors and level-3 and 4 have only two floors, that means the leve-2 carries 27.5 kg as a total additional masses and each of level-3 and 4 carries as a total additional masses of 9 kg in each level, as shown in *Figure 5.44*. For the level-5, 6, 7 and 8 where only one floor is there, one concrete block has 10.5 kg is used as additional mass for both leve-5 and 6, while a steel block has 13.5 kg is used in level-7. Another steel mass of 16.2 kg is used for level-8 which is also connected the steel plate by bolts. For the

last two levels-9 and 10 where no floor is there, two additional masses of marble are used for each level with 32 kg as a total mass which are connected together by bolt, as shown in *Figure 5.44*.

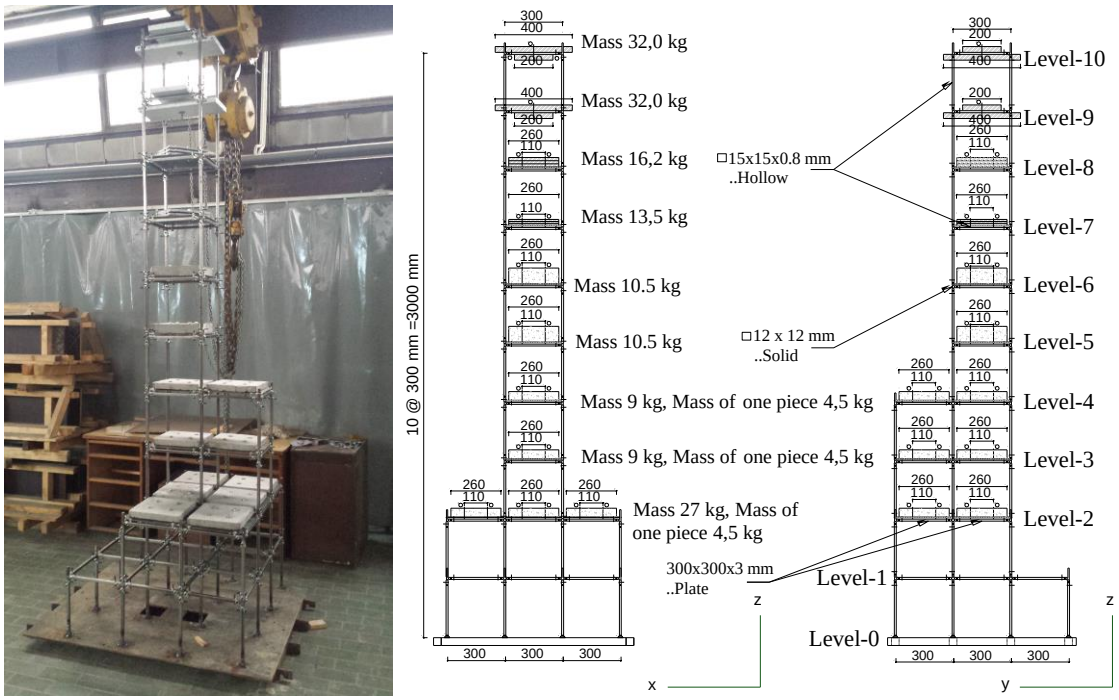

Figure 5.44. Layout of steel multi-storey building structural model

The multi-storey building model has two types of cross sections which used in the this frame model for beams and columns. The first section is hollow square section of (15x15x0.8) mm, while the second section for all beam-column joints. The second section has solid square section of (12x12) mm dimension for entire length of 100 mm for both sides of a beam-column joint that is taken in through columns and beams endings, as shown in *Figure 5.45*. This beam column joint consists of rigid element that is inserted through beams and columns and connected by suitable size of bolts from each side of the joints, as shown in *Figure 5.45*.

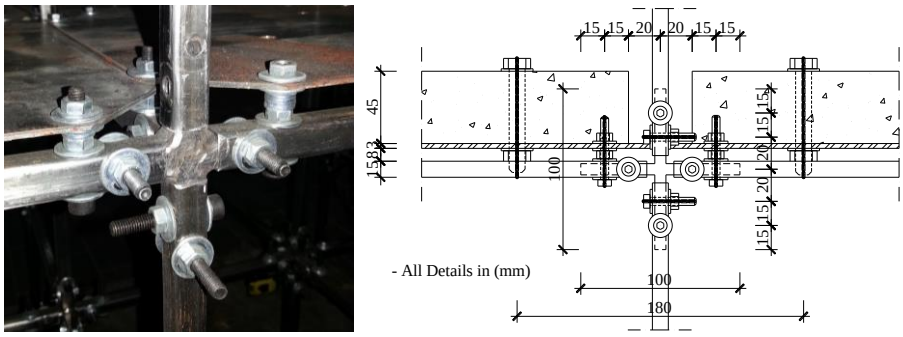

Figure 5.45. Details of beam-column joint used in multi-storey building structural model

The multi-storey building model is installed on the lab through four erection stages. The first stage is to connect the building frame model in two parts, the first part consists of the first four levels with all steel plate floors and the second part consists the other six levels. The second stage is to fix the first part of the building model with a rigid base plate by welding all supprts of the lower columns and all supports are fixed support type, as shown in *Figure 5.46.*

Figure 5.46. Multi-storey steel building model during erection stages

The third stage is to connect the second part of the building model over the first part to form the whole multi-storey building model without additional masses. Whereas, the

final stage is to connect all additional masses on the floors by bolts and praper the model for experimental testing. All stages of the building model erection are carried out by the lab staff and author and started from the lower level up to upper level, as shown in *Figure 5.46*. The way of fixed the supports is necessary in the experimental testing to prevent any undesirable movement in the supports during the excitation of the structural model by simulated ambient vibration using shaker device.

5.6.2. Positions of the accelerometers on the multi-storey building model

For multi-storey building model, several trials also are implemented to fix the appropriate distribution of accelerometers positions using only eight accelerometers which are available. Due to the geometry of the building frame model, the accelerometers positions (measurement points) are desigened in five sets along the height of the model to cover the large number of degrees of freedom of the all 10-storey with limited numbers of accelerometers. All five sets have the same distribution of the accelerometers positions and directions on the measurement points, as shown in *Figure 5.47*.

(a)  (b) 

Figure 5.47. Distribution of eight accelerometers of the measurement points with movement directions of muti-storey building model in (a) the second set and (b) the third set

All five set are distributed only in the xz-plane of height of the building model and included ten levels where each set consists of two levels respectively. Each set of the five sets contains four measurement points, two points in the right side and two points in the left side. The measurement points in the right side include two degrees of freedom using 2-accelerometers to measure the transverse movement direction of y-axis of the model. In other two measurement points in the left side have four degrees of freedom using 4-acceleroemeter to measure two transverse movement directions of y-axis and two transverse movement directions of x-axis of the model, as shown in *Figure 5.48*.

The other two accelerometers are used in the reference measurement point with two degrees of freedom. The reference point is located at level-9 at the oppesite side of xz-plane. This reference point is required to be in the same position for all five sets during recording ambient vibration measurements to extract the modal properties of the building model using ARTeMIS software.

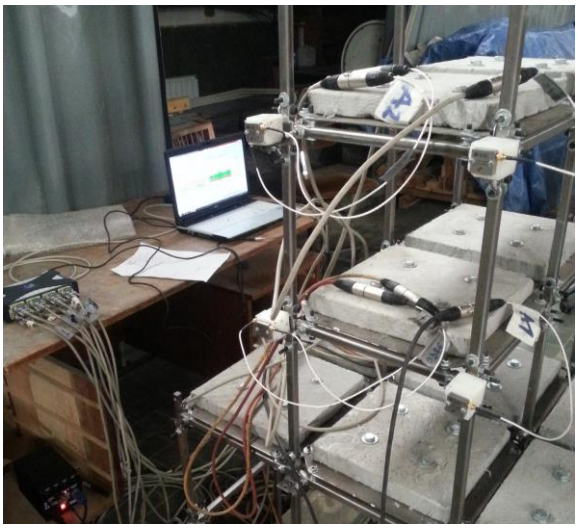

Figure 5.48. Positions of accelerometers of measurement points and movement directions of second set of multi-storey model

All accelerometers are set up on cubes and those cubes are installed by screws on steel angle section glued on the specified measurement points on the model, as shown in *Figure 5.48*. This way of connection helps to carry out the experimental testing fast by

facilitating move the accelerometers through the five sets during ambient vibration measurements. All accelerometers are set up on the intersecting nodes of the beams with columns of the specified plane of the building model. The distribution of measurement points is adopted in five sets to present and reflect the real structural behavior, flexural and torsion, of the building model from ambient vibration measurements.

5.6.3. Data acquisition system and signal processing using simulated ambient vibration of the multi-storey building model

Simulation of ambient vibration measurements of the multi-storey building model is carried out using the shaker device, acquisition device of 24-bits 8 channel and PC-storage system, as shown in *Figure 5.49*. The shaker device is installed on the thick wood plate by bolts and this plate iis fixed on the main rigid base plate of the structural model by bolts to allow waves of vibration to influence on the model base directly. In this way, the excitation is insured to influence on the base of the model, which simulates the ambient vibration.

Figure 5.49. Data acquisition system of the multi-storey building model

The process of experimental testing is started by holding the shaker device with specified intensity value of 5 using the same random vibration signals generated by MATALB software. The recording the acceleration time history of each specified

accelerometers installed on the building model is stored in the PC as data file. The frequency range of the vibration response of the model has been investigated using numerical model. The selected of appropriate sampling frequency of the vibration response and the value of filtering frequency are adopted of 600 Hz and 50 Hz, respectively. The time of data recording is 30 min for each set.

For the building model, the recorded data of each set of accelerometers consist 5-transverse in y-axis and 3-transverse in x-axis movements including the reference point. The sample of acceleration history time of the first transverse movement accelerometers of the building model for the first 100 seconds of the recording are shown in *Figure 5.50*. The figures of acceleration time history of other accelerometers only for model are shown in Appendix - A4.

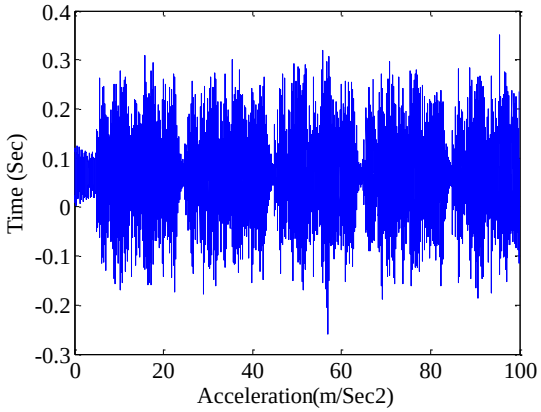

(a)

Figure 5.50. Acceleration history time for one accelerometer during simulated ambient vibration measurements using shaker of intact multi-storey model

The geometry of the structural model in coordinate system, the title of the project, the sampling frequency, the names of recorded data file of all five sets and description of the accelerometers and their direction of movements during excitation are written in CFG file defined in ARTeMIS software. The geometry of the building model and distribution of accelerometers in each set of the five sets along the height of building model are presented in ARTeMIS software, as shown in *Figure 5.51*.

(a) 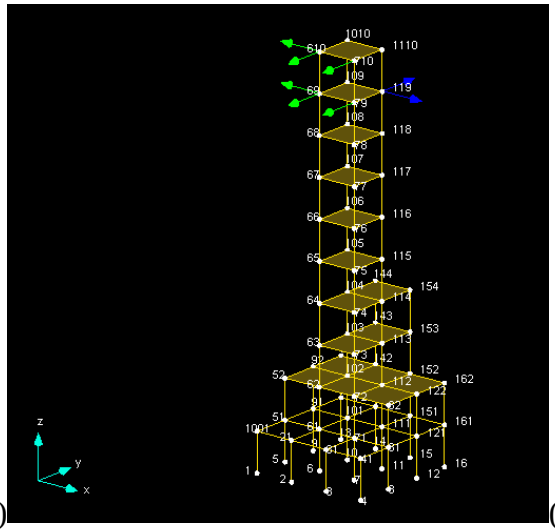 (b) 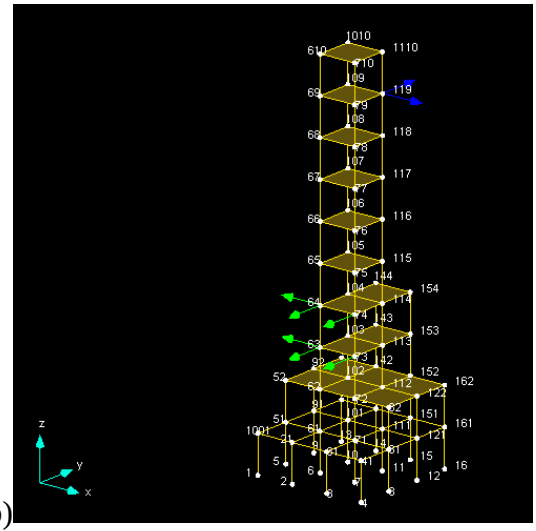

Figure 5.51. Geometry and distribution of accelerometers with reference point for (a) first set and (b) fourth set of measurements of intact multi-storey building model

Figure 5.51 (a) shows one sample of set of measurement of the five sets, in each set the blue arrows are the two movements (accelerometers) of the reference point, while the green arrows are six movements of the set measurements of the building model.

Then, the data processing is conducted to estimate the average of the normalized singular value of spectral density matrices of all ten data sets and from which the peak picking procedure is applied to extract the modal properties of the multi-storey building model.

5.6.4. Extraction of modal properties of the intact multi-storey building model using ARTeMIS extractor software

The modal frequencies and mode shapes of the intact multi-storey building model are extracted using ARTeMIS - extractor software by the FDD technique. The peak picking procedure of FDD technique is implemented with number of frequency line of 8192 to get the appropriate frequency resolution and overlap of 66.67 %, filtering (Butterworth) and window function (Hanning). Several trials of measurements are conducted to provide more confidence of the extracted modal properties, according to the spectral density matrices

estimated based on the recorded ambient vibration data. The diagram of the spectral density matrices of all data sets for the building model are shown in *Figure 5.52*.

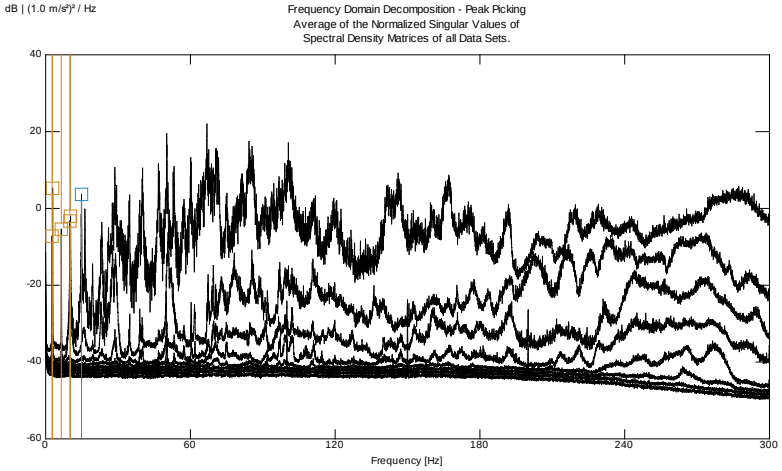

Figure 5.52. Spectral density matrices with selected modes using FDD estimation procedure in ARTeMIS extractor software of intact muti-storey building model

The structural modes are estimated using the peak-picking procedure, according to FDD estimation technique explanation in paragraph 3.5.4. The vertical lines in the figures represent the peak picking modal modes in FDD method, which means only the real structural modes are selected from the peaks. The results of the first six modal frequencies and the modes characters of the multi-storey building model are listed in Table 5.16.

Table 5.16: Experimental extracted modal frequencies using ARTeMIS extractor for multi-storey building model

Mode No.	Frequency Value of Intact Model (Hz)	Mode Character
1	2.637	1st Bending about y-axis
2	2.893	1st Bending about x-axis
3	6.555	1st Torsion
4	10.030	2nd Bending about y-axis
5	10.290	2nd Bending about y-axis
6	14.870	2nd Torsion

On the other hand, the first six mode shapes results and their characters corresponding to the natural frequencies of the multi-storey building model are shown in *Figure 5.53*. The values of the first six mode shape vectors of the multi-storey building model are provided as output SVS system file from the ARTeMIS software.

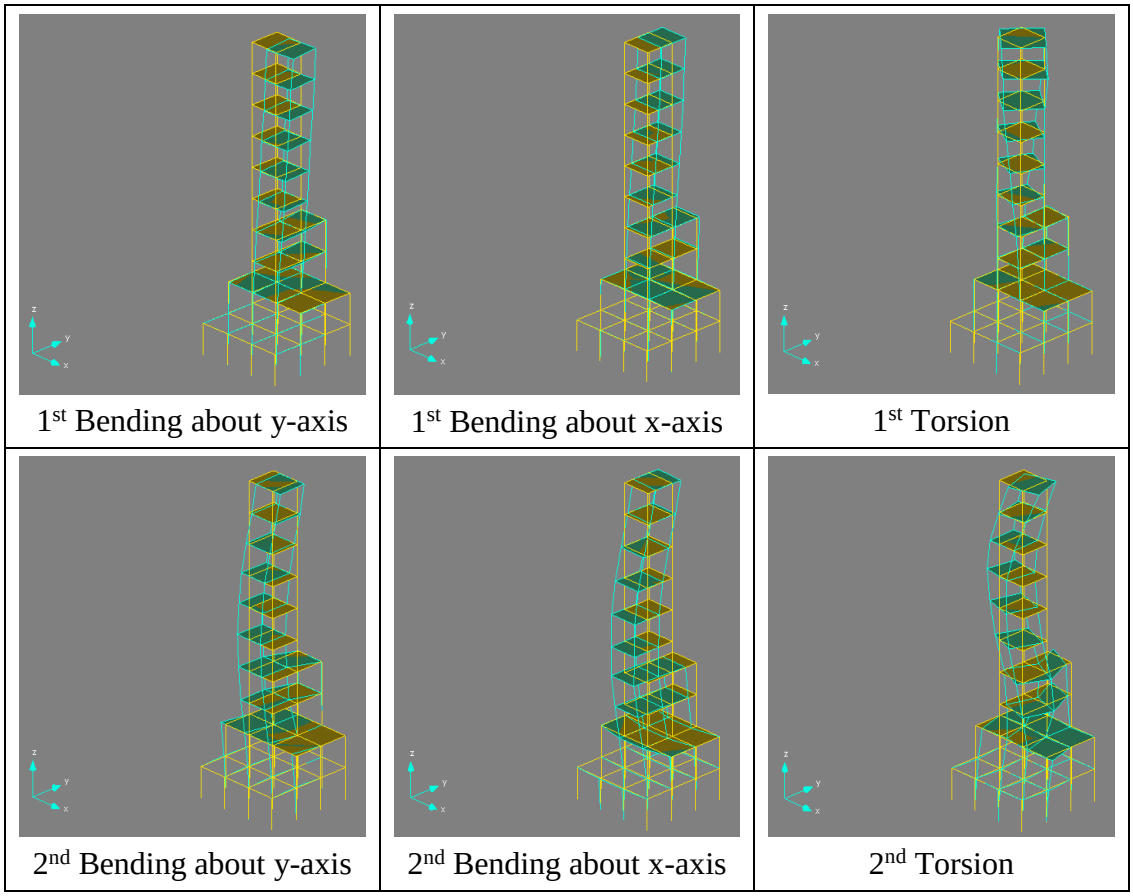

Figure 5.53. Experimental modal properties of the intact multi-storey building model by FDD technique procedure using ARTeMIS extractor software

The values of the first and second mode shape vectors of the the multi-storey model for the 80 nodes, numbered as shown in *Figure 5.51*, including reference point are listed in Table 5.17. The mode shape vectors in table are for three movement directions, where in this model the X and Y-axis are included for the transverse movements in both directions X and Y-axis, respectively, of the measurement points. The third movement in the vertical

axis is very small and neglected. It is clear from Table 5.17 that the maximum value of displacement vector for the first mode shape about y-axis is at node number 610 and 710 in the displacement of x-axis of the building model and equal of 1.00, numbered as shown in *Figure 5.51*. Whereas, for the second mode shape about x-axis is at node number 710 and 1110 in the displacement of y-axis of the building model and equal of 1.00. For the first and second mode shape, first bending about y and x-axis, the maximum displacement is in the upper end and this verifying the results.

Table 5.17: Experimental extracted mode shape vectors using ARTeMIS extractor for both intact multi-storey building model

Node No.	First Mode Shape Vectors of Building Model About Y-Axis			Second Mode Shape Vectors of Building Model About X-Axis		
	Disp. Vector-X (Trans.)	Disp. Vector-Y (Trans.)	Disp. Vector-Z (Vert.)	Disp. Vector-X (Trans.)	Disp. Vector-Y (Trans.)	Disp. Vector-Z (Vert.)
1	0.0000	0.0000	0.0000	0.0000	0.0000	0.0000
2	0.0000	0.0000	0.0000	0.0000	0.0000	0.0000
3	0.0000	0.0000	0.0000	0.0000	0.0000	0.0000
4	0.0000	0.0000	0.0000	0.0000	0.0000	0.0000
5	0.0000	0.0000	0.0000	0.0000	0.0000	0.0000
6	0.0000	0.0000	0.0000	0.0000	0.0000	0.0000
7	0.0000	0.0000	0.0000	0.0000	0.0000	0.0000
8	0.0000	0.0000	0.0000	0.0000	0.0000	0.0000
9	0.0000	0.0000	0.0000	0.0000	0.0000	0.0000
10	0.0000	0.0000	0.0000	0.0000	0.0000	0.0000
11	0.0000	0.0000	0.0000	0.0000	0.0000	0.0000
12	0.0000	0.0000	0.0000	0.0000	0.0000	0.0000
13	0.0000	0.0000	0.0000	0.0000	0.0000	0.0000
14	0.0000	0.0000	0.0000	0.0000	0.0000	0.0000
15	0.0000	0.0000	0.0000	0.0000	0.0000	0.0000
16	0.0000	0.0000	0.0000	0.0000	0.0000	0.0000
1001	0.0000	0.0000	0.0000	0.0000	0.0000	0.0000
21	0.0000	0.0025	0.0000	0.0000	0.0209	0.0000
31	0.0000	0.0029	0.0000	0.0000	0.0268	0.0000
41	0.0000	0.0000	0.0000	0.0000	0.0000	0.0000
51	0.0249	0.0000	0.0000	0.0025	0.0000	0.0000

61	0.0249	0.0025	0.0000	0.0025	0.0209	0.0000
71	0.0249	0.0029	0.0000	0.0025	0.0268	0.0000
81	0.0249	0.0000	0.0000	0.0025	0.0000	0.0000
91	0.0000	0.0000	0.0000	0.0000	0.0000	0.0000
101	0.0000	0.0025	0.0000	0.0000	0.0209	0.0000
111	0.0000	0.0029	0.0000	0.0000	0.0268	0.0000
121	0.0000	0.0000	0.0000	0.0000	0.0000	0.0000
131	0.0000	0.0000	0.0000	0.0000	0.0000	0.0000
141	0.0000	0.0025	0.0000	0.0000	0.0209	0.0000
151	0.0000	0.0029	0.0000	0.0000	0.0268	0.0000
161	0.0000	0.0000	0.0000	0.0000	0.0000	0.0000
52	0.0779	0.0000	0.0000	0.0054	0.0000	0.0000
62	0.0779	0.0077	0.0000	0.0054	0.0690	0.0000
72	0.0779	0.0084	0.0000	0.0054	0.0715	0.0000
82	0.0779	0.0000	0.0000	0.0054	0.0000	0.0000
92	0.0000	0.0000	0.0000	0.0000	0.0000	0.0000
102	0.0000	0.0077	0.0000	0.0000	0.0690	0.0000
112	0.0000	0.0084	0.0000	0.0000	0.0715	0.0000
122	0.0000	0.0000	0.0000	0.0000	0.0000	0.0000
132	0.0000	0.0000	0.0000	0.0000	0.0000	0.0000
142	0.0000	0.0077	0.0000	0.0000	0.0690	0.0000
152	0.0000	0.0084	0.0000	0.0000	0.0715	0.0000
162	0.0000	0.0000	0.0000	0.0000	0.0000	0.0000
63	0.1844	0.0127	0.0000	0.0028	0.1503	0.0000
73	0.1844	0.0197	0.0000	0.0028	0.1512	0.0000
103	0.1532	0.0127	0.0000	0.0026	0.1503	0.0000
113	0.1532	0.0197	0.0000	0.0026	0.1512	0.0000
143	0.0000	0.0127	0.0000	0.0000	0.1503	0.0000
153	0.0000	0.0197	0.0000	0.0000	0.1512	0.0000
64	0.3110	0.0470	0.0000	0.0204	0.2370	0.0000
74	0.3110	0.0463	0.0000	0.0204	0.2407	0.0000
104	0.2177	0.0470	0.0000	0.0169	0.2370	0.0000
114	0.2177	0.0463	0.0000	0.0169	0.2407	0.0000
144	0.0000	0.0470	0.0000	0.0000	0.2370	0.0000
154	0.0000	0.0463	0.0000	0.0000	0.2407	0.0000
65	0.4515	0.0460	0.0000	0.0041	0.3751	0.0000
75	0.4515	0.0431	0.0000	0.0041	0.3755	0.0000
105	0.3625	0.0460	0.0000	0.0033	0.3751	0.0000
115	0.3625	0.0431	0.0000	0.0033	0.3755	0.0000
66	0.5773	0.0757	0.0000	0.0338	0.5247	0.0000
76	0.5773	0.0217	0.0000	0.0338	0.5322	0.0000
106	0.4800	0.0757	0.0000	0.0268	0.5247	0.0000
116	0.4800	0.0217	0.0000	0.0268	0.5322	0.0000

67	0.6971	0.0972	0.0000	0.0455	0.6669	0.0000
77	0.6971	0.0230	0.0000	0.0455	0.6835	0.0000
107	0.5786	0.0972	0.0000	0.0307	0.6669	0.0000
117	0.5786	0.0230	0.0000	0.0307	0.6835	0.0000
68	0.8303	0.0843	0.0000	0.0433	0.8162	0.0000
78	0.8303	0.0211	0.0000	0.0433	0.8199	0.0000
108	0.7250	0.0843	0.0000	0.0398	0.8162	0.0000
118	0.7250	0.0211	0.0000	0.0398	0.8199	0.0000
69	0.9181	0.1021	0.0000	0.0581	0.9076	0.0000
79	0.9181	0.0121	0.0000	0.0581	0.9249	0.0000
109	0.8019	0.1021	0.0000	0.0135	0.9076	0.0000
119	0.8019	0.0503	0.0000	0.0135	0.9290	0.0000
610	1.0000	0.0833	0.0000	0.0574	0.9914	0.0000
710	1.0000	0.0879	0.0000	0.0574	1.0000	0.0000
1010	0.8291	0.0833	0.0000	0.0487	0.9914	0.0000
1110	0.8291	0.0879	0.0000	0.0487	1.0000	0.0000

Those vector values are normalized depend on the maximum vector value, therefore all other points vectors are less than the maximum vector value of 1, as listed in Table 5.17. The exported output file from ARTeMIS software provide vector values with positive signs for all measurement points, therefore for the purposes of computations, the vectors values signs are assumed and taken as in the numerical results.

In addition, to verify the results of the extracted modal properties, the MAC values for the building model are calculated by Eq. (4.10) to obtain an indication for the relationship between each two modes, as listed in Table 5.18. The table shows the correlation between each two extracted modes of the model where the MAC values for each different modes are very small close to zero and equal 1 for each equal modes. Those MAC values verify the validity of the extracted modes with respect to their stability and the modes represent the real structural modes.

Also, the MAC values could be presented as a bar charts which is provided in ARTeMIS software, as shown in *Figure 5.54* for the building model. It is clear from figure, the validity of the extracted modes with respect to the same mode of value equal to 1 and different mode of value close to zero.

Table 5.18: MAC values of extracted mode shapes corresponding to natural frequencies using ARTeMIS extractor for intact multi-storey building model

Frequency Value (Hz)	2.637	2.893	6.555	10.03	10.290	14.870
2.637	1	0.01639	0.112	0.3145	0.03201	0.2661
2.893	0.01639	1	0.0228	0.01637	0.288	0.01221
6.555	0.112	0.0228	1	0.097	0.01662	0.04011
10.03	0.3145	0.01637	0.097	1	0.1027	0.32
10.290	0.03201	0.288	0.01662	0.1027	1	0.01928
14.870	0.2661	0.01221	0.04011	0.32	0.01928	1

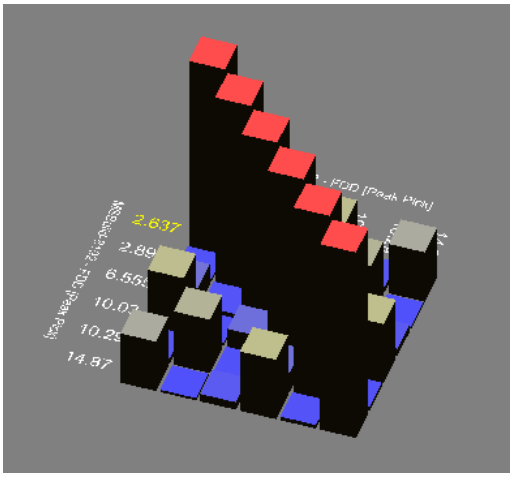

Figure 5.54. Bar charts of MAC values of experimental modal properties using ARTeMIS extractor software of the intact multi-storey building model

5.6.5. Implemented damage scenarios in the multi-storey building model

For the multi-stoery building model, two different damage scenarios are implemented to investigate the behavior of structural model and efficiency of the proposed procedure for detecting damage location and severity in different positions on the model. The first damage scenario is at the column as it is true that the column in the building frame has significant effect and the second damage scenario is at the beam, as shown in *Figure 5.55*.

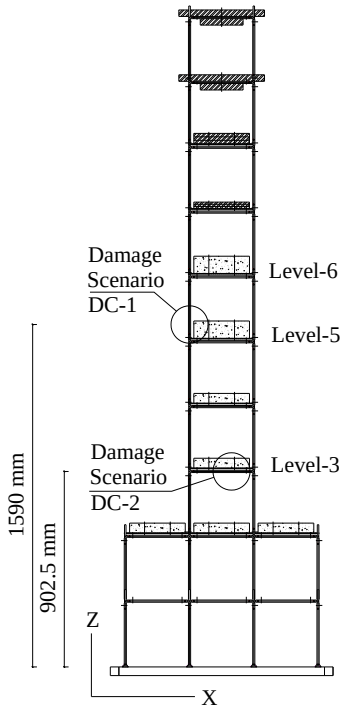

Figure 5.55. Location of damage scenarios, DC-1 and DC-2, on the damaged multi-storey building model

The first damage scenario, DC-1, is located at the lower third of column between level-5 and 6 at the right hand side of the xz-plane at the distance of 1590 mm c/c from the model base plate of the building model, as shown in *Figure 5.55*. The implemented damage scenario in DC-1 has crack height of 60 mm and crack depth of 5 mm of the total depth of 15 mm which represents 33.34 % of the total depth of the column cross section (i.e. damage ratio of 0.334), as shown in *Figure 5.56* (a).

The second implemented damage scenario, DC-2, is located at the right third part of the beam at level-3 of the xz-plane at distance of 902.5 mm c/c from the model base plate of the building model, as shown in *Figure 5.55*. The implemented damage scenario in DC-2 has the length of 60 mm and depth of 5 mm of the total depth of 15 mm which also represents 33.34 % of the total depth of the beam cross section (i.e. damage ratio of 0.334), as shown in *Figure 5.56* (b).

(a)  (b) 

Figure 5.56. Extent of damage scenarios of the damaged multi-storey building model in (a) in DC-1 and (b) in DC-2

For experimental testing, the first damage scenario, DC-1, is first examined and repaired, after which the second damage scenario, DC-2, is implemented. The ambient vibration testing and estimation procedure for the intact case of the structural model is repeated after repairing the damage created in DC-1. In this way, the same modal properties were ensured as in the intact case.

5.6.6. Extraction of modal properties of the damaged multi-storey building model using ARTeMIS extractor software

After implementation of damage scenarios, two trials of ambient vibration measurements are carried out for each of the two damage scenarios in order to improve reliability in the extracted modal properties of the damaged multi-storey building model. The first six values of modal properties, natural frequencies and mode shapes, of the damaged building model for both damage scenarios are extracted using ARTeMIS software. The results of natural frequency values of the intact and damaged model with percentage of reduction are listed in Table 5.19.

Table 5.19: Experimental extracted modal frequencies using ARTeMIS extractor for both damaged and intact multi-storey building model

Mode No.	Frequency Value of Intact Building Model (Hz)	Frequency Value of Damaged Building Model (Hz)			
		DC-1	Relative Reduction (%)	DC-2	Relative Reduction (%)
1	2.637	2.637	0	2.637	0
2	2.893	2.893	0	2.893	0
3	6.555	6.482	1.11	6.555	0
4	10.03	9.997	0.33	9.997	0.33
5	10.290	10.25	0.39	10.29	0
6	14.870	14.87	0	14.87	0

Respect to the intact building model, in the case of DC-1 the reduction is in the third, fourth and fifth mode with no reduction in the first, second and sixth mode, whereas for the case of DC-2 the reduction is in the fourth mode only. Also, in the case of DC-1, the maximum reduction in frequency value are extracted in the third modes (torsion mode), while in the case of DC-2, the reduction only in frequency value are extracted in the fourth mode (bending mode about y-axis).

It is obvious from Table 5.19 that the DC-1 (located at the column) has more significant reduction in natural frequency values than DC-2 (located at the beam) and this verify that the damage in column has more dangerous than in beam. In addition, the maximum value of reduction in the DC-1, respect to the intact model, is in the third mode (torsion mode) and it is different mode for the case in the DC-2, while there is no effect in the first, second and sixth mode in both damage scenarios as well as in the third and fifth mode for the DC-2.

6. NUMERICAL MODELING SIMULATION (FEM) AND MODEL CALIBRATION PROCESS BETWEEN EXPERIMENTAL AND NUMERICAL DYNAMIC CHARACTERISTICS

6.1. General

This chapter deals with the numerical investigations, which are conducted to extract the dynamic characteristics of the adopted four structural models. In presented thesis, this part of the study represents a second part of the main three parts included in the proposed SHM procedure to detect damages in structural models, as shown in Figure 1.1. The numerical analysis is performed for all adopted structural models; overhang beam, grid bridge, Vierendeel bridge and 10-storey building model. The simulation of Finite Element Model (FEM) for each structural model are created using ANSYS Parametric Desigen Language (APDL) within ANSYS package software [133]. The dynamic characteristics of the structural model are estimated using modal analysis by block Lanczos method. To analyze the structural models, the isotropic elastic linear structure is assumed and the estimated modal properties of the structural model are natural frequencies and mode shapes.

The main objective of this chapter is outlying a numerical study that is implemented to estimate vibration response of adopted structural models at different states of loading for intact initial FE models. In the FE analysis, two types of elements are applied to the FEM of the structural models, Beam4 and Mass21 element type. The Beam4 element type is used for all element in the FE models, whereas the Mass21 element type is used for the additional masses, which represent the concrete cubes and cubes of accelerometers. Two loading state, without and with additional masses, are applied for two types of the structural model, grid and Vierendeel bridge model, and the original state is adopted for the other two structural model, overhang beam and multi-storey building model.

On the other hand, the calibration process is carried out on the initial FE models to converge the estimated modal properties to those are extracted of experimental testing of the models. The sensitive parameters are selected from assumed initial parameters of the FE model to implement the calibration process. The updating of the selected parameter is made during the numerical process until the results of calibrated FE model correspond or very close to the results of experimental model. The compatibility between the numerical calibrated FE and experimental model is high important for proposed SHM procedure to detect damage in structural models.

6.2. Modal analysis of FE model

The modal analysis of the FE model is one of the dynamic analysis of the structure, which is applied to determine the dynamic (vibration) characteristics, natural frequencies and mode shape, of the structures while they are being designed or under operational condition [133]. The natural frequencies and mode shapes are important parameters in the design of the structure for dynamic loading conditions or in the structural health monitoring (SHM) under operational condition. The modal analysis can also assist as a starting procedure for another advance dynamic analysis such as transient dynamic and harmonic analysis ... etc.. There are two type of the modal analysis based on the damping in the structure, undamped and damped modal analysis. For the system becoming a damped modal analysis, the modal properties become complex. In this study, the modal analysis without damping in the structure is adopted to analyze the created FE models and estimate the modal properties.

In present study, ANSYS software [133] is used to estimate the dynamic characteristic of the FE model of the structures using modal analysis by Block Lanczos method as a mode-extraction method. The modal analysis analyzes the FE model for isotropic elastic linear structure with defining the initial material properties such as Young's modulus (E) and mass density (ρ). Also, the initial real constants of the FE model are required for specific element type in the FE structural model. After defining the analysis method type, the mode-extraction method and number of modes to estimate are specified to finish the analysis of the FE model. The loads applicable in the modal analysis are zero-

value displacement constrains with specifying their directions and they are applied on nodes or elements of the FE model. The solve of the problem starts after specifying all required parameters of the modal analysis method and then the results of the analysis could be estimated for natural frequencies and mode shape vectors.

The Block Lanczos extraction method used in modal analysis in ANSYS software is available for large symmetric eigenvalue problems. The method is performed using a block of vectors as opposed to single vector [133]. The Block Lanczos method could solve FE model with 1,000,000 degrees of freedom (DOFs) with many constraint equations and that requires large amount of computer memory and computing time. Therefore, in present study the high quality of PC laptop Inspiron Dell, with Core-i7 processor type and 2-Giga memory storage, is used to perform the dynamic modal analysis of the four adopted structural models.

On the other hand, in ANSYS software there are two way to create and describe the FE model of the structural model and then analyze it, using either Graphical User Interface (GUI) or ANSYS Parametric Design language (APDL). In this study and due to the feature of the APDL, the second way using APDL is adopted to create the FE models and perform the modal analysis and extract the dynamic characteristics of the structural models.

6.3. Features of APDL environment in ANSYS software

In ANSYS software, the standard APDL is a scripting language that can use to automate common tasks or even build the model in term of parameters/variables. Also, the APDL consists a wide range of other features such as repeating commands, macros, if-then-else branching, do-loops, scalar, vector and matrix operations [134]. The APDL variables are more similar to Fortran language variable and all numeric values, integer or real, are stored as double-precision values. It is also provides several types of array parameters such as numeric, character, string and table.

The APDL is used as sophisticated features such as design optimization and adaptive meshing and it is also offers many flexibility during analyzing the FE model.. In the APDL can do multi change on the parameters of the created FE model and import the geometry file. The analyzing of the FE model with quick batch process to integrate its preprocess and

postprocessor and then export data files of the results to another software which can automatic connect with them such as MATLAB to solve hard optimization problems for example [4]. However, the APDL environment needs high experience from user to work with it and programming the problem of the structure with all details of the geometry, real constant, material properties,... etc. In this study, the standard APDL environmental is used to create FE model and analyze the model using modal analysis method for the adopted structural models.

6.4. Numerical analysis of the simply supported overhang model

As mentioned before, the first numerical structural model in this study is a simply supported steel overhang beam. The selection of this beam model is as simple case to implement the numerical investigation and estimate the modal properties. The present study adopted this model as a simple beam structure has only the flexural behavior. This beam model has only movement in one direction, vertical displacement, and the transverse and longitudinal displacements are very small and neglected.

6.4.1. Description of initial FE model

The simply supported steel overhang beam has the total length of 1500 mm with rectangular cross section of dimensions of (5x50) mm. The overhang of 20 mm was made on the left-hand side to provide support, while the overhang of 380 mm was made on the right-hand side to make the structure unsymmetrical. The mid-span length between the supports was 1100 mm, as shown in *Figure 5.1*. Initial material properties adopted by modulus of elasticity of E_initial=2x10^5 N/mm^2, Poisson's ratio ν = 0.3 and mass density ρ_initial=7.860x10^3 kg/m^3. The numerical simulation of the beam model is created using ANSYS software by APDL environmental. The created FE model of the examined structure includes of 60 elements and 61 nodes, each element length in the range of 20-30 mm. The first element at left overhang has 20 mm length and the last element at right overhang has length of 30 mm, while the other middle 58-element have the same length of

25 mm, as shown in *Figure 6.1*. The element length assumed to provide possibility for detecting the precise damage location for the adopted damage scenarios.

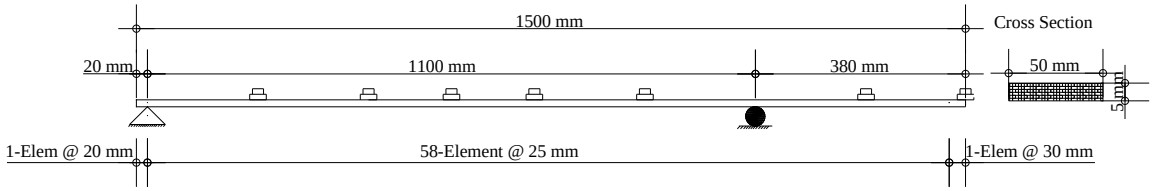

Figure 6.1. Finite element model of overhang steel beam model

The numerical simulation analysis is carried out using ANSYS software for structural analysis using Beam4 element type and linear elastic isotropic material. Due to the low mass of the model, masses of instruments and supporting cubes were included in the FE model. Masses of seven transducers used during the experimental investigations were added to the FE model using Mass21 element type, with the average mass of 34.525×10^{-3} kg and the appropriate mass moment of inertia of 5.3945×10^{-6} kg.m^2.

6.4.2. Estimation of modal properties

The modal analysis using Block Lanczos method is applied to estimate the first four modes for the intact initial beam model. The assumed initial values of geometry and material parameters are used in this analysis. The created input file in ANSYS-APDL environment is written for the geometry, real constant, material properties, boundary condition and solving method with all required parameters of the overhang beam model, as listed in Appendix -D. In this file also the commands to export the requierd output results, modal frquencies and mode shape vectors, is included by opening new file of results, which can import and read it in another software. All units of the geometry, real constant and material properties of the FE model should be entered consistent in ANSYS-APDL input file, which are in mm and Newton.

The boundary conditions (supports types) for this FE beam model are assumed as, one is hinge support at left side and the other is roller support at right side. the hinge support is restricted in movement direction x-axis (longitudinal), z-axis (vertical) and y-axis

(transverse) as well as the rotation about x-axis, and the other is restrained only in the vertical z-axis and transverse y-direction.

The estimated first four modal frequencies values and mode characters of the overhang beam model are listed in Table 6.1. In this table, the corresponding modal frequencies which are extracted from experimental model,Table 5.1, are also listed with the differences in numerical estimated modal frequencies values corresponding to experimental extracted modal frequencies values.

Table 6.1: Numerical estimated modal frequencies values using ANSYS software for intact initial FE overhang beam model and comparison with experimental extracted values

Mode No.	Modal Frequency Value of Intact Overhang Beam Model (Hz)		Difference in Frequency		Mode Character
	Experimental Model	Numerical Initial FE Model	(Hz)	Relative (%)	
1	7.910	7.724	-0.186	-2.35	1st Bending
2	18.750	18.378	-0.372	-1.98	2nd Bending
3	42.480	42.510	0.030	0.07	3rd Bending
4	90.820	86.223	-4.597	-5.06	4th Bending

It is evident from table, the are significant different between the experimental and numerical results. Therefore, the calibtation process of the initial FE model is needed to tune this differences. In addition, it is noted that the higher difference is in the fourth mode and the lower is in the third mode.

Also, the first four mode shapes results and their characters corresponding to the natural frequencies of the overhang model are shown in *Figure 6.2*. The values of the first four mode shape vectors of the overhang beam model are provided as output file from the ANSYS software. The values of mode shape vectors of 61 nodes of the first mode shape, exported from ANSYS software, of the overhang beam model are listed in Appendix -E. It is clear from *Figure 6.2*, the mode shapes characters estimated numerically is the same extracted experimentally of the overhang beam model, as shown in *Figure 5.9*.

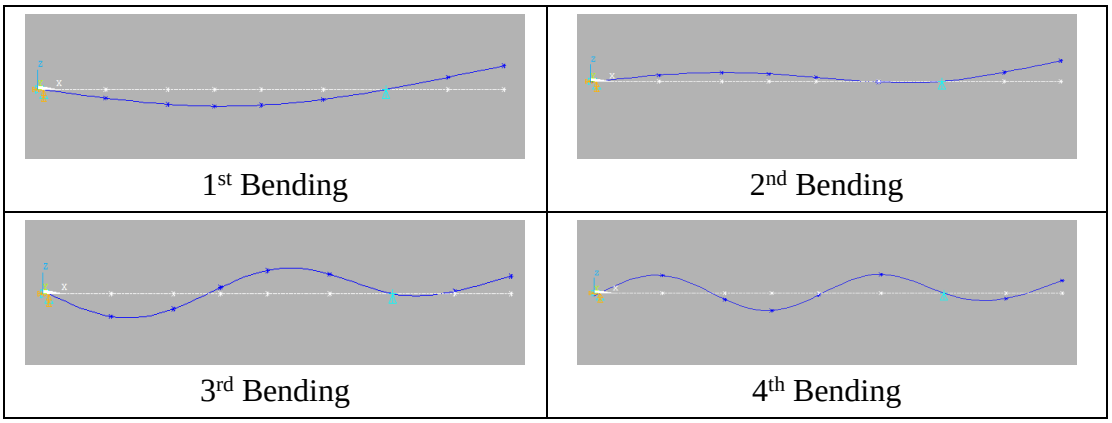

Figure 6.2. Numerical modal properties of the intact initial overhang beam model using ANSYS software

6.5. Numerical analysis of the grid bridge model

The second numerical simulation of structural model in this study is a simply supported steel grid bridge model. The selection of this bridge model is as an advanced case to implement the numerical investigation and estimate the modal properties. The present study adopted this model as a plane structure has the flexural and torsion behavior. This bridge model has two movements and two rotations in two directions, vertical and transverse displacement as well as rotation about x and y-axis, and the longitudinal displacements and rotation about z-axis are neglected.

6.5.1. Description of initial FE model

The simply supported steel grid bridge model has 6800 mm long and 830 mm wide with 10-grid length of 672 mm c/c. The main longitudinal edge and cross steel beams are rectangular hollow section dimensions of (30x50x2.8) mm. The deck of the bridge model is formed as a thin orthotropic plate made of steel, with thickness of 1.5 mm and with 7 longitudinal stiffeners spaced on 100 mm, *Figure 5.13*. The initial values of material properties are assumed as follows: modulus of elasticity of E_initial=2x10^5 N/mm^2, Poisson's ratio ν=0.3 and ρ_initial=7.860x10^3 kg/m^3. The bridge model has four supports, three hinge supports and one roller support. The left side has two hinge supports and one hinge and roller supports at other right side. As mentioned in pagraph 5.4.1, to study the

modal frequencies in different frequency ranges, the model is adopted in two loading states, without additional masses and with additional masses. The loading state with additional mass included 10 masses (concrete cubes) placed at joints of the main longitudinal and cross beams inside the span. Each concrete mass has average mass of 7.925 kg distirbuted equaly along the grid bridge model length, as shown in *Figure 5.16*.

The numerical simulation of the grid bridge model is created using ANSYS software by APDL environmental. The created FE model of the steel grid bridge structural model consists of 928 elements and 609 nodes with three element lengths (42 mm, 100 mm and 168 mm), as shown *Figure 6.3*.

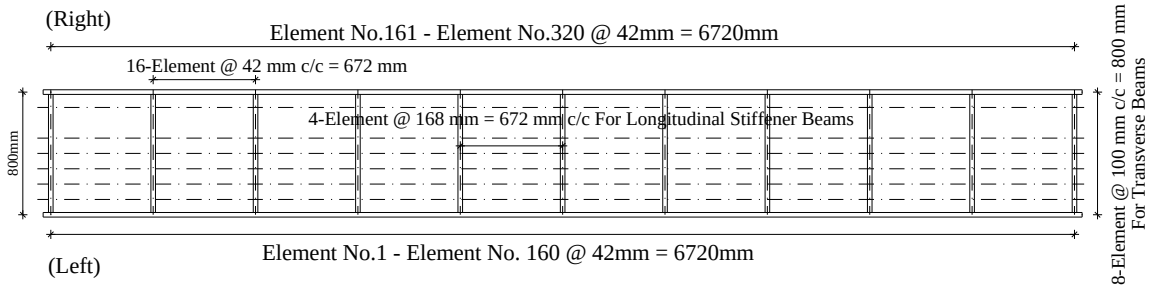

Figure 6.3. Finite element model of grid bridge steel model

According to the importance of the main longitudinal beams for structural integrity, those parts are modeled with the smallest length of 42 mm, to provide the possibility for determining the precise damage location. The length of beam elements of 100 mm is adopted for the main and hidden transverse beams in lateral direction of the orthotropic plate. Those elements of hidden transverse beams are adopted to suppress local behavior of longitudinal stiffener beams of the orthotropic plate. Thus, zero mass density is assumed for those elements with rectangular solid cross section dimensions of (1.5x50) mm. Those dimensions of hidden transverse beams are calculated from many trials to choose the appropriate estimated values of results to be as possible as close to the experimental extracted values. The length of 168 mm is adopted of elements of longitudinal stiffener beams of the orthotropic plate. The section of the longitudinal stiffener beams is assumed in FE model as T-section with web cross section (1.5x45) mm and symmetry length of flange

with cross section (1.5x100) mm. The stiffener beams at the both edge have unsymmetry length of flange with 50 mm in one side and 100 mm in the other side The selection of different element lengths is adopted in order to reduce the number of dergrees of freedom of FE model. In this study, it is focused on 320 elements of both longitudinal main edge beam as a main girders with element length of 42 mm.

The numerical simulation analysis is carried out using ANSYS software for structural analysis using Beam4 element type and linear elastic isotropic material. Due to both studied loading state, without and with additional masses, the element type of Mass21 is used for the FE model with additional masses to simulate the concrete cubes as well as to the Beam4. Additional masses of ten concrete cubes used during the experimental investigations have average mass (*M*_initial) of 7.925 kg and mass moment of inertia of 0.07925 kgm^2, which are added to the FE model using Mass21 element type.

6.5.2. Estimation of modal properties

The modal analyses using Block Lanczos method are applied to estimate the first five modes for both the intact initial bridge model loading state, without and with additional masses. The assumed initial values of geometry, material parameters and additional masses properties are used in those analyses. The created input files in ANSYS-APDL environment are written for the geometry, real constant, material properties, boundary condition and solving method with all required parameters of both the bridge model state. In those input files also the commands to export the requierd output results, modal frquencies and mode shape vectors, are included by opening new files of results, which can import and read them in another software. All units of the geometry, real constant and material properties of both the FE models should be entered consistent in ANSYS-APDL input files, which are in mm and Newton.

For both FE models, four types of boundary conditions (supports types) are assumed same and consisted of three higes supports and one roller support. Two supports are at left side of the bridge model, one hinge support is supress in three movement directions x (longitudinal), y (transverse) and z-axis (vertical) and the other in the same side also hinge support is restricted in two movement directions x and z-axis. The other two supports are in

the right side of the bridge model, one hinge support is restrained in two movement directions y and z-axis, and thee second support is roller and restricted only in z-axis moement direction.

The estimation of the first five modal frequencies values and their mode characters of the intact initial FE grid bridge model state without additional masses are listed in Table 6.2. In this table, the corresponding modal frequencies that are extracted from experimental model state without additional masses, Table 5.6, are also listed with the differences in numerical estimated modal frequencies values corresponding to experimental extracted modal frequencies values.

Table 6.2: Numerical estimated modal frequencies values using ANSYS software for intact initial FE grid bridge model state without additional masses and comparison with experimental extracted

Mode No.	Modal Frequency Value of Intact Grid Bridge Model State without Additional Masses (Hz)		Difference in Frequency		Mode Character
	Experimental Model	Numerical Initial FE Model	(Hz)	Relative (%)	
1	2.490	2.488	-0.002	-0.08	1st Bending
2	9.814	9.943	0.129	1.31	2nd Bending
3	10.550	10.835	0.285	2.70	1st Torsion
4	22.410	22.328	-0.082	-0.37	3rd Bending
5	23.580	23.492	-0.088	-0.37	2nd Torsion

It is evident from table, there are small differences between the results of experimental model and numerical FE model. Those small differences in natural frequencies values reflect the high accuracy of the numerical simulation of initial FE model to the real structural bridge grid model. However, the calibration process of the initial FE model is still needed for more convergence to detect damage in structure precisely. In addition, it is noted from Table 6.2 that the higher difference is in the third mode and the lower is in the first mode.

In addition, the first five mode shapes and their characters corresponding to the natural frequencies of the grid bridge model state without additional masses are shown in *Figure 6.4*. The values of the first five mode shape vectors of the bridge model are stored as output file from the ANSYS software. It is clear from *Figure 6.4*, the mode shapes characters estimated numerically is the same extracted experimentally of the grid bridge model state without additional masses, as shown in *Figure 5.24*.

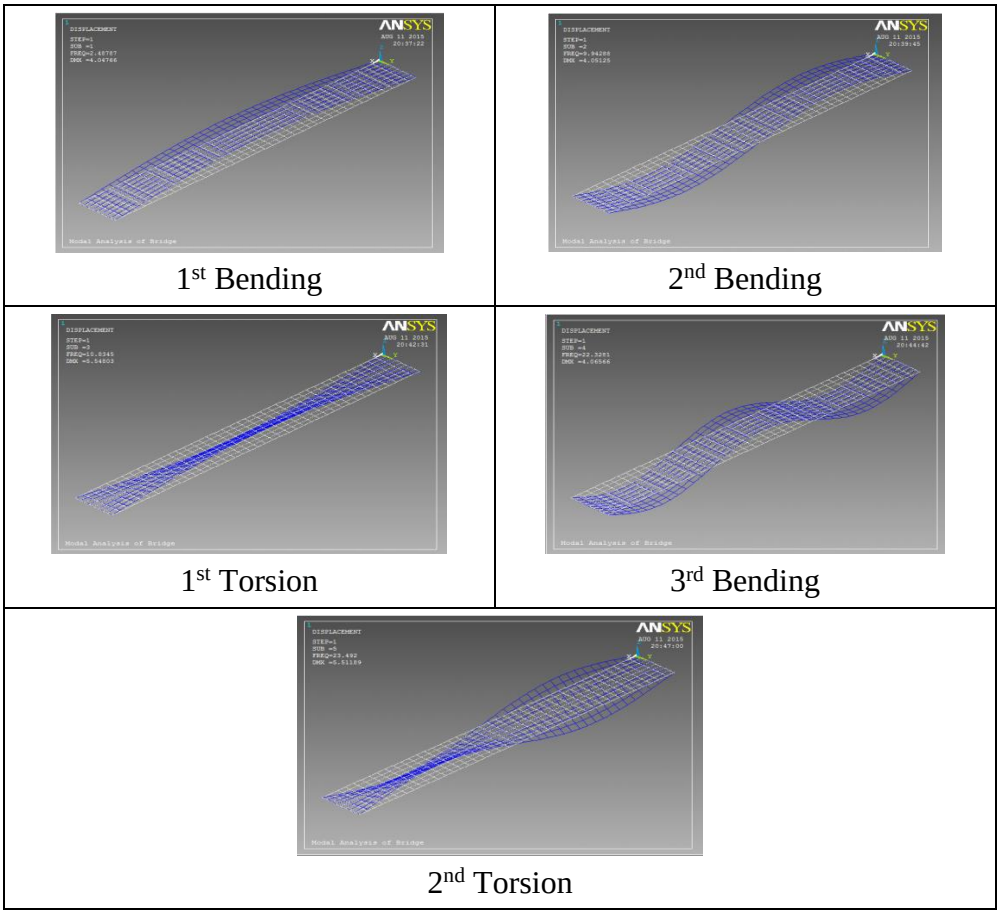

Figure 6.4. Numerical mode shapes of the intact initial FE grid bridge model state without additional masses using ANSYS software

For the loading state of the intact initial FE grid bridge model with additional masses, the estimation of the first five modal frequencies values and their mode characters are listed in Table 6.3. In this table, the corresponding modal frequencies that are extracted from

experimental model state with additional masses, Table 5.6, are also listed with the differences in numerical estimated modal frequencies values corresponding to experimental extracted modal frequencies values.

Table 6.3: Numerical estimated modal frequencies values using ANSYS software for intact FE initial grid bridge model state with additional masses and comparison with experimental extracted values

Mode No.	Modal Frequency Value of Intact Grid Bridge Model State with Additional Masses (Hz)		Difference in Frequency		Mode Character
	Experimental Model	Numerical Initial FE Model	(Hz)	Relative (%)	
1	2.051	1.930	-0.121	-5.90	1st Bending
2	8.093	7.720	-0.373	-4.61	2nd Bending
3	8.313	8.290	-0.023	-0.28	1st Torsion
4	18.240	17.260	-0.980	-5.37	3rd Bending
5	18.640	17.870	-0.770	-4.13	2nd Torsion

It is evident from Table 6.3, there are significant differences between the results of experimental model and numerical FE model. This loading state of the FE model with additional masses is unlike the original state of the FE model without additional masses with small differences in the natural frequencies. Those differences between two loading states of the grid bridge model exhibits the significant effect of the additional masses of the dynamic structural behavior of the real structural model. Therefore, the calibration process of the initial FE model state with additional masses is needed to tune the modal properties of the model to detect damage in structure precisely. Also, it is obvious from Table 6.3 that the higher difference is in the fourth mode and the lower is in the third mode.

In addition, the mode shape characters corresponding to the natural frequencies of the FE grid bridge model state with additional masses are same to those estimated for state FE mode without additional masses, as shown in *Figure 6.4*.

6.6. Numerical analysis of the Vierendeel bridge model

The third numerical structural model in this study is a simply supported steel Vierendeel bridge model. As mentioned before, the selection of this type of bridge model is a complex case to implement the numerical investigation and estimate the modal properties. The present study adopted this model as a 3D-space structure has the flexural and torsion behavior as well as to truss-bending action comes from both fences on the two sides of the bridge model. For the purposes of this study, two movements and two rotations in two directions, vertical and transverse displacement as well as rotation about x and y-axis of this bridge model are adopted, and the longitudinal displacements and rotation about z-axis are neglected. This structural bridge model type is as special complex civil structural applications and it is state-of-the-art of this study.

6.6.1. Description of initial FE model

The Vierendeel bridge model is a complex structure consists of a grid floor and two fences on the both sides with 11-column in each side. Total length of the model is 6800 mm and width is 800 mm, which consists of 10-bay at 672 mm c/c for each, as shown in *Figure 5.28*, and the width of the model contains 8-grid of 100 mm c/c as stiffener beams. This model consists of two main parts, the first is the grid floor, which has the same geometry description of the second adopted model of the grid bridge model, as discussed in paragraph 5.4.1. The second part of this model is the two fences located on the both sides of the bridge model left and right hand side, which consist of 11-column and upper beam in each side, as shown in *Figure 5.28*. The columns sections of the fences have (30x40x2.25) mm dimensions and the columns connect the two main longitudinal beams in the grid floor with main longitudinal upper beams. The main longitudinal upper beams have the same cross section as in the main longitudinal lower beams of grid floor. Each column is stiffened by two triangular steel parts have dimensions of (71x71x100x2.8) mm on the top and bottom, as shown in *Figure 5.28*. The initial values of material properties are assumed as follows: modulus of elasticity of E_initial=2x10^5 N/mm^2, Poisson's ratio ν=0.3 and ρ_initial=7.860x10^3 kg/m^3.

In present study, the numerical simulation of the Vierendeel bridge model is created using APDL enviroment in ANSYS software. The created FE model of the Vierendeel bridge structural model consists 1402 elements and 1063 nodes using Beam4 element type, as shown in *Figure 6.5*. Those element is devided into elements of the grid floor and elements of the both fences. The FE model of the grid floor of the Vierendeel bridge model have the same distribution of elements lengths used in the previous grid bridg model, as discussed in paragraph 5.4.1. Due to the importance of the width of the rectangular solid hidden beam to supress the local behviour of the longitudinal stiffener beams, the width is adopted of 100 mm instead of 50 mm in this FE model. Whereas, for the both fences of FE Vierendeel bridge model consist of additional elements for columns, stiffener parts of columns and longitudinal upper beams. Two different lengths of columns elements are adopted, a 60 mm length for elements of stiffener parts of columns in the lower and upper of each column is used and 54.8 mm length for middle parts of columns. In addition, the same element length of 42 mm used for the main lower beams in grid floor are adopted for the main upper beams in both sides, as shown in *Figure 6.5*.

The triangular cross section of the stiffener parts of the beam-column joint, *Figure 5.28*, can be offset to rectangular cross section to be easiest in computations. Therefore, two assumed equivalent rectangular cross sections are adopted for the stiffener parts elements of the beams and columns in the FE model based on the dimensions. The equivalent cross section of stiffener parts elements of beam has dimension of (85x30x2.8) mm, while the origin cross section of beam has dimension (50x30x2.8) mm. Also, the equivalent cross section of stiffener parts elements of columns has dimension of (110x30x2.25) mm, while the origin cross section of column has dimension (40x30) mm, as shown in *Figure 6.5*.

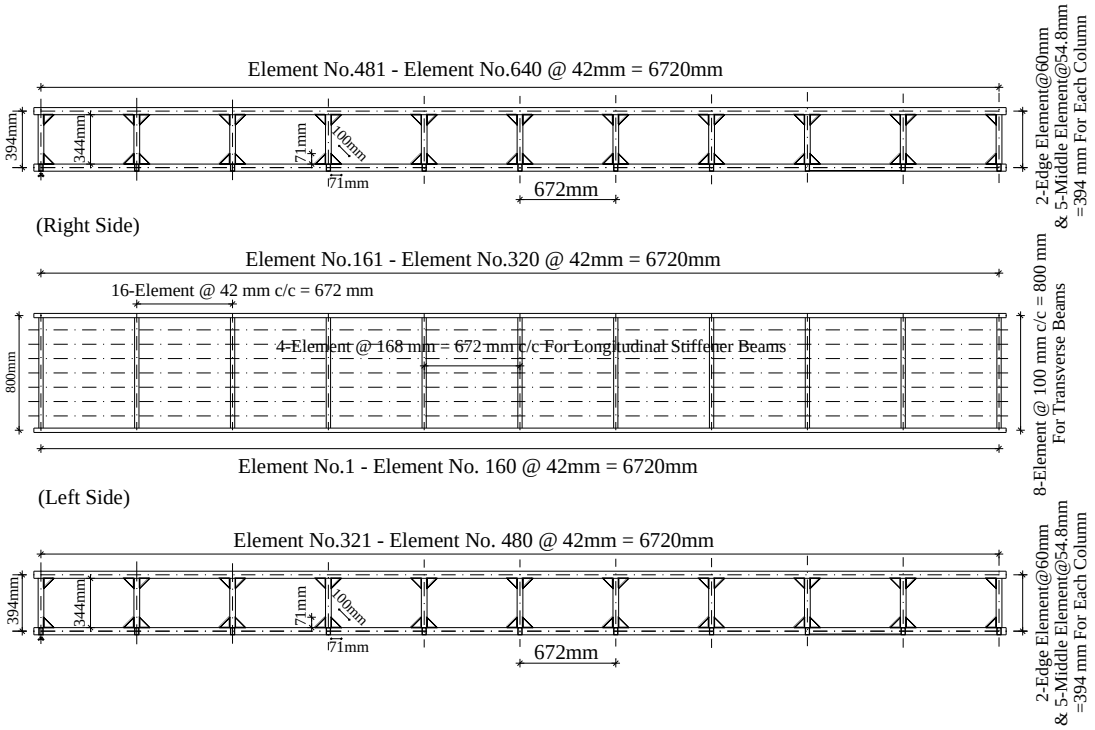

Figure 6.5. Finite element model of Vierendeel bridge steel model

According to the importance of the main longitudinal lower beams in grid floor and the truss-bending action of the both fences for structural integrity, those parts are modeled with the smallest length of 42, 54.8 and 60 mm, to provide the possibility for determining the precise damage location. The selection of different element lengths is adopted in order to reduce the number of dergrees of freedom of FE model and thereby decrease run time of ANSYS software. In this study, it is focused on 794 elements, which consist 640-element of both longitudinal main lower beams and upper beams of fences with element length of 42 mm as well as to 154-elemnt of columns of both fences with element length of 54.8 and 60 mm.

The numerical simulation analysis is carried out using ANSYS software for structural analysis using Beam4 element type and linear elastic isotropic material. Due to both studied loading state, without and with additional masses, the element type of Mass21 is used for the FE model with additional masses to simulate the concrete cubes. Additional masses of ten concrete cubes used during the experimental investigations have average mass

M_initial=7.925 kg and mass moment of inertia of 0.07925 kgm^2, which are added to the FE model using Mass21 element type.

6.6.2. Estimation of modal properties

The modal analyses using Block Lanczos method are applied to estimate the modal properties for both the intact initial bridge model loading state, without and with additional masses. The assumed initial values of geometry, material parameters and additional masses properties are used in those analyses. The created input files in ANSYS-APDL environment are written for the geometry, real constant, material properties, boundary condition and solving method with all required parameters of both the bridge model states. In those input files also the commands to export the requierd output results, modal frquencies and mode shape vectors, are included by opening new files of results, which can import and read them in another software. All units of the geometry, real constant and material properties of both the FE models should be entered consistent in ANSYS-APDL input files, which are in mm and Newton. For both FE models, four types of boundary conditions (supports types) are assumed the same used for the previous grid bridge model which are discussed in 6.5.2.

The estimation of the first four modal frequencies values and their mode characters of the intact initial FE Vierendeel bridge model state without additional masses are listed in Table 6.4. In this table, the corresponding modal frequencies that are extracted from experimental model state without additional masses, Table 5.11, are also listed with the differences in numerical estimated modal frequencies values corresponding to experimental extracted modal frequencies values.

It is evident from table, there are differences between the results of experimental model and numerical FE model. Therefore, the calibration process of the initial FE model is needed to tune the modal properties and for more convergence to detect damage in structure precisely. In addition, it is noted from Table 6.4 that the higher difference is in the first mode and the lower is in the third mode.

Table 6.4: Numerical estimated modal frequencies values using ANSYS software for intact initial FE Vierendeel bridge model state without additional masses and comarison with experimental extracted values

Mode No.	Modal Frequency Value of Intact Vierendeel Bridge Model State without Additional Masses (Hz)		Difference in Frequency		Mode Character
	Experimental Model	Numerical Initial FE Model	(Hz)	Relative (%)	
1	15.234	15.534	0.300	1.97	1st Bending
2	16.552	16.713	0.161	0.97	1st Torsion
3	35.852	35.845	-0.007	-0.02	2nd Bending
4	36.291	36.445	0.154	0.42	2nd Torsion

In addition, the first four mode shapes and their characters corresponding to the natural frequencies of the grid bridge model state without additional masses are shown in *Figure 6.6*. The values of the first four mode shape vectors of 1063 nodes of the bridge model are stored as output file from the ANSYS software. It is clear from *Figure 6.6*, the mode shapes characters estimated numerically is the same extracted experimentally of the Vierendeel bridge model state without additional masses, as shown in *Figure 5.40*.

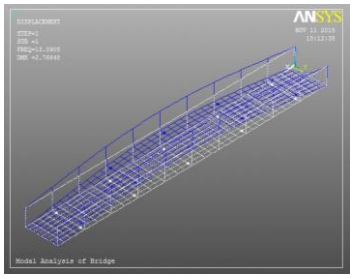

1st Bending

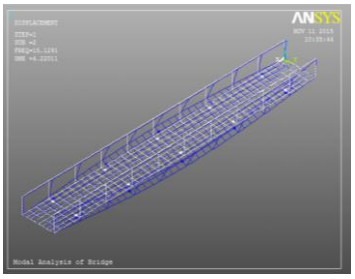

1st Torsion

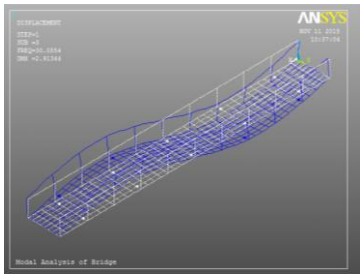

2nd Bending

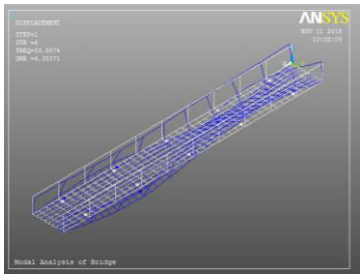

2nd Torsion

Figure 6.6. Numerical mode shapes of the intact initial FE Vierendeel bridge model state without additional masses using ANSYS software

For the loading state of the intact initial FE Vierendeel bridge model with additional masses, the estimation of the first four modal frequencies values and their mode characters are listed in Table 6.5. In this table, the corresponding modal frequencies that are extracted from experimental model state with additional masses, Table 5.11, are also listed with the differences in numerical estimated modal frequencies values corresponding to experimental extracted modal frequencies values.

Table 6.5: Numerical estimated modal frequencies values using ANSYS software for intact initial FE Vierendeel bridge model state with additional masses and comparison with experimental extracted values

Mode No.	Modal Frequency Value of Intact Vierendeel Bridge Model State with Additional Masses (Hz)		Difference in Frequency		Mode Character
	Experimental Model	Numerical Initial FE Model	(Hz)	Relative (%)	
1	13.220	13.090	-0.13	-0.98	1st Bending
2	15.197	15.129	-0.068	-0.45	1st Torsion
3	30.908	30.085	-0.823	-2.66	2nd Bending
4	34.570	33.587	-0.983	-2.84	2nd Torsion

It is evident from Table 6.5, there are significant differences between the results of experimental model and numerical FE model. This loading state of the FE model with additional masses is like the original state of the FE model without additional masses with differences in the natural frequencies. Those differences between two loading states of the Vierendeel bridge model exhibits the significant effect of the additional masses of the dynamic structural behavior of the real structural model. Therefore, the calibration process of the initial FE model state with additional masses is needed also to tune the modal properties of the model to detect damage in structure precisely. Also, it is obvious from

Table 6.5 that the higher difference is in the fourth mode and the lower is in the second mode.

In addition, the mode shape characters corresponding to the natural frequencies of the FE Vierendeel bridge model state with additional masses are same to those estimated for state FE mode without additional masses, as shown in *Figure 6.6* with difference vectors values.

6.7. Numerical analysis of the multi-storey building model

The fourth adopted numerical structural model is a steel multi-stoery building (MSB) The selection of this structural model is as a complex space frame structure to implement the numerical investigation and estimate the modal properties. The present study adopted this model as a 3D-space frame tall building structure has the torsion behavior, the flexural behavior as well as to plate-bending and beam-column action comes from 10-storey model consist from beams, floors and columns. In addition, this 3D-space frame structural building model has movements in three directions, transverse in two directions. As, the vertical movement is very small, therefore, it is neglected in this study. For the purposes of this study, two movements directions and three rotations in three axes, transverse displacement in x and y-axis as well as rotation about x, y and z-axis (vertical) of this building model are adopted, and the vertical displacements (z-axis) is neglected. For the purposes of verification of proposed SHM procedure to detect damage in the structure, this structural building model is as common complex civil structural applications and it is state-of-the-art of this study.

6.7.1. Description of initial FE model

The multi-storey building model consists of 10 storeys (11 levels from 0 to 10) have 300 mm height for each one and the total height is 3000 mm, as shown in *Figure 5.44*. For simulation of actual behavior of the model, different types of masses are applied in order to simulate its modal properties of natural frequencies and mode shapes values. The building frame model consists of 25 floors, for each square floor has (300x300) mm span length c/c. The model consists in the first floor 9-bay, second floor 6-bay, third and fourth 2-bay and

from fifth to tenth are one bay, as shown in *Figure 5.44*. In the building model, the supports type and details of distributed floor plate and additional masses are discussed in 5.6.1. The building model has two types of cross sections which used in the this building frame model for beams and columns. The first section is hollow square section of (15x15x0.8) mm, while the second section for all beam-column joints. The second section has solid square section of (12x12) mm dimension for entire length of 100 mm for both sides of a beam-column joint that is taken in through columns and beams endings, as shown in *Figure 5.45*. This beam column joint consists of rigid element that is inserted through beams and columns and connected by suitable size of bolts from each side of the joints, as shown in *Figure 5.45*.

The numerical simulation of the multi-storey model is created using APDL enviroment in ANSYS software. The created FE model of the building structural model consists 1294 elements, 1223 nodes and 14 areas. In this FE building model three element types are applied, Beam4 for columns and beams elements, shell63 for plate element and Mass21 for additional masses, as shown in *Figure 6.7*. The FE building model has the same element length of 60 mm for all columns and beams, where, each column and beam consist of 5 elements. For beam-column joint, the different real constant of columns and beams elements are adopted with higher stiffness of element. The initial values of material properties are assumed as follows: modulus of elasticity of E_initial=$2x10^5$ N/mm^2, Poisson's ratio ν=0.3 and initial mass density ρ_initial=$7.860x10^3$ kg/m^3.

Figure 6.7. Finite element model of multi-storey building steel model

According to the importance of the columns and beams in building frame for structural integrity, those parts are modeled with the small length of 60 mm, to provide the possibility for determining the precise damage location. The selection of equal element lengths for columns and beams is adopted due to the symmetry of dimensions of the building model in columns and beams. In this study, it is focused on the elements of columns and beams for damage detection procedure, which consist 793-element of both columns and beams of element length 60 mm and the plate elements are excluded..

The area simulates the plate of the floor in FE building model and connected with the underneath beams by eight surrounding points. Due to distribution of additional masses over the floors of the building model, the element type of Mass21 is used for the FE model to simulate the concrete and streel masses. All additional masses are applied on the surface of the floors except for the level 9 and 10 of the model which are simulated as concentrated

masses distributed on four cross beams in each level. In the levels 9 and 10, the masses are initially distributed as 8 masses with 4 kg for each one of the total concentrated masses of 32 kg, as shown in *Figure 6.7*.

In the present study, the mass of the actual steel floor plate and the applied additional mass are assembled to obtain an equivalent mass density for both materials, concrete and steel, in order to be simulated easily in the FE building model. The equivalent mass density is calculated, based on the assumption that both steel floor plate and the applied additional mass are in the same volume of equivalent steel floor plate which has the same dimensions of actual steel floor plate of (300x300x3) mm, according to Eq. (6.1) as following:

$$Mass\_Density^{equivalent} = \frac{Mass^{actual}_{additional\_mass} + Mass^{actual}_{floor\_plate}}{Volume^{actual}_{floor\ plate}} \quad 6.1$$

where are:

$Mass\_Density^{equivalent}$ - the equivalent mass density in kg/mm^3 of the floor from both actual steel floor plate and additional mass in that floor,

$Mass^{actual}_{additional\_mass}$ - the actual mass in kg of the additional mass distributed on each floor,

$Mass^{actual}_{floor\_plate}$ - the actual mass in kgof the steel floor plate of the original structural model of each floor,

$Volume^{actual}_{floor\ plate}$ - the actual volume of the steel floor plate in mm^3 of the original structural model of each floor,

The mass density of equivalent floor plate of each applied additional mass on each steel floor plate of the FE model are summarized in Table 6.6. The mass and volume of the Actual steel floor plate is calculated based on the assumed initial mass density of the steel material and the dimensions of the steel floor plate. The equivalent masses densities are adopted in the FE model as initial value with the initial other material properties and real constant of the structural building model for the numerical analysis.

Table 6.6: Equivalent mass density values according to Eq. (6.1) of the applied additional masses on the floors of the intact initial FE multi-storey building model using ANSYS software

No. of Floor	Mass of the Applied Additional Masses (kg)	Mass of the Actual Steel Floor Plate (kg)	Volume of the Actual Steel Floor Plate (mm^3)	Mass Density of Equivalent Floor Plate (kg/mm^3)
2-4	4.500	2.122	270000	$2.4526x10^{-5}$
5 and 6	10.500	2.122	270000	$4.6748x10^{-5}$
7	13.500	2.122	270000	$5.7859x10^{-5}$
8	16.200	2.122	270000	$6.7859x10^{-5}$

The numerical simulation analysis is carried out using ANSYS software for structural analysis using Beam4 for coluns and beams and Shell63 for areas and Mass21 for additional masses with linear elastic isotropic material.

6.7.2. Estimation of modal properties

The modal analysis using Block Lanczos method is applied to estimate the modal properties for the intact initial multi-storey building model. The assumed initial values of geometry, material parameters and equivalent floors plates properties are used in this analysis. The created input file in ANSYS-APDL environment is written for the geometry, real constant, material properties, boundary condition and solving method with all required parameters of the building model. In this input file the commands to export the requierd output results, modal frquencies and mode shape vectors, are included by opening new file of results, which can import and read it in another software. All units of the geometry, real constant and material properties of both the FE models should be entered consistent in ANSYS-APDL input file, which are in mm and Newton. For the FE building model, the boundary conditions (supports types) are assumed the fixed end supports for all columns in the first storey of the building model which are discussed in 6.5.2.

The estimation of the first six modal frequencies values and their mode characters of the intact initial FE multi-storey model are listed in Table 6.7. In this table, the corresponding modal frequencies that are extracted from experimental model, Table 5.16, are also listed with the differences in numerical estimated modal frequencies values corresponding to experimental extracted modal frequencies values.

Table 6.7: Numerical estimated modal frequencies values using ANSYS software for intact initial FE multi-storey model and comparison with experimental extracted values

Mode No.	Modal Frequency Value of Intact Multi-Storey Model (Hz)		Difference in Frequency		Mode Character
	Experimental Model	Numerical Initial FE Model	(Hz)	Relative (%)	
1	2.637	2.647	0.010	0.38	1st Bend. about y-axis
2	2.893	2.794	-0.099	-3.42	1st Bend. about x-axis
3	6.555	6.517	-0.038	-0.58	1st Torsion
4	10.030	9.632	-0.398	-3.97	2nd Bend. about y-axis
5	10.290	9.735	-0.555	-5.39	2nd Bend. about y-axis
6	14.870	14.920	0.050	0.34	1st Bend. about y-axis

It is evident from Table 6.7, there are differences between the results of experimental model and numerical FE model. Therefore, the calibration process of the initial FE model is needed to tune the modal properties and for more convergence to detect damage in structure precisely. In addition, it is noted from Table 6.7 that the higher difference is in the fifth mode and the lower one is in the first and sixth mode.

In addition, the first six mode shapes and their characters corresponding to the natural frequencies of the multi-storey building model are shown in *Figure 6.8*. The values of the first six mode shape vectors of 1223 nodes of the bridge model are stored as output file from the ANSYS software. It is clear from *Figure 6.8*, the mode shapes characters estimated numerically are the same extracted experimentally of the multi-storey building model, as shown in *Figure 5.53*.

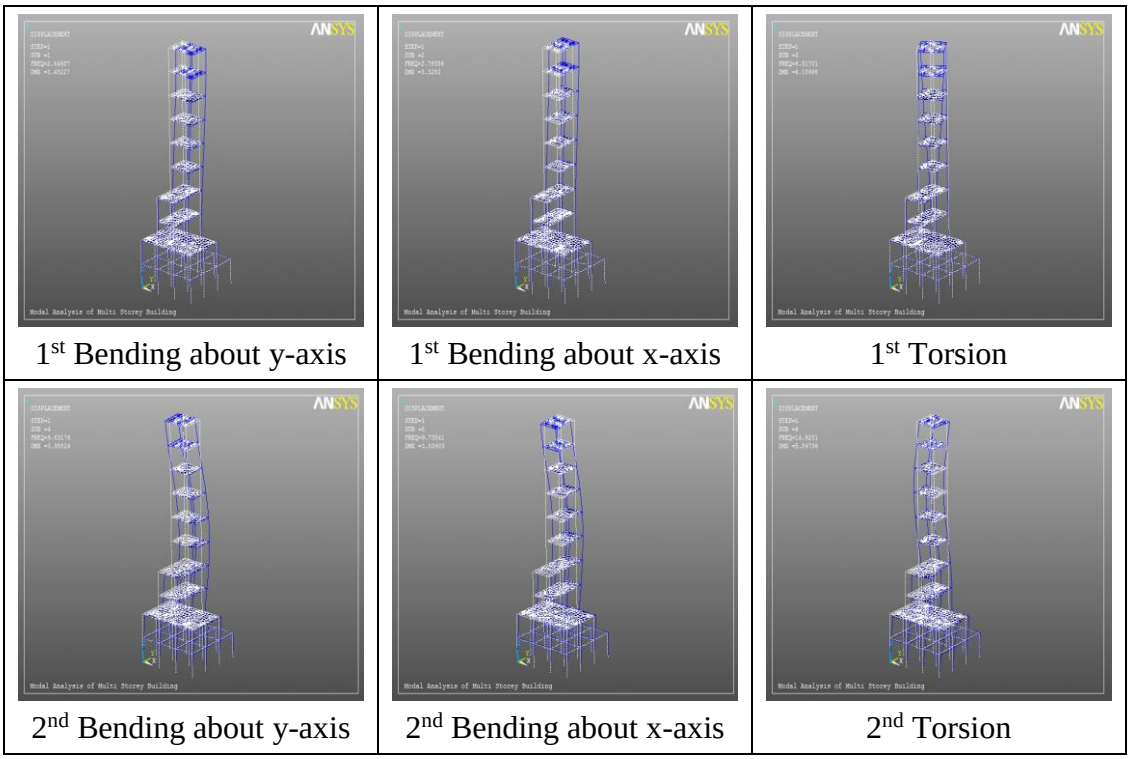

Figure 6.8. Numerical mode shapes of the FE model of the intact initial multi-storey building model using ANSYS software

6.8. Calibration process for initial FE models

There are usually some differences between numerically estimated and experimentally extracted modal properties due to inaccuracy in modeling of the complex real structures [135]. Those differences in FE model come from the considerable uncertainties due to boundary conditions, joint flexibilities and damping, etc.. Because of that, the initial FE model has to be calibrated to closely correspond to the actual structure, using the so-called Finite Element Model Updating technique. In order to match closer modal properties, initial FE model parameters such as mass density, modulus of elasticity, geometry, etc. [51], which significantly affect modal properties, have to be tuned. Generally, two structural model updating techniques are proposed: classical approach using sensitivity analysis, and direct FE model updating using the chosen parameters.

In addition, the FE model updating technique can sometimes be classified into another two categories: direct (non - iterative) techniques and iterative techniques. The first

one represents the model calibration just in one step, updating the system stiffness and mass matrices, according to modal test data. The drawback of this technique is that the experimental data are reproduced exactly, and the consequent system matrices are not symmetrical and positive definite, [135]. Therefore, such techniques require very high quality of modal testing and the analysis procedure. The iterative techniques are updating the values of material and structural parameters of FE model during iterations with the aim to reduce the mismatch between experimental and FE response. The process will continue until the iterations case, when the values of updated parameters stop converging or the error function minimize to the prescribed level. These techniques require a reasonable number of iterations to reach the final result.

For the observed structure, the FE model has to represent all main types of structural modal behavior, vertical and lateral bending, as well as torque of the structure. The most significant element properties, which affect the dynamic behavior, are element stiffness and mass [136]. For the tuning of modal properties for application in vibration-based damage detection procedures, FE model updating has to be performed. Optimization of objective function, which includes variation of the chosen, most significant parameters, is a common way to achieve the optimal solution. The optimal solution should represent the minimum "distance" between experimentally extracted and numerically estimated modal properties. The "distance" (error) is also known in the model updating community as the output error residue $R(p_k)$, [137], as the quantities being compared are the properties of the system. Values of $p_{k=1,2,\ldots,K}$ represent the updated parameters and K is the number of included parameters in the calibration.

Generally, most calibration techniques for structural dynamics applications are based on the functional relationship between the measured responses and structural parameters that can be expressed in terms of the Taylor series expansion limited to the linear term. Calibration methods based on optimization function require estimation of the numerical modal properties in each iteration. When the change of the parameters between two successive iterations becomes small, a good estimation of the modal model is available and may be used to improve the Eigensystem computation efficiently. Those methods use linear

approximation, based on Taylor series, of modal data as a function of the change of uncertain parameter [136]:

$$\delta d_{j=1,2,...,n} = \mathbf{S_{jk}} \delta p_{k=1,2,...,K} \quad 6.2$$

where are:

n - the modal parameters included,

δd_j - the differences between the experimentally extracted and numerically estimated modal properties,

S - the sensitvity matrix which contains the first derivatives with respect to the assumed model parameters,

δp_k - the variation of the updated parameter.

The discrepancy between the initial model predictions and properties extracted from testing data has to be resolved by minimizing the weighted error (weighted residues) [138] between modal properties of the included mode shapes. Different forms of the residue $\{R(p_{k=1,2,...,K})\}$ are available, while the one of them, which includes weighted modal frequencies and mode shapes [137], is represented by Eq. (6.3).

$$\{R(p_{k=1,2,...,K})\} = \begin{Bmatrix} W_f \begin{Bmatrix} f_1^{Exp\_Intact} - f_1^{Udated\_Intact}(p_k) \\ \vdots \\ f_i^{Exp\_Intact} - f_i^{Udated\_Intact}(p_k) \\ \vdots \\ f_n^{Exp\_Intact} - f_n^{Udated\_Intact}(p_k) \end{Bmatrix} \\ W_d \begin{Bmatrix} \phi_{11}^{Exp\_Intact} - \phi_{11}^{Udated\_Intact}(p_k) \\ \vdots \\ \phi_{ij}^{Exp\_Intact} - \phi_{ij}^{Udated\_Intact}(p_k) \\ \vdots \\ \phi_{nm}^{Exp\_Intact} - \phi_{nm}^{Udated\_Intact}(p_k) \end{Bmatrix} \end{Bmatrix} \quad 6.3$$

where are:

$i = 1,2,...,n$ - the i^{th} modal mode

n - the number of included modal mode in the computations,

m - the number of included FE mode degrees of fredom in the computations,

W_f and W_d - the weighting factors for the natural frequency residuals and normalized mode shape vector residuals, respectively.

It is required that mode shapes are normalized in an adequate way so that they could be consequently compared.

The objective function, which is defined as a norm of the weighted residues, has to be minimized subjected to constrains, according to the prescribed boundaries of physical FE model parameters, as following in Eq. (6.4).

$$p_k^{\min} \le p_k \le p_k^{\max} \qquad k = 1,2,...,\mathrm{K} \tag{6.4}$$

Prior to applying any FE model updating technique, the experimental and FE model data sets need to be compared to ensure the existence of correlation between experimental and FE model responses and to determine whether it is worth to update the proposed FE model, or a completely new model is required. These techniques include comparison of FRFs, natural frequencies, mode shapes and Modal Assurance Criterion (MAC) [135].

6.9. Proposed calibration process using SA algorithm

In present study, the proposed SHM procdure for damage detection includes the calibration process, direct updating technique, of the initial FE models of the adopted structural models using the adopted heurstic optimization method, Simulated Annealing (SA). The proposed procedure of the calibration process of the initial FE model adoptes the minimization of differences between experimental and numerical natural frequencies as comparative parameters used in the selected objective function.

The SA method applied in the calibration process has the same features and parameters that used in the proposed SHM procedure for damage detection which is discussed in chapter four in paragraph 4.5. The randomly selection of the intial and generated solution is one of the feature applied in the proposed calibration process. The standard SA method of searching configuration type is adopted to generate the new solutions by generating one solution from the current soltion. The relation of linear reduction is used to reduce the temperature, T, of the system using reduction factor, α, during improving the optimal solution by iterations which is called Cooling Schedule. The

Initial temperature, T_o, is assumed depend on the optimization problem. The value of the reduction factor is selected in the range of $[0.70, 0.95]$ coming from trial and error to choise the appropriate value. The termination criteria are selected either by specifying the maxinun number of iterations to explore the optimal solution or using SA itself feature of the system frozing, which means stop the iterations when the system is cool i.e. temperature is close to zero. As mentioned previously in current study, the flowchart of proposed SA algorithm procedure used in the calibration process with adopting the strategy of SA features is shown in *Figure 4.2*.

The form of objective function used in the calibration process is minimizing the differences, residue $R(p_k)$, in the modal frequencies only between the experimental and numerical modal frequencies. The selection of modal frequencies only in the objective function of the calibration process is due to the high sensitivity of this modal property to change in the stiffness or mass density of the structure. Three forms of objective functions are used in the calibration process of the adopted four structural models.

The first form is the square of relative difference in the updated modal frequency respect to the experimental modal frequency, as defined in Eq. (6.5). This form of objective function is close to the first part of the adopted objective function, Eq. (4.32), of present study in proposed SHM procedure for damage dection in structure, as discussed in chapter four in paragraph 4.7.

$$R(p_k)^{calib} = \sum_{i=1}^{n} \left(\frac{f_i^{exp} - f_i^{num\text{-}updated}}{f_i^{exp}} \right)^2 \qquad 6.5$$

where are:

f_i^{exp} and $f_i^{num\text{-}updated}$ - the i^{th} modal natural frequencies extracted from experimental testing and estimated from numerical updated intact FE model, respectively,

n - the number of included modal modes in the computations of the calibration process.

The second form is square of the direct difference between the updated modal frequency and the experimental modal frequency, as defined in Eq. (6.6).

$$R(p_k)^{calib} = \sum_{i=1}^{n} \left(f_i^{exp} - f_i^{num\text{-}updated} \right)^2 \qquad 6.6$$

The third form is absolute of the direct difference between the updated modal frequency and the experimental modal frequency, as defined in Eq. (6.6).

$$R(p_k)^{calib} = \sum_{i=1}^{n} \left| f_i^{exp} - f_i^{num\text{-}updated} \right| \qquad 6.7$$

The application of any form of the objective function in the calibration process of the adopted four structural models is depended on the type of problem and the number of selected parameters as well as to the values of the differences, error residue, between the compartive modal properties. In addition, the three forms of the objective functions were applied on some of the structural models, then the best results were adopted.

The stages of the calibration process in the proposed SHM procedure was explained in the flow chart, as shown in *Figure 6.9*.

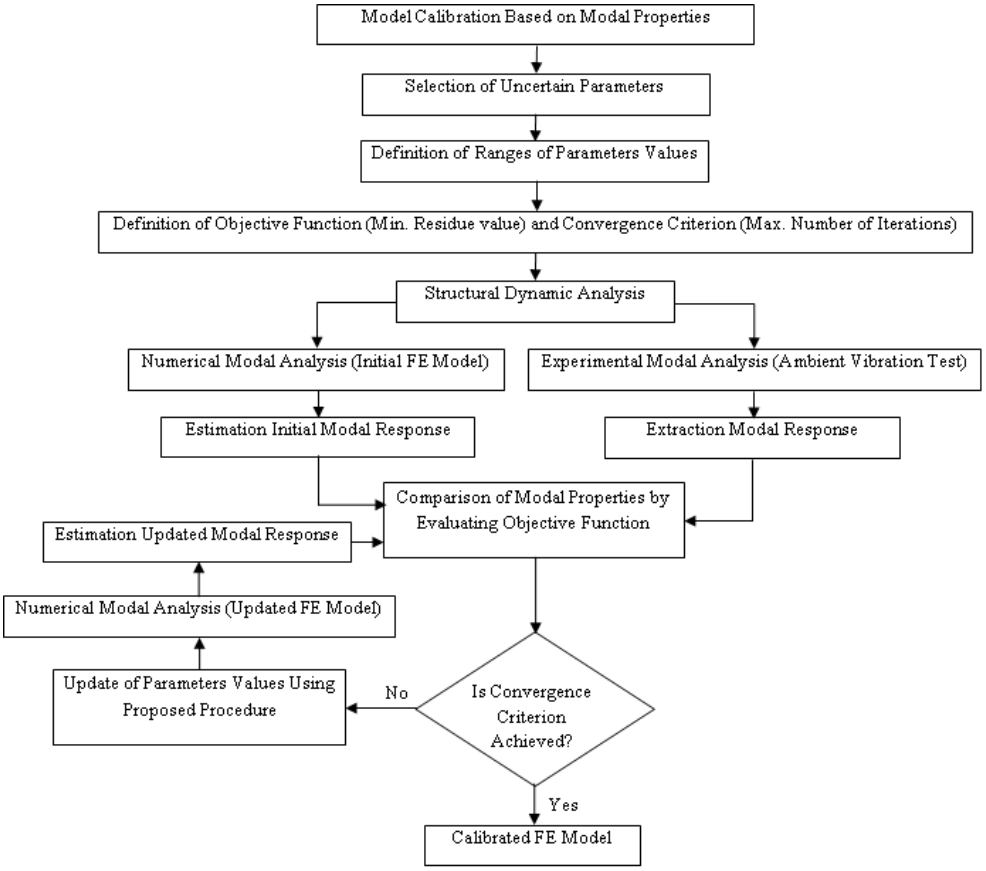

Figure 6.9. Flow chart of the proposed calibration process of the initial FE model

The selection of the uncertian parameters depends on the simplicity or complexity, geometry, of the structural model and the sensitivity of the parameters. In addition, the range of the updated parameters values is specified to the reseanable limitations of change possibility under the structural and material specifications.

On the other hand, the subroutine in environment MATLAB software is written to implement calibration process with the proposed SHM procedure for damage detection. The updating process is perfomed by generating randomly new values of the selected parameters during iterations and then exported output file with new generated parametrs values to update the FE model. The subroutine is connecting with envionment APDL in ANSYS software to conduct the new modal analysis of updated FE model. The new modal analyses are implemented to estimate the updated modal frequencies during iterations and so on untill the termination criteria are achieved, as shown in *Figure 6.9*. That means the high convergence between the comparative modal frequencies is reached based on the adopted objective function.

6.10. Calibration process for FE overhang beam model

For the first initial FE model of the overhang model, *Figure 6.1*, due to the differences in the initial numerical modal frequencies values respct to the experimental extracted values, as listed in Table 6.1, the calibration process is implemented. In this study, to select the parameters that have significant effect on the calibration process, sensitivity analysis is conducted. The selected parameters in sensitvity analysis is done for uncertainty parameters values to study which parameters have hig sensitvity to change in the modal frequencies values of the FE model.

6.10.1. Sensitvity analysis of selected parameters of FE overhang beam model for calibration process

For the purpose of selection significant parameters to be included in the calibration process of the initial FE overhang beam model, the sensivity analysis is conducted for four parameters. Those four parameters are mass density of the steel material, modulus of

elasiticity of the steel material, width and thickness of the rectangular cross section of the overhan beam model. The change in values of selected parameters for this analysis study is in the range of ±(5-8) % from the initial assumed value of the parameters. The analysis is implemented on the each frequency of the first four modal frequencies of the FE model, as shown in *Figure 6.10*.

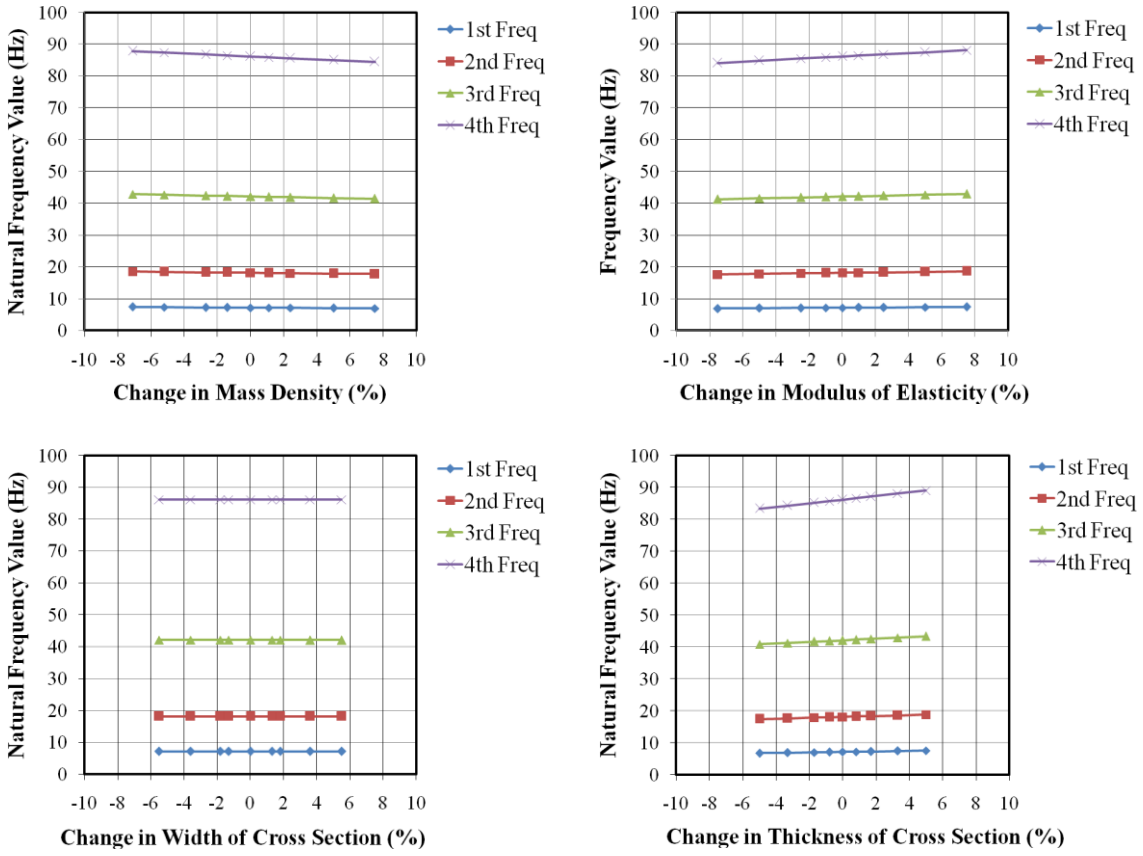

Figure 6.10. Sensitivity analysis of the selected parameters on the first four modal frequencies of initial FE overhang beam model

It is obvious from *Figure 6.10* that the mass density, modulus of elasticity and thickness (height) of the rectangular cross section have significant effect on the percentage of change in modal frequencies values of the initial FE model. In addition, the fourth modal frequency has higher perentage of change than other three modal frequencies. Due to the various changes of the modal frequencies to the changes in selected parameters of the FE

model, therefore the implementation of manually parametric study to calibrate this model is difficult and inappropriate.

For the initial FE overhang model, the mass density of the model as well as the additional masses of the accelerometers on the model are calculated preciesly in the lab and equal to $7.752443x10^{3}$ kg/m^{3} and $34.525x10^{-3}$ kg, respectively. Also, due to sensitivity analysis study that the change in the width of the rectangular cross section in the specified value range has not significant effect on the modal frequencies of the FE overhang beam model, as shown in *Figure 6.10*. Therefore, the calibration process includes two selected parameters only, $K = 2$, of modulus of elasitcity and thickness of the rectangular cross section. The initial values of parameters included in the calibration process are the same values assumed in the initial FE model, as explained in paragraph 6.4.1. The initial parameters values are E_initial=$2x10^{5}$ N/mm^{2}, ρ_initial=$7.752443x10^{3}$ kg/m^{3}, average additional mass of M_initial=$34.525x10^{-3}$ kg and thicness of cross section of t_CS=50 mm.

6.10.2. Estimated modal properties of calibrated FE overhang beam model

The calibration process for the initial FE overhang beam model is implemented using the subroutine of the proposed SHM procdure by SA method. A paper is published in the internation conference civil engineering (GNP) in Montenegro deals with the calibration procedure of the FE overhang beam model [139]. The parameters of SA optimization method are designd by many trials to get the best and quick convergence of the iterations. The selected SA features are the initial temperature $T_o = 20$ and the reduction factor $\alpha = 0.8$.of the cooling schedule. The searching space included in the SA optimization of the calibration process of this model is configured according to the adopted changes ranges, ±(5-8) %, of specified parameters values. The adopted ranges is discretized by nine for thickness of cross section and 20 for the modulus of elasticity, therefore the total searching space has 180 possible solutions. The proposed calibration procedure starts with the initial value of objective function of the intial differences between the experimental and initial FE overhang beam model, as listed in Table 6.1. The termination criterion for this

optimization problem of calibrated FE model is limited to the maximum number of iterations of 50, which represents 28 % of the total searching space.

The adopted objective function for calibration process of FE overhang beam model is represented by the sum of absolute direct difference between experimental and numerical udated natural frequency value, as defined in Eq. (6.7). The first two modal frequencies, $n = 2$, and two discrete variables, $K = 2$, are included in the calibration process for this FE model due to the high divergence in the natural frequencies values if more than two modes are included. This type of optimization for small searching space, it can be considered as a simple optimization problem.

The improvement of the optimum solution according to minimize objective function value during the iterations of SA optimization method is shown in *Figure 6.11* (a). In addition, the modification of the two chosen parameters during updating procedure in the calibration process by three steps is shown in *Figure 6.11* (b).

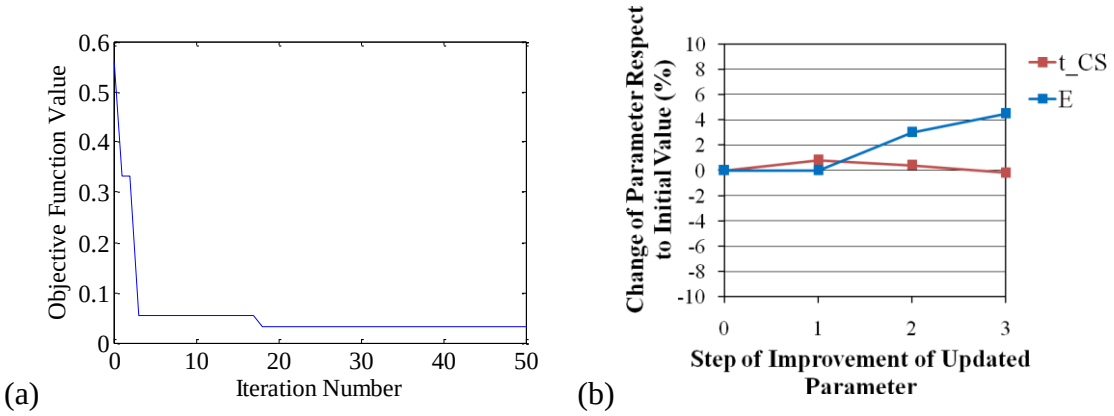

Figure 6.11. Calibrated FE overhang beam model according to the adopted objective function during SA optimization iterations (a) improvement of optimal solution and (b) step of improvement in updated parameters respect to initial values

It is obvious from *Figure 6.11* (a) that the SA optimization procedure catches the optimal solution after 18 iterations, which represent only 10 % of the total searching space. Also, it is clear in *Figure 6.11* (b) that significant change is in the modulus of elasticity during updating process, while smooth change is in thickness of cross section. The

calibration process results the optimum values of the updated parameters of modulus of elasticity of $2.09x10^5$ N/mm^2 and thickness of cross section of 4.99 mm.

The first four calibrated modal frequencies and corresponding experimental, Table 5.1, and initial, Table 6.1, values are listed in Table 6.8. It is evident from table that the proposed procedure minimized the differences in modal frequencies according to of objective function from initial value of 0.558 to the optimal value of 0.032. Therefore, the percentage of the relative difference in modal frequency respect to the experimental model is decreased from 2.35 for the first mode to be 0.39 and lower for the second mode and the reduction in the difference of the fouth mode is clear.

Table 6.8: Calibrated modal frequencies values using proposed SHM procedure by SA optimization method of intact calibrated FE overhang model and comparison with initial values respect to the experimental values

Mode No.	Experimental Modal Frequency (Hz)	Numerical Initial Modal Frequency (Hz)	Difference in Frequency		Numerical Calibrated Modal Frequency (Hz)	Difference in Frequency	
			(Hz)	Relative (%)		(Hz)	Relative (%)
1	7.910	7.724	-0.186	-2.35	7.879	-0.031	-0.39
2	18.750	18.378	-0.372	-1.98	18.749	-0.001	-0.01
According to Eq. (6.7) the sum = 0.558						0.032	
3	42.480	42.510	0.030	0.07	43.365	0.885	2.08
4	90.820	86.223	-4.597	-5.06	87.956	-2.864	-3.15
According to Eq. (6.7) the sum = 5.185						3.781	

The results show that calibration procedure using the SA optimization method has high and quick convergence. Also, the differences in modal frequencies of calibrated FE model is reduced, as shown in *Figure 6.12*.

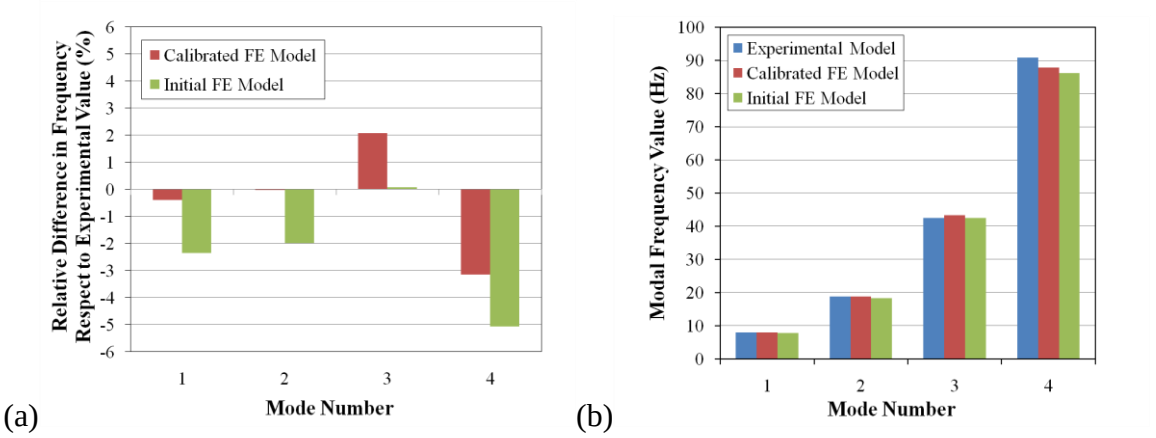

Figure 6.12. Results of calibration process using SA method of FE overhang beam model (a) differences in modal frequencies of the calibrated and initial FE model respect to the experimental model and (b) convergence in modal frequencies values

It is evident from *Figure 6.12* (a) that the significant reductions are in modal frequency differences for the first, second and fourth mode, whereas there is increase in the third mode. Figure 6.12 (b) shows the convergence in the modal frequencies of calibrated FE model with the experimental model and this achieves the advantage and importance of the performed calibration process. It is concluded from the calibration process, the all four modal frequencies of the calibrated FE model are increased from the initial FE model in percentages of 2 %, as listed in Table 6.9.

Table 6.9: Improvement in the modal frequencies values of calibrated FE overhang beam model using proposed SHM procedure by SA optimization method respect to the initial FE model

Mode No.	Modal Frequency Value of Intact Overhang Beam Model (Hz)		Difference in Frequency	
	Initial FE Model	Calibrated FE Model	(Hz)	Relative (%)
1	7.724	7.879	+0.155	+2.01
2	18.378	18.749	+0.371	+2.02
3	42.510	43.365	+0.855	+2.01
4	86.223	87.956	+1.733	+2.01

The results prove the efficiency and robustness of the calibration process subroutine in the proposed SHM procedure for damage detection using SA heuristic optimization method.

6.11. Calibration procedure for FE grid bridge model

For the second initial FE model of the grid bridge model, *Figure 6.3*, and due to the differences in the initial numerical modal frequencies values respct to the experimental extracted values of both model loading states, without and with additional masses, as listed in Table 6.2 and Table 6.3, the calibration process is implemented. In this study, to select the parameters that have significant effect on the calibration process, sensitivity analysis is also performed for the model state without additional masses. The sensitvity analysis includes the uncertainty parameters to study which parameters have hig sensitvity to change in the modal frequencies values of the FE model state without additional masses.

6.11.1. Sensitvity analysis of selected parameters of FE grid bridge model for calibration process

For the purpose of selection significant parameters to be included in the calibration process of the initial FE overhang beam model, the sensivity analysis is conducted for four parameters. Those four parameters are mass density of the steel material, modulus of elasiticity of the steel material, thickness of the T-section web of the stiffener beams and thickness of the rectangular hollow section of the main longitudinal beams of the the model. The change in values of selected parameters for this analysis study is in the range of ±(7-10) % from the initial assumed value of the parameters. The analysis is implemented on the each frequency of the first five modal frequencies of the FE model, as shown in *Figure 6.13*.

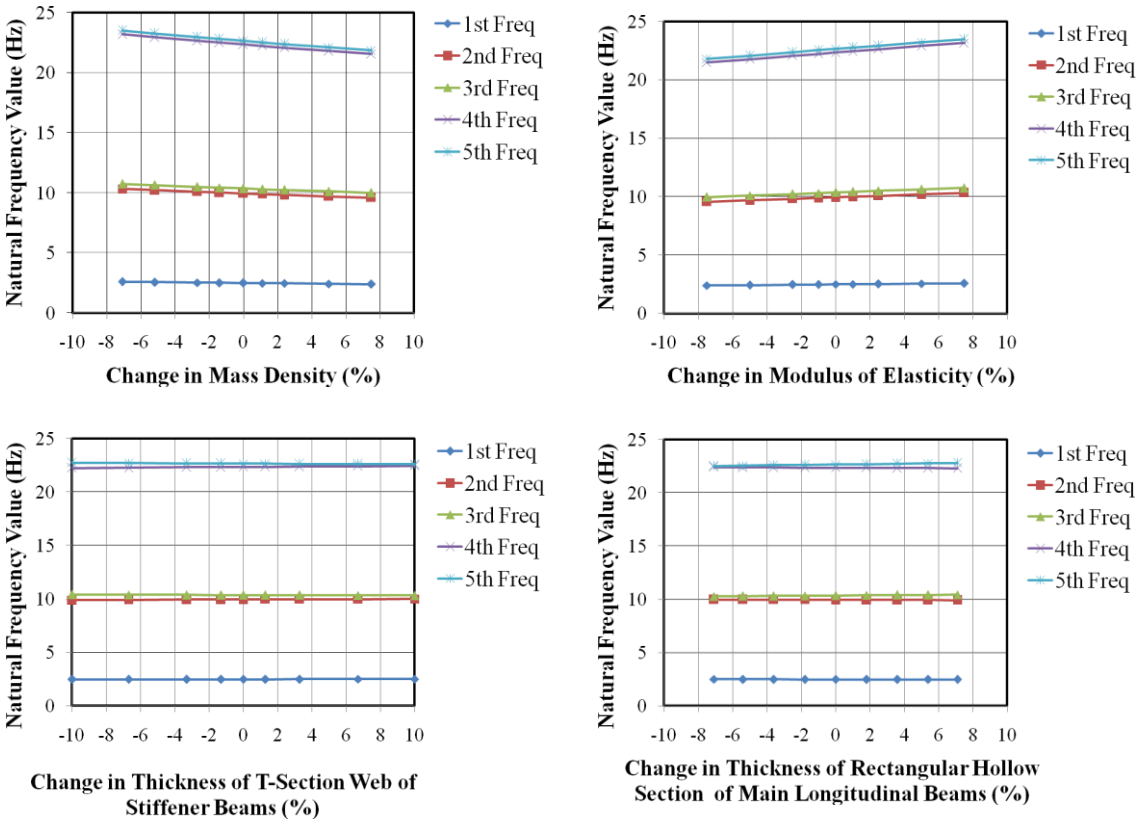

Figure 6.13. Sensitivity analysis of the selected parameters on the first five modal frequencies Values of initial FE grid bridge model state without additional masses

It is obvious from *Figure 6.13* that the mass density and modulus of elasticity have significant effect on the percentage of change in modal frequencies values of the initial FE model. The thickness of the rectangular hollow section of main longitudinal beams has effect on the precentage of change in modal frequencies values, but the thickness of T-section web of stiffener beams has small effect, as shown in *Figure 6.13*. In addition, the fourth and fifth modal frequencies have higher perentage of change than other three modal frequencies. Due to the various changes of the modal frequencies to the changes in selected parameters and complixity of of the FE bridge model, therefore the implementation of automatic calibration process using subroutine using SA method to calibrate the initial FE model is needed.

As mentioned previously, the structural grid bridge model is erected from different types of steel cross sections and those sections are fabricated from variety of origins

thereby, the mass density value of the steel material of the structural model is uncertain parameter. As well as, for the structural bridge model state with additional masses, the mass value of additional masses, concrete cubes, installed on the model are taken approximatley as an average value for all ten additional masses. In addition, the created hidden transverse beams, with zero mass density, in the FE model to supress the local behaviour of the stiffener beams have initial assumed cross section of $(1.5x50)$ mm, as discussed in paragraph 6.5.1. Those hidden transverse beams affect on the global behaviour of the FE bridge model, thus on its modal properties values.

Consequently, the calibration process of this FE grid bridge model includes five selected parameters, $K = 5$, for updating for the model state without additional masses. Those five chosen parameters are the four selected parameters in the sensitivity analysis, mass density, modulus of elasticity, thickness of T-section web of stiffener beams and thickness of the rectangular hollow section of the main longitudinal beams, as well as to the width of the hidden transverse beams. Whereas, for the calibration process of the FE bridge model state with additional masses, six parameters, $K = 6$, are included. Those six chosen parameters are the same five parameters used in the calibration process of first FE bridge model state, without additional masses, as well as to the mass value of the additional masses.

6.11.2. Estimated modal properties of calibrated FE grid bridge model

The calibration process for the both initial FE grid bridge model states, without and with additional masses, is implemented using the subroutine of the proposed SHM procdure by SA method. The parameters of SA optimization method are selected by many trials to obtain the high and quick convergence of the iterations. The selected SA features are the initial temperature $T_o = 20$ and the reduction factor $\alpha = 0.8$.of the cooling schedule for both states of the model. The searching space included in the SA optimization of the calibration process of this model is configured according to the adopted changes ranges, ±(7-10) %, of specified four parameters values. For the fifth parameter of width of hidden

transverse beams, different large range is adopted of ±20 % due to the signifcant effect of this parameter on the FE bridge model. The initial values of parameters included in the calibration process are the same values assumed in the initial FE model, as explained in paragraph 6.5.1. The initial parameters values are thicness of rectangular hollow section of longitudinal beams of 2.8 mm, flange and web thickness of T-section of stiffener beams of 1.5 mm, width of hidden transverse beams of 50 mm, E_initial=2x10^5 N/mm^2, mass density ρ_initial=7.860x10^3 kg/m^3 and average mass value of additional masses M_initial=7.925 kg.

6.11.2.1. Calibrated modal properties of FE grid bridge model without additional masses

For this FE model state, the number of selected parameters included in the calibration process is five. The adopted ranges of those five parameters are discretized by nine, nine, four, nine and six for thickness of rectangular hollow section (t_RHS), thickness of T-section (t_TS), width of rectangular solid hidden beam section (w_RSHBS), modulus of elasticity (E) and mass density (ρ) value, respectively. Therefore, the adopted total searching space in this optimization problem of calibration process has 17496 possible solutions. The proposed calibration procedure starts with the initial value of objective function of the intial differences between the experimental and initial FE bridge model state without additional masses, as listed in Table 6.2. The termination criterion for this optimization problem of calibrated FE bridge model is limited to the maximum number of iterations of 500, which represents 2.9 % of the total searching space.

The adopted objective function for calibration process of FE bridge model state without additional masses is represented by the sum of square relative difference between experimental and numerical udated natural frequency value, as defined in Eq. (6.7). The first five modal frequencies, $\mathrm{n}=5$, and five discrete variables, $\mathrm{K}=5$, are included in the calibration process for this FE bridge model. This type of optimization due to the large searching space with five discrete variables can be regarded as a complex optimization problem.

The improvement of the optimum solution, according to minimize value of adopted objective function, during the iterations of SA optimization method in the proposed calibration procedure of the FE bridge model state without additional masses is shown in *Figure 6.14* (a). In addition, the modification of the five chosen parameters during updating procedure in the calibration process of the same FE bridge model state by four steps is shown in *Figure 6.14* (b).

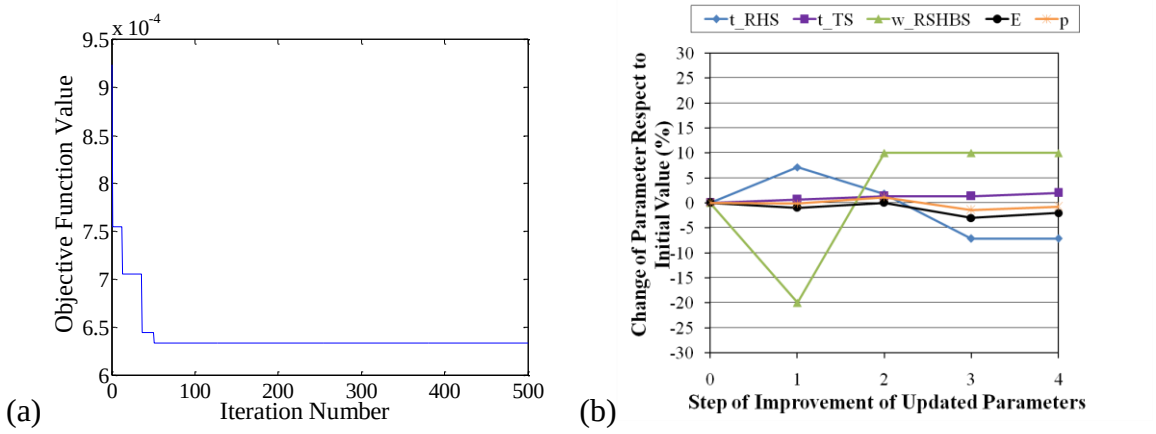

Figure 6.14. Calibrated FE grid bridge model state without additional masses according to the adopted objective function during SA optimization iterations (a) improvement of optimal solution and (b) step of improvement in updated parameters respect to initial values

The results show that calibration procedure using the SA optimization method has high and quick convergence. Also, the differences in modal frequencies values of calibrated FE model is reduced, as shown in *Figure 6.14*. It is obvious from *Figure 6.14* (a) that the SA optimization procedure obtains the optimal solution after 51 iterations, which represent only 0.29 % of the total searching space. Also, it is clear in *Figure 6.14* (b) that significant change is in the width of hidden transverse beams (*w*_RSHBS) and thickness of rectangular hollow section of the longitudinal beams (*t*_RHS) during updating process, while smooth changes are in other three parameters. The calibration process results the optimum values of the selected parameters of, *t*_RHS_opt=2.6 mm, *t*_TS_opt=1.53 mm, *w*_RSHBS_opt=55 mm, *E*_opt= 1.96x10^5 N/mm^2 and ρ_opt= 7.80x10^{+3} kg/m^3.

The first five estimated calibrated modal frequencies values and corresponding experimental extracted values of the grid bridge mode; state without additional masses, Table 5.6, and numerical initial estimated values, Table 6.2, are listed in Table 6.10. It is evident from table that the proposed procedure minimized the differences in modal frequencies according to of objective function from initial value of 0.00093 to the optimal value of 0.00063. Therefore, the percentage of the relative difference in modal frequency respect to the experimental model is decreased from 2.7 % for the third mode to be 1.80 % and lower for the second mode and the the differences of the other three modes are little increased, as listed in Table 6.10.

Table 6.10: Calibrated modal frequencies values using proposed SHM procedure by SA optimization method of intact calibrated FE grid bridge model state without additional masses and comparison with initial values respect to the experimental values

Mode No.	Experimental Modal Frequency (Hz)	Numerical Initial Modal Frequency (Hz)	Difference in Frequency		Numerical Calibrated Modal Frequency (Hz)	Difference in Frequency	
			Relative Square	Relative (%)		Relative Square	Relative (%)
1	2.490	2.488	6.4E-07	-0.08	2.477	2.7E-05	-0.52
2	9.814	9.943	1.7 E-04	1.31	9.901	7.8E-05	0.89
3	10.550	10.835	7.2 E-04	2.70	10.740	3.2E-04	1.80
4	22.410	22.328	1.3E-05	-0.37	22.230	6.4E-05	-0.80
5	23.580	23.492	1.3E-05	-0.37	23.302	1.3E-04	-1.18
According to Eq. (6.7) the sum = 0.0009305						0.0006337	

The percentages of relative differences between the initial and calibrated FE model modal frequencies, with respect to the experimental values, are shown in *Figure 6.15*. The zero percent of difference means that there is no difference between the observed frequencies. According to *Figure 6.15* (a), significant improvement is observed for the second and third frequency differences, while the other frequency differences remain in the range of 1%.

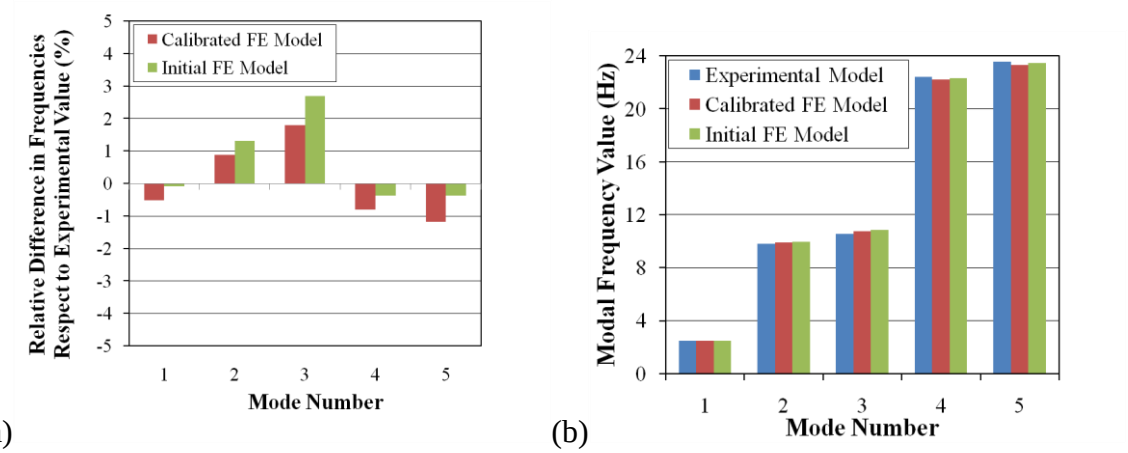

Figure 6.15. Results of calibration process using SA method of FE grid bridge model state without additional masses (a) differences in modal frequencies of the calibrated and initial FE model respect to the experimental model and (b) the convergence in modal frequencies values

Figure 6.15 (b) shows the convergence in the modal frequencies of calibrated FE model with the experimental model. The small percentage of differences of initial FE bridge modal frequencies values with respect to experimental values, Table 6.10, reflects high accuracy of numerical simulation of initial FE bridge model. The objective function minimum value is improved from the initial value of 0.00093 to 0.00063 for calibrated FE model within four steps, as shown in *Figure 6.14* (a) and (b). Consequently, the calibration process with adopted form of the objective function Eq. (6.7), reduced the high relative differences, thus causing the calibrated FE model to become very close to the real experimental model, which is the most important for further damage detection procedure.

It is concluded from the calibration process, the all five modal frequencies of the calibrated FE model are decreased from the initial FE model in percentages of (0.44-0.88) %, as listed in Table 6.11.

Table 6.11: Improvement in the modal frequencies values of calibrated FE grid bridge model state without additional using proposed SHM procedure by SA optimization method respect to the initial FE model

Mode No.	Modal Frequency Value of Intact Grid Bridge Model (Hz)		Difference in Frequency	
	Initial FE Model	Calibrated FE Model	(Hz)	Relative (%)
1	2.488	2.477	-0.011	-0.44
2	9.943	9.901	-0.042	-0.42
3	10.835	10.740	-0.095	-0.88
4	22.328	22.230	-0.098	-0.44
5	23.492	23.302	-0.190	-0.81

The presented proposed calibration procedure proves the efficiency and robustness of the adopted calibration process subroutine in the proposed SHM procedure for damage detection using SA heuristic optimization method for FE model updating according to modal frequencies, where even the initial differences of modal frequencies are small.

6.11.2.2. Calibrated modal properties of FE grid bridge model with additional masses

For this FE model state with additional masses, the number of selected parameters included in the calibration process is six. The adopted ranges of those six parameters are discretized by nine, nine, four, nine, six and six for thickness of rectangular hollow section (t_RHS), flange and web thickness of T-section (t_TS), width of rectangular solid hidden beam section (w_RSHBS), modulus of elasticity (E), mass density (ρ) and mass value (M) of additional cubic mass, respectively. Therefore, the adopted total searching space in this optimization problem of calibration process has 104976 possible solutions. The proposed calibration procedure starts with the initial value of objective function of the intial differences between the experimental and initial FE bridge model state with additional masses, as listed in Table 6.3. The termination criterion for this optimization problem of calibrated FE bridge model is limited to the maximum number of iterations of 5000, which represents 4.8 % of the total searching space.

The adopted objective function for calibration process of FE bridge model state with additional masses is the same applied for the first model state without additional masses. It

is represented by the sum of square relative difference between experimental and numerical udated natural frequency value, as defined in Eq. (6.7). The first five modal frequencies, $n = 5$, and six discrete variables, $K = 6$, are included in the calibration process for this FE bridge model. This type of optimization due to the very large searching space with six discrete variables can be considered as a hard optimization problem.

The improvement of the optimum solution, according to minimize value of adopted objective function, during the iterations of SA optimization method in the proposed calibration procedure of the FE bridge model state with additional masses is shown in *Figure 6.16* (a). In addition, the modification of the six chosen parameters during updating procedure in the calibration process of the same FE bridge model state by 12 steps is shown in *Figure 6.16* (b).

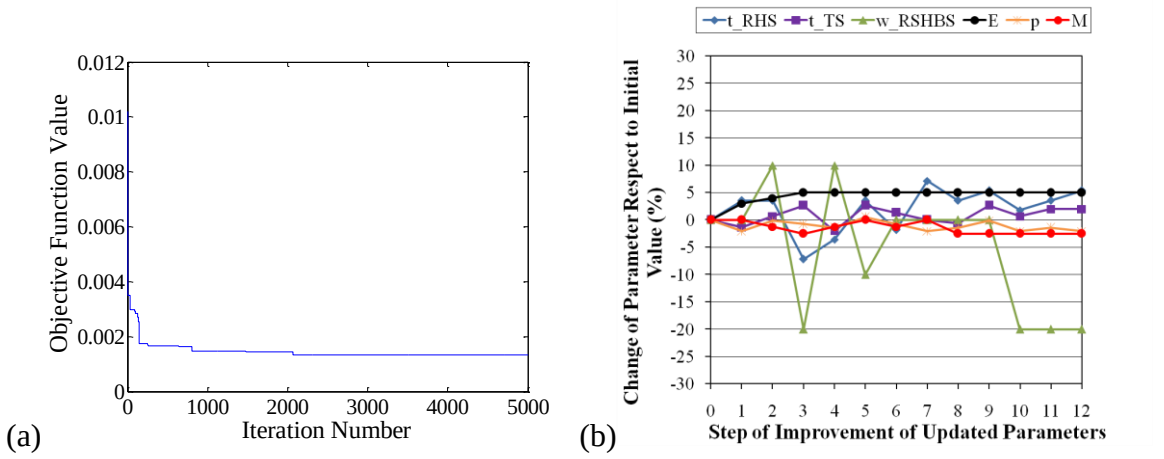

Figure 6.16. Calibrated FE grid bridge model state with additional masses according to the adopted objective function during SA optimization iterations (a) improvement of optimal solution and (b) step of improvement in updated parameters respect to initial values

The results show that calibration procedure using the SA optimization method has high and quick convergence. Also, the differences in modal frequencies values of calibrated FE model are reduced significantly, as shown in *Figure 6.16*. It is obvious from *Figure 6.16* (a) that the SA optimization procedure obtains the optimal solution after 2064

iterations, which represent only 1.96 % of the total searching space. Also, it is clear in *Figure 6.16* (b) that significant change is in the width of hidden transverse beams (*w*_RSHBS), thickness of rectangular hollow section of the longitudinal beams (*t*_RHS), mass value (*M*) of additional cubic masses and modulus of elasticity (*E*) during updating process, while smooth changes are in other two parameters. The calibration process results the optimum values of the selected six parameters of *t*_RHS_opt=2.95 mm, *t*_TS_opt=1.53 mm, *w*_RSHBS_opt=40 mm, *E*_opt=2.10x10^{5} N/mm^{2}, ρ_opt=7.70x10^{+3} kg/m^{3}, and *M*_opt=0.007725 kg.

The first five estimated calibrated modal frequencies values and corresponding experimental extracted values of the grid bridge mode; state with additional masses, Table 5.6, and numerical initial estimated values, Table 6.3, are listed in Table 6.12. It is evident from table that the proposed procedure minimized the differences in modal frequencies according to of objective function from initial value of 0.0102 to the optimal value of 0.0013. Therefore, the percentage of the relative difference in modal frequency respect to the experimental model is decreased from 5.90 % for the first mode to be 1.66 % and lower for the other three modes except for the third mode there is slight increase in its difference.

Table 6.12: Calibrated modal frequencies values using proposed SHM procedure by SA optimization method of intact calibrated FE grid bridge model state with additional masses and comparison with initial values respect to the experimental values

Mode No.	Experimental Modal Frequency (Hz)	Numerical Initial Modal Frequency (Hz)	Difference in Frequency		Numerical Calibrated Modal Frequency (Hz)	Difference in Frequency	
			Relative Square	Relative (%)		Relative Square	Relative (%)
1	2.051	1.930	0.0034805	-5.90	2.017	0.0002748	-1.66
2	8.093	7.720	0.0021242	-4.61	8.048	0.0000309	-0.56
3	8.313	8.290	0.0000077	-0.28	8.540	0.0007457	2.73
4	18.240	17.260	0.0028867	-5.37	17.993	0.0001834	-1.35
5	18.640	17.870	0.0017064	-4.13	18.461	0.0000922	-0.96
According to Eq. (6.7) the sum = 0.0102055						0.0013270	

The percentages of relative differences between the initial and calibrated FE model modal frequencies, with respect to the experimental values, are shown in *Figure 6.17*. According to *Figure 6.17* (a), significant improvement is noted for the four modal frequencies differences, first,second fourth and fifth, while the third modal frequency has increase in the difference.

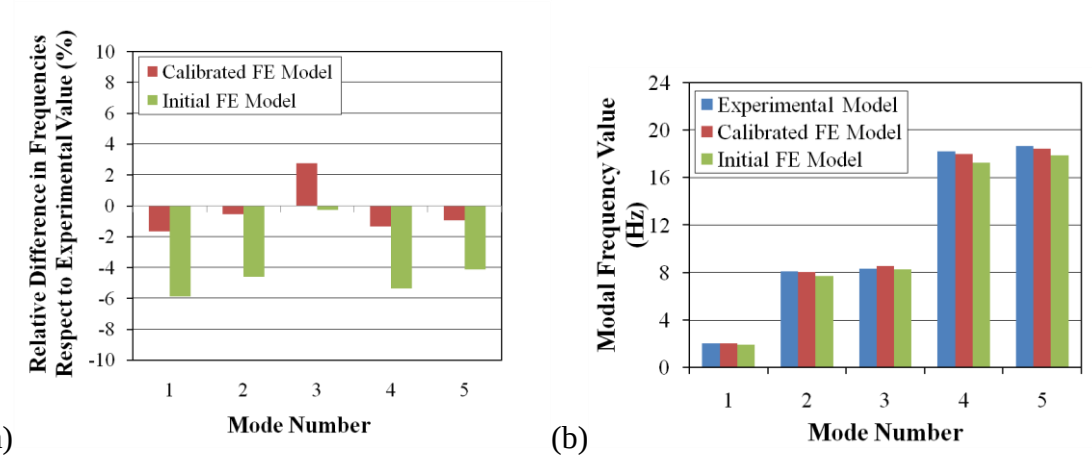

Figure 6.17. Results of calibration process using SA method of FE grid bridge model state with additional masses (a) differences in modal frequencies of the calibrated and initial FE model respect to the experimental model and (b) the convergence in modal frequencies values

Figure 6.17 (b) shows the convergence in the modal frequencies of calibrated FE model with the experimental model and this achieves the advantage and importance of the performed calibration process. The objective function minimum value is improved from the initial value of 0.0102 to 0.0013 for calibrated FE model within 12 steps, as shown in *Figure 6.16* (a) and (b). Consequently, the calibration process with adopted form of the objective function Eq. (6.7), reduced the high relative differences, thus causing the calibrated FE model to become very close to the real experimental model, which is the most important for further damage detection procedure.

It is concluded from the calibration process, the all five modal frequencies of the calibrated FE model are decreased from the initial FE model in percentages of (3.0-4.5) %, as listed in Table 6.13.

Table 6.13: Improvement in the modal frequencies values of calibrated FE grid bridge model state with additional using proposed SHM procedure by SA optimization method respect to the initial FE model

Mode No.	Modal Frequency Value of Intact Grid Bridge Model (Hz)		Difference in Frequency	
	Initial FE Model	Calibrated FE Model	(Hz)	Relative (%)
1	1.930	2.017	0.087	4.51
2	7.720	8.048	0.328	4.25
3	8.290	8.540	0.250	3.02
4	17.260	17.993	0.733	4.25
5	17.870	18.461	0.591	3.31

The herein presented calibration procedure proves the efficiency and robustness of the adopted calibration process subroutine in the proposed SHM procedure for damage detection using SA heuristic optimization method according to modal frequencies.

6.12. Calibration procedure for FE Vierendeel bridge model

For the third initial FE model of the Vierendeel bridge model, *Figure 6.5*, and due to the differences in the initial numerical modal frequencies values respect to the experimental extracted values of both model loading states, without and with additional masses, as listed in Table 6.4 and Table 6.5, the calibration process is implemented. For the calibration of this structural FE model, the parameters represent the flexural stiffness, mass density of model material and mass of the additional cubic masses are selected for both model states, without and with additional masses.

6.12.1. Adopted parameters in the calibration process of initial FE Vierendeel bridge model

The number of adpoted parameters in the calibration process of the FE Vierendeel bridge mode state without additional masses are eight selected parameters. Those selected parameters are thickness of rectangular hollow section for main longitudinal lower and upper beams (*t*_RHSB); equivalent hieght of rectangular hollow section for stiffener part of main longitudinal upper and lower beams (*h*_RHSBS); flange and web thickness of T-section longitudinal stiffener beams (*t*_TS); width of hidden transverse beams (w_RSHBS); thickness of rectangular hollow section for columns (*t*_RHSC); equivalent hieght of rectangular hollow section for stiffener upper and lower part of columns (*h*_RHSCS); modulus of elasticity (*E*) and mass density (ρ) of steel material.

For the FE bridge model state with additional masses, one more parameter is included in addition to the eight selected parameters in the model state without additional masses. This parameters is the mass value (*M*) of additional masses to be total number of selected parameters in the calibration process of this state of the FE bridge model is nine.

The selection of those parametera is based on the previous sensitivity analysis of the grid bridge model and the uncertainty parameters of the second part of the Vierendeel bridge model represented by both fences on the two sides of the model. As well the significant effect of the column cross sections and the assumed equivalent cross sections of the stiffener parts elements of the main beams and columns, as discussed in paragraph 6.6.1. Thus, the existance of uncertainty values of various cross sections dimensions and assumed equivalent values of another cross sections of such complex structural FE Vierendeel bridge model, the implementation of automatic calibration process for such initial FE model using subroutine by SA method is necessary.

6.12.2. Estimated modal properties of calibrated FE model

The calibration process for the both initial FE Vierendeel bridge model states, without and with additional masses, is implemented using the subroutine of the proposed

SHM procdure by SA method. The selected SA features are the initial temperature $T_o = 20$ and the reduction factor $\alpha = 0.8$.of the cooling schedule for both states of the model. The searching space included in the SA optimization of the calibration process of this model is configured according to the adopted changes ranges, ±(5-12) %, of specified seven parameters values. For the parameter of width of hidden transverse beams (w_RSHBS), different large range is adopted of ±20 % due to the signifcant effect of this parameter on the FE bridge model. The initial values of parameters included in the calibration process are the same values assumed in the initial FE Vierendeel bridge model, as explained in paragraph 6.4.1. The initial parameters values are *t*_RHSB_initial=2.8 mm, *h*_RHSBS_initial=85 mm, *t*_TS_initial=1.5 mm, *w*_RSHBS_initial=100 mm, *t*_RHSC_initial=2.25 mm, *h*_RHSCS_initial=110 mm, *E*_initial=2x10^{-5} N/mm^2, ρ_initial=7.86x10^3 kg/mm^3. For the FE bridge model with additional masses, one more parameter is included of the mass value of additional masses with initial average value of *M*_initial=7.925 kg.

6.12.2.1. Calibrated modal properties of FE Vierendeel bridge model without additional masses

For this FE model state, the number of selected parameters included in the calibration process is eight. The adopted ranges of those eight parameters are discretized by four steps for all eight selected parameters. Therefore, the adopted total searching space in this optimization problem of calibration process has 65536 possible solutions. The proposed calibration procedure starts with the initial value of objective function of the intial differences between the experimental and initial FE bridge model state without additional masses, as listed in Table 6.4. The termination criterion for this optimization problem of calibrated FE bridge model is limited to the maximum number of iterations of 1000, which represents 1.5 % of the total searching space. Such type of searching space with 8-dimension is called hyper space.

The adopted objective function for calibration process of FE bridge model state without additional masses is represented by the sum of square direct difference between

experimental and numerical udated natural frequency value, as defined in Eq. (6.7). The first four modal frequencies, $n = 4$, and eight discrete variables, $K = 8$, are included in the calibration process for this FE bridge model. This type of optimization due to the large searching space with eight discrete variables could be considered as a complex optimization problem.

The improvement of the optimum solution, according to minimize value of adopted objective function, during the iterations of SA optimization method in the proposed calibration procedure of the FE bridge model state without additional masses is shown in *Figure 6.14* (a). In addition, the modification of the five chosen parameters during updating procedure in the calibration process of the same FE bridge model state by five steps is shown in *Figure 6.18* (b).

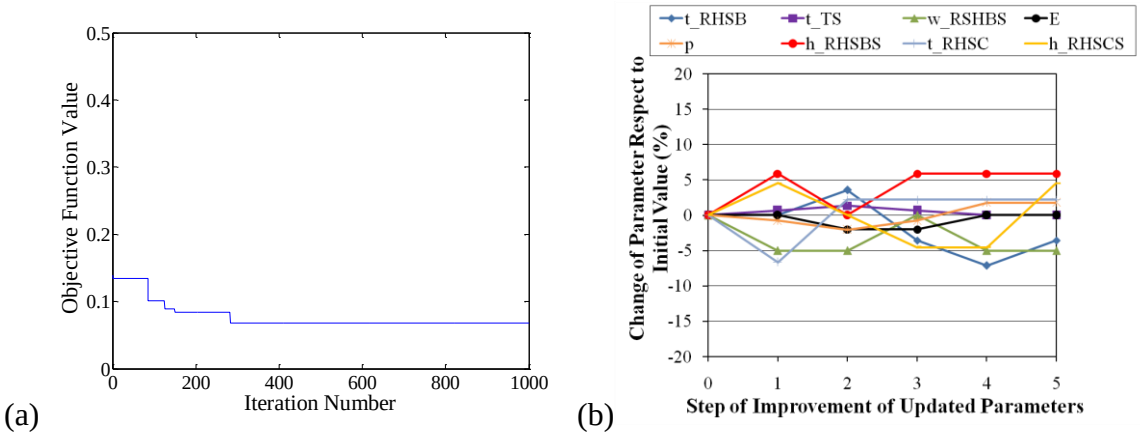

Figure 6.18. Calibrated FE Vierendeel bridge model state without additional masses according to the adopted objective function during SA optimization iterations (a) improvement of optimal solution and (b) step of improvement in updated parameters respect to initial values

The results show that calibration procedure using the SA optimization method has high and quick convergence. Also, the differences in modal frequencies values of calibrated FE model is reduced. It is obvious from *Figure 6.18* (a) that the SA optimization procedure obtains the optimal solution after 283 iterations, which represent only 0.43 % of the total searching space. Also, it is clear in *Figure 6.18* (b) that significant change is in the

thickness of rectangular hollow section of the longitudinal beams (t_RHSB) and the equivalent heights of the stiffener parts of beams (h_RHSBS) and columns (h_RHSCS) during updating process, while slight changes are in other five parameters. The calibration process results the optimum values of the selected parameters of t_RHSB_opt=2.7 mm, h_RHSBS_opt=90 mm, t_TS_opt=1.5 mm, w_RSHBS_opt=95 mm, t_RHSC_opt=2.3 mm, h_RHSCS_opt=115 mm, E_opt=2x10^{-5} N/mm^2 and ρ_opt=8.0x10^3 kg/mm^3.

The first four estimated calibrated modal frequencies values and corresponding experimental extracted values of the Vierendeel bridge mode state without additional masses, Table 5.11, and numerical initial estimated values, Table 6.4, are listed in Table 6.14. It is evident from table that the proposed procedure minimized the differences in modal frequencies according to of objective function from initial value of 0.1396 to the optimal value of 0.0682. Therefore, the percentage of the relative differences in modal frequency respect to the experimental model are decreased from 1.97 % for the first mode to be 1.58 % and lower for the second and fourth mode and the the difference of the third modes is slightly increased, as listed in Table 6.14.

Table 6.14: Calibrated modal frequencies values using proposed SHM procedure by SA optimization method of intact calibrated FE Vierendeel bridge model state without additional masses and comparison with initial values respect to the experimental values

Mode No.	Experimental Modal Frequency (Hz)	Numerical Initial Modal Frequency (Hz)	Difference in Frequency		Numerical Calibrated Modal Frequency (Hz)	Difference in Frequency	
			Square (Hz^2)	Relative (%)		Square (Hz^2)	Relative (%)
1	15.234	15.534	0.090000	1.97	15.475	0.058081	1.58
2	16.552	16.713	0.025921	0.97	16.618	0.004356	0.40
3	35.852	35.845	0.000049	-0.02	35.788	0.004096	-0.18
4	36.291	36.445	0.023716	0.42	36.250	0.001681	-0.11
According to Eq. (6.7) the sum = 0.139686						0.068214	

The percentages of relative differences between the initial and calibrated FE model modal frequencies, with respect to the experimental values, are shown in *Figure 6.19*. According to *Figure 6.19* (a), significant improvement is observed for the first, second and

fourth frequency differences, while the third frequency difference is increased but remains in the range of less than 0.2 %.

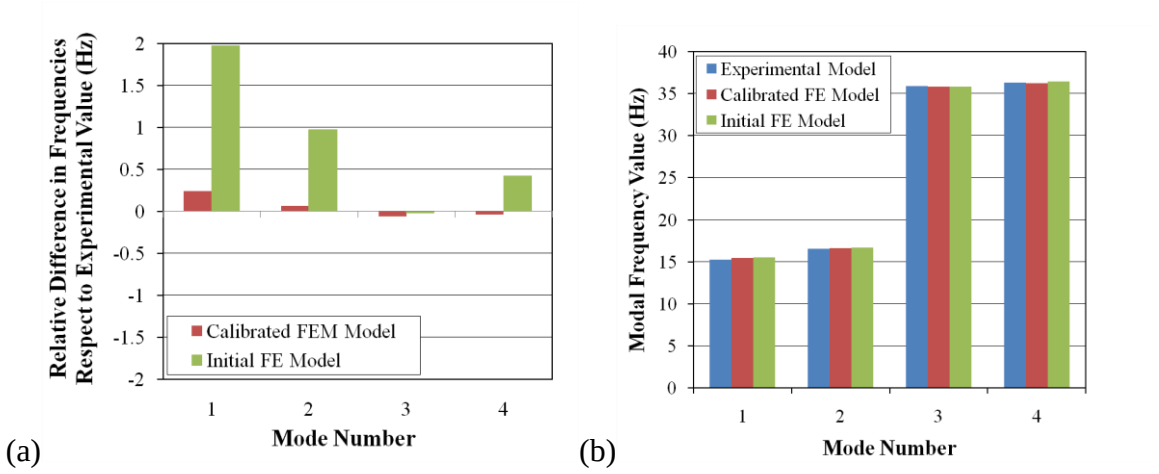

Figure 6.19. Results of calibration process using SA method of FE Vierendeel bridge model state without additional masses (a) differences in modal frequencies of the calibrated and initial FE model respect to the experimental model and (b) the convergence in modal frequencies values

Figure 6.19 (b) shows the convergence in the modal frequencies of calibrated FE model with the experimental model. The small percentage of differences of initial FE bridge modal frequencies values with respect to experimental values, Table 6.14, reflects high accuracy of numerical simulation of initial FE bridge model. The objective function minimum value is improved from the initial value of 0.1396 to 0.0682 for calibrated FE model within five steps, as shown in *Figure 6.18* (a) and (b). Consequently, the calibration process with adopted form of the objective function Eq. (6.7), reduced the high relative differences, thus causing the calibrated FE model to become very close to the real experimental model, which is the most important for further damage detection procedure.

It is concluded from the calibration process, the all four modal frequencies of the calibrated FE model are decreased from the initial FE model in percentages of (0.16-0.57) %, as listed in Table 6.15.

Table 6.15: Improvement in the modal frequencies values of calibrated FE Vierendeel bridge model state without additional using proposed SHM procedure by SA optimization method respect to the initial FE model

Mode No.	Modal Frequency Value of Intact Vierendeel Bridge Model (Hz)		Difference in Frequency	
	Initial FE Model	Calibrated FE Model	(Hz)	Relative (%)
1	15.534	15.475	-0.059	-0.38
2	16.713	16.618	-0.095	-0.57
3	35.845	35.788	-0.057	-0.16
4	36.445	36.250	-0.195	-0.54

The presented proposed calibration procedure proves the efficiency and robustness of the adopted calibration process subroutine in the proposed SHM procedure for damage detection using SA heuristic optimization method for FE model updating according to modal frequencies, where even the initial differences of modal frequencies are small.

6.12.2.2. Calibrated modal properties of FE Vierendeel bridge model with additional masses

For this FE Vierendeel bridge model state with additional masses, the number of selected parameters included in the calibration process is nine. The adopted ranges of those nine parameters are discretized also by four steps for all nine selected parameters. Therefore, the adopted total searching space in this optimization problem of calibration process has 262144 possible solutions. The proposed calibration procedure starts with the initial value of objective function of the intial differences between the experimental and initial FE bridge model state with additional masses, as listed in Table 6.5. The termination criterion for this optimization problem of calibrated FE bridge model is limited to the maximum number of iterations of 1000, which represents very small perecentage of the total searching space of 0.38 %.

The adopted objective function for calibration process of FE bridge model state with additional masses is the same applied for the first model state without additional masses. It

is represented by the sum of square of direct difference between experimental and numerical udated natural frequency value, as defined in Eq. (6.7). The first four modal frequencies, $n = 4$, and nine discrete variables, $K = 9$, are included in the calibration process for this FE bridge model state. This type of optimization due to the very large searching space with nine discrete variables can be considered as a so hard optimization problem. Such type of searching space with 9-dimension is hyper space.

The improvement of the optimum solution, according to minimize value of adopted objective function, during the iterations of SA optimization method in the proposed calibration procedure of the FE Vierendeel bridge model state with additional masses is shown in *Figure 6.20* (a). In addition, the modification of the nine chosen parameters during updating procedure in the calibration process of the same FE Vierendeel bridge model state by eight steps is shown in *Figure 6.20* (b).

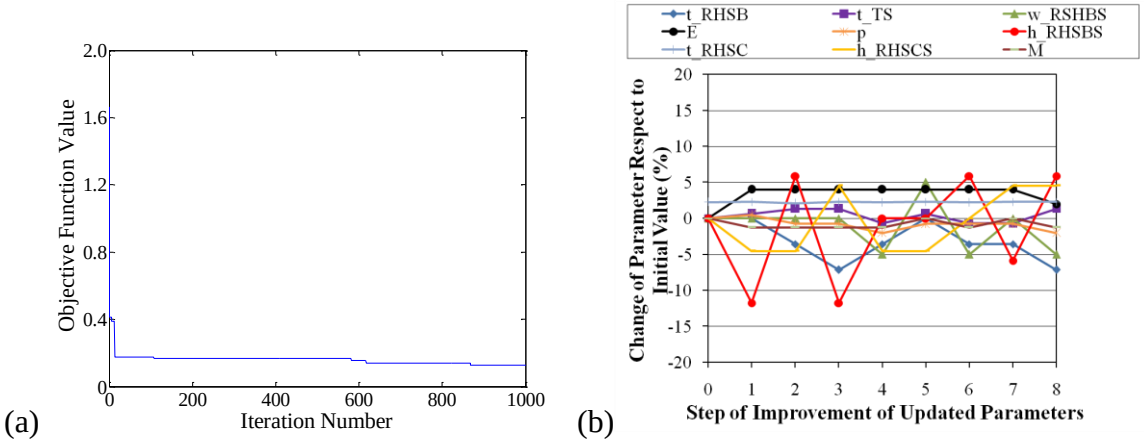

Figure 6.20. Calibrated FE Vierendeel bridge model state with additional masses according to the adopted objective function during SA optimization iterations (a) improvement of optimal solution and (b) step of improvement in updated parameters respect to initial values

The results show that calibration procedure using the SA optimization method has high and quick convergence. Also, the differences in modal frequencies values of calibrated FE model are reduced significantly. It is obvious from *Figure 6.20* (a) that the SA optimization procedure obtains the optimal solution after 868 iterations, which represent

only 0.33 % of the total searching space. Also, it is clear in *Figure 6.16* (b) that significant changes are in the equivalent height of the stiffener parts of beams (*h*_RHSBS) and columns (*h*_RHSCS), width of rectangular solid hidden transverse beams section (*w*_RSHBS), thickness of rectangular hollow section of the longitudinal beams (*t*_RHSB) and modulus of elasticity (*E*) during updating process, while slight changes are in other four parameters. The calibration process results the optimum values of the selected parameters of *t*_RHSB_opt=2.6 mm, *h*_RHSBS_opt=90 mm, *t*_TS_opt=1.52 mm, *w*_RSHBS_opt=95 mm, *t*_RHSC_opt=2.3 mm, *h*_RHSCS_opt=115 mm, *E*_opt=2.04x10^{-5} N/mm^2, ρ_opt=7.7x10^3 kg/mm^3 and *M*=0.007825 kg.

The first four estimated calibrated modal frequencies values and corresponding experimental extracted values of the Vierendeel bridge mode state with additional masses, Table 5.11, and numerical initial estimated values, Table 6.5, are listed in Table 6.16. It is evident from table that the proposed procedure minimized the differences in modal frequencies according to of objective function from initial value of 1.6651 to the optimal value of 0.1268. Therefore, the percentage of the relative difference in modal frequency respect to the experimental model is decreased from 2.84 % for the fourth mode to be 0.34 % and so on for the other two modes except for the second mode there is increase in its difference but remain less than 1.8 %.

Table 6.16: Calibrated modal frequencies values using proposed SHM procedure by SA optimization method of intact calibrated FE Vierendel bridge model state with additional masses and comparison with initial values respect to the experimental values

Mode No.	Experimental Modal Frequency (Hz)	Numerical Initial Modal Frequency (Hz)	Difference in Frequency		Numerical Calibrated Modal Frequency (Hz)	Difference in Frequency	
			Square (Hz^2)	Relative (%)		Square (Hz^2)	Relative (%)
1	13.22	13.09	0.016900	-0.98	13.34	0.014400	0.91
2	15.197	15.129	0.004624	-0.45	15.462	0.070225	1.74
3	30.908	30.085	0.677329	-2.66	30.739	0.028561	-0.55
4	34.57	33.587	0.966289	-2.84	34.453	0.013689	-0.34
According to Eq. (6.7) the sum = 1.665142						0.126875	

The percentages of relative differences between the initial and calibrated FE model modal frequencies, with respect to the experimental values, are shown in *Figure 6.21*. According to *Figure 6.21* (a), significant improvement is noted for the three modal frequencies differences, first, third and fourth, while the second modal frequency has increased in the difference.

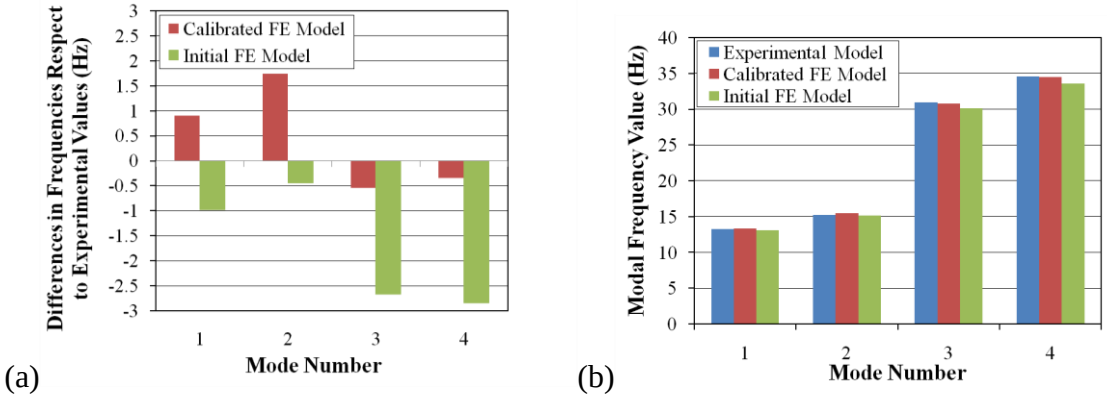

Figure 6.21. Results of calibration process using SA method of FE Vierendeel bridge model state with additional masses (a) differences in modal frequencies of the calibrated and initial FE model respect to the experimental model and (b) the convergence in modal frequencies values

Figure 6.21 (b) shows the convergence in the modal frequencies of calibrated FE model with the experimental model and this achieves the advantage and importance of the performed calibration process. The objective function minimum value is improved from the initial value of 1.665 to 0.126 for calibrated FE model within eight steps, as shown in *Figure 6.20* (a) and (b). Consequently, the calibration process with adopted form of the objective function Eq. (6.7), reduced the high relative differences, thus causing the calibrated FE model to become very close to the real experimental model, which is the most important for further damage detection procedure.

It is concluded from the calibration process, the all four modal frequencies of the calibrated FE model are increased from the initial FE model in percentages of (1.9-2.5) %, as listed in Table 6.17.

Table 6.17: Improvement in the modal frequencies values of calibrated FE Vierendeel bridge model state with additional using proposed SHM procedure by SA optimization method respect to the initial FE model

Mode No.	Modal Frequency Value of Intact Vierendeel Bridge Model (Hz)		Difference in Frequency	
	Initial FE Model	Calibrated FE Model	(Hz)	Relative (%)
1	1.930	2.017	0.250	1.91
2	7.720	8.048	0.333	2.20
3	8.290	8.540	0.654	2.17
4	17.260	17.993	0.866	2.58

The herein presented calibration procedure proves the efficiency and robustness of the adopted calibration process subroutine in the proposed SHM procedure for damage detection using SA heuristic optimization method according to modal frequencies.

6.13. Calibration procedure for FE multi-storey model

For the fourth initial FE model of the multi-storey building model, *Figure 6.7*, and due to the differences in the initial numerical modal frequencies values respect to the experimental extracted values, as listed in Table 6.7, the calibration process is implemented. For the calibration of this structural FE model, the parameters represent the flexural stiffness, mass density and mass of the additional masses on the floors of the strucutral model are selected.

6.13.1. Adopted parameters in the calibration process of initial FE multi-stoery building

The number of adpoted parameters in the calibration process of the FE multi-storey building model are seven selected parameters. Those selected parameters are thickness of square hollow section for main beams and columns (t_SHS), dimension of square hollow

section for main beams and columns (*h*_SHS), dimension of square solid section for beam-column joint section (*h*_SSS), thickness of square steel floor plate (*t*_Plate), modulus of elasticity (*E*), mass density (ρ) of steel material and mass value (*M*) of additional masses over the floors of the last two level of building model, level-9 and 10, as shown in *Figure 5.44*, and discussed in paragraph 6.7.1. The additional masses over floors of the other levels are assembled within the mass density of origin steel floor plate of each level in the equivalent mass density of steel floor plate, according to Eq. (6.1).

The selection of those seven parametera is based on the manually parametric study of the FE analysis of the FE multi-storey model for some of them and the uncertainty parameters values of the other parameters. As well the significant effect of the beam-column joint cross section, as discussed in paragraph 6.6.1. Thus, the existance of uncertainty values of various cross sections dimensions and assumed equivalent distribution of additional masses positions in beams of the level-9 and 10 of such complex structural FE multi-storey building model, the implementation of automatic calibration process for such initial FE model using subroutine by SA method is necessary.

The initial values of selected seven parameters included in the calibration process are the same values assumed in the initial FE multi-storey building model, as mentioned in paragraph 6.4.1. The initial parameters values are *t*_SHS_initial=0.8 mm, *h*_SHS_initial=15 mm, *h*_SSS_initial=12 mm, *t*_Plate_initial=3 mm, *E*_initial=$2\text{x}10^{-5}$ N/mm^2, ρ_initial=$7.86\text{x}10^3$ kg/mm^3 and *M*=4 kg.

6.13.2. Estimated modal properties of calibrated FE model

For the FE multi-storey building model, the number of selected parameters included in the calibration process is seven. The adopted ranges of those seven parameters are discretized by four steps for five of them and six steps for two parameters of dimension of beam-column joint section and mass value of additional masses. Therefore, the adopted total searching space in this optimization problem of calibration process has 36864 possible solutions. The proposed calibration procedure starts with the initial value of objective function of the intial differences between the experimental and initial FE building model, as

listed in Table 6.7. The termination criterion for this optimization problem of calibrated FE bridge model is limited to the maximum number of iterations of 500, which represents very small perecentage of the total searching space of 1.36 %.

The adopted objective function for calibration process of FE building model is represented by the sum of square of direct difference between experimental and numerical udated natural frequency value, as defined in Eq. (6.7). The first six modal frequencies, $n = 6$, and seven discrete variables, $K = 7$, are included in the calibration process for this FE building model. This type of optimization due to the very large searching space with seven discrete variables can be considered as a so hard optimization problem with hyper space.

The improvement of the optimum solution, according to minimize value of adopted objective function, during the iterations of SA optimization method in the proposed calibration procedure of the FE multi-storey building model is shown in *Figure 6.22* (a). In addition, the modification of the seven chosen parameters during updating procedure in the calibration process of the FE building model by five steps is shown in *Figure 6.22* (b).

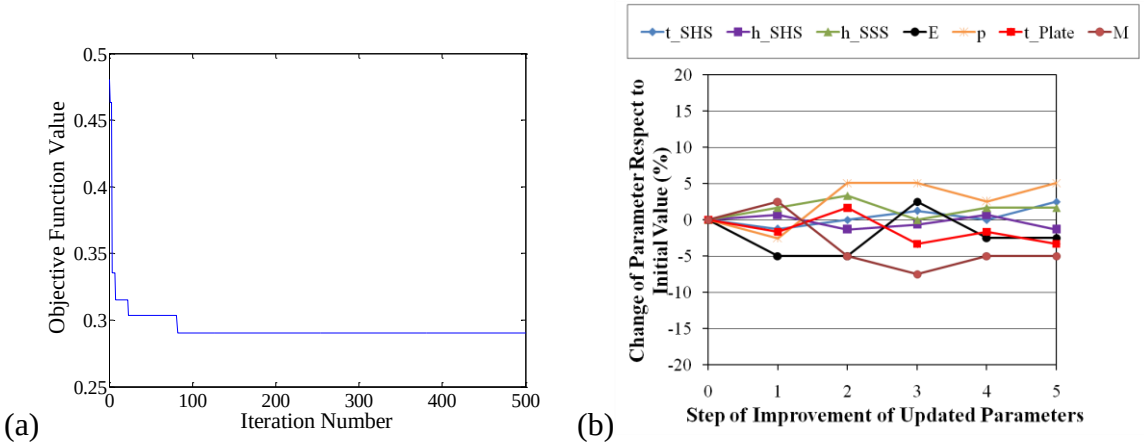

Figure 6.22. Calibrated FE multi-storey building model according to the adopted objective function during SA optimization iterations (a) improvement of optimal solution and (b) step of improvement in updated parameters respect to initial values

The results show that calibration procedure using the SA optimization method has high and quick convergence. Also, the differences in modal frequencies values of calibrated

FE model are reduced. It is obvious from *Figure 6.22* (a) that the SA optimization procedure obtains the optimal solution after 82 iterations, which represent only 0.22 % of the total searching space. Also, it is clear in *Figure 6.22* (b) that significant changes are in the thickness of the steel floors plates (*t*_Plate), modulus of elasticity (*E*), mass density (ρ) and mass value of equivalent distribution of additional masses positions (*M*) during updating process, while slight changes are in other two parameters. The calibration process results the optimum values of the selected parameters of *t*_SHS_initial=0.82 mm, *h*_SHS_initial=14.8 mm, *h*_SSS_initial=12.2 mm, *t*_Plate_initial=2.9 mm, *E*_initial=1.96x10^{-5} N/mm^2, ρ_initial=8.26x10^3 kg/mm^3 and *M*=3.8 kg.

The first six estimated calibrated modal frequencies values and corresponding experimental extracted values of the multi-storey building model, Table 5.16, and numerical initial estimated values, Table 6.7, are listed in Table 6.18. It is evident from table that the proposed procedure minimized the differences in modal frequencies according to of objective function from initial value of 0.4802 to the optimal value of 0.2903. Therefore, the percentage of the relative difference in modal frequency respect to the experimental model is decreased from 5.39 % for the fifth mode to be 3.59 % and lower for the other two modes, but for the first, third and sixth mode there are slight increase in their differences.

Table 6.18: Calibrated modal frequencies values using proposed SHM procedure by SA optimization method of intact calibrated FE multi-storey building model and comparison with initial values respect to the experimental values

Mode No.	Experimental Modal Frequency (Hz)	Numerical Initial Modal Frequency (Hz)	Difference in Frequency		Numerical Calibrated Modal Frequency (Hz)	Difference in Frequency	
			Square (Hz^2)	Relative (%)		Square (Hz^2)	Relative (%)
1	2.637	2.647	0.0001	0.38	2.713	0.0058	2.88
2	2.893	2.794	0.0098	-3.42	2.865	0.0008	-0.97
3	6.555	6.517	0.0014	-0.58	6.630	0.0056	1.14
4	10.030	9.632	0.1584	-3.97	9.816	0.0458	-2.13
5	10.290	9.735	0.3080	-5.39	9.921	0.1362	-3.59
6	14.870	14.920	0.0025	0.34	15.180	0.0961	2.08
According to Eq. (6.7) the sum = 0.4802						0.2903	

The percentages of relative differences between the initial and calibrated FE model modal frequencies, with respect to the experimental values, are shown in *Figure 6.23*. According to *Figure 6.23* (a), significant improvement is apparent for the three modal frequencies differences, second, fourth and fifth, while the first, third and sixth modal frequencies have increased in the differences.

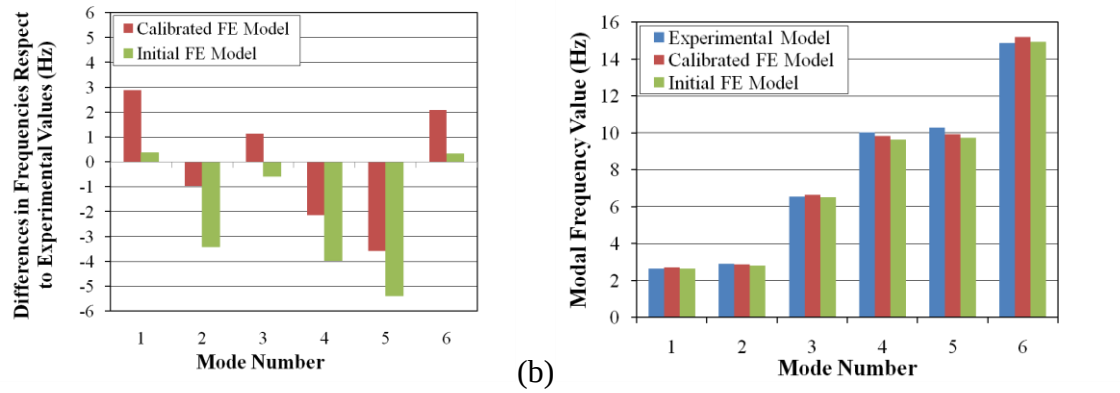

Figure 6.23. Results of calibration process using SA method of FE multi-storey building model (a) differences in modal frequencies of the calibrated and initial FE model respect to the experimental model and (b) the convergence in modal frequencies values

Figure 6.23 (b) shows the convergence in the modal frequencies of calibrated FE model with the experimental. The objective function minimum value is improved from the initial value of 0.4802 to 0.2903 for calibrated FE model within five steps, as shown in *Figure 6.22* (a) and (b). Consequently, the calibration process with adopted form of the objective function Eq. (6.7), reduced the high relative differences, thus causing the calibrated FE model to become very close to the real experimental model, which is the most important for further damage detection procedure.

It is concluded from the calibration process, the all six modal frequencies of the calibrated FE model are increased from the initial FE model in percentages of (1.7-2.5) %, as listed in Table 6.19.

Table 6.19: Improvement in the modal frequencies values of calibrated FE multi-storey building model using proposed SHM procedure by SA optimization method respect to the initial FE model

Mode No.	Modal Frequency Value of Intact Multi-Storey Building Model (Hz)		Difference in Frequency	
	Initial FE Model	Calibrated FE Model	(Hz)	Relative (%)
1	2.647	2.713	0.066	2.49
2	2.794	2.865	0.071	2.54
3	6.517	6.630	0.113	1.73
4	9.632	9.816	0.184	1.91
5	9.735	9.921	0.186	1.91
6	14.920	15.180	0.260	1.74

The herein presented calibration procedure of the multi-storey building model and previous three structural models proves the efficiency and robustness of the adopted calibration process subroutine in the proposed SHM procedure for damage detection using SA heuristic optimization method according to modal frequencies.

So, the all calibrated FE structural models are ready to verify of the proposed SHM procedure to detect the damages in which based on the adopted damages scenarios for each model.

7. VERIFICATION OF THE PROPOSED DAMAGE DETECTION PROCEDURE USING OPTIMIZATION ALGORITHM

7.1. General

In this chapter, the verification of the proposed **S**tructural **H**ealth **M**onitoring procedure for damage detection **U**sing **S**imulated **A**nnealing optimization method (SHMUSA-procedure) are conducted to detect the damage in the adopted four structural models. This chapter represents a sophisticated part of the proposed SHMUSA-procedure, which includes the artificial intelligent technique (AIT) to connect multi aspects to monitor states of the structures, as shown in Figure 1.1. The verfication includes test of the adopted bjective function with its features, number of included modes, number of included components and weighting factors, for each adopted structural model. The objective function with its parameters and designed searching space plays an important aspect to detect damage characteristics precisely. The sensitvity of the adopted objective function function are studied for the implemented damage scenarios for the damaged structural models to verify the ability in such problems. Different values of objective function parametres are applied to select the appropriate values which have to catch the best optimum that represents the damage characteristics, location of damaged element and damage ratio. Therefore, the check of the adopted objective function with its parameters is performed for each structural model.

In addition, the iterative numerical simulation is implemented to estimate dynamic response of the structural models at different locations and severities of damage in each structural model. The simulated damage is applied on the clibrated FE models of the all adopted structural models. Then, the modal analysis is implemented for the damaged FE models after simulation of the adopted damage scenarios for all adopted structural models to estimate the dynamic properties, natural frequency and normalized mode shape vector. The orthogonality between the experimental and the numerical FE model mode shapes is

checked using the MAC indicator, Eq. (4.10), which allows to compare between each other and used them in the computations.

Thereafter, the improvements optimal solutions,damage characteristics, during performance of the SMHUSA-procedure in each structural models are verified using all its features adopted such as size of searching space, cooling schedule, configuration type of neighborhood and termination criteria. Also, the improvements of the each parameter of the damage characteristics, location and extent of the damage, are verified during iterations of the adopted proposed procedure.

Also, two loading states, without and with additional masses, are verified for two types of the structural models, grid and Vierendeel bridge model, and the original state is adopted for verification of the other two structural model, overhang beam and multi-storey building model. In addition, the verification of the SHMUSA-procedure is implemented to simply supported steel beam by simulating damage scenario numerically only in the FE model. In the present study, all those structural models are adopted to prove the ability, efficiency and robustness of the proposed structural health monitoring procedure using simulated annealing method (SHMUSA-procedure) to detect damage due to various dynamic behaviours in different types of damaged structures.

7.2. Proposed SHM procedure for damage detection using SA algorithm (SHMUSA-procedure)

The SHMUSA-procedure is based on the methods of damage detection based on updating FE model using optimization method, as discussed in chapter two paragraph 2.5. The SHMUSA-procedure performs the comparison between the dynamic characteristics extracted from the experimental (actual) damaged structure and estimated from iterative numerical simulation states of the damaged FE model, as shown in *Figure 2.3* (a) and (b). The heuristic SA optimization method adopted in the SHMUSA-procedure conducts the statistical analysis of the dynamic responses of structural models using the adopted objective function, Eq. (4.32), as shown in *Figure 4.2*.

In the SHMUSA-procedure, the damage is simulated numerically and applied on the calibrated FE models of the all adopted structures, as shown in *Figure 2.3*. The

implemented damage scenario of each structures is represented by reducing in the flexural stiffness of the damaged element in the FE models. The reduction in stiffness matrix is calculated by decreasing the depth of the cross section of the damaged element by multiplying it in reduction factor, β, during analyzing the FE models. The reduction factor, β, specifies the damage ratio in the damaged element as a ratio from the total depth of the cross section. Those damage characteristics, damage location and damage severity, are selected randomly during the iterations in the SHMUSA-procedure from designed ranges for each parameter. The first damage characteristic is damage location which is presented in SHMUSA-procedure as damaged element number (D_e) from the adopted number of included elements in the FE model of each structure. The other damage characteristic is the damage severity which represents damage ratio (D_r). The damage ratio (D_r) is represented in SHMUSA-procedure as reduction factor, β, value in the range of [0.01-0.99]. The searching space of optimization problem for each structural model is calculated from those ranges of damage characteristics values, D_e and D_r.

The termination criteria control the system time of SHMUSA-procedure to explore the optimal solution, damage characteristics. Those termination criteria were adopted either the system reaches the cold state "frozen" or the maximum number of iteration is achieved. The frozen state is reached when the temperature, T, of the system is reduced by the cooling sechdule to be less than one (i.e. close to zero) during improving the optimal solution by iterations. The linear relation of the cooling schedule is applied in the SHMUSA-procedure to control the system with range of the reduction factor, α, of [0.70-0.90]. The Initial temperature, T_o, is assumed depend on the optimization problem. The maximum number of the iterations was limited in the range of [500-2000] checked solutions of the total possible solutions in the searching space of the structural models problems. Those ranges of reduction factor, α, and maximum number of the iterations come from many trials of trial and error to design the approperiate values of parameters of the SHMUSA-procedure to catch the best solutions.

In the SHMUSA-procedure, two types of the selection of neighborhood in the searching space are adopted based on the structural problem, simplicity or complixity. The

randomly selection of the intial solution from the searching space and a generated solution from the neighborhood of the cuurent solution is one of the important feature applied in the SHMUSA-procedure. The standard SA method and ordinary SA method of searching configuration type are adopted to generate the new solution from the neighboring solutions of the current solution. The Standard SA method generates one neighboring solution from the current soltion, while the ordinary SA method generates a set of neighboring solutions from the current soltion. As mentioned previously in current study, the flowchart of proposed SHM procedure using SA heuristic optimization metod with adopting strategy of SA features is shown in *Figure 2.3* (a) and (b).

The form of objective function adopted in SHMUSA-procedure consists of two parts, as defined in chapter four in Eq. (4.32). The first part is the square of relative difference in the updated modal frequency of the damaged FE model respect to the experimental modal frequency extracted from implemenyed damage scenario, as defined in Eq. (4.32). The second parts of the objective function represents the differences in normalized mode shape vectors values between the experimentally extracted respect to implemented damage scenario and numerically updated of the damaged FE model, as defined in Eq. (6.5). The second part of the objective function represents the form of mathematiclly norm and this is the modification of the present study on the adopted objective fnction. After that, the difference between the experimental and numerical updated modal propoerties of the damaged model are calculated. The adopted objective function in the SHMUSA-procedure minimize the differences between the compartive modal properties untill the optimal solution is explored, as shown in *Figure 2.3* and *Figure 4.2*. The optimal solution of the objective function represents the exact or very close to actual implemented damage scenario characteristics, damage location and damage severity, in the experimental testing. The compatibility between the numerical calibrated FE and experimental model is high important for proposed SHMUSA-procedure to detect damage in structural models preciesly.

The proposed SHMUSA-procedure is written in a high-level technical computing language of enviroment MATLAB-Software that could properly handle all these things to monitor the structures system. In envoment MATLAB software can connect among multi

tasks during performance of SHMUSA-procedure, as shown in *Figure 2.3* (b) and *Figure 4.2*. Firstly, the SHMUSA-procedure, in MATALAB envioment, selects randomly the new values of damage characteristics, damaged element number (D_e) and reduction factor value , β , from matrices created in the dimension of the designed ranges. Then, the procedure calculates the updated real constants for all elements as well the damaged element in the FE model based on the new damage characteristics. After that, the SHMUSA-procedure save the updated real constants in the output file. Secondly, the SHMUSA-procedure connects with ANSYS software in APDL enviroment to conduct the new analysis. The enviroment APDL calls the stored file of the updated real constants to ANSYS software as input file. Thereafter, the SHMUSA-procedure, in ANSYS software, performs the new modal analysis of the updated FE model and estimates the updated modal properties, natural frequencies and mode shape vector and save the results in output file. Thirdly, the SHMUSA-procedure, in MATALAB software, calls the stored file results of the updated modal properties. The normalization of the estimated mode shape vectors is computed based on the experimental mode shape vectors for the updated FE model. Herein, the number of DOFs of numerical FE model are specified to be the same number of DOFs of the measurement points used to record acceleration data in the experimental testing of the structural model during ambient vibration testing. Fourthly, the SHMUSA-procedure, using SA method with its features which is discussed in chapter four in paragraph 4.5, performs statistical analysis to compare the updated damaged FE model (new current solution) with actual damaged scenario model. The SHMUSA-procedure continue repeat these analyses processes and estimate the updated modal frequencies of the damaged FE model and compare them with experimental damaged model during iterations and so on until the termination criteria are achieved and the SHMUSA-procedure explores the optimal solution, which represents damage characteristics, as shown in *Figure 2.3*. That means the high convergence between the comparative modal properties, experimental and numerical updated, is reached based on the minimizing of the adopted objective function.

7.3. Verification of proposed SHM procedure numerically on simply supported beam structural model

The first verification of the SHMUSA-procedure was done using a simply supported beam model, as show in *Figure 7.1*. This verfication of the proposed procedure is adopted only the numerical simulation of the damage scenario. In this section, efficiency and effectiveness of the proposed procedure are evaluated firstly through some simulated damage identification tests using modal data. Paper in the 14th initernational conference of DGKS in 2014 is published dealt with this verification of the SHMUSA-procedure [140].

A simply supported steel beam of 10 m length is chosen with two different damage scenarios of damage. FE model of the steel beam is created using ANSYS software for structural analysis, as shown in *Figure 7.1*.

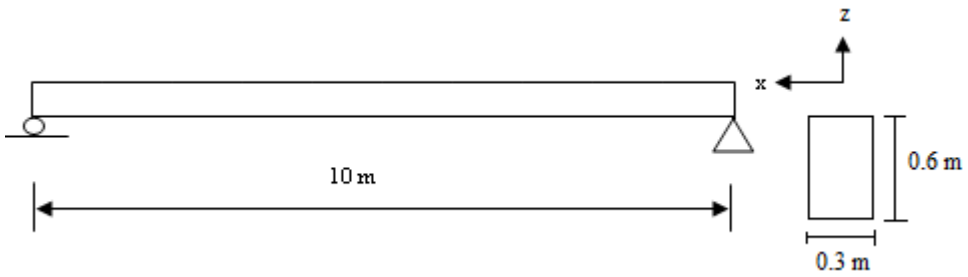

Figure 7.1. FE model of simply supported steel beam

The FE model consists of 100 elements and 101 nodes, while the Beam4 finite element type used. The material properties include Young's modulus of E=200x10^5 N/mm^2 and mass density of ρ =7860 kg/m^3. Cross-sectional area and second moment of area of the beam are A=0.18 m^2 and I=0.0054 m^4, respectively.

Thereafter, the modal analysis of the FE simply supported beam model was performed and modal properties, the natural frequencies and mode shape, were estimated by Block Lanczos method using ANSYS software. The first five estimated modal frequencies and the mode shape characters of the intact FE model are shown in Table 7.1.

Table 7.1: Modal properties of FE simply supported beam model using ANSYS software

Mode No.	Modal Frequency Value of Intact Simply Supported Beam Model (Hz)	Modw Shapr Characters
1	6.8595	1st bending
2	13.7038	1st Lateral
3	27.4077	2nd bending
4	54.5742	2nd Lateral
5	61.5538	3rd bending

In this first model study, two damage scenarios were implemented with damage characteristics, damage location and severity. The first damage characteristc is the location of damage in the scenarios, which represents the number of selected damaged element in the FE model. The second one is the damage severity which is defined in the presented study by the ratio of crack_depth/total_depth, D_r, damage ratio, in the form defined by Eq. (7.1).

$$D_r = \gamma \frac{d}{t} \qquad 7.1$$

where are:

d - the crack depth from the bottom side of the cross section,

t - the total depth of the cross section,

γ - the weighting factor of damaged stiffness.

During the numerical simulation of damage, the stiffness of the entire element has to be reduced. Hence, in order to get adequate stiffness, because the crack width could be smaller than the element length, parameter γ needs to be introduced to weight an adequate stiffness of the element and its real stiffness with narrow crack. This parameter takes value in the range of $0 < \gamma \leq 1$. It is considered, herein, that $\gamma = 1$, because the width of actual crack was the same as the element length of 100 mm, *Figure 7.1*, and the actual damage ratios were computed according to Eq. (7.1), Table 7.2. The crack depth d is calculated by assumed the value of reduction factor β which multiply by the total intact depth of cross section t to produce the damage/crack depth d of damaged element, as defined in Eq. (7.2).

$$d = \beta \, . \, t \qquad 7.2$$

where are:

β - the reduction factor of damage in the range of [0.01-1.00].

The intact remaining depth of the cross section of the damaged element is calculated by multiplying the value of $(1-\beta)$ by the total depth, t, of cross section. The both damage scenarios were implemented with damage characteristics, damage location and ratio, as listed in Table 7.2.

Table 7.2: Implemented damage scenarios on the FE simply supported beam model

Description	Damage Scenario-1 (DC-1)	Damage Scenario-2 (DC-2)
Damage Location D_e (Damaged Element Number)	30	50
Damage Ratio D_r	0.30	0.50

During the performance of the SHMUSA-procedure, its parameters for optimization problem were designed to achieve the convergence and accuracy of exploration the optimal solution, damage characteristics. The included number of elements in the computations is 100 elements, *Figure 7.1*, of all elements in the FE model, while the damage ratio represented by reduction factor β is considered as a discrete variable with accuracy of 0.01, as listed in Table 7.3. Therefore, the size of the searching space, which represents the total number of all possible solutions in the searching space, is 10000.

Table 7.3: Input Parameters in the SHMUSA-procedure for damage detection in the the simply supported beam model

Parameter Description	Parameter Value
Number of Included Elements	100
Range of Damage Reduction Factor β	[0.01 - 1.00]
Size of Searching Space	10000
Max Number of Iterations	500
Percentage (%)	5 %
Initial Temperature T_o	20
Temperature Reduction Factor α	0.7
Weighting Factors W_f , W_d	1000, 0.001

The termination criteria in this structural model problem are specified by frozen of the system, i.e. temperature less than one degree, and the maximum number of iterations, which is limited to 500, i.e. 5 % of the total number of possible solutions in searching space, as listed in Table 7.3.

On the other hand, There are other designed parameters in the SHMUSA-procedure for SA method, which represents the features of SA optimization method such as the linear relation of cooling schedule included initial temperature T_o and reduction factor, α. For this type of simply supported beam model, those parameters are listed in Table 7.3.

In addition, one of the important parameters used in the SHMUSA-procedure are the weighting factors W_f and W_d which have to be suitable enough for the proposed objective function in the procedure, Eq.(4.32), to enable it of detect damage characteristics precisely. The selection of these parameters is based on several studies by trial and error for specified damage cases. To check the ability of the adopted function in the SHMUSA-procedure to detect the optimal solution, one case study was implemented. This case study includes damage ratio of 0.10 at element number 50 using weighting factors of $W_f = 1000$ and $W_d = 0.001$, as shown in *Figure 7.2*.

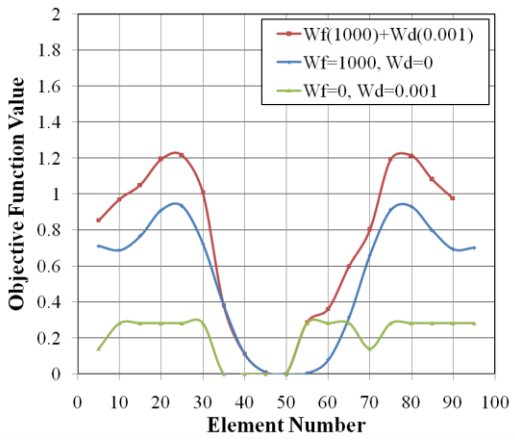

Figure 7.2. Test of adopted objective function with weighting factors of $W_f = 1000$ and $W_d = 0.001$, case study of D_e=50 and D_r=0.10, used in the SHMUSA-procedure on the simply supported beam model

This case study included only 90 elements of the 100 element in the FE model in the range of [5-95]. It is obvious from *Figure 7.2* that the adopted objective function, Eq.(4.32), in the SHMUSA-procedure has high accuracy to detect exactly the damage location at element number 50. Also, the differences in modal frequencies, which represents the first part of the objective function Eq. (4.32), have significant effect on the results, as shown in *Figure 7.2*. Therefore, the appropriate values of weighting factors depend on the strutural model type and thus the values of natural frequencies and normalized mode shape vectors of the structure. Therefore, for this type of simply supported beam model, the selected values of the weighting factors W_f and W_d are 1000 and 0.001, respectively, as listed in Table 7.3.

In the SHMUSA-procedure and for the simply supported bem model, the objective function, Eq. (4.32), is included the first five modes, $n=5$, natural frequencies and normalized mode shapes in the computations. The number of components of the mode shape vectors included in the computations for this structural model is two, $m=2$. The first component is the vertical displacement in z-axis and the second one is the transverse displacement in y-axis, while the longitudinal displacement in x-axis is neglected, as shown in *Figure 7.1*.

After performance of the proposed SHMUSA-procedure to detect damage in the simply supported beam model, the improvements of the objective function during the iterations for both tested damage scenarios, are shown in *Figure 7.3*. It is evident from *Figure 7.3* (a) and (b) for both damage scenarios, that the SHMUSA-procedure has high and quick convergence during the iterations which are the most significant advantage of the applied procedure for damage detection based on optimization metod. The termination criterion for DC-1 is the frozen of the system, as shown *Figure 7.3* (a) , while in the DC-2 is the max number of iterations, as shown *Figure 7.3* (b).

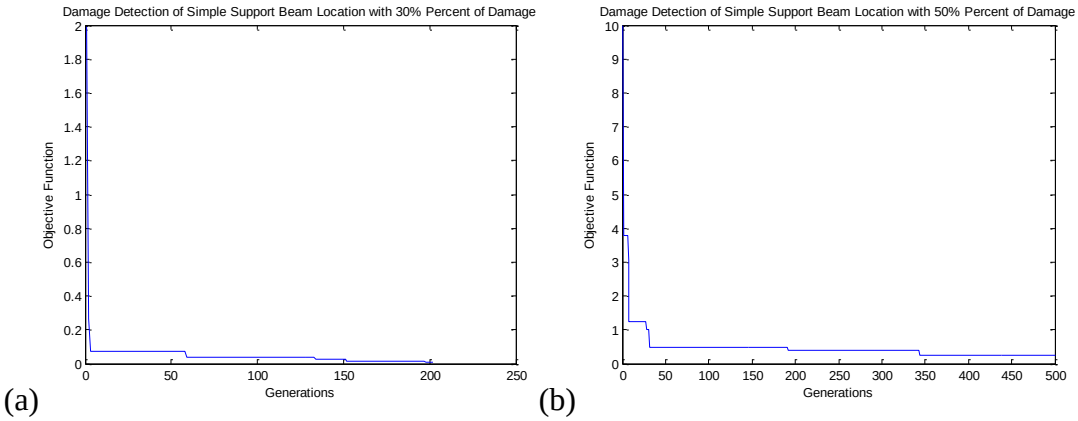

(a) (b)

Figure 7.3. Improvement of the adopted objective function used in the SHMUSA-procedure for implemented both damage scenarious (a) for DC-1 and (b) for DC-2

The final results of verification the SHMUSA-procedure to detect damage characteristics in the simply supported beam model are shown in *Figure 7.4*. It is quite obvious from *Figure 7.4*, that the SHMUSA-procedure in damage scenario of DC-1, Table 7.2, detected the optimal solution which represents damage characteristics, damage location and damage ratio, at element no. 30 and damage ratio of 0.31, as shown in *Figure 7.4* (a), after number of iteration of 202. Whereas, for damage scenario of DC-2, Table 7.2, the SHMUSA-procedure detected damage location at element no. 50 with damage ratio of 0.52, as shown in *Figure 7.4* (b), after number of iteration of 500.

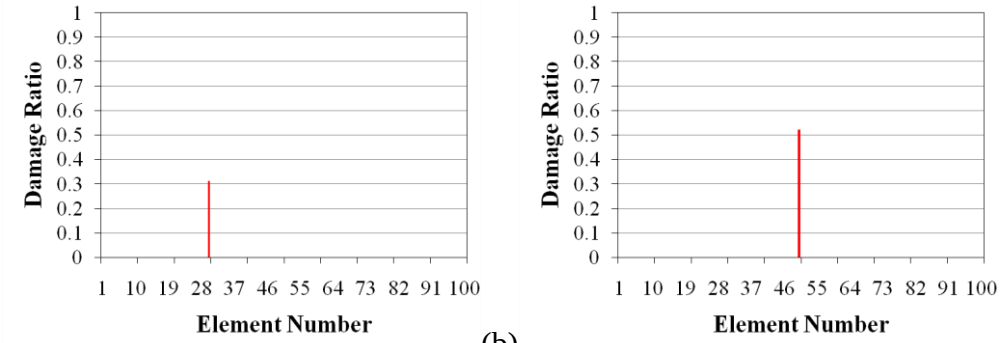

(a) (b)

Figure 7.4. Detected damage characteristics, damage location and damage severity by the SHMUSA-procedure in the simply supported beam model for (a) DC-1 and (b) DC-2

The results, *Figure 7.3* and *Figure 7.4*, show that the SHMUSA-procedure explored the exact damage location and severity in the simply supported beam model for DC-1 and DC-2. The results indicate that the SHMUSA-procedure has a robustness, efficiency and effectivness in detecting and quantifying of various damage scenarios and it has avoided trapping in local solution with fast running in short time.

7.4. Verification of proposed SHM procedure on overhang structural model

The verification of the SHMUSA-procedure on the first adopted structural model of overhang beam is started with numerical test of the adopted objective function for the implemented damage scenarios. Paper in the, Journal of the Croatian Assocaition of Civil Engineers (Gradevinar) in 2014 is puplised dealt with this verification of the SHMUSA procedure [141].

In this second model, two damage scenarios were implemented with damage characteristics, damage location and severity, as discussed five paragraph 5.2.5 in chapter five. Both of damage scenarios are at the same element number 17 of the FE overhange beam model, *Figure 5.11*, but with different damage severities. The first damage scenarios, DC-1, has damage severity of 0.38, while the second scenario, DC-2, has damage severity of 0.55, which means more seroius damage in DC-2, as listed in table Table 7.4. Herein, the weighting factor of the element stiffness $\gamma = 1$, because the width of actual crack was the same as the element length of 25 mm, *Figure 6.1*, and the actual damage ratios were computed according to Eq. (7.1).

Table 7.4: Implemented damage scenarios on the simply supported overhang beam model

Description	Damage Scenario-1 (DC-1)	Damage Scenario-2 (DC-2)
Damage Location D_r (Damaged Element Number)	17	17
Damage Severity D_e	0.38	0.55

Prior to the application of the proposed SHMUSA-procedures, tests of the objective function efficiency were conducted. The proposed form of objective function, defined by Eq. (4.32), was analyzed in order to find out the most effective values of the weighting factors for different severity of damages.

Also, for this model parametric study to find the most suitable values of the weight factor influence on objective function efficiency for the SHMUSA-procedure, Eq. (4.32), was carried out, in order to insure that the adopted objective function will be sensitive enough to any changes in modal properties due to damage existence. The studied values of W_f and W_d weighting factors, varied in the range listed in Table 7.5. The parameteric study included the first four modes of the overhang beam model into consideration during testing the objective function.

Table 7.5: Studied values of weighting factors of adopted objective function, Eq. (4.32), used in the SHMUSA-procedure for overhang beam model

	W_f	W_d
Weighting Factor Value	0, 1, 10, 100	0, 1

For the first damage scenario, DC-1, with damage ratio of $D_r = 0.38$, the most suitable values of the weighing factors $W_f = 10$ and $W_d = 1$ were found in the modified objective function Eq. (4.32), which result in exact minimum at the actual position of damage, *Figure 7.5* (a). In the case of examined first damage scenario, DC-1, with small differences in frequencies in the range of 3%, the differences in displacements (mode shapes) with adopted weighting factors, more significantly participate in the objective function total value than natural frequency differences. It practically explored the most suitable values of the weighting factors to amplify the participation of the small frequency differences. Also, the displacements have to be included to get minimum value of the objective function at the exact position of damage, on element no. 17, as it is marked in red line in *Figure 7.5* (a).

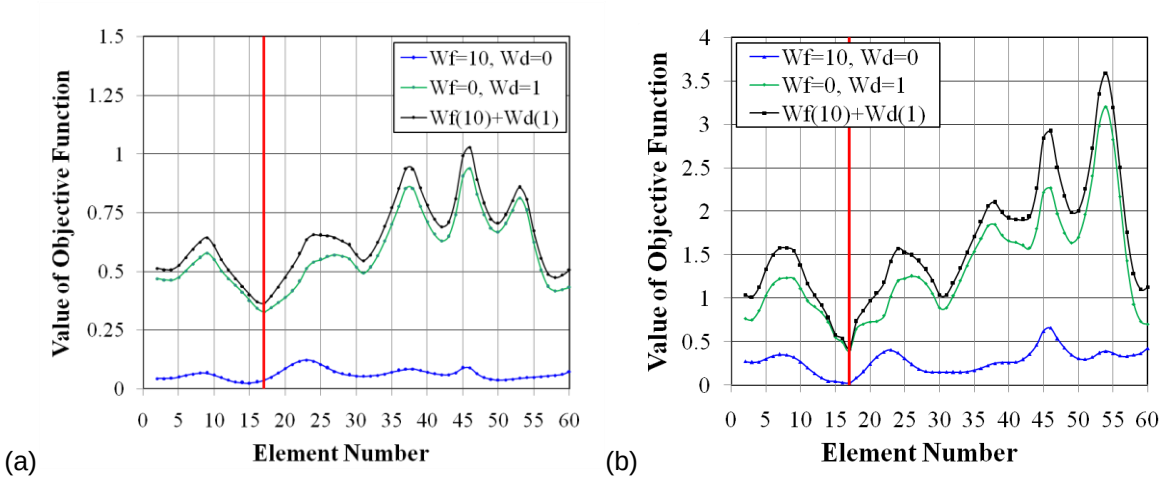

Figure 7.5. Influence of the weighting factors in objective function, Eq. (4.32), for studied damage scenarios with variation of the positions of damage (a) for DC-1 with $D_r = 0.38$ *and (b) for DC-2 with* $D_r = 0.55$

The same analysis was carried out for the second adopted damage scenario, DC-2, with more significant damage with ratio of $D_r = 0.55$, Table 7.4, using the same proposed weighting factor values, $W_f = 10$ and $W_d = 1$. The behaviour of the adopted modified objective function, Eq. (4.32), shows that the proposed weighting factors are adequate and provide ability to explore the global minimum at the exact damage position, element no.17, *Figure 7.5* (b). The adopted weighting factors were applied in all further analyses, as the most suitable values in the objective function for the SHMUSA-procedure in the form defined by Eq. (4.32).

Further investigation was conducted to examine the efficiency of objective function defined by Eq. (4.32), with previously defined most suitable weighting factor values and different severity of damage. Firstly, the study was carried out for the adopted scenario of damage DC-1, varying the damage ratio D_e in the range [0.1, 0.6], and position of the damage along the beam as shown in *Figure 7.6* (a). Figure 7.6 (a) shows objective function change during the numerical simulation of damage for the actual results for DC-1. The global minimum of the objective function achieved for damage ratio $D_e = 0.38$ and at the exact damage position, element no. 17, with more local minimums, *Figure 7.6* (a).

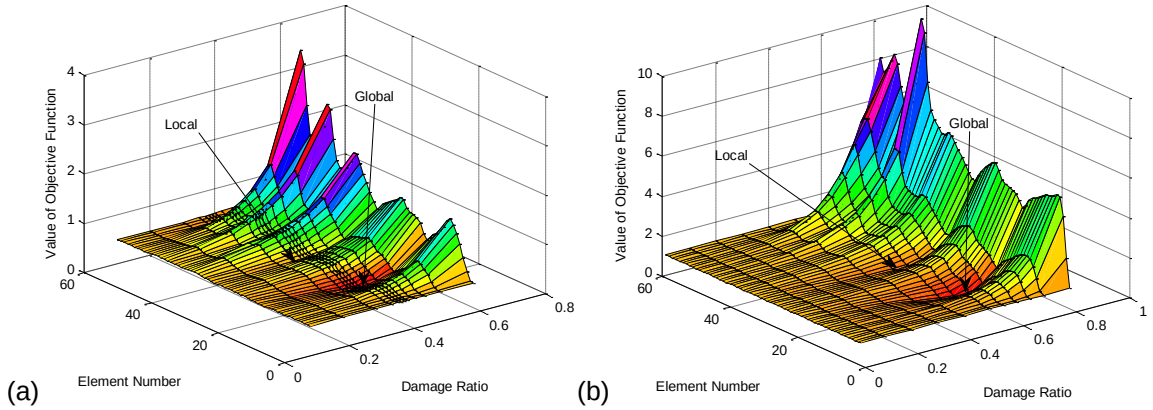

Figure 7.6. Numerical simulatation testing of the adopted objective function with $W_f = 10$ and $W_d = 1$ *used in the SHMUSA-procedure for the FE overhang beam model with global and local minimums (a) for DC-1 and (b) for DC-2*

Based on the experimental results of DC-2, damage simulation was conducted for damage ratio D_e in the range [0.01, 0.8] and position of the damage element along the beam. As in the previous case, DC-1, simulation of the modified objective function detected the global minimum for the actual damage ratio of DC-2 and at exact position on element no.17, *Figure 7.6* (b). The parametric study proves that the modified objective function, Eq. (4.32), with adopted weighing factors, in the SHMUSA-procedure reflects actual damage location and severity with its global minimum.

During the performance of the SHMUSA-procedure, its parameters for optimization problem were designed to achieve the convergence and accuracy of exploration the optimal solution, damage characteristics. The included number of elements in the computations is 60 elements, *Figure 6.1*, of all elements in the FE model, while the damage ratio represented by reduction factor β is considered as a discrete variable with accuracy of 0.01, as listed in Table 7.6. Therefore, the size of the searching space, which represents the total number of all possible solutions in the searching space, is 10000. The termination criteria in this structural model problem are specified by frozen of the system, i.e. temperature less than one degree, and the maximum number of iterations, which is limited to 200, i.e. 4.1 % of the total number of possible solutions in searching space, as listed in Table 7.6.

Table 7.6: Input Parameters in the SHMUSA-procedure for damage detection in the the simply supported overhang beam model

Parameter Description	Parameter Value
Number of Included Elements	60
Range of Damage Reduction Factor β	[0.01 - 0.80]
Size of Searching Space	4800
Max Number of Iterations	200
Percentage (%)	4.1 %
Initial Temperature T_o	20
Temperature Reduction Factor α	0.8
Weighting Factors W_f , W_d	10, 1

On the other hand, There are other designed parameters in the SHMUSA-procedure for SA method, which represents the features of SA optimization method such as the linear relation of cooling schedule included initial temperature T_o and reduction factor α. For this type of simply supported beam model, those parameters are listed in Table 7.6.

In the SHMUSA-procedure and for the simply supported overhang bem model, the objective function, Eq. (4.32), is included the first four modes, $n=4$, natural frequencies and normalized mode shapes in the computations. The number of components of the mode shape vectors included in the computations for this structural model is one, $m=1$. This component is the vertical displacement only in z-axis and the second, transverse displacement in y-axis, and third, longitudinal displacement in x-axis, are neglected according to the adopted mode shapes for this model, as shown in *Figure 6.2*.

After performance of the proposed SHMUSA-procedure to detect damage in the simply supported overhang beam model, the improvements of the objective function during the iterations for both tested damage scenario, DC-1 and DC-2, are shown in *Figure 7.7*. It is evident from *Figure 7.7* (a) and (b) for both damage scenarios, that the SHMUSA-procedure has also high and quick convergence during the iterations for this model which are the most significant features of the applied procedure for damage detection based on optimization metod. The termination criterion for both DC-1 and DC-2 are the max number

of iterations, as shown *Figure 7.7* (a) and (b). The optimal solution in DC-1 was reached after 184 iterations, which exactly corresponds to the actual DC-1, damaged element no. 17 with damage ratio $D_r^* = 0.38$. Whereas, the optimal solution in DC-2 was reached after 179 iterations, which is so-called near-optimal solution of $D_r^* = 0.56$, which is very close to the actual damage ratio with the exact damage position, element no.17, as listed in Table 7.4.

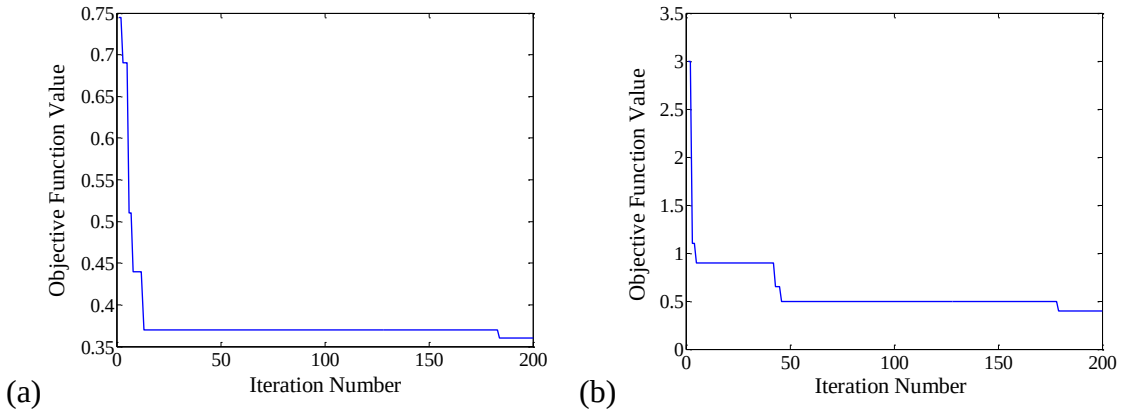

Figure 7.7. Improvement of the adopted objective function used in the SHMUSA-procedure for implemented both damage scenarious (a) for DC-1 and (b) for DC-2

The checked solutions in the searching space during implementation of the SHMUSA-procedure for both damage scenarios, DC-1 and DC-2, are shown in *Figure 7.8*. Figure 7.8 (a) and (b) present the adequate random distribution of randomly selected solution in the SHMUSA-procedure for DC-1 and DC-2, respectively. The red line in the figur specifies the explored optimal solution (i.e. damage characterisitcs, damage location and ratio) by the SHMUSA-procedure. From *Figure 7.8* is evident that the proposed procedure covers the whole searching space, required to explore the global optimal solution and avoid local minimums. The type of configuration of single neighboring solution used in the standard SA method was adopted in the SHMUSA-procedure for this model, as shown in *Figure 7.8*. This type of SA method is adeqaute and effective because the small searching space is included.

High agreement in results, *Figure 7.7* and Figure 7.8, between the implemented damage scenarios and detected damage characteristics, damage location and ratio, by SHMUSA-procedure shows robustness and efficiency of the proposed procedure during the limited number of iterations.

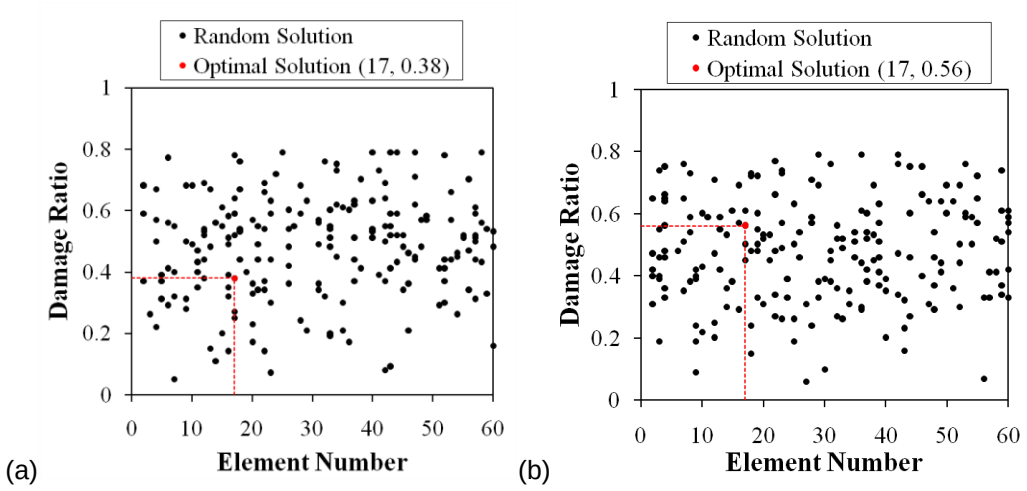

Figure 7.8. Distributions of checked solutions during iterations in the SHMUSA-procedure with global minimal which represents damage charecteristics, damage location D_e^* *and severity* D_r^* *(a) for DC-1 and (b) for DC-2*

7.5. Verification of proposed SHM procedure on grid bridge structural model

Further verification was performed of the SHMUSA-procedure on the second adopted structural model of grid bridge model. In this type of structural model, the structural optimization problem is complex because the large searching space and different structural behviour of the model were included. Different structural loading states of the grid bridge model are adopted, wihtout and with additional masses, as shown in *Figure 5.16*. In addition, the damage size in the implemented damage scenarios is very small comparative with large entire size of the structural model with large number of included elements of the FE model in the computations of the SHMUSA-procedure. The verification of the SHMUSA procedure on the second adopted structural model of grid bridge model is

puplised in paper dealt with this verification of the SHMUSA procedure in the Technical Gazette (Tehnički vjesnik) Journal in 2015 [141].

In this third model, two damage scenarios were implemented with damage characteristics, damage location and severity, as discussed five paragraph 5.2.5 in chapter five. The damage scenarios are at different locations of the FE grid bridge model, *Figure 5.26*, but with the same damage severities, as shown in *Figure 5.27*. Both damage scenarios, DC-1 and DC-2 , have damage severity of 0.4 which means damage ratio, D_r , as listed in table Table 7.7. Also, the weighting factor of the element stiffness in this model is equal one, $\gamma = 1$, because the width of actual damage was the same as the element length of 42 mm, *Figure 6.3*, and the actual damage ratios were computed according to Eq. (7.1). According to the numbering of elements in the FE grid bridge model, the location of the damage in the DC-1 is at element no. 54 which is located at 2247 mm c/c from support at left side and in the DC-2 is at element no. 200 which is located at 1659 mm c/c from support at right side, as shown in *Figure 5.26* and *Figure 6.3*.

Table 7.7: Implemented damage scenarios on the simply supported grid bridge model

Description	Damage Scenario-1 (DC-1)	Damage Scenario-2 (DC-2)
Damage Location D_r (Damaged Element Number)	54	200
Damage Severity D_e	0.4	0.4

The verification of the SHMUSA-procedure was performed on both states of grid bridge model, without and with additional masses, its parameters for optimization problem were designed to achieve the convergence and accuracy of exploration the optimal solution, damage characteristics. The included number of elements are 320, *Figure 6.3*, with damage ratio accuracy of 0.01, as listed in Table 7.8. Therefore, the size of the searching space, which represents the total number of all possible solutions in the searching space, is 31680. The termination criteria in this structural model problem are specified by frozen of the system, i.e. temperature less than one degree, $T < 1$, and the maximum number of

iterations, which is limited to 1000, i.e. 3.2 % of the total number of possible solutions in searching space, as listed in Table 7.8.

Table 7.8: Input Parameters in the SHMUSA-procedure for damage detection in the the simply supported grid bridge model

Parameter Description	Parameter Value
Number of Included Elements	320
Range of Damage Reduction Factor β	[0.01 - 0.99]
Size of Searching Space	31680
Max Number of Iterations	1000
Percentage (%)	3.2 %
Initial Temperature T_o	20
Temperature Reduction Factor α	0.8
Weighting Factors W_f , W_d	10, 1

On the other hand, There are other designed parameters in the SHMUSA-procedure for SA method, which represents the features of SA optimization method such as the linear relation of cooling schedule included initial temperature T_o and reduction factor α. For this type of simply supported beam model, those parameters are listed in Table 7.6.

In the SHMUSA-procedure and for the simply supported grid bridge model, the adopted objective function is included the first five modes, $n=5$, natural frequencies and normalized mode shapes in the computations. The number of components of the mode shape vectors included in the computations for this structural model is two, $m=2$. The first component is the vertical displacement in z-axis and the second one is transverse displacement in y-axis, while the third component, longitudinal displacement in x-axis, is neglected according to the adopted mode shapes for this model, as shown in *Figure 6.4*.

Because of the complexity of this structural model with two loading states without and with additional masses, numerical investigation was conducted to examine the efficiency of adopted objective function, Eq. (4.32) in the SHMUSA-procedure, with most suitable weighting factor values and different severities of damage.

7.5.1. For the state of the model without additional masses

Firstly, the study was carried out numerical testing of the adopted objective function for both adopted damage scenarios of DC-1 and DC-2 of the FE model state without additional masses, with varying damage ratio D_r in the range of [0.1, 0.6] and positions of the damage along the main beams. The first part of the objective function, Eq. (4.32), used in the SHMUSA-procedure for this grid bridge model is adopted square direct difference in the modal frequencies instead of the realtive difference. The numerical simulation of the adopted objective function used in the SHMUSA-procedure for this bridge model of both damage scenarios, DC-1 and DC-2, is shown in *Figure 7.9* shows. The global minimum of the objective function is achieved for damage ratio $D_r = 0.4$ and at the exact damage position in DC-1, element no. 54, with more local minimums, as shown in *Figure 7.9* (a). Whereas, the global minimum of the objective function is achieved for damage ratio $D_r = 0.4$ and at the exact damage position also in DC-2, element no. 200, with more local minimums, as shown in *Figure 7.9* (b). The study testifies that the modified objective function Eq. (4.32), with adopted weighing factors, used in the SHMUSA-procedure reflects actual damage location and severity with its global minimum.

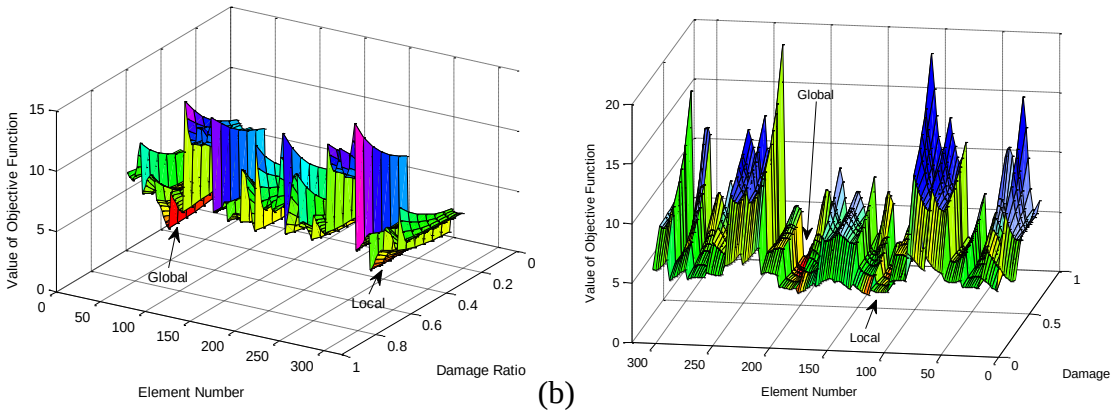

Figure 7.9. Numerical simulatation testing of the adopted objective function with $W_f = 10$ and $W_d = 1$ *used in the SHMUSA-procedure for the FE grid bridge model state without additional masses with global and local minimums (a) for DC-1 and (b) for DC-2*

The improvement of the optimal solution detected by the SHMUSA-procedure during iterations for the first studied damage scenario, DC-1, of damaged model state without additional mass is shown in *Figure 7.10* (a). The system energy of the acceptance propability in SA method, boltzmman mechine in Eq. (4.20), in the SHMUSA-procedure during improving the optimal solution is shown *Figure 7.10* (b). Figure 7.10 (b) shows the accepted current solutions during the iterations when the cooling schedule decrease the temerature of the system and the acceptance probability is more restricted, as discussed in paragraph 4.5.2. A very quick improvement of the optimal solution, *Figure 7.10* (a), and convergence during the SHMUSA-procedure can be observed, without achieving the prescribed maximum number of iterations. Also, the appropriate values of designed parameters of the SHMUSA-procedure is verified by the explaination of the final results in *Figure 7.10* (b). The optimum solution was reached after *839* iterations (with percentage 2.7 % of whole search space). That means the frozen state of the system controled the termination criteria instead of the max number of iterations, as shown *Figure 7.10* (a).

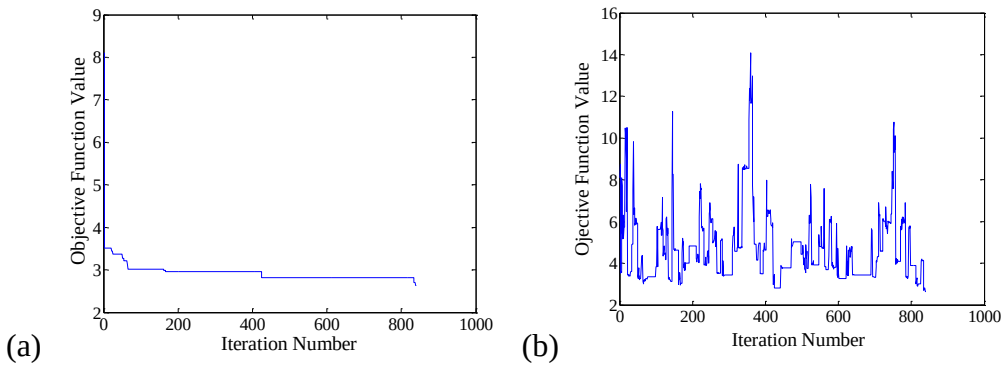

Figure 7.10. Improvement of the objective function global minimum estimation during the SHMUSA-procedure for the studied DC-1 for the grid bridge mode state without additional masses (a) improvement of the optimal solution (b) system energy of accepted solutions

In this grid bridge model and for the state without additional masses, the second type of ordinary simulated annealing (OSA), as discussed in paragraph 4.5.4.2, was applied in the SHMUSA-procedure for damage detection. Herein, the generated new solution from the neighborhood is consists a set of solutions adopted 6-solution, $N^T = 6$. The generation process is by generating randomly one new neighboring solution, then six new solutions are generated from the first random solution using normal distribution. The total new generated solutions will be 7-solution and this configuration is defined as a set of solutions, as shown in *Figure 7.11* (a).

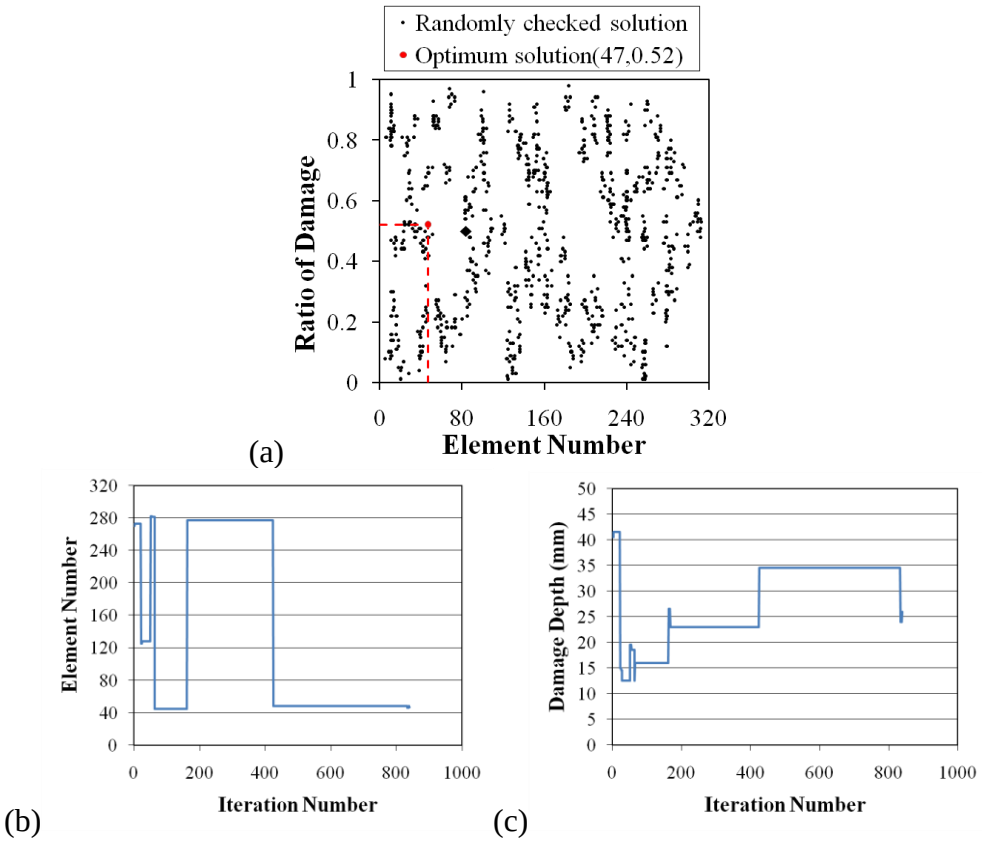

Figure 7.11. Checked solutions during iterations in the SHMUSA-procedure with global improvement of minimal solution of damage charecteristics for DC-1 of the grid bridge model state without additional masses (a) distribution of checked solution (b) improvement of damage location and (c) improvement of damage severity

It closely corresponds to the actual damage characteristics implemented in DC-1. The SHMUSA-procedure detected position of damage on element $D_e^* = 47$ with damage ratio of $D_r^* = 0.52$, *Figure 7.11* (i.e. damage crack =26 mm), while the actual damage parameters are $D_e = 54$ and $D_r = 0.40$ (i.e. damage crack =20 mm), as shown in *Figure 7.11*. Generated solutions in the search space, *Figure 7.11* (a), show that the SHMUSA-procedure covers the whole search space to avoid local minimums and explore the global optimum solution. A small percentage of the total number of solutions was checked, just a 2.7 % of the total number of possible solutions. It is concluded that for complex structural model, the OSA is more effective and efficincy than standard simulated annealing (SSA) used for simple structural model.

The improvement of the optimal solution which represents damage characteristics, damage location and damage severity, during iterations of performance the SHMUSA-procedure are shown in *Figure 7.11* (b) and (c). Figure 7.11 (b) shows the improvement of the first parameter of the damage which is the damage location represented by the number of damaged element during the iterations, detected no. 47 of damaged element. While, the *Figure 7.11* (c) shows the improvement of the second parameter of the damage which is the damage severity represented by damage ratio during the iterations, detected damage ratio of 0.52 (i.e. damage depth of 26 mm)

The performance the proposed SHMUSA-procedure for the second damage scenario, DC-2, exhibits quick convergence, as shown in *Figure 7.12* (a). The system energy of the acceptance propability, Eq. (4.20), in the SHMUSA-procedure during improving the optimal solution is shown *Figure 7.12* (b). Figure 7.12 (b) shows the accepted current solutions during the iterations during the cooling schedule decrease the temerature of the system and also verifies the ability of the proposed procedure to detect damage wirh suitable designed parameters. The optimal solution, damage characteristics, was reached after 819 iterations (the number of checked solutions), which represents 2.6 % of the total possible solutions.

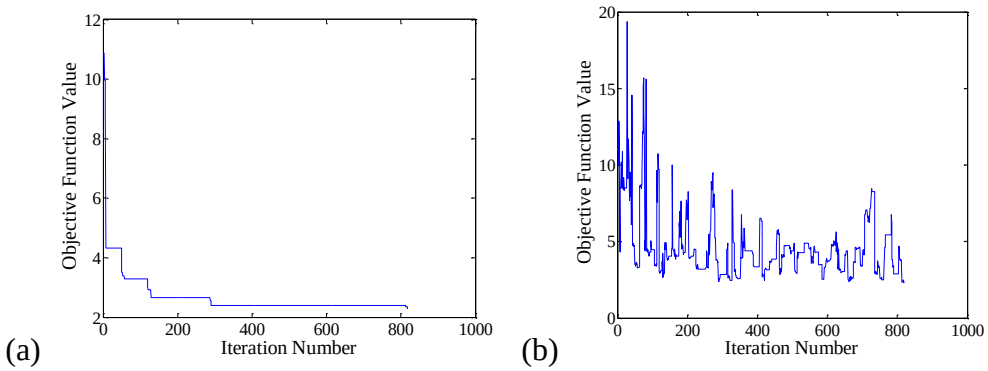

Figure 7.12. Improvement of the objective function global minimum estimation during the SHMUSA-procedure for the studied DC-2 for the grid bridge mode state without additional masses (a) improvement of the optimal solution (b) system energy of accepted solutions

In this case, the procedure detected very close position of damage on element $D_e^* = 201$ with the damage ratio of $D_r^* = 0.47$ (i.e. damage crack =23.5 mm), *Figure 7.13*. The optimum solution is very close to the actual damage scenario DC-2, represented by damage parameters $D_e = 200$ and $D_r = 0.40$ (i.e. damage crack depth of 20 mm), Table 7.7.As in the previous case, the search solutions are also randomly distributed throughout the whole search space, *Figure 7.13* (a).

The improvement of the optimal solution which represents damage characteristics, damage location and damage severity, during iterations of performance the SHMUSA-procedure are shown in *Figure 7.13*. Figure 7.13 (b) shows the improvement of the first parameter of the damage which is the damage location represented by the number of damaged element during the iterations, detected no. 201 of damaged element. While, the *Figure 7.13* (c) shows the improvement of the second parameter of the damage which is the damage severity represented by damage ratio during the iterations, detected damage ratio of 0.47 (i.e. damage depth of 23.5 mm).

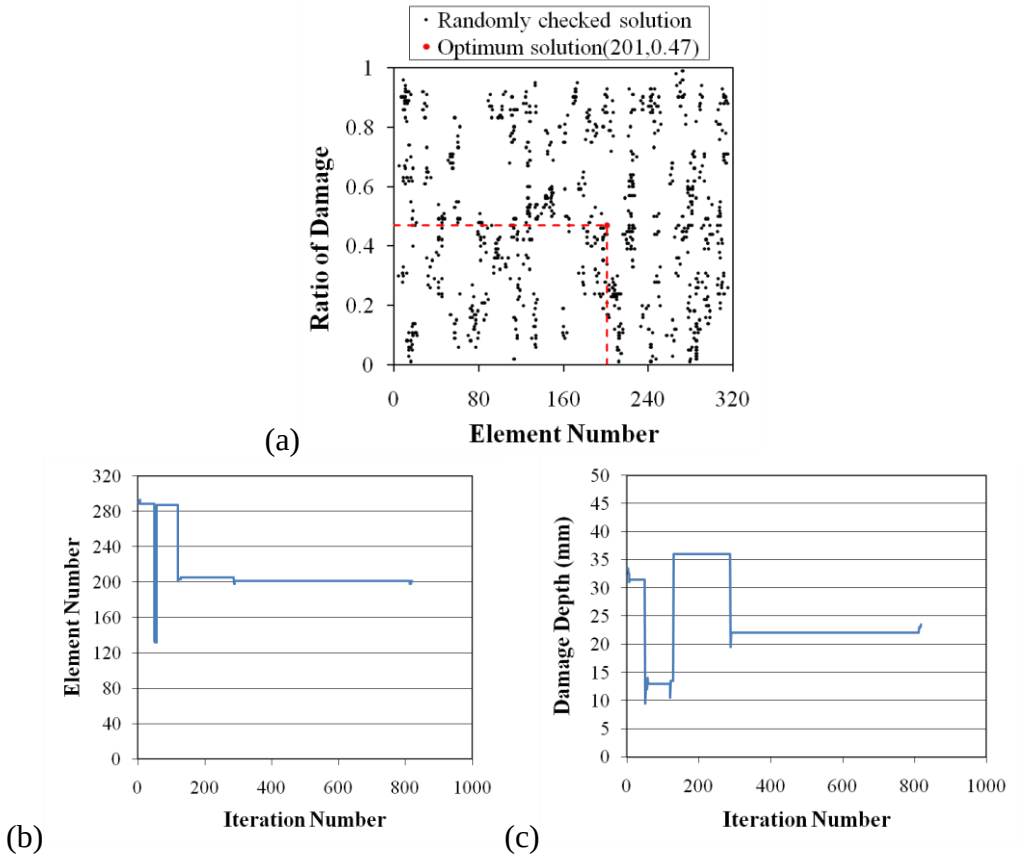

Figure 7.13. Checked solutions during iterations in the SHMUSA-procedure with global improvement of minimal solution of damage charecteristics for DC-2 of the grid bridge model state without additional masses (a) distribution of checked solution (b) improvement of damage location and (c) improvement of damage severity

Excellent and very satisfactory agreement between the implemented scenarios and estimated damage locations and damage ratios, exhibits the robustness and reliability of the proposed SHMUSA-procedure for damage detection in this type of structure. Based on the accuracy of the results, the proposed SHMUSA-procedure is very efficient to detect damage in complex structures, even with minor differences in modal properties between the intact and damage state.

7.5.2. For the state of the model with additional masses

For model state with additional masses the study was carried out test for the adopted objective function with its parameters, $W_f = 10$ and $W_d = 1$, only for adopted damage scenario of DC-2 with varying the damage ratio D_r in the range of [0.3, 0.7] and positions of the damage along the beam. The same form of the square direct difference in the modal frequencies of the first part in the objective function was adopted in this state of the grid bridge model. The numerical simulation of the objective function used in the SHMUSA-procedure is performed for damage scenario of DC-2 to check the ability of adopted form for this loading state with additional masses of the model, as shown in *Figure 7.14*. The figure shows objective function change during the implementation of different locations and severities of damage. For the DC-2, the SHMUSA-procedure detected the global miminum with damage ratio of 0.4 the exact damage location at element no. 200, as shown in *Figure 7.14*. The study testifies that the modified objective function with adopted weighing factors reflects actual damage location and severity with its global minimum.

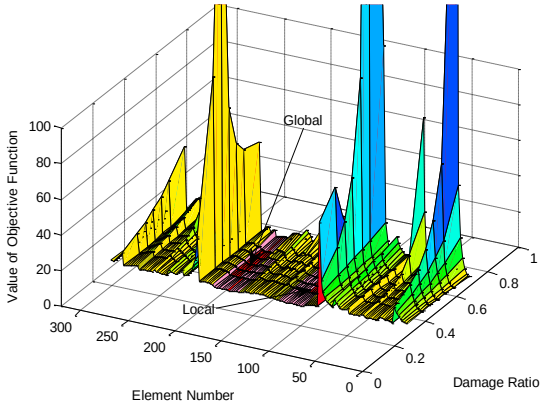

Figure 7.14. Numerical simulatation testing of the adopted objective function with $W_f = 10$ and $W_d = 1$ *used in the SHMUSA-procedure for the FE grid bridge model state with additional masses with global and local minimums for DC-2*

For the loading state with additional masses, the verification of the SHMUSA-procedure is performed only for the second damage scenario, DC-2. The improvement of the objective function during damage detection (via SHMUSA-procedure) for the studied damage scenario of DC-2 of damaged model with additional mass is shown in *Figure 7.15*

(a). Figure 7.15 (b) shows the accepted current solutions during the iterations during the cooling schedule decrease the temerature of the system and also verifies the ability of the proposed procedure to detect damage wirh suitable designed parameters. A small percentage of the total number of solutions was checked, just a 3.2 % of the total number of possible solutions.

A very quick improvement of the optimal solution approximation, *Figure 7.15* (a), and convergence during SA optimization can be observed, without achieving the prescribed maximum number of iterations.

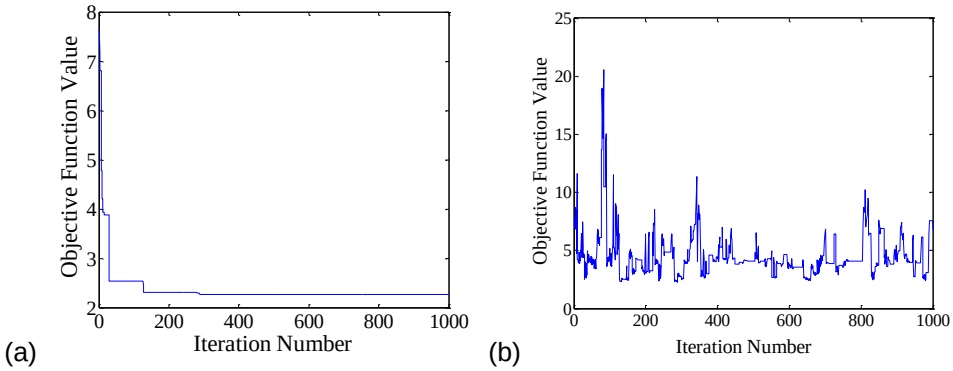

Figure 7.15. Improvement of the objective function global minimum estimation during the SHMUSA-procedure for the studied DC-2 for the grid bridge mode state with additional masses (a) improvement of the optimal solution (b) system energy of accepted solutions

Generated solutions in the search space, *Figure 7.16* (a) show that the SHMUSA-procedure covers the whole search space to avoid local minimums and explore the global optimum solution. Distribution of checked solutions during the process in the search space is shown in *Figure 7.16* (a). It is evident from *Figure 7.16* (a) that in this state of the model, also the second type of ordinary simulate annealing (OSA) was applied in the SHMUSA-procedure for damage detection. Herein, the generated new solution from the neighborhood is consists of different configuration of a set of solutions adopted 8-solution, $N^T = 8$,. The generation process is by generating randomly one new neighboring solution, then eight new solutions are generated from the first random solution using normal distribution. The total

new generated solutions will be 9-solution and this configuration is defined as a set of solutions, as shown in *Figure 7.16* (a). It is concluded that for complex structural model, the OSA is more effective and efficincy than standard simulated annealing (SSA) used for simple structural model.

The improvement of the damage characteristics, location damaged element and damage severity, are shown in *Figure 7.16*. The SHMUSA-procedure detected the optimal solution exactly corresponds to the actual parameters of damage produced in DC-2. The detected location of damage at element no. 200, *Figure 7.16* (b), with damage ratio of 0.5 (i.e. damage depth of 25mm), *Figure 7.16* (c), while the actual damage parameters are element no. 200 and damage ratio of 0.4 (i.e. damage crack =20 mm).

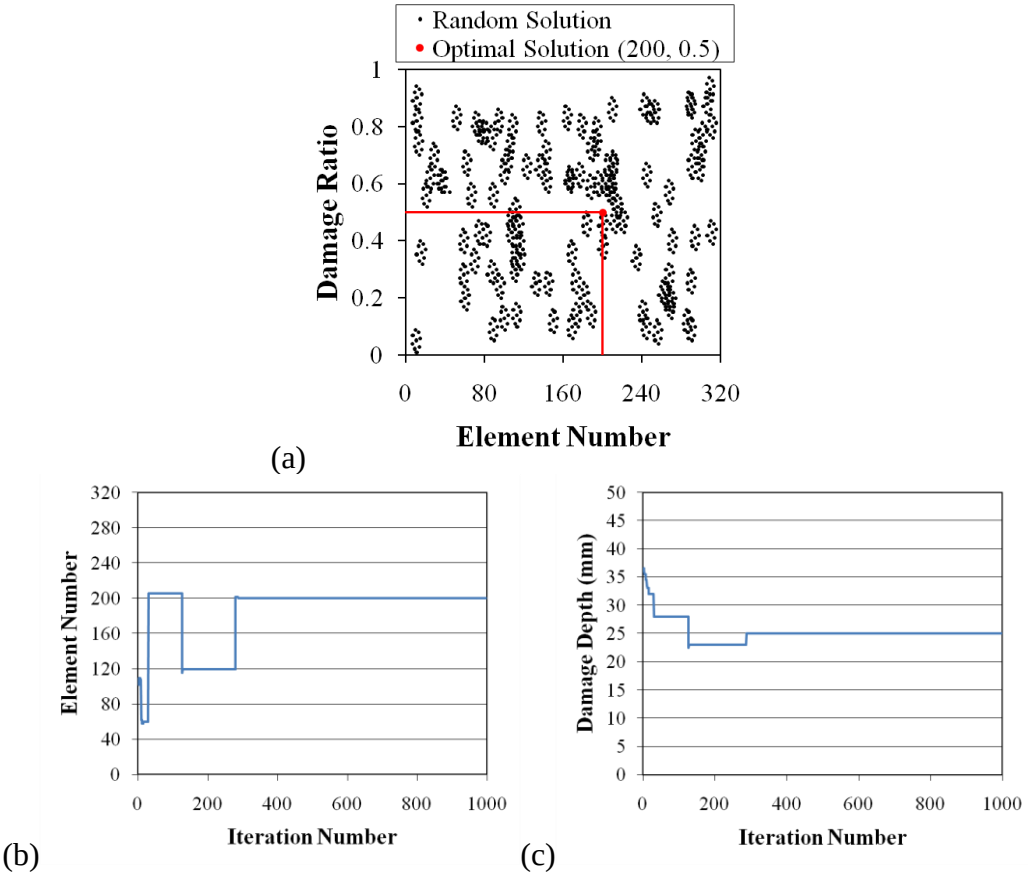

Figure 7.16. Checked solutions during iterations in the SHMUSA-procedure with global improvement of minimal solution of damage charecteristics for DC-2 of the grid

bridge model state with additional masses (a) distribution of checked solution (b) improvement of damage location and (c) improvement of damage severity

Excellent and very satisfactory agreement between the implemented scenarios and estimated damage locations and damage ratios, exhibits the robustness and reliability of the proposed SHMUSA-procedure for damage detection in this complex structure of grid bridge model. particularly, the application of the second type of the OSA method in the SHMUSA-procedure with different configurations. Based on the accuracy of the results, the proposed SHMUSA-procedure is very efficient to detect damage in complex structures, even with minor differences in modal properties between the intact and damage state.

7.6. Verification of proposed SHM procedure on Vierendeel bridge structural model

The verification of SHMUSA procedure on the third adopted Vierendeel bridge structural mode was made based on the changing in modal properties, natural frequency and mode shape It was studied to verify the high sensitivity of the SHMUSA-procedure to the presence of damage in column and beam of the model. For this adopted structural model, paper was submitted for Iranian Journal of Science and Technology-Transactions of Civil Engineering, publishing in Springer [143]. In this type of structural model, the structural optimization problem is more complex because the very large searching space and different structural behviour of the model were included with beams and columns. Different structural loading states of the Vierendeel bridge model are adopted, wihtout and with additional masses, as shown in *Figure 5.31*. In addition, the damage size in the implemented damage scenarios is so small comparative with large entire size of the structural model with very large number of included elements of the FE model in the computations of the SHMUSA-procedure.

In this fourth model, two damage scenarios were implemented with damage characteristics, damage location and severity, as discussed in paragraph 5.2.5 in chapter five. The damage scenarios are at different locations, beam and column, of the Vierendeel bridge model, *Figure 5.42*, with the different damage severities, as shown in *Figure 5.43*.

The damage scenario of DC-1 has damage severity of 0.4 which means damage ratio, D_r, as listed in table Table 7.9. While, the damage scenario of DC-2 has damage section of tapered section of 5 mm from upper and 57 mm from lower side, as shown in *Figure 5.43*. Therefore, the eqiuvalent rectangular section was adopted to compensate the tapered section, as mention in paragraph 6.6.1, and eqiuvalent damage ratio is assumed. The damage ratio in this model was calculated according to Eq. (7.1) and the weighting factor of the element stiffness in this model is equal one, $\gamma = 1$, because the length of actual damage was the same as the element length of 42 mm for beam and 54.8 mm for column, *Figure 6.5*. According to the numbering of elements in the FE Vierendeel bridge model, the location of the damage in the DC-1 is at beam element no. 291 which is located at 483 mm c/c from support at left side in the upper main beam (i.e. at left fence) , as listed in table Table 7.9. The damage location in the DC-2 is at column element no. 651 (or 1251 if all elemnts of FE model are included) which is located at 1364 mm c/c from support at the same left side, as shown in *Figure 5.42* and *Figure 6.5*.

Table 7.9: Implemented damage scenarios on the simply supported Vierendeel bridge model

Description	Damage Scenario-1 (DC-1)	Damage Scenario-2 (DC-2)
Damage Location D_e (Damaged Element Number)	291	651 or 1251
Damage Severity D_r	0.4	Equivalent

The verification of the SHMUSA-procedure was performed on both states of Vierendeel bridge model, without and with additional masses. The parameters of the SHMUSA-procedure for optimization problem were designed to achieve the convergence and accuracy of exploration the optimal solution, damage characteristics. The included number of elements are 794, *Figure 6.5*, with damage ratio accuracy of 0.01, as listed in Table 7.10. The number of 794-element is distributed as 640-element for the main upper and lower beams (i.e. 160-element for each main beam of 4-beam) and 154-element for columns of both left and right fences of the bridge model (i.e. 7-element for each column of

22-column), as shown in *Figure 6.5*. Therefore, the size of the searching space, which represents the total number of all possible solutions in the searching space, is 71460 solutions. The termination criteria in this structural model problem are specified by frozen of the system, i.e. temperature less than one degree, $T < 1$, and the maximum number of iterations, which wass limited to 1000, i.e. 1.4 % of the total number of possible solutions in searching space, as listed in Table 7.10.

Table 7.10: Input Parameters in the SHMUSA-procedure for damage detection in the the simply supported Vierendeel bridge model

Parameter Description	Parameter Value
Number of Included Elements	794
Range of Damage Reduction Factor β	[0.01 - 0.90]
Size of Searching Space	71460
Max Number of Iterations	1000
Percentage (%)	1.4 %
Initial Temperature T_o	20
Temperature Reduction Factor α	0.8
Weighting Factors W_f , W_d	Without Masses = 10, 1 With Masses = 100, 1

On the other hand, There are other designed parameters in the SHMUSA-procedure for SA method, which represents the features of SA optimization method such as the linear relation of cooling schedule included initial temperature T_o and reduction factor, α. For this type of simply supported bridge model, those parameters are listed in Table 7.10.

In the SHMUSA-procedure and for the simply supported Vierendeel bridge model, the adopted objective function, Eq. (4.32), includes the first four modes, $n = 4$, natural frequencies and normalized mode shapes in the computations. The number of components of the mode shape vectors included in the computations for this structural model is two, $m = 2$. The first component is the vertical displacement in z-axis and the second one is transverse displacement in y-axis, while the third component, longitudinal displacement in

x-axis, was neglected according to the adopted mode shapes for this model, as shown in *Figure 6.6*.

Because of the high complexity of this structural model with two loading states, without and with additional masses, numerical investigation was conducted to examine the efficiency of adopted objective function, Eq. (4.32), used in the SHMUSA-procedure, with most suitable weighting factor values and different severities of damage.

7.6.1. For the state of the model without additional masses

Firstly, the numerical test of the adopted objective function, Eq. (4.32), for adopted damage scenario of DC-2 only of the FE model state without additional masses was carried out. The study adopted damage depth in equivalent section of column of 4 mm and it is very small compared with equivalent cross section of stiffener part of column of (110x30) mm, as mention in paragraph 6.6.1, and varied locations of the damage along the main upper and lower beams and all columns. The numerical test of the adopted objective function, Eq. (4.32), used in the SHMUSA-procedure with adopted weighting factor of $W_f = 10$ *and* $W_d = 1$, for this bridge model state implemented for damage scenario DC-2, was shown in *Figure 7.17.* The global minimum of the objective function is achieved at very close to the exact damage location in DC-2 at element no. 651, even with more local minima, as shown in *Figure 7.17*. The study testifies that the modified objective function Eq. (4.32), with adopted weighing factors, used in the SHMUSA-procedure reflects actual damage location and severity with its global minimum. It is evident from figure that the differences in mode shape vectors only has significant effect to detect optimal minimum, damage characteristics, close to exact location, element no. 651, as shown in *Figure 7.17 (b)*, while there are more local minima for only natural frequencies differences, as shown *Figure 7.17 (a).* The detected damage location is obvoius from *Figure 7.17 (c)* for the explored damage location when both parts of objective function is participated with their adopted weighting factors values. The study testifies that the modified objective function with adopted weighing factors reflects actual damage location and severity with its global minimum.

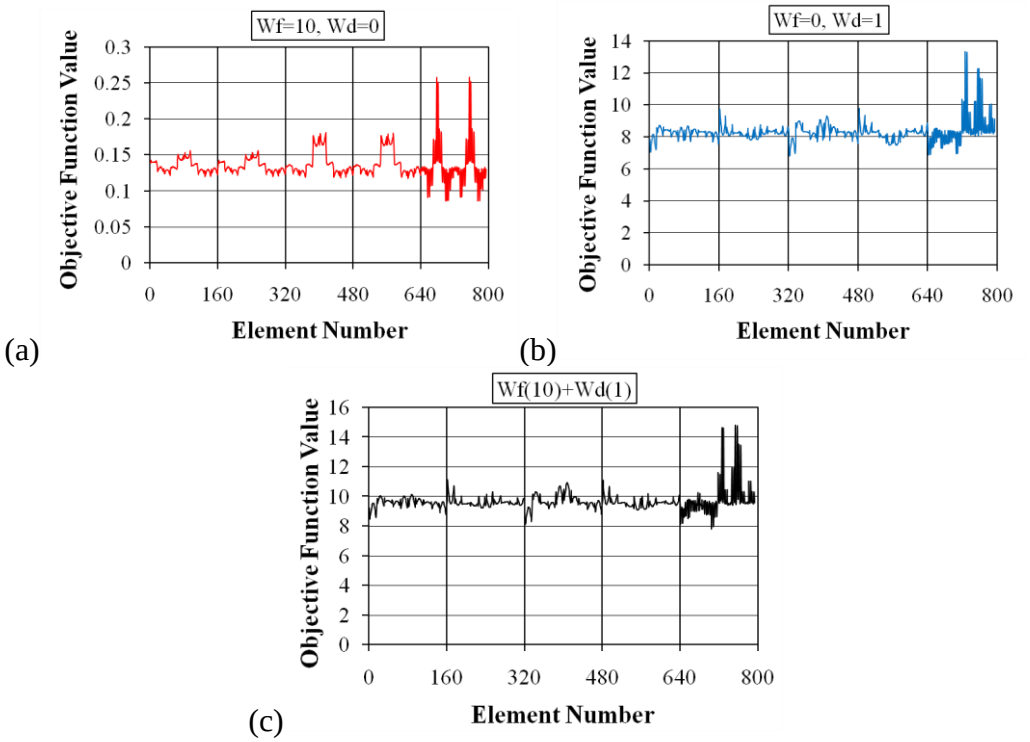

Figure 7.17. Numerical rest of adopted objective function with $W_f = 10$ and $W_d = 1$ used the SHMUSA-procedyre application for DC-2 of Vierendeel Bridge model state without additional masses with global and local minimums

The improvement of the optimal solution detected by the SHMUSA-procedure during iterations for the first studied damage scenario, DC-1, of damaged model state without additional mass is shown in *Figure 7.18* (a). The system energy of the acceptance propability in SA method, boltzmman mechine in Eq. (4.20), in the SHMUSA-procedure during improving the optimal solution is shown *Figure 7.18* (b). Figure 7.18 (b) shows the accepted current solutions during the iterations when the cooling schedule decrease the temerature of the system and the acceptance probability is more restricted. A very quick improvement of the optimal solution, *Figure 7.18* (a), and convergence during the SHMUSA-procedure can be observed, with achieving the specified maximum number of iterations of 1000. The optimum solution was reached after 221 iterations (with percentage 0.31 % of whole searching space). That means for this state of the Vierendeel bridge model,

the max number of iterations controled the termination criteria instead of the system frozen, as shown *Figure 7.18* (a).

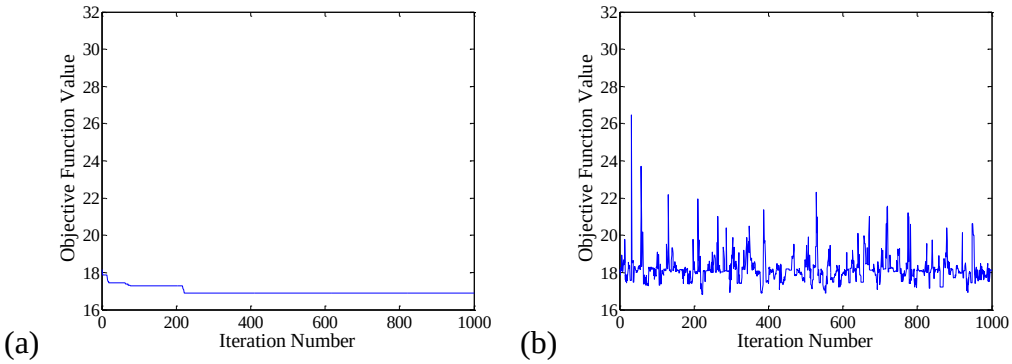

Figure 7.18. Improvement of the objective function global minimum estimation during the SHMUSA-procedure for the studied DC-1 for the Vierendeel bridge mode state without additional masses (a) improvement of the optimal solution (b) system energy of accepted solutions

According to the actual damage characteristics implemented in DC-1, th SHMUSA-procedure detected damage location exactly on element no. 291, $D_e^* = 291$, with small error in damage ratio of 0.59, $D_r^* = 0.59$, *Figure 7.19* (i.e. damage depth =29.5 mm), while the actual damage characteristics are $D_e = 291$ and $D_r = 0.40$ (i.e. damage crack =20 mm). Herein, also the generated new solution from the neighborhood consists different configuration of a set of solutions adopted 6-solution, $N^T = 6$, of the OSA method. The six new solutions are generated from the first random solution using normal distribution. The total new generated solutions will be 7-solution and this configuration is defined as a set of solutions, as shown in *Figure 7.19* (a). The distributions of generated solutions in the search space, *Figure 7.19* (a), show that the SHMUSA-procedure covers the whole search space to avoid local minimums and explore the global optimum solution.

The improvement of the optimal solution which represents damage characteristics, damage location and damage severity, during iterations of performance the SHMUSA-procedure are shown in *Figure 7.19* (b) and (c). Figure 7.19 (b) shows the improvement of

the first parameter of the damage which is the damage location represented by the number of damaged element during the iterations, detected no. 291 of damaged element. While, the *Figure 7.19* (c) shows the improvement of the second parameter of the damage which is the damage severity represented by damage depth during the iterations, detected damage ratio of 0.59 (i.e. damage depth of 29.5 mm).

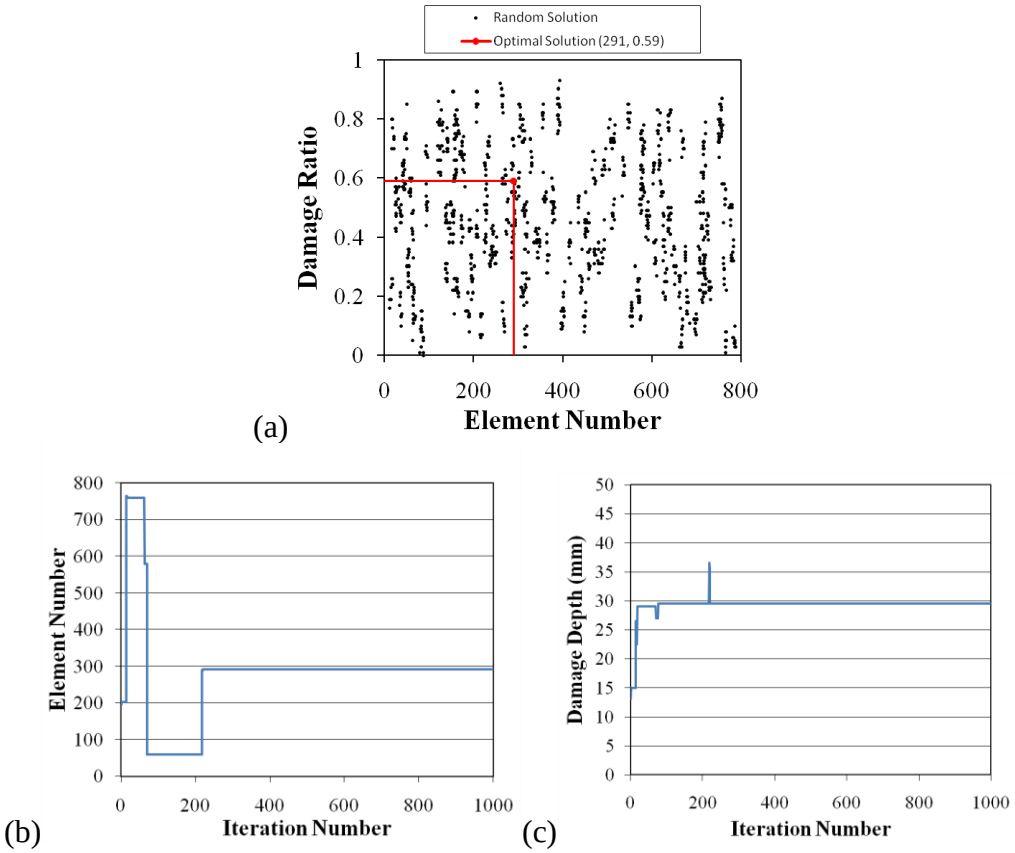

Figure 7.19. Checked solutions during iterations in the SHMUSA-procedure with global improvement of minimal solution of damage charecteristics for DC-1 of the Vierendeel bridge model state without additional masses (a) distribution of checked solution (b) improvement of damage location and (c) improvement of damage severity

For the damage scenario of DC-2, the improvement of the optimal solution detected by the SHMUSA-procedure during iterations for the damaged model state without additional mass is shown in *Figure 7.20* (a). The acceptance propability energy in the system of SA method, Eq. (4.20), used in the SHMUSA-procedure during improving the

optimal solution is shown *Figure 7.20* (b). Figure 7.20 (b) shows the accepted current solutions during the iterations when the cooling schedule decrease the temerature of the system and the acceptance probability is decreased with decreasing system temperature. A very quick improvement of the optimal solution, *Figure 7.20* (a), and convergence during the SHMUSA-procedure can be noted, with achieving the specified maximum number of iterations of 1000. The optimum solution was reached after 872 iterations (with percentage 1.22 % of whole searching space). That means for this state of the Vierendeel bridge model, the max number of iterations controled the termination criteria instead of the system frozen, as shown *Figure 7.20* (a).

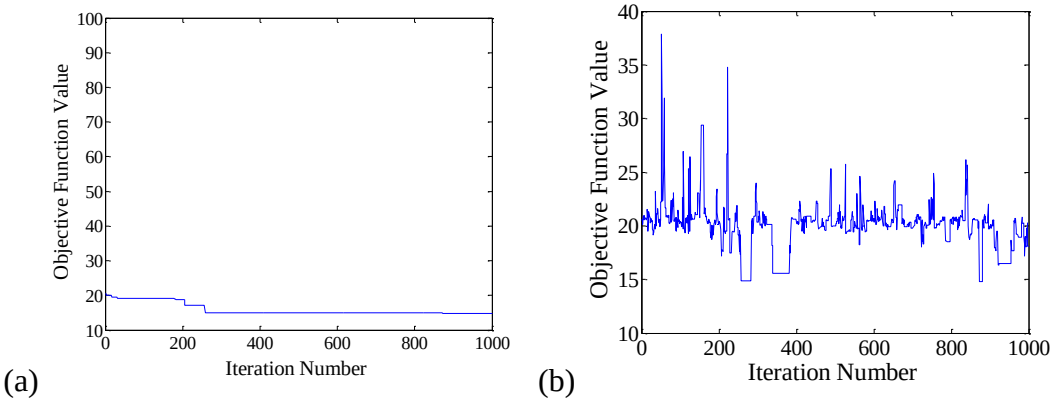

Figure 7.20. Improvement of the objective function global minimum estimation during the SHMUSA-procedure for the studied DC-2 for the Vierendeel bridge mode state without additional masses (a) improvement of the optimal solution (b) system energy of accepted solutions

According to the actual damage characteristics implemented in DC-2, th SHMUSA-procedure detected damage location on element no. 1259 (corresponding to element no. 659 if only the included elements of FE model are adopted in computations), $D_e^* = 1259$, with damage ratio of 0.37, $D_r^* = 0.37$ (i.e. damage depth of 16.4 mm), *Figure 7.21* (here the equivalent damage depth was assumed based on the total cross section depth of 40 mm), while the actual damage characteristics are $D_e = 1251$. In this case study, there is small

error between the implemented damage location and the detected location. Also, the generated new solution from the neighborhood consists of a set of solutions adopted 6-solution, $N^T = 6$, of the OSA method. The six new solutions are generated from the first random solution using normal distribution. The total new generated solutions will be 7-solution and this configuration is defined as a set of solutions, as shown in *Figure 7.21* (a).

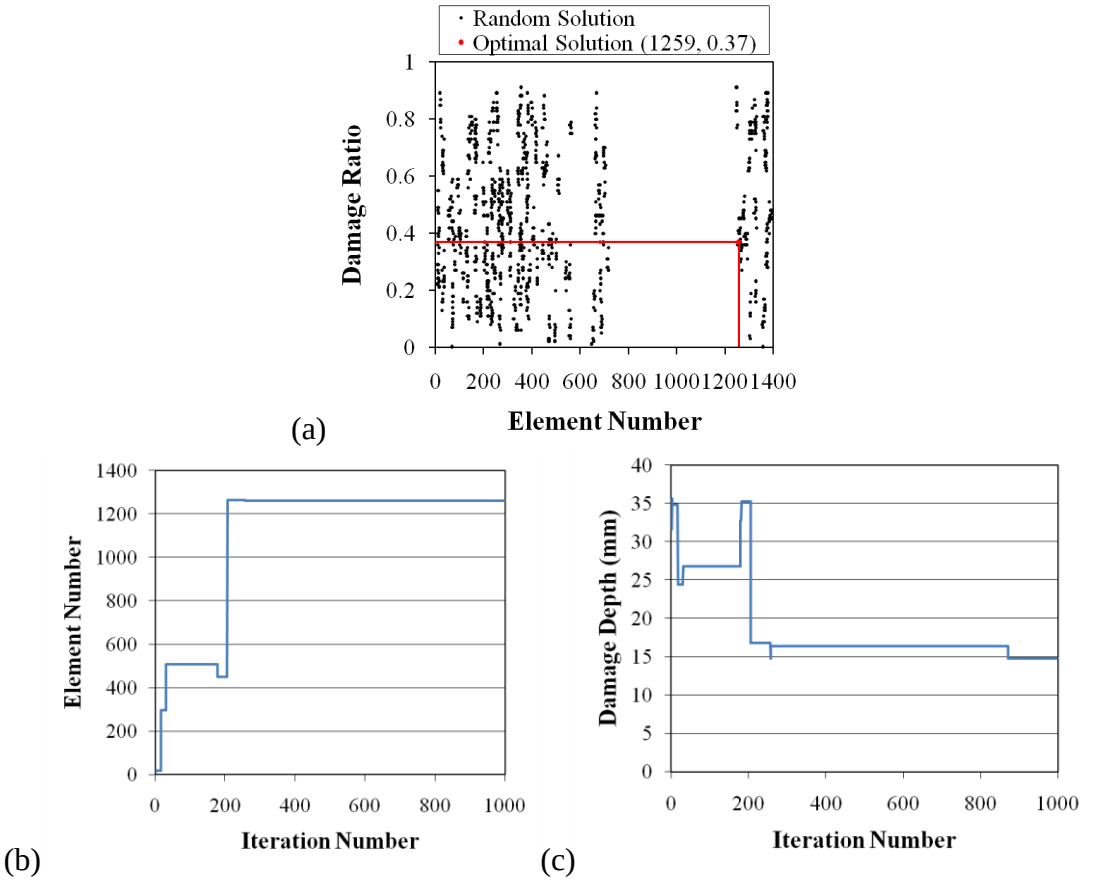

Figure 7.21. Checked solutions during iterations in the SHMUSA-procedure with global improvement of minimal solution of damage charecteristics for DC-2 of the Vierendeel bridge model state without additional masses (a) distribution of checked solution (b) improvement of damage location and (c) improvement of damage severity

The distributions of checked solutions in the search space has a gap, *Figure 7.21* (a), this gap is due to the sequence of the included elements in the computations of damage detection in the SHMUSA-procedure, as discussed before. Figure 7.21 (a) show that the

SHMUSA-procedure covers the whole search space to avoid local minimums and explore the global optimum solution close to the exact implemented. The improvement of the optimal solution which represents damage characteristics, damage location and damage severity, during iterations of performance the SHMUSA-procedure are shown in *Figure 7.21* (b) and (c). Figure 7.21 (b) shows the improvement of the first parameter of the damage which is the damage location represented by the number of damaged element during the iterations, detected no. 1259 of damaged element. While, the *Figure 7.21* (c) shows the improvement of the second parameter of the damage which is the damage severity represented by damage depth during the iterations, detected damage ratio of 0.37 (i.e. damage depth of 16.4 mm).

Good and very satisfactory agreement between the implemented scenarios and estimated damage locations and damage ratios, exhibits the robustness and reliability of the proposed procedure using SA optimization for damage detection in structures. Based on the accuracy of the results, the proposed procedure is very efficient to detect damage in complex structures.

7.6.2. For the state of the model with additional masses

For the model state with additional masses, the numerical test of the adopted objective function, Eq. (4.32), for adopted damage scenario of DC-2 only of the FE model was carried out. The study adopted the same damage depth in equivalent section of column of $4\,\text{mm}$ in the previous study for model state witjout additional masses and varied locations of the damage along the main upper and lower beams and all columns. The numerical test of the adopted objective function, Eq. (4.32), used in the SHMUSA-procedure with adopted weighting factor of $W_f = 100$ *and* $W_d = 1$, for this bridge model state implemented for damage scenario DC-2, was shown in *Figure 7.22.* The global minimum of the objective function is achieved at exact damage location in DC-2 at element no. 651, even with more local minima, as shown in *Figure 7.22*. The study testifies that the modified objective function Eq. (4.32), with adopted weighing factors, used in the SHMUSA-procedure reflects actual damage location and severity with its global minimum.

It is evident from *Figure 7.22* that the differences in mode shape vectors only has significant effect to detect optimal minimum, damage characteristics, exact location, element no. 651, as shown in *Figure 7.22 (b)*, while there are more local minima for only natural frequencies differences, as shown *Figure 7.22 (a).* The detected damage location is obvoius from *Figure 7.22 (c)* for the explored damage location when both parts of objective function is participated with their adopted weighting factors values.

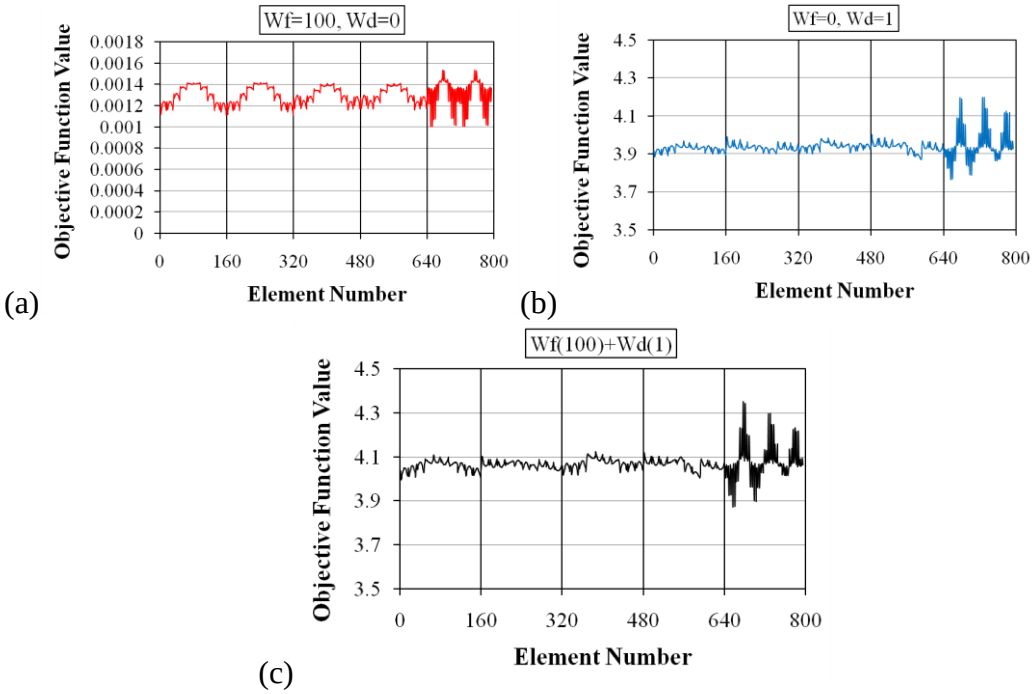

Figure 7.22. Numerical rest of adopted objective function with $W_f = 100$ and $W_d = 1$ used the SHMUSA-procedyre application for DC-2 of Vierendeel Bridge model state with additional masses with global and local minimums

The study testifies that the objective function with adopted weighing factors reflects actual damage location and severity with its global minimum.

The improvement of the optimal solution detected by the SHMUSA-procedure during iterations for the first studied damage scenario, DC-1, of damaged model state with additional mass is shown in *Figure 7.23* (a). The system energy of the acceptance propability in SA method in Eq. (4.20), in the SHMUSA-procedure during improving the

optimal solution is shown *Figure 7.23* (b). Figure 7.23 (b) shows the accepted current solutions during the iterations when the cooling schedule decrease the temerature of the system and the acceptance probability decreased with decreasing system temerature. A very quick improvement of the optimal solution, *Figure 7.23* (a), and convergence during the SHMUSA-procedure can be seen, with achieving the limited maximum number of iterations of 1000. The optimum solution was reached after 159 iterations (with percentage 0.22 % of whole searching space) and the max number of iterations controled the termination criteria for this state of the Vierendeel bridge model, as shown *Figure 7.23* (a).

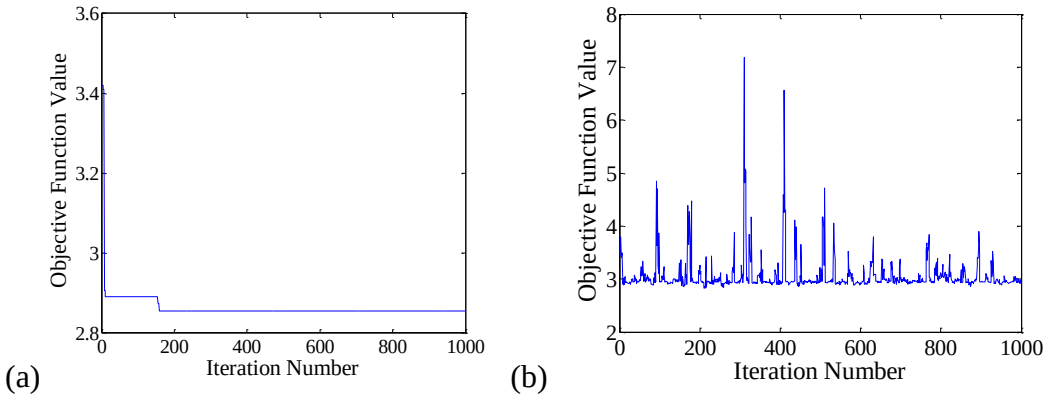

Figure 7.23. Improvement of the objective function global minimum estimation during the SHMUSA-procedure for the studied DC-1 for the Vierendeel bridge mode state with additional masses (a) improvement of the optimal solution (b) system energy of accepted solutions

According to the actual damage characteristics implemented in DC-1, th SHMUSA-procedure detected damage location very close to the exact location at element no. 284, $D_e^* = 284$, with very small error in damage ratio of 0.42, $D_r^* = 0.42$, *Figure 7.24* (i.e. damage depth =21 mm), while the actual damage characteristics are $D_e = 291$ and $D_r = 0.40$ (i.e. damage crack =20 mm). Herein, also the generated new solution from the neighborhood consists of a set of solutions adopted 6-solution, $N^T = 6$, of the OSA method. The six new solutions are generated from the first random solution using normal

distribution. The total new generated solutions will be 7-solution and this configuration is defined as a set of solutions, as shown in *Figure 7.24* (a).

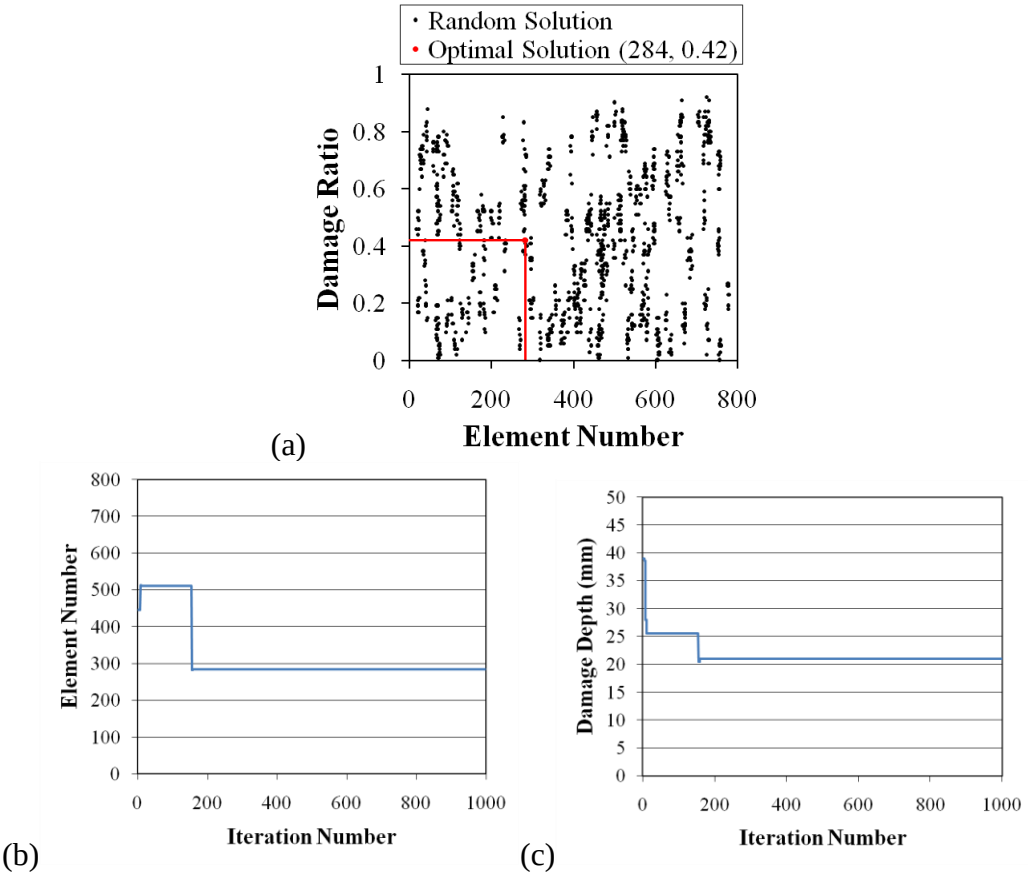

Figure 7.24. Checked solutions during iterations in the SHMUSA-procedure with global improvement of minimal solution of damage charecteristics for DC-1 of the Vierendeel bridge model state with additional masses (a) distribution of checked solution (b) improvement of damage location and (c) improvement of damage severity

The distributions of checked solutions in the search space, *Figure 7.24* (a), show that the SHMUSA-procedure covers the whole search space to avoid local minimums and explore the global optimum solution. The improvement of the optimal solution which represents damage characteristics, damage location and damage severity, during iterations of performance the SHMUSA-procedure are shown in *Figure 7.24* (b) and (c). Figure 7.24 (b) shows the improvement of the first parameter of the damage which is the damage

location represented by the number of damaged element during the iterations, detected no. 284 of damaged element. While, the *Figure 7.24* (c) shows the improvement of the second parameter of the damage which is the damage severity represented by damage depth during the iterations, detected damage ratio of 0.42 (i.e. damage depth of 21 mm).

For the damage scenario of DC-2, the improvement of the optimal solution detected by the SHMUSA-procedure during iterations for the damaged model state with additional mass is shown in *Figure 7.25* (a). The acceptance propability energy in the system of SA method used in the SHMUSA-procedure during improving the optimal solution is shown *Figure 7.25* (b). Figure 7.25 (b) shows the system energy to accept current solutions during the iterations still has high acceptance probability of the system until close the end of the optimization process. That means there is no large number of steps and the high improvement of the optimal solution was achieved during the SHMUSA-procedure and it is terminated due to the max number of iteration was reached and still the system has high temperature.

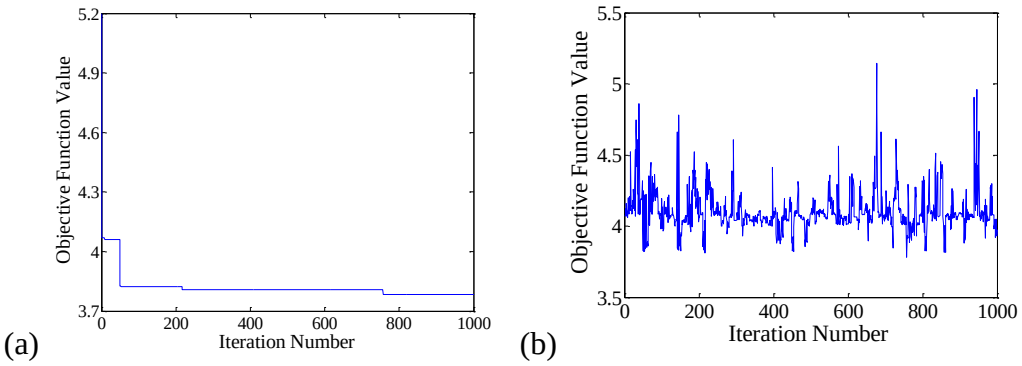

Figure 7.25. Improvement of the objective function global minimum estimation during the SHMUSA-procedure for the studied DC-2 for the Vierendeel bridge mode state with additional masses (a) improvement of the optimal solution (b) system energy of accepted solutions

A very quick convergence of the optimal solution, Figure 7.25 (a), and convergence during the SHMUSA-procedure can be noted, with achieving the limited maximum number

of iterations of 1000. The optimum solution was reached after 757 iteration (with percentage 1.06 % of whole searching space).

According to the actual damage characteristics implemented in DC-2, th SHMUSA-procedure detected damage location exactly at element no. 651, $D_e^* = 651$, with very small error in damage ratio of 0.34, $D_r^* = 0.34$, *Figure 7.26* (i.e. damage depth =21 mm), while the actual damage characteristics are $D_e = 651$ (here equivalent damage was assumed). Also, the generated new solution from the neighborhood consists of a set of solutions adopted 6-solution, $N^T = 6$, of the OSA method. The six new solutions are generated from the first random solution using normal distribution. The total new generated solutions will be 7-solution and this configuration is defined as a set of solutions, as shown in *Figure 7.26* (a). The distributions of checked solutions in the search space, *Figure 7.24* (a), show that the SHMUSA-procedure covers the whole search space to avoid local minimums and explore the global optimum solution. The improvement of the optimal solution which represents damage characteristics, damage location and damage severity, during iterations of performance the SHMUSA-procedure are shown in *Figure 7.24* (b) and (c). Figure 7.24 (b) shows the improvement of the first parameter of the damage which is the damage location represented by the number of damaged element during the iterations, detected no. 284 of damaged element. While, the *Figure 7.24* (c) shows the improvement of the second parameter of the damage which is the damage severity represented by damage depth during the iterations, detected damage ratio of 0.42 (i.e. damage depth of 21 mm).

Good and very satisfactory agreement between the implemented scenarios and estimated damage locations and damage ratios, exhibits the robustness and reliability of the proposed SHMUSA-procedure for damage detection in the Vierendeel bridge structural model. Based on the accuracy of the results, the SHMUSA-procedure is very robust and efficient to detect damage in complex structures due to the precense of small damage.

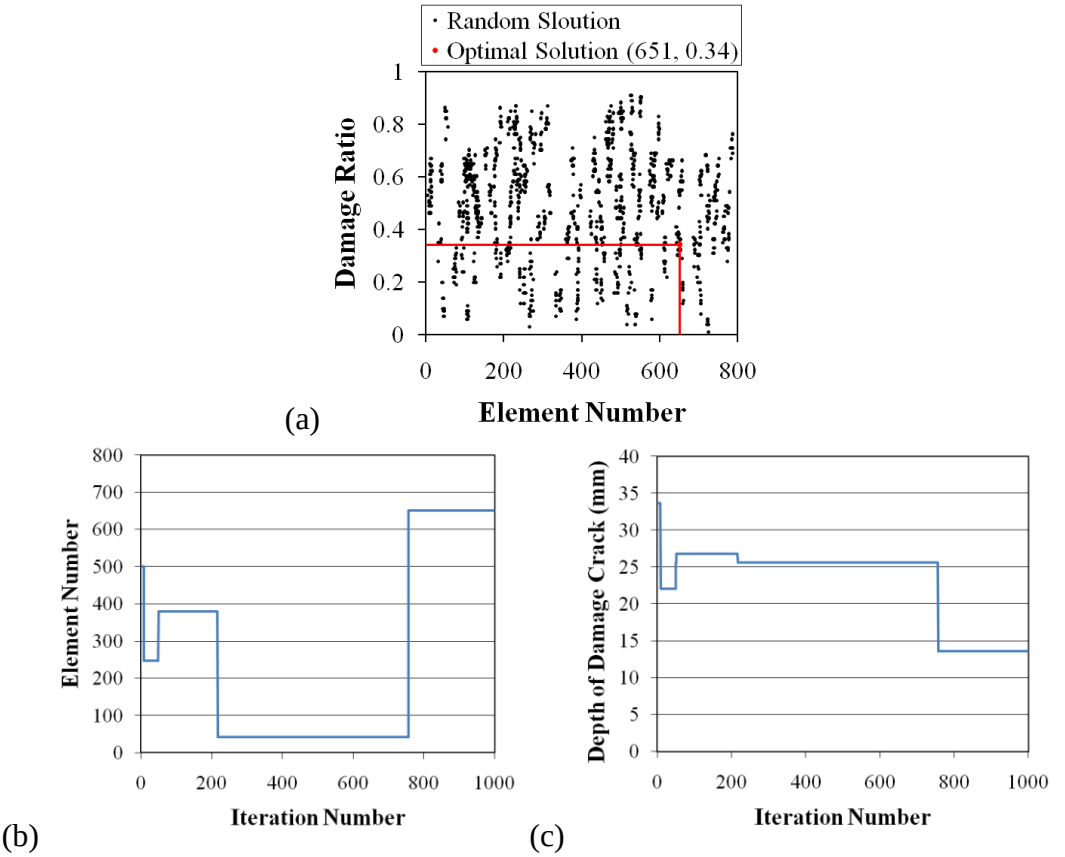

Figure 7.26. Checked solutions during iterations in the SHMUSA-procedure with global improvement of minimal solution of damage charecteristics for DC-2 of the Vierendeel bridge model state with additional masses (a) distribution of checked solution (b) improvement of damage location and (c) improvement of damage severity

7.7. Verification of proposed SHM procedure on multi-storey structural model

The verification of SHMUSA procedure on the fourth structural model was studied to prove the high sensitivity to the presence of damage in beam and column. The study previously testified that the modified objective function Eq. (4.32), with adopted weighing factors reflects actual damage location and severity with its global minimum. For the multi-storey building structural model, the SHMUSA procedure was improved with large searching space and different structural behviour of the model were included with beams

and columns and applied upon the implemented both damage scenarisos for the sake of damage detection.

In this fifth model, two damage scenarios were implemented with different damage characteristics, damage location and severity, as discussed in paragraph 5.6.5 in chapter five. The damage scenarios are at different locations, column and beam, of the multi-storey building model, *Figure 5.55*, with the different damage severities, as shown in *Figure 5.56*. The damage scenario of DC-1 is in the left column between the leve-5 and 6 in the xz-plane, as shown in *Figure 5.55*. The damage scenario in DC-1 has damage length of 60 mm and damage severity of 0.5 which means damage ratio, D_r, as listed in table Table 7.11. While, the damage scenario of DC-2 is in the right side of the beam in the leve-3 in the same xz-plane, as shown in *Figure 5.55*. The damage scenario in DC-1 has damage length of 60 mm and damage severity of 0.5 mm, as shown in *Figure 5.56*. The damage ratio in this model was calculated according to Eq. (7.1) and the weighting factor of the element stiffness in this model is equal one, $\gamma = 1$, because the length of actual damage was the same as the element length of 60 mm for columns and beams, *Figure 6.7*. According to the numbering of elements in the FE multi-storey building model, the location of the damage in the DC-1 is at column element no. 142 which is located at 1590 mm c/c from lower fixed support at rigid base plate, as listed in Table 7.11. The damage location in the DC-2 is at beam element no. 462 which is located at 902.5 mm c/c from lower fixed support at rigid base plate, as shown in *Figure 5.55* and *Figure 6.5*. In addition, in this multi-stoery building model, there are 64 columns and 79 beams with the same length of 300 mm c/c, which is divided into 5-element for each member.

Table 7.11: Implemented damage scenarios on the simply supported Vierendeel bridge model

Description	Damage Scenario-1 (DC-1)	Damage Scenario-2 (DC-2)
Damage Location D_e (Damaged Element Number)	142	642
Damage Severity D_r	0.5	0.5

Therefore, the damage size in the implemented damage scenarios is so small comparative with large entire size of the structural model with large number of included elements of the FE model in the computations of the SHMUSA-procedure.

The verification of the SHMUSA-procedure was performed on multi-storey model with the parameters of the SHMUSA-procedure for optimization problem. The parameters were designed to achieve the convergence and accuracy of exploration the optimal solution, damage characteristics. The included number of elements are 715, *Figure 6.5*, with damage ratio accuracy of 0.01, as listed in Table 7.12. The number of 715-element is distributed as 395-element for the all beams of the building model (i.e. 5-element for each beam of 79-beam) and 320-element for all columns of building model (i.e. 5-element for each column of 64-column), as shown in *Figure 6.5*. Therefore, the size of the searching space, which represents the total number of all possible solutions in the searching space, is 71460 solutions. The termination criteria in this structural model problem are also specified by frozen of the system, i.e. temperature less than one degree, $T < 1$, and the maximum number of iterations, which wass limited to 1000, i.e. 1.4 % of the total number of possible solutions in searching space, as listed in Table 7.12.

Table 7.12: Input Parameters in the SHMUSA-procedure for damage detection in the the simply supported Vierendeel bridge model

Parameter Description	Parameter Value
Number of Included Elements	715
Range of Damage Reduction Factor β	[0.01 - 0.99]
Size of Searching Space	71500
Max Number of Iterations	1000
Percentage (%)	1.4 %
Initial Temperature T_o	20
Temperature Reduction Factor α	0.8
Weighting Factors W_f , W_d	100, 1

On the other hand, There are other designed parameters in the SHMUSA-procedure for SA method, which represents the features of SA optimization method such as the linear

relation of cooling schedule included initial temperature T_o and reduction factor, α. For this type of building model, those parameters are listed in Table 7.12.

In the SHMUSA-procedure and for the multi-storey building model, the adopted objective function, Eq. (4.32), includes the first six modes, $n = 6$, natural frequencies and normalized mode shapes in the computations. The number of components of the mode shape vectors included in the computations for this structural model is two, $m = 2$. The first component is the transverse displacement in x-axis and the second one is transverse displacement in y-axis, while the third component, vertical displacement in z-axis, was neglected according to the mode shapes for this model, as shown in *Figure 6.8*. The values of weighting factors in the adopted objective function are $W_f = 100$ *and* $W_d = 1$, those appropriate value came from many tials and erorrs to fix the fadopted values

The improvement of the optimal solution detected by the SHMUSA-procedure during iterations for the first damage scenario, DC-1, of damaged model in column is shown in *Figure 7.27* (a). The system energy of the acceptance propability in SA method in Eq. (4.20), in the SHMUSA-procedure during improving the optimal solution is shown *Figure 7.27* (b). Figure 7.27 (b) shows that the system energy to accept current solutions during the iterations still has high acceptance probability of the system until close the end of the optimization process. That means there is no large number of steps and the high improvement of the optimal solution was achieved during the SHMUSA-procedure and it is terminated due to the max number of iteration was reached and still the system has high temperature. A very quick improvement of the optimal solution, *Figure 7.27* (a), and convergence during the SHMUSA-procedure can be seen, with achieving the limited maximum number of iterations of 1000. The optimum solution was reached after 892 iterations (with percentage 1.25 % of whole searching space) and the max number of iterations controled the termination criteria for this state of the multi-storey building model, as shown *Figure 7.23* (a).

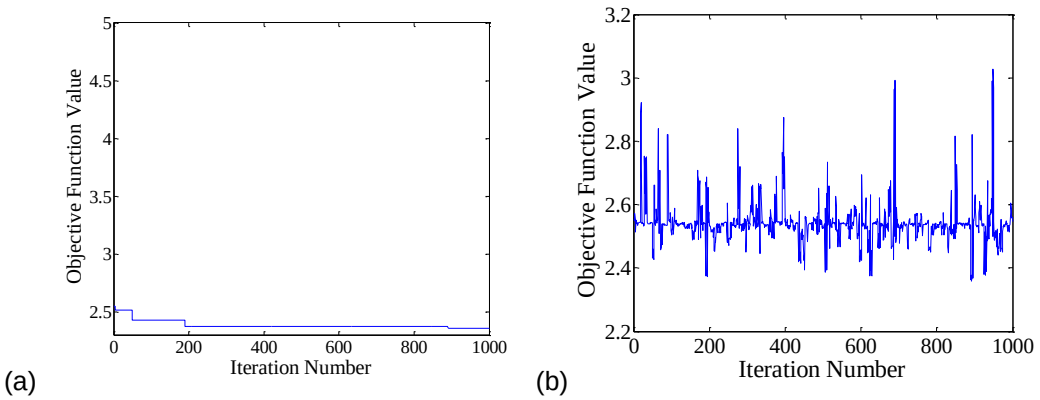

Figure 7.27. Improvement of the objective function global minimum estimation during the SHMUSA-procedure for the studied DC-1 for the multi-storey building model (a) improvement of the optimal solution (b) system energy of accepted solutions

According to the actual damage characteristics implemented in DC-1 in column, th SHMUSA-procedure detected damage location prescisely at the exact location at element no. 142, $D_e^* = 142$, with error in damage ratio of 0.82, $D_r^* = 0.82$, *Figure 7.28* (i.e. damage depth =12.1 mm), while the actual damage characteristics are $D_e = 142$ and $D_r = 0.50$ (i.e. damage crack =7.5 mm). Herein, also the generated new solution from the neighborhood consists of a set of solutions adopted 6-solution, $N^T = 6$, of the OSA method. The six new solutions are generated from the first random solution using normal distribution. The total new generated solutions will be 7-solution and this configuration is defined as a set of solutions, as shown in *Figure 7.28* (a). The distributions of checked solutions in the search space, *Figure 7.28* (a), show that the SHMUSA-procedure covers the whole search space to avoid local minimums and explore the global optimum solution. The improvement of the optimal solution which represents damage characteristics, damage location and damage severity, during iterations of performance the SHMUSA-procedure are shown in *Figure 7.28* (b) and (c). Figure 7.28 (b) shows the improvement of the first parameter of the damage which is the damage location represented by the number of damaged element during the iterations, detected no. 142 of damaged element. While, the *Figure 7.28* (c) shows the improvement of the second parameter of the damage which is the

damage severity represented by damage depth during the iterations, detected damage ratio of 0.82 (i.e. damage depth of 12.1 mm).

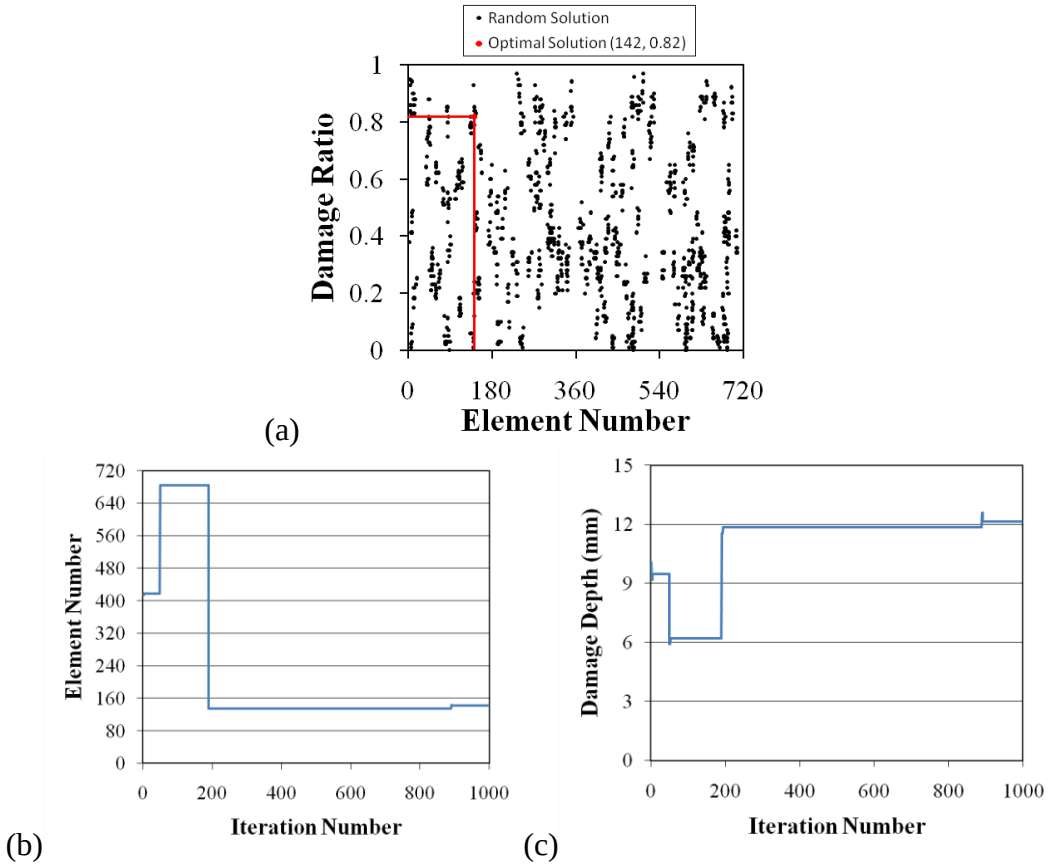

Figure 7.28. Checked solutions during iterations in the SHMUSA-procedure with global improvement of minimal solution of damage charecteristics for DC-1 in column of the multi-storey building model (a) distribution of checked solution (b) improvement of damage location and (c) improvement of damage severity

For damage scenario of DC-2 in beam, the improvement of the optimal solution detected by the SHMUSA-procedure during iterations of damaged model in beam is shown in *Figure 7.29* (a). The system energy of the acceptance propability in SA method in Eq. (4.20), in the SHMUSA-procedure during improving the optimal solution is shown *Figure 7.29* (b). Figure 7.29 (b) shows the accepted current solutions during the iterations when the cooling schedule decrease the temerature of the system and the acceptance probability is

decreased with decreasing system temerature. A very quick improvement of the optimal solution, *Figure 7.29* (a), and convergence during the SHMUSA-procedure can be seen, with achieving the limited maximum number of iterations of 1000. The optimum solution was reached after 595 iterations (with percentage 0.83 % of whole searching space) and the max number of iterations controled the termination criteria for this state of the multi-storey building model, as shown *Figure 7.29* (a).

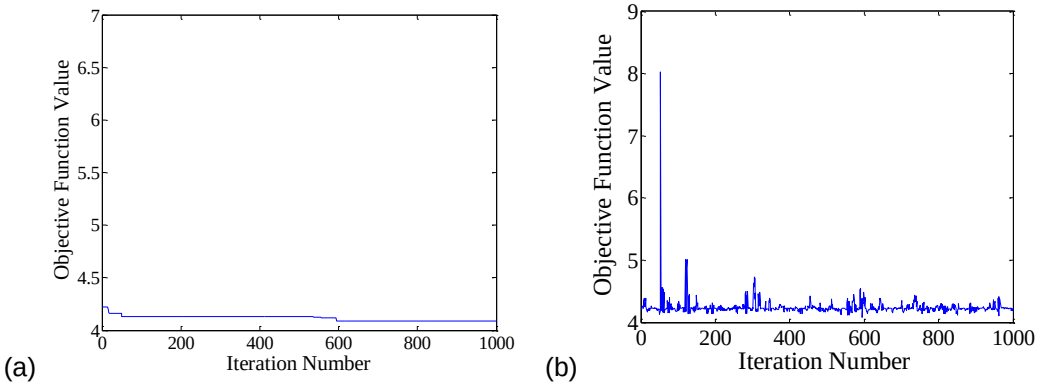

Figure 7.29. Improvement of the objective function global minimum estimation during the SHMUSA-procedure for the studied DC-2 for the multi-storey building model (a) improvement of the optimal solution (b) system energy of accepted solutions

According to the actual damage characteristics implemented in DC-2 in beam, th SHMUSA-procedure detected damage location very close to the exact location at element no. 649, $D_e^* = 649$, with small error in damage ratio of 0.62, $D_r^* = 0.62$, *Figure 7.30* (i.e. damage depth =9.3 mm), while the actual damage characteristics are $D_e = 642$ and $D_r = 0.50$ (i.e. damage crack =7.5 mm). Herein, also the generated new solution from the neighborhood consists of a set of solutions adopted 6-solution, $N^T = 6$, of the OSA method. The six new solutions are generated from the first random solution using normal distribution. The total new generated solutions will be 7-solution and this configuration is defined as a set of solutions, as shown in *Figure 7.30* (a). The distributions of checked solutions in the search space, *Figure 7.30* (a), show that the SHMUSA-procedure covers

the whole search space to avoid local minimums and explore the global optimum solution. The improvement of the optimal solution which represents damage characteristics, damage location and damage severity, during iterations of performance the SHMUSA-procedure are shown in *Figure 7.30* (b) and (c). Figure 7.30 (b) shows the improvement of the first parameter of the damage which is the damage location represented by the number of damaged element during the iterations, detected no. 649 of damaged element. While, the *Figure 7.30* (c) shows the improvement of the second parameter of the damage which is the damage severity represented by damage depth during the iterations, detected damage ratio of 0.62 (i.e. damage depth of 9.3 mm).

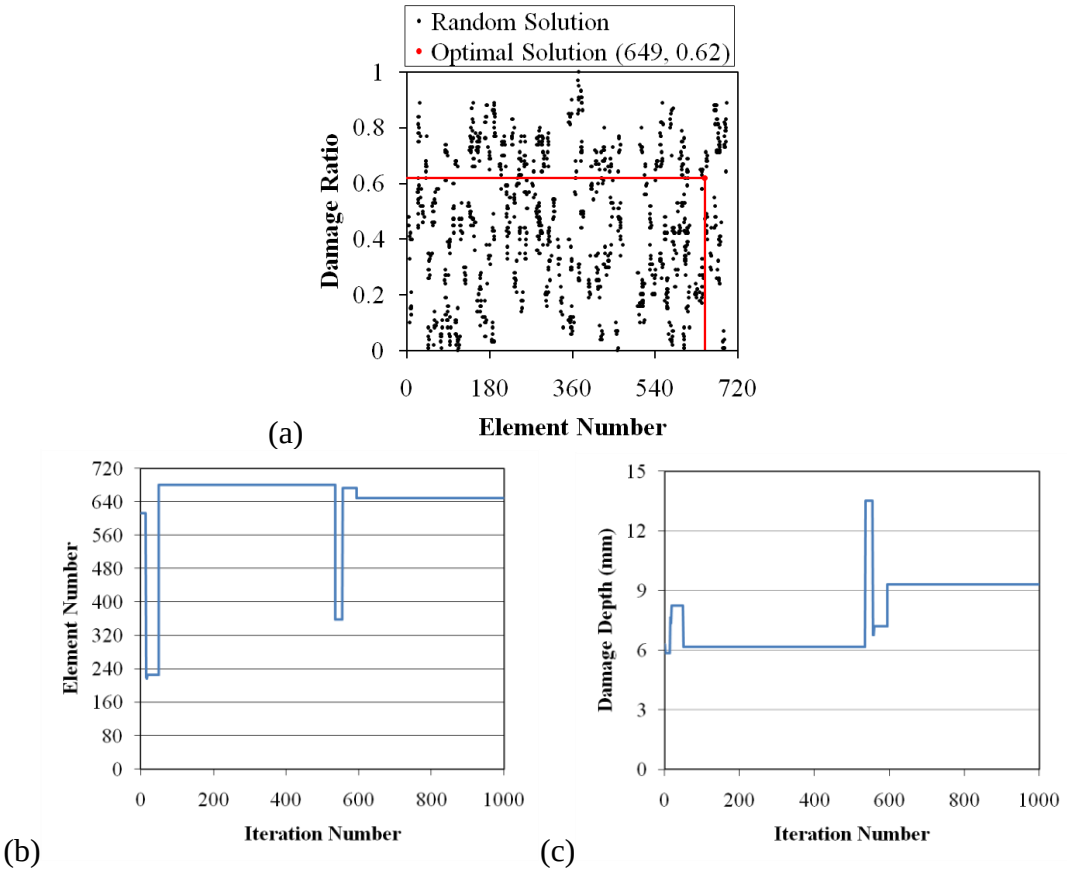

Figure 7.30. Checked solutions during iterations in the SHMUSA-procedure with global improvement of minimal solution of damage charecteristics for DC-2 in beam of the multi-storey building model (a) distribution of checked solution (b) improvement of damage location and (c) improvement of damage severity

In this case the SHMUSA-procedure detected the damage very close to the exact implemented damage scenario of DC-2 in neighboring beam of the same level-3 of the eaxct damaged beam, where 79 beams in the all 10-level of building model. Whereas, for the damage scenario of DC-1 in column, the SHMUSA-procedure detected the exact damage location in the implemented damaged column. Excellent and very satisfactory agreement between the implemented scenarios and estimated damage locations and damage ratios for this building model and all other bridge and simple model, exhibits the robustness and reliability of the proposed SHMUSA-procedure using SA optimization method for damage detection in structures.

8. CONCLUSIONS AND RECOMMENDATIONS

8.1. Conclusions

In this study on damage detection and localization for civil structural health monitoring (SHM), the following main conclusions can be drawn:

1- The type of structural model can have a significant effect on detecting damage characteristic presicely, damaged element and damage ratio. The proposed SHMUSA-procedure detected exactly the implemented damage scenarios for the simple and complex structure of the adopted models or very close.

2- The detection of the damage characteristics for the structural models, grid and Vierendeel bridge, has significant effect due to the loading state with additional masses of the strucutral models with reduction in the dynamic characteristics value with different dynamic behviour of the structure and that represents the effect of operational conditions on the structural behaviour.

3- The designed max number of iterations, which specified the terminal criterion, for the heuristic optimization simulated annealing method has significant effect on detecting exactly the damage characteristics. However, the large number of iterations, large number of trials with time consuming some time have very small improvements on the optimal solutions.

4- The number of selected paramaters in the calibration process of the initial FE model has significant effect on the convergence between the experimental extracted and numerical estimated modal properties of the strucutral models.

5- The adoption of the modal frequencies only in the calibration process of the initial FE models are sufficient to tune the calibrated modal properties corresponding to the experimental modal properties.

6- The large number of modes are included in the calibration process, the high percentages of the convergence are achieved between the comparative modal properties, particularly, for the complex structural models.

7- The large number of modes are included in the proposed SHM procedure for damage detection, the high accuracy to detect damage characteristics are achieved, particularly, for the complex structural models.

8- The selected appropriate values of the simulated annealing features have significant effect on the performance of the heuristic optimization method to catch the optimal solution with low consuming time. Those features values are cooling schedule parameters, initial temperature and reduction factor, neighboring configurations type of the generated solution in the searching space. Also, the linear relation of the reduction temperature in cooling schedule is sufficient to control the cooling of the system.

9- The standard simulated annealing (SSA) with neighboring configuration of single randomly generated solution is efficient and suitable for simple structural problems such as simply supported and overhang beam model. Whereas, the ordinary simulated annealing (OSA) with neighboring configuration of set randomly generated solutions is more advisable and efficient, particularly for complex structural model such as grid, Vierendeel and multi-storey building.

10- The increase of the change ranges of the selected parameters in the calibration process of FE model, the increase the improvement on the optimal solution to tune the dynamic properties of the structural models. Those ranges values of selected parameters are about (5-12)% of the assumed initial values of the parameters in the initial FE models.

11- The equivalenet parameters due to the numerical simulation of real structural models in the FE models have significant effect on the convergence of the modal properties between the experimental and numerical estimations, initial and calibrated FE model. Those parameters are the width of the hidden transverse beams in the FE grid bridge model, equivalenet height of stiffener parts cross section of main beams elements in the FE Vierendeel bridge, equivalenet height of stiffener parts cross section of columns elements in the FE Vierendeel bridge and the equivalent and equivalent mass density of the steel floors plates due to the additional masses in the FE multi-storey building model.

12- The duration of the recorded data in the ambient vibration testing is very important to reflect the real structural behviour of the models. Also, the sampling frequency value of the recording process has significant effect to present the appropriate modal properties of the

structural models. In addition, the repetition of trials of experimental testing is useful to ensure that the recording data are correct and with lower percentage of noise. Also, the reduction of the effect of noise of the recording data reduces the undesirable unreal modes.

13- The number of the measurement points in the tested structural model have significant effect on the presentation of the real structural dynamic properties of the structures. In addition, the number of accelerometers used in the ambient vibration testing increase the accuracy of the testing results. The results of present study improve that with few limited number of accelerometers, eight only, can perform structural health monitoring (SHM) of the simple or complex structures.

14- The distribution of the measurement points over the structural models has high importance to obtain the correct mode shapes of the strucutres, particularly for complex structures.

15- The device type used for excitation method such as shaker device is enough and suitable to gain the real dynamic behviour of the structural model with adopted frequency value range of (2-200)Hz. Also, the position of the shaker device on the structural model during excitation and the way to install it on the structure is very important to be the recording data correct. In addition, it could not control perfectly on the experimental testing without small errors or noise.

16- The modal frequencies values of the structural models due to the sensitvity analysis using modal analysis method increase with increasing the thickness of the cross section of the structural models and this increase is more pronounced for complex structures.

17- The modal frequencies values of the structural models due to the sensitvity analysis using modal analysis method increase with increasing modulus of elacticity of steel metrial of all the structural models.

18- The modal frequencies values of the structural models due to the sensitivity analysis using modal analysis method decrease gradually with increasing mass density of steel metrial of all the structural models.

19- The modal frequencies values of the structural models due to the sensitivity analysis using modal analysis method increase gradually with increasing height of the cross sections FE models of all the structural models.

20- The excellent results of the detecting damage characteristics, damaged element location and damage severity, of the implemented damage scenarios of the adopted four structural models improve the efficiency and robustness of the proposed SHM procedure for damage identification.

21- The high accuracy results of damages detection in the structural models verify the effectiveness of the heuristic optimization method such as simulated annealing to solve such complex and nonlinear structural problems.

22- Ambient vibration testing with suitable excitation method using shaker device is favorable to extract the dynamic properties of the structures with easiest and not expensive way with acceptable real structural modal properties.

23- It is rare to applied one form of objective function for detecting damage in different structures. The adopted form of objective function, Eq. (4.32), is effective and efficiency for all types of adopted structural models with varied values of its parameters.

24- The verifications of the proposed SHMUSA-procedure detected the damage locations in all adopted structural model exactly and some times with very close to the exact implemented damage scenarios. While, there are some relative errors in detecting the damage severity during application of the proposed SHMUSA-procedure. In fact, the detection of damage location is more important than damage severity in the civil structural health monitoring

8.2. Recommendations

On the basis of the present study on damage detection and localization for civil structural health monitoring (SHM), the following recommendations for future research are proposed:

1- It is recommended to extend this study to the case of the other heurestic optimization method such as; particale swarm optimization (PSO) or tabu search (TS).

2- It is recommended to extend this study to implement the damage scenarios of multi-damages cases of damaged models with different damage locations.

3- It is recommended to extend this study to apply other excitation method to extract dynamic properties of structural models.

4- It is recommended to extend this study to use those stuctural models with another methods to detect damage in structure.

5- It is recommended to extend this study to apply non-linear analysis of FE structural models with nonlinear damage crack theory.

6- It is recommended to extend this study to use another objective function with another included parameters with including largre number of modes in the computations to detect damages in the structures.

7- It is recommended to extend this study to test the third type of the direct simulated annealing (DSA) and compare the results.

8- It is recommended to extend this study to include damping ratio in the modal analysis method and effect of the damping ratio on the accuracy of detecting the damage characteristices, damaged element location and damage severity.

9- It is recommended to extend this study to include more selected parameters in the calibration process.

10- It is recommended to apply the proposed SHM procedure on the real structure in the site and detect the damages or monitor the structures during operational conditions.

9. REFERENCES AND APPENDICES

9.1. References

[1] F. Kang, J. Li and S. Liu, 2013, "Combined data with partical swarm optimization damage detection", Journal of mathematical problem in engineering, artical ID 416941, 10 pages.

[2] M. Biswas, A.K. Pandey and M.M. Samman, 1990, "Diagnostic Experimental Spectral/Modal Analysis of a Highway Bridge", Modal Analysis: The International Journal of Analytical and Experimental Modal Analysis, vol. 5, pp. 33–42.

[3] FHWA, 2001, "Reliability of visual inspection", Federal Highway Administration (FHA), Report No. FHWA-RD-01-020 and FHWA-RD-01-021, Washington DC, USA.

[4] R.S. He and S.F. Hwang, 2006, "Damage detection by an adaptive real-parameter simulated annealing genetic algorithm", Journal of computers and structures, vol. 84, pp.2231-2243.

[5] M. Sahin and R.A. Shenoi, 2003, "Quantification and localization of damage in beam-like structures by using artificial neural networks with experimental validation", Journal of engineering structures, vol. 25, pp. 1785-1802.

[6] A.S. Kobayashi, 1993, "Non-destructive evaluation", Hand Book on Experimental Mechanics, VCH, New York, N.Y., and SEM, Bethel, CT, USA.

[7] T.E. Uomoto, 2000, "Non-destructive testing in civil engineering", Elsevier Science Ltd., Amsterdam.

[8] Chong, K.P., Carino, N.J., and Washer, G. 2001. Health monitoring of civil infrastructures. Health Monitoring and Management of Civil Infrastructure Systems,Proceedings of SPIE's International Symposium on NDE and Health Monitoring Diagnostics, Vol. 4337, S.B. Chase and A.E. Aktan, eds., SPIE, Bellingham, WA, pp. 1-16.

[9] B. Raj, T. Jayakumar and M. Thavasimuthu, 2002, "Practical non-destructive testing", 2nd edition, Narosa Publishing House, New Delhi, India.

[10] G.M. Owolabi, A.S.J. Swamidas and R. Seshadri, 2003, "Crack detection in beam using changes in frequencies and amplitudes of frequency response function", Journal of sound and vibration, vol. 265, pp. 1-22.

[11] C.T. Ng, M. Veidt and H.F. Lam, 2009, "Guided wave damage characterization in beams utilizing probabilistic optimization", Journal of engineering structures, vol. 31, pp. 2842-2850.

[12] S.W. Doebling, C.R. Farrar and M.B. Prime, 1997, "A summery review of vibration-based damage identification methods", Journal, artical ID 416941, 34 pages.

[13] L.D. Wegner, Z. Zhou, M. Alwash, A.B. Siddique and B.F. Sparling, 2004, "Vibration-based damage detection on bridge superstructures", Proceedings of the 2nd International Workshop on Structural Health Monitoring of Innovative Civil Engineering Structures, pp. 429-439.

[14] V.H. Antonio, 2014, "Model updating and structural health monitoring of horizontal axis wind turbines via advanced spinning finite elements and stochastic subspace identification methods", PhD Dissertation, Michigan Technological University.

[15] C.R. Farrar and K. Worden, 2013, "Structural Health Monitoring", 1st Edition Published Book by John Wiley & Sons, ISBN: 978-1-119-99433-6, UK.

[16] Web site: https://en.wikipedia.org/wiki/Structural_health_monitoring.

[17] C.R. Farrar and S.C. Doebling, 1998, "Damage detection II: Field application to a large structure", Proceedings Modal Analysis.

[18] H.Y. Hwang and C. Kim, 2004, "Damage detection in structures using a few frequency response measurements", Journal of sound and vibration, vol. 270, pp. 1-14.

[19] A. Rytter, 1993, "Vibrational based inspection of civil engineering structures", PhD thesis, Aalborg University, Denmark.

[20] O.S. Salawu, 1997, "Detection of structural damage through changes in frequency - a review", Engineering Structures, vol. 19, no. 9, pp. 718–723.

[21] R.W. Clough and J. Penzien, 1975, "Dynamics of Structures", 2nd edition, Mcraw-Hill, ISBN 0-07-011392-0.

[22] A. L. Materazzi and I. Venanzi: Structural damage detection using dynamic response state-of-the-art and prospects, International Journal (2008), 5: 33–42.

[23] A. E. Aktan, C. Chuntavan and T. Aksel, 1994: Modal Testing for Structural Identification and Condition Assessment of Constructed Facilities, in Proc. of 12th International Modal Analysis Conference, pp. 462–468.

[24] C. Farrar and D. Jauregui,1996: Damage Detection Algorithms Applied to Experimental and Numerical Modal Data from the 1-40 Bridge, LA-13074-MS, Los Alamos national Laboratory.

[25] R. W. Clough and J. Penzien, 1975," Dynamics of Structures", Library of Congress Cataloging in Publication Data, McGraw-Hill Inc, USA.

[26] A. K. Chopra, 1995,"Dynamics of Structures: Theory and Application to Earthquake Engineering", Library of Congress Cataloging in Publication Data, Prentice Hall, New Jersey Inc, USA.

[27] D. Inman, 2000, "Engineering Vibration", 2nd edition, Prentice Hall publishing Inc, New Jersey, USA.

[28] B. Schwarz and M. Richardson, 2003, "Scaling Mode Shapes Obtained from Operating Data", 21th International Modal Analysis Conference (IMAC), Kissimmoo, Florida, USA, pp. 18-22.

[29] B. Schwarz and M. Richardson, 2006, "Using FEA Modes to Scale Experimental Mode Shapes", 24th International Modal Analysis Conference (IMAC), California, USA, pp. 1-8.

[30] B. Davison and G.W. Owens, 2003, "Steel Designer's Manual", 6th edition of book, The Steel Construction Institute, Blackwell publishing.

[31] Tomaszewska A. Influence of statistical errors on damage detection based on structural flexibility and mode shape curvature. Elsevier, Computers and Structures 2010; 88: 154 - 164 .

[32] Tomaszewska A., 2010, Influence of statistical errors on damage detection based on structural flexibility and mode shape curvature, J. of Computers and Structures, Vol. 88, No. 3-4, pp. 154 – 164.

[33] S. W. Doebling, C. R. Farrar, M. B. Prime and D. W. Shevltz, 1996, " Damage Identification and Health Monitoring of Structural and Mechanical Systems from Changes in Their Vibration Characteristics: A Literature Review", Los Alamos National Laboratory, University of California, LA-13070-MS, 134 pages.

[34] J. J. Sinou, 2013, "A review of Damage Detection and Health Monitoring of Mechanical System from Changes in the Measuerment of Linear and Non-Linear Vibrations", HAL Archives-Ouvertes, UHAL Id: hal-00779322, Laboratoire de Tribologie et Dynamique des Systemes, France, 60 pages.

[35] Doebling, S. W., Farrar, C. R., Prime, M. B., and Shevitz, D. W., 1996a, "Damage Identification and Health Monitoring of Structural and Mechanical Systems from Changes in their Vibration Characteristics: A Literature Review", Los Alamos National Laboratory report LA-13070-MS.

[36] R. J. Allemang and D. L. Brown: A correlation coefficient for modal vector analysis", Proceedings of the 1st International Modal Analysis Conference, pages 110-116, 1982.

[37] R. J. Allemang: The modal assurance criterion (MAC): twenty years of use and abuse", Proceedings of 20th International Modal Analysis Conference, Los Angeles, CA, USA, pp. 397-405, 2002.

[38] Fox, C. H. J., 1992, "The Location Of Defects In Structures: A Comparison Of The Use Of Natural Frequency And Mode Shape Data," in Proc. of the 10th International Modal Analysis Conference, pp. 522–528.

[39] H. Nahvi and Jabbari M., 2005, Crack detection in beams using experimental modal data and finite element model, Elsevier, International Journal of Mechanical Sciences, Vol. 47, No. 10, pp. 1477 - 1497.

[40] M. M. Fayyadh and A. Abdul Razak, 2011, Detection of Damage Location Using Mode Shape Deviation: Numerical Study, International Journal of Physical Sciences, Vol. 6, No. 24, pp. 5688 - 5698.

[41] M. A. Abdo, 2012, "Damage Detection in Plate-Like Structure Using High-Order Mode Shape Derivatives", International Journal of Civil and Structural Engineering, Vol. 2, No. 3, pp. 801 - 816.

[42] E. Ekinovic, S. Ekinovic and R. Sunulahpasic, 2013, A Glance to a Mode Shape Based Damage Detection Technique, 17th International Research/Expert Conference, Trends in the Developement of Machinery and Associated Technology, pp. 381-384.

[43] E. Ernest, 2012, "Detection of Structural Damage in Building Using Changes in Modal Damping Mechanism, International Journal of Engineering and Management Scinces, Vol 3 (3), pp. 250-255.

[44] D. J. Ewins, 1984,"Modal Testing: Theory and Practice", Research Studies Presss LTD, John Wiley and Sons Inc, England, UK.

[45] M. K. Yoon, D. Heider, J. W. Gillespie, C. P. Ratcliffe and R. M. Crane, 2010, "Local damage detection with the global fitting method using operating deflection shape data", J Nondestruct Eval, Vol. 29, pp. 25-37.

[46] U. Baneen, N.M. Kinkaid, J.E. Guivant, I. Herszberg, 2012, "Vibration based damage detection of a beam-type structure using noise suppression method", Journal of Sound and Vibration, Vol. 331, No. 8, pp. 1777 - 1788.

[47] A. K. Pandey, and M. Biswas, , 1994, “Damage Detection in Structures Using Changes In Flexibility,” Journal of Sound and Vibration, Vol. 169, No. 1, pp. 3–17.

[48] Salawu, O. S. and Williams, C., 1993, “Structural Damage Detection Using Experimental Modal Analysis–A Comparison Of Some Methods,” in Proc. of 11th International Modal Analysis Conference, pp. 254–260.

[49] H. Lam and T. Yin, 2011, “Dynamic Reducton-Based Structural Damage Detection of Transmission Towers: Practical Issues and Experimental Verification,” Elsevier, Engineering Structures, Vol. 33 (2011), pp. 1459–1478.

[50] P.H. Kirkegaard and A. Rytter, 1995, “A Comparative Study of Three Vibration Based Damage Assessement Techniques,” Fracture and Dynamics, ISSN 0902-R9435, pp. 1–10.

[51] R. Ruotolo and C. Surace, 1997, “Damage Assessment of Multiple Cracked Beams: Numerical Results and Experimental Validation,” Journal of Sound and Vibration, Vol. 206(4), pp. 567-588.

[52] M.I. Friswell, J.E.T. Penny and S.D. Garvey, 1998, "A Combined Genetic and Eignsensitivity Algorithm for the Location of Damage in Structures," Pergamon, Computers and Structures, Vol. 69, pp. 547–556.

[53] Y. Xia and H. Hao, 1998, "A Genetic Algorithm for Structural Damage Detection Based on Vibration Data," School of Civil Engineering, Nanyang Technological University, Singapore, pp. 1–7.

[54] F. Au, Y. Cheng, L. Tham and Z. Bai, 2003, "Structural Damage Detection Based on a Micro-Genetic Algorithm Using Incomplete and Noisy Modal Test Data," Journal of Sound and Vibration, Vol. 259(5), pp. 1081–1094.

[55] M. Sahin and R.A. Shenoi, 2003, "Quantification and Localisation of Damage in Beam-Like Structures by Using Artificial Neural Networks with Experimental Validation," Elsevier, Engineering Structures, Vol. 25 (2003), pp. 1785–1802.

[56] M.A. Rao, J. Srinivas and B.S.N. Murthy, 2004, "Damage Detection in Vibrating Bodies Using Genetic Algorithms," Elsevier, Computers and Structures, Vol. 82 (2004), pp. 963–968.

[57] J.J. Lee, J.W. Lee, J.H. Yi, C.B. Yun and H.Y. Jung, 2005, "Nueral Networks-Based Damage Detection for Bridges Considering Errors in Baseline Finite Element Models," Elsevier, Journal of Sound and Vibration, Vol. 280 (2005), pp. 555–578.

[58] J.H. Park, D.S. Hong, J.M. Lee, J.T. Kim and W.B. Na, 2006, "GA-Based Damage Detection in Structure Using Frequency and Modal Strain-Energy," Department of Ocean Engineering, Pukyong National University, Korea.

[59] R. P. Bandara, T. H.T. Chan and D. P. Thambiratnam, 2007, " Frequency Response Function Based Structural Damage Detection Using Artificial Neural Networks," pp. 1-12.

[60] R.S. He and S.F. Hwang, 2007, "Identifying Damage in Spherical Laminate Shells by Using a Hybrid Real-Parameter Genetic Algorithm," Elsevier, Compsite Structures, Vol. 80 (2007), pp. 32–41.

[61] H. M. Gomes and N. R. S. Silva, 2011, "Some Comparison for Damage Detection on Structures Using Genetic Algorithm and Modal Sensitivity Method," Elsevier, Applied Mathematical Modelling, Vol. 32 (2008), pp. 2216–2232.

[62] V. Meruane, W. Helyen and K. U. Leuven, 2008, “Damage Detection on a Multi-Cracked Beam by Parallel Genetic Algorithms Using Modal Characteristics,” Proceedings of ISMA 2008, pp. 3319–3332.

[63] S. K. Panigrahi, S. Chakraverty and B. K. Mishra, 2008, “Genetic Algorithm Based Damage Detection Identification in Non-Homogeneous Structural members,” Elsevier, Engineering Structures, Vol. 33 (2011), pp. 1459–1478.

[64] M. B. Rosales, C. P. Filipich and F. S. Buezas, 2009, “Crack Detection in Beam-Like Structures,” Elsevier, Engineering Structures, Vol. 31 (2009), pp. 2257–2264.

[65] S.K. Panigrahi, S. Chakraverty and B.K. Mishra, 2009, “Vibration Based Damage Detection in a Uniform Strength Beam Using Genetic Algorithm,” Springer, Meccanica, Vol. 44 (2009), pp. 697–710.

[66] N. Bakhary, H. Hao and A. J. Deeks, 2010, “Structure Damage Detection Using Neural Network with Multi-Stage Substructuring,” Advances in Structural Engineering, Vol. 13, No.1, pp. 1–16.

[67] N. Bakhary, H. Hao and A. J. Deeks, 2006, “Neural Network Based Damage Detection Using a Substructure Technique,” School of Civil and resource Engineering, University of Western Australia, Australia, pp. 1–11.

[68] V. Meruane and W. Heylen, 2010, “An Hybrid Real Genetic Algorithm to Detect Structural Damage Using Modal Properties,” Elsevier, Mechanical System and Signal, doi:10.1016/j.ymssp.2010.11.020.

[69] M.H. Arafa, A.M.A. Youssef and A. Nassef, 2010, "A Modified Continuous Reactive Tabu Search for Damage Detection in Beam", International Design Engineering Technical Conferences Computers and Information in Engineering Conference ASME 2010, DOI: 10.1115/DETC2010-28389.

[70] H. Aghabarati and M. Tehranizadeh, 2011, “Comparison Study on Neural Networks in Damage Detection of Steel Truss Bridge,” Journal of Structural Engineering and Geotechnics, Qazvin Islamic Azad University, Vol. 1 (1), pp. 37–48.

[71] H. Liu, K. Xin and Q. Qi, 2011, “Study of Structural Damage Detection with Multi-Objective Function Genetic Algorithm,” Elsevier, Procedia Engineering, Vol. 12 (2011), pp. 80–86.

[72] N. H. Hadi and A. A. Abdulkareem, 2012, “Damage Detection and Assessement of Stiffness and Mass Matrices in Curved Simply Supported Beam Using Genetic Algorithm”, Journal of Engineering, University of Baghdad, Vol. 18 (1), pp. 1-21.

[73] S.M. Pourhoseini Nejad, Gh.R. Ghodrati Amiri, A. Asadi, E. Afshari and Z. Tabrizian, 2012, “Damage Detection of Skeletal Structures Using Particle Swarm Optimizer with Passive Congregation (PSOPC) Algorithm via Incomplete Modal Data”, Computational Methods in Civil Engineering CMCE, Vol. 3 (1), pp. 1-13.

[74] S. S. Kourekli, A. Bagheri, C. G. Amiri and M. Ghafory-Ashtiany, 2013, “Structural Damage Detection Using Incomplete Modal Data and Incomplete Static Response”, Structural Engineering, KSCE Journal of Civil Engineering, Structural Engineering, Vol.17 (1), pp. 216–223.

[75] J. Zhan and L. Yu, 2014, "Optimal Sensor Placement based on Tabu Search Algorithm", Applied Mechanics & Materials, Issue 578-579, Page 1069.

[76] Z. Miskovic, S. Al-Wazni and A. Alalikhan, 2015, "Methods of Damage Detection of Structures Based on Changes of Dynamic Characteristics", Gradevinski Kalendar, Journal of the Union of Engineers and Technicians ISSN 0352-2733, Vol. 47, pp. 163-191.

[77] Structural Vibration Solutions A/S, 2004, “ARTeMIS - Extractor, Release 3.41 Academic License, User’s Manual”, NOVI SciencePark, Aalborg, Denmark.

[78] M. Friswell, E. Mottershead, "Finite Element Model Updating in Structural Dynamics", Kluwer Academic Publisher, The Netherlands, ISBN 0-7923-3431-0, 1995.

[79] FEMtools - Integrating Test and Analysis, Version 1.0., Dynamic Design Solutions, Leuven, Belgium: FEMtools, 1995.

[80] A. Pavić, Z. Mišković, P. Reznolds, "Modal Testing and Finite-Element Model Updating of a Lively Open-Plan Composite Building Floor", ASCE – Journal of Structural Engineering, Vol.133, No-4 , pp.550-558., 2007.

[81] MATLAB- Software (R2010b)-Version 7.11.0.584, 2010, The language of Technical Computing, The MathWorks Inc., USA.

[82] J.Z. Zhang, J. Prader, K.A. Grimmelsman, F. Moon, A.E. Aktan and A. Shama, 2009, “Challenges in Experimental Vibration Analysis for Structural Identification and

Corresponding Engineering Strategies", 3rd Experimental Vibration Analysis for Civil Engineering Structures Conference, Third Edition, Wroclaw.

[83] https://en.wikipedia.org/wiki/Seismic_noise#cite_note-17

[84] R. Li, A. Mita and J. Zhou, 2013, "Hybrid Methodology for Structural Health Monitoring Based on Immune Algorithms and Symbolic Time Series Analysis", Journal of Intelligent Systems and Applications, Vol. 5, pp. 48-56.

[85] C.R. Farrar, T.A. Duffey, P.J. Cornwell and S.W. Doebling, 1999, "Excitation Methods for Bridge Structures", Proceedings of the 17th International Modal Analysis Conference IMAC, Kissimmee, Florida, USA.

[86] https://en.wikipedia.org/wiki/Operational_Modal_Analysis.

[87] H. Wenzel and P. Furtner, 2006, "Damage Detection and Bridge Classification by Ambient Vibration Monitoring-Application of BRIMOS at Two Stay Cable Bridges in China", The Proceeding of 4th China-Japan-US Symposium on Structural Control and Monitoring, Chaina.

[88] T. Yin, H,F. Lam, H.M. Chow and H.P. Zhu, 2009, "Dynamic Reducton-Based Structural Damage Detection of Transmission Towers Utilizing Ambient Vibration Data", Elsevier, Engineering Structures, Vol. 31 (2009), pp. 2009–2019.

[89] H. Wenzel and D. Pichler, 2005, "Ambient Vibration Monitoring", Book published by John Wiley and Sons Inc, England.

[90] M.Q. Feng, J.M. Kim and H. Xue, 1998, "Identification of a Dynamic Sysytem Using Ambient Vibration Measurements", Journal of Applied Mechanics, ASME, vol. 65, pp. 1010-1021.

[91] M.D. Kohler, P.M. Davis and E. Safak, 2005, "Earthquake and Ambient Vibration Monitoring of the Steel-Frame UCLA Factor Building", Earthquake Spectra, Vol. 21, No. 3, pp. 1-22.

[92] J.F. Lord, C.E. Ventura and E. Dascotte, 2003, "Automated Model Updating Using Ambient Vibration Data from a 48-Storey Building in Vancouver", Vancuover,Canada, pp. 1-7.

[93] X.H. Chen P. Omenzetter and S. Beskhyroun, 2014, "Ambient Vibration Based Evaluation of a Curved Post-tensioned Concrete Box-Girder Bridge", International Conference NZSEE, pp. 1-8.

[94] C.P. Fritzen, 2005, "Vibration-Based Structural Health Monitoring-Concepts and Applications", Key Engineering Materials, Vols. 293-294, pp. 3-20.

[95] V.B Ali, S. Zivanovic, H.V. Dang, M. Istrate and A.L. Iban, 2012, "Modal Testing and FE Model Updating of a Lively Staircase Structure", Proceedings of the SEM, IMAC XXX Conference, Florida, USA, pp. 2009–2019.

[96] R. Brincker, L. Zhang and P. Anderson, 2000, "Modal Identification from Ambient Responses Using Frequency Domain Decomposition", Proceedings of 18th International Modal Analysis Conference (IMAC), Texas, USA, pp. 625–630.

[97] P. Anderson, R. Brincker, B. Peeters, G.D. Roeck, L. Hermans and C. Kramer, 1999, "Comparison of System Identification Methods Using Ambient Bridge Test Data", Proceedings of 17th International Modal Analysis Conference (IMAC), Kissimee, Florida, USA, pp. 1035–1041.

[98] R. Bricker, J.B. Frandsen and P. Andersen, 2000, "Ambient Response Analysis of the Great Belt Bridge", Proceedings of the 18th International Modal Analysis Conference IMAC, San Antonio, Texas, USA.

[99] R.S. Pappa, K.B. Elliott and A. Schenk, 1992, "A Consistent-Mode Indicator for the Eigensystem Realization Algorithm", NASA Technical Memorandum 107607, N92-24707, Virginia, USA.

[100] J.W. Lee, J.D. Kim, C.B. Yun, J.H. Yi and J.M. Shim, 2002, "Health-Monitoring Method for Bridges Under Ordinary Traffic Loadings", Elsevier, Journal of Sound and Vibration, 257(2), pp. 247-264.

[101] C.E. Ventura, T. Horyna, 2000, "Measured and Calculated Modal Characteristics of The Heritage Court Tower in Vancouver, B.C.", International Modal Analysis Conference IMAC–XX, A Conference on Structural Dynamics, Proceedings of the Conference held in, pp. 1070-1074.

[102] C.E. Ventura, J.F. Lord, M. Turek, R. Brincker, P. Andersen and E. Dascotte, 2005, "FEM Updating of Tall Building Using Ambient Vibration Data", Proceedings of 6th International Conference on Structural Dynamics, Paris, France, pp. 4-7.

[103] P. Reynolds, A. Pavic and Z. İbrahim, 2003, "A Remote Monitoring Sytem for Stadia Dynamics", Proceedings of the 22nd International Modal Analysis Conference (IMAC), Florida, USA.

[104] C.P. Lamarche, P. Paultre J. Proulx and S. Mousseau, 2008, "Assessment of the Frequency domain decomposition technique by forced-vibration test of a Full-Scale Structure", Earthquake Engineering and Structural Dynamics, Vol. 37, pp. 487-494.

[105] W.C. Su, C.S. Huang, S.L. Hung, L.J. Chen and W.J. Lin, 2012, "Locating Damage Storey in a Shear Building Based on its Sub-Structural natural Frequencies", Elsevier, Engineering Structures, Vol. 39, pp. 126-138.

[106] http://www.svibs.com/products/ARTeMIS_Modal_software.aspx?

[107] Z. Mišković, A. Alalikhan, S. Al-Wazni, R. Salatić and L. Mišković, 2014, "Vibration Ambient Test of Cazela Bridge Approach Structure in Belgrade", 5th International Conference of GNP, University of Montenegro, pp. 34-41.

[108] S. Al-Wazni, Z. Mišković, A. Alalikhan and R. Salatić, 2014, "Comparison of FDD and SSI modal identification methods from ambient vibration data-case study", 5th International Conference of GNP, University of Montenegro, pp. 8-12.

[109] R. Brincker, L. Zhang and P. Andersen, 2000, "Output-Only Modal Analysis by Frequency Domain Decomposition", Proceedings of the 25th International Seminar on Modal Analysis (ISMA), Leuven, 2000.

[110] P. Miroslav, B. Michal and H. Tomas, 2012, "Modal Assurance Criteria", Elsevir, Journal of Procedia Engineering, Vol. 48, pp. 543–548.

[111] K.D. Nagesh, 2000,"Water Resources Systems Planning and Management: Advanced Topics – Genetic Algorithms, IISc, Bangalore, M9L2, pp. 1 - 14.

[112] M. Heikki, M. Kaisa, P. Antti, 2007, On initial populations of a genetic algorithm for continuous optimization problems, Springer, Journal Global Optimum, Vol. 37, No. 3, pp. 405–436.

[113] S.O. Degertekin, 2007, "A comparison of simulated annealing and genetic algorithm for optimum design of nonlinear steel space frames", Springer, Structural Multidisc Optimum, Vol. 34, No. 4, pp. 347–359.

[114] H.A.O. Junior, L. Ingberg, A. Petraglia, M.R. Petraglia and M.A.S. Machado, 2012, "Stochastic Global Optimization and Its Application with Fuzzy Adaptive Simulated Annealing", Springer Heidelberg New York Dordrecht London, DOI 10.1007/978-3-642-27479-4, USA.

[115] https://en.wikipedia.org/wiki/optimization.

[116] S. Kirkpatrick, C.D. Gelatt and M.P. Vecchi, 1983, "Optimization by simulated annealing", Journal of science (Jstor), volume 220, No. 4598, pp. 671-680.

[117] L. Hui, X. Kegui, Q. Quanquan, 2011, "Study of Structural Damage Detection with Multi-objective Function Genetic Algorithms", SREE Conference on Engineering Modeling and Simulation, Elsevier, Procedia Engineering Vol. 12, pp. 80–86.

[118] R.C. Chakraborty, 2010, "Fundamental of Genetic Algorithm", AI Course, Lecture 39-40, 42- pages.

[119] J. Kennedy and R. Eberhart, 1995, "Particle Swarm Optimization", International Conference of IEEE, pp. 1942-1948.

[120] D. Merkle and M. Middendorf, 2004, "Chapter 14: Swarm Intelligence", chapter 14 in book, Department of Computer Science, University of Leipzig, Germany.

[121] M.A. Khanesar, H. Tavakoli, M. Teshnehlab and M.A. Shoorehdeli, 2009, "Novel Binary Particle Swarm Optimization", Chapter one in book of "Particle Swarm Optimization", Edited by Aleksendar Lazinica, ISBN: 978-953-7619-48-0, published by InTech, KN. Toosi University of Technology, Iran.

[122] Y. Habib, M. Sadiq, A. Hakim, 2001, "Evolutionary algorithms, simulated annealing and tabu search: a comparative study", Engineering Applications of Artificial Intelligence, Vol. 14, pp. 167–181.

[123] G. Michel, P. Jean-Y, 2014, "Chapter 6: Tabu Search, in Search Methodologies: Introductory Tutorials in Optimization and Decision Support Techniques," 2nd edition, edit by Edmund K. Burke and Graham Kendall, ISBN 978-1-4614-6940-7, Springer, New York, USA.

[124] M. Pastor, M. Binda and T. Harcarik, 2012, "Modal Assurance Criterion", Procedia Engineering, Vol. 48, pp. 543-548.

[125] B. Ceranic, C. Fryer and R.W. Baines, 2001, "An application of simulated annealing to the optimum design of reinforced concrete retaining structures", Journal of computers and structures, Vol. 79, pp. 1569-1581.

[126] D. Henderson, S.H. Jacobson and A.W. Johnson, 2005, "The Theory and Practice of Simulated Annealing", Chapter 10 in book, pp. 287-318, USA.

[127] C. Tsallis and D. Stariolo, 1995, "Generalized simulated annealing", Journal, vol. 1, Rio de Janeiro, Brazil.

[128] Z. Miskovic, 2000, "Application of the stress fields based on the theory of plasticity for determination load carrying capacity of the reinforced concrete walls", PhD thesis, Belgrade university, Belgrade, Serbia.

[129] O. Hasancebi, F. Erbatur, 2002, "Layout optimization of trusses using simulated annealing", Journal of Engineering Software, Vol. 33, pp. 681-696.

[130] M. Akbulut and F.O. Sonmez, 2011, "Design optimization of laminated composites using a new variant of simulated annealing", Journal of computers and structures, Vol. 89, pp. 1712-1724.

[131] F.O. Sonmez, 2007, "Shape Optimization of 2D Structures Using Simulated Annealing", Elsevier, Comput. Methods Appl. Mech. Engrg, Vol. 196, pp. 3279-3299.

[132] H. G. Harris and G. M. Sabnis, 1999, "Structural Modeling and Experimental Techniques", Second Edition, USA.

[133] Academic ANSYS, version 2011, Release 14.0, http://www.ansys.com.

[134] ANSYS Parametric Design Language guide, 2011, Release 14.0.

[135] S. Sehgal and H. Kumar, 2015, "Structural Dynamic model updating techniques: a state of the art review", Journal of Arch Computat Methods Eng, Vol. 54, pp. 56-65.

[136] E. Mottershead and M. Friswell, 1993, "Model updating in structural dynamics: a survey", Journal of Sound and Vibration, Vol. (167), No. (2), pp. 347-375.

[137] F.M. Hemez and S.W. Doebling, 2000, "Review and assessment of model updating for nonlinear, transient dynamics", Journal of Mechanical System and Signal Processing, Vol. (14), pp. 1-44.

[138] J. Guggenberger, 2005, "In search of simulating reality: validation and updating of FE models for structural analysis", International Congress on FEM Technology with ANSYS CFX & ICEM CFD Conference, pp. 1-10.

[139] Z. Mišković, S. Al-Wazni, A. Alalikhan, 2016, "FE model updating based on dynamic properties by heurstic optimization", 6th International Conference of GNP, University of Montenegro, Montenegro, pp. 8-12.

[140] S. Al-Wazni, A. Alalikhan, Z. Mišković, R. Salatić, 2014, "Numerical Test of Damage Detection Using Simulated Annealing Method", 14th International Conference of DGKS, Association of Structural Engineering of Serbia,University of Novi Sad, Serbia, pp. 50-59.

[141] A. Alalikhan, S. Al-Wazni, Z. Mišković, R. Salatić, L. Mišković, 2015, "Test of Heuristic Techniques in Vibration Based Damage Detection", (Paper ID: 1410-2015 – under revision), Građevinar – Jorunal of the Croatian Association of Civil Engineers, ISSN (print) 0350-2465, ISSN (on-line) 1333-9095.

[142] Z. Mišković, S. Al-Wazni, A. Alalikhan, 2015, "Damage Detection for Civil Structural Health Monitoring Application-A Case Study of the Steel Grid Bridge Structural Model", Technical Gazette (paper ID: TV-20160411065936 – under revision), ISSN 1330-3651 (print) ISSN 1848-6339 (On-line).

[143] S. Al-Wazni, A. Alalikhan, Z. Mišković, 2015, "Damage Detection for Civil Structural Health Monitoring Application-A Case Study of the Steel Grid Bridge Structural Model", Submitted paper in the Iranian Journal of Science and Technology-Transactions of Civil Engineering, Springer,.

9.2. Appendices

Appendix - A: Acceleration time history of adopted structural models

Appendix - A1: Acceleration time history of overhang beam model

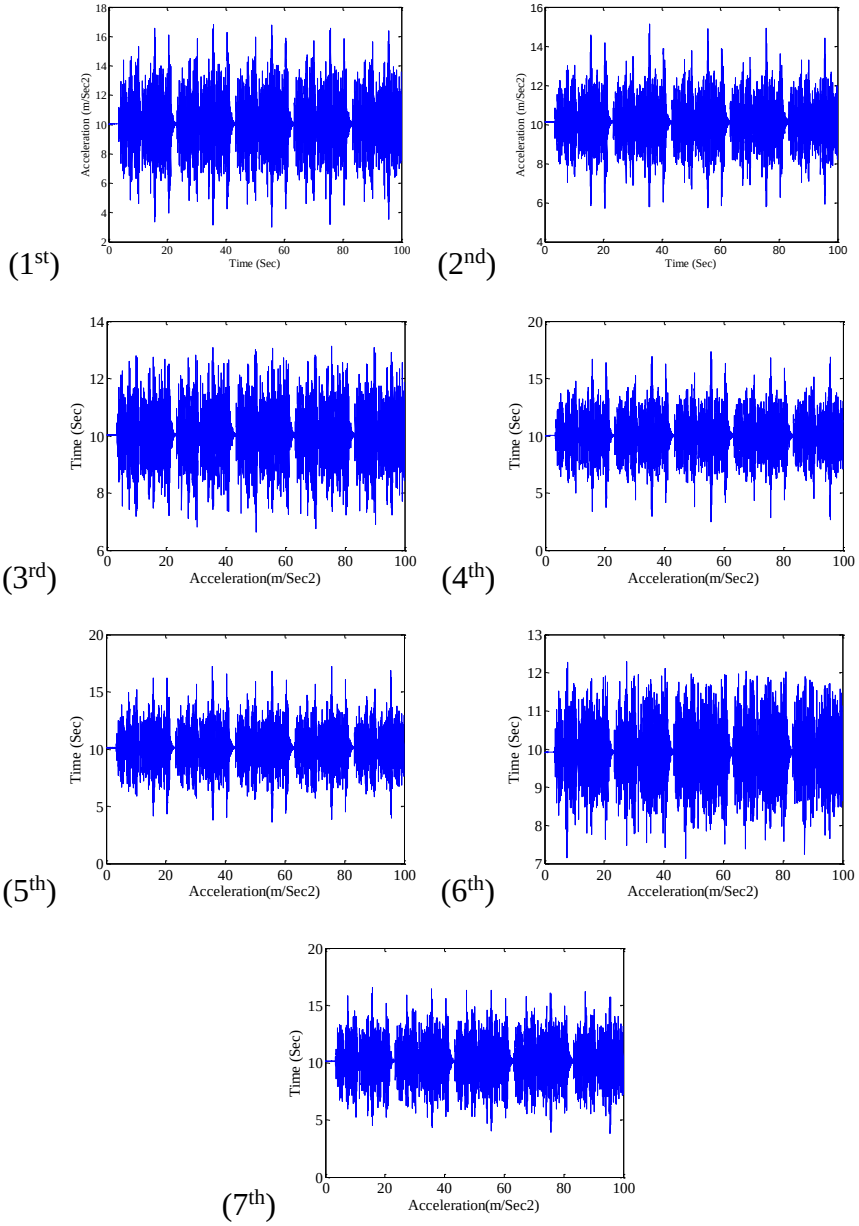

Figure A.1. Acceleration history time of the seventh accelerometers during simulated ambient vibration measurements using shaker of intact overhang beam model

Appendix - A2: Acceleration time history of grid bridge model

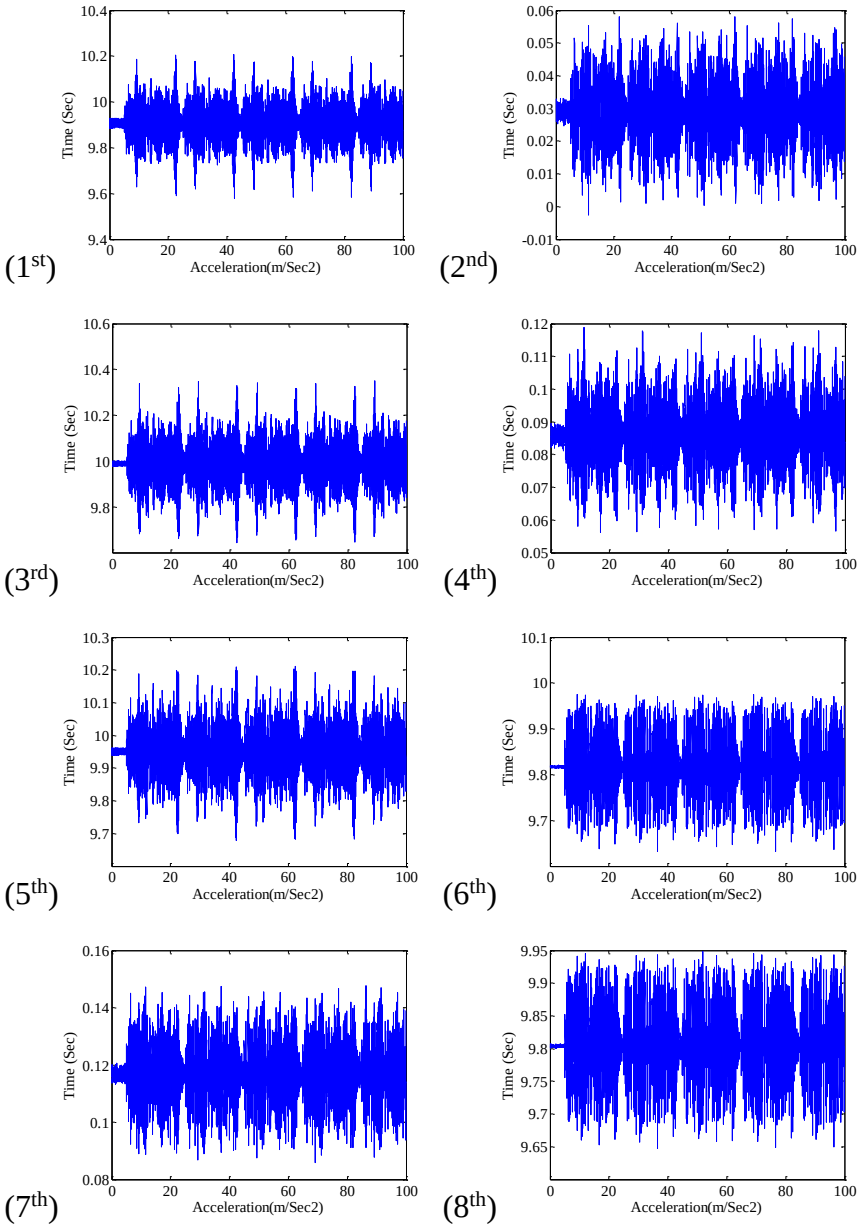

Figure A.2. Acceleration history time of the eight accelerometers during simulated ambient vibration measurements using shaker of intact grid bridge model

Appendix - A3: Acceleration time history of Vierendeel bridge model

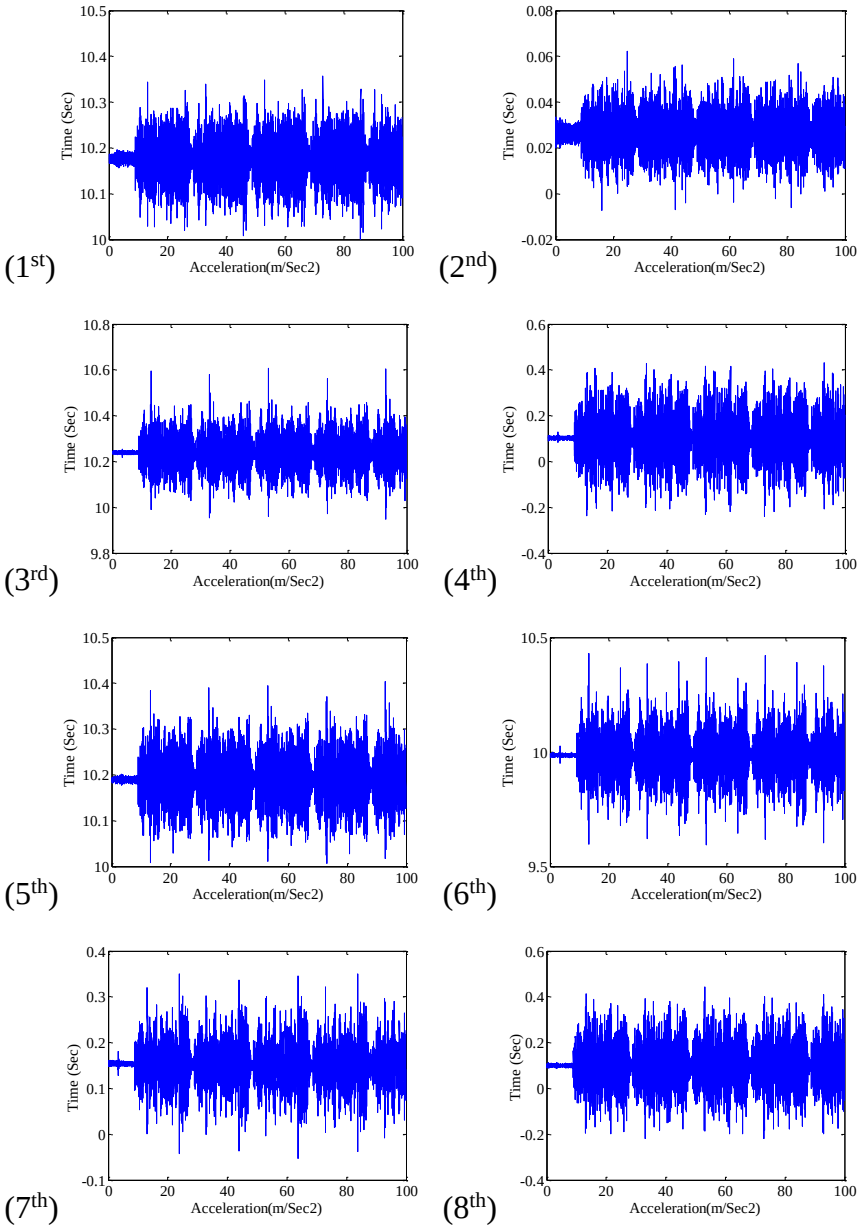

Figure A.3. Acceleration history time of the eight accelerometers during simulated ambient vibration measurements using shaker of intact Vierendeel bridge model

Appendix - A4: Acceleration time history of multi-storey building model

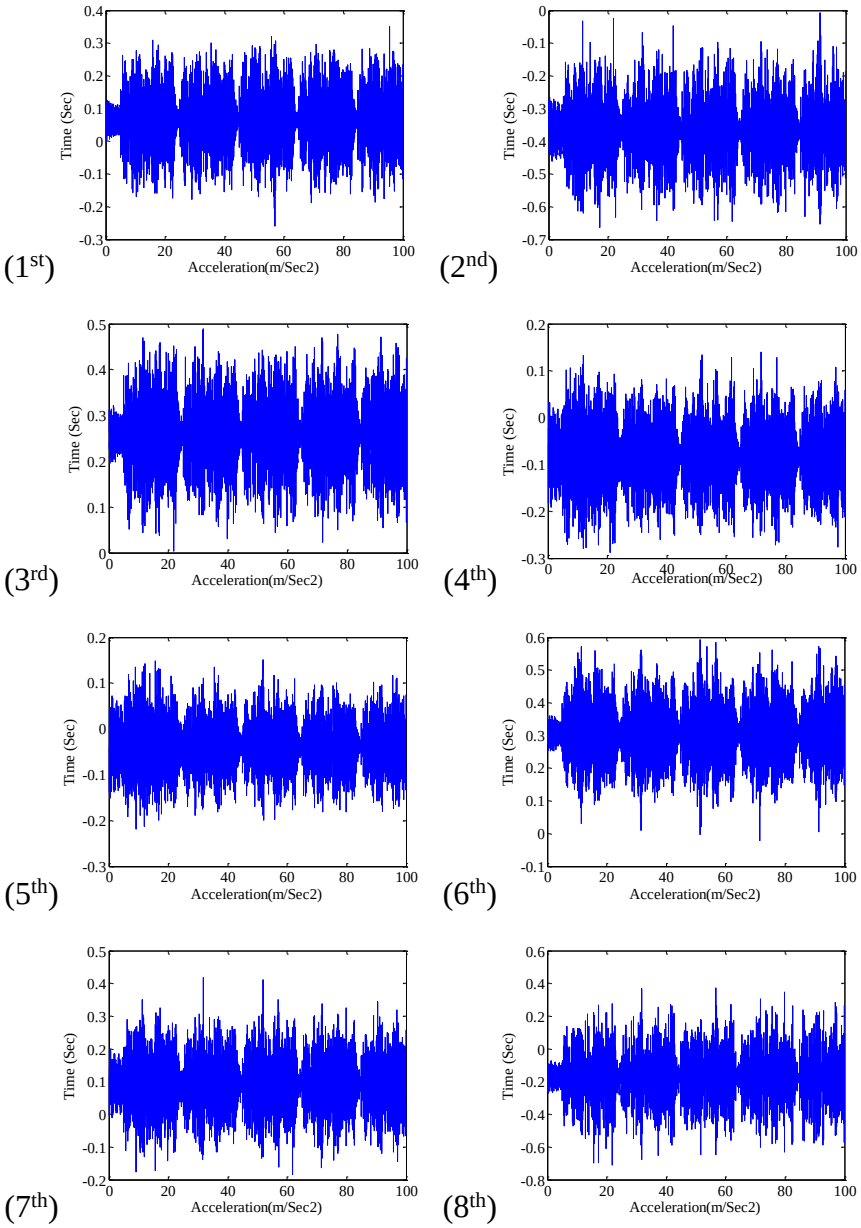

Figure A.4. Acceleration history time of the eight accelerometers during simulated ambient vibration measurements using shaker of intact multi-storey building model

Appendix -B: CFG input file used in ARTeMIS extractor software

Header: Overhang Beam Model with Closely Spaced Modes

T: 0.0016666666

Node Number, X-coordinate, Y-coordinate, Z-coordinate.
Nodes
1 0 0 0
2 20 0 0
3 220 0 0
4 420 0 0
5 570 0 0
6 720 0 0
7 920 0 0
8 1120 0 0
9 1320 0 0
10 1500 0 0

From Node Number, To Node Number.
Lines
1 2
2 3
3 4
4 5
5 6
6 7
7 8
8 9
9 10

Setups
Measurement1
OverHangBeamSET.asc
3 0 0 1 0.000001 m/s² Acceleration Transducer 1
4 0 0 1 0.000001 m/s² Acceleration Transducer 2
5 0 0 1 0.000001 m/s² Acceleration Transducer 3
6 0 0 1 0.000001 m/s² Acceleration Transducer 4
7 0 0 1 0.000001 m/s² Acceleration Transducer 5
9 0 0 1 0.000001 m/s² Acceleration Transducer 6
10 0 0 1 0.000001 m/s² Acceleration Transducer 7

Appendix -C: SVS output file exported from ARTeMIS extractor software

BEGIN MODE DEFINITION
PROJECT
Overhang Beam New Model-2nd-1024
ESTIMATOR
FDD
FREQUENCY [HZ]: MEAN / SDEV
7.910157e+000 0.000000e+000
DAMPING [%]: MEAN / SDEV
0.000000e+000 0.000000e+000
MODE SHAPE: NODE / X-ABS / X-ANG / Y-ABS / Y-ANG / Z-ABS / Z-ANG
1 0.000000e +000 0.000000e+000 0.000000e+000 0.000000e+000 0.000000e+000 0.000000e+000
2 0.000000e+000 0.000000e+000 0.000000e+000 0.000000e+000 0.000000e+000 0.000000e+000
3 0.000000e+000 0.000000e+000 0.000000e+000 0.000000e+000 3.649350e-001 -3.131186e+000
4 0.000000e+000 0.000000e+000 0.000000e+000 0.000000e+000 6.136370e-001 -3.136658e+000
5 0.000000e+000 0.000000e+000 0.000000e+000 0.000000e+000 6.831053e-001 -3.133360e+000
6 0.000000e+000 0.000000e+000 0.000000e+000 0.000000e+000 6.374503e-001 -3.133888e+000
7 0.000000e+000 0.000000e+000 0.000000e+000 0.000000e+000 3.954244e-001 -3.137308e+000
8 0.000000e+000 0.000000e+000 0.000000e+000 0.000000e+000 0.000000e+000 0.000000e+000
9 0.000000e+000 0.000000e+000 0.000000e+000 0.000000e+000 5.214784e-001 6.754151e-004
10 0.000000e+000 0.000000e+000 0.000000e+000 0.000000e+000 1.000000e+000 1.454144e-018
END MODE DEFINITION
BEGIN MODE DEFINITION
PROJECT
Overhang Beam New Model-2nd-1024
ESTIMATOR
FDD
FREQUENCY [HZ]: MEAN / SDEV
1.875000e+001 0.000000e+000
DAMPING [%]: MEAN / SDEV
0.000000e+000 0.000000e+000

MODE SHAPE: NODE / X-ABS / X-ANG / Y-ABS / Y-ANG / Z-ABS / Z-ANG
1 0.000000e+000 0.000000e+000 0.000000e+000 0.000000e+000 0.000000e+000 0.000000e+000
2 0.000000e+000 0.000000e+000 0.000000e+000 0.000000e+000 0.000000e+000 0.000000e+000
3 0.000000e+000 0.000000e+000 0.000000e+000 0.000000e+000 2.978601e-001 2.156173e-003
4 0.000000e+000 0.000000e+000 0.000000e+000 0.000000e+000 4.119616e-001 -3.370361e-003
5 0.000000e+000 0.000000e+000 0.000000e+000 0.000000e+000 3.436510e-001 9.169825e-003
6 0.000000e+000 0.000000e+000 0.000000e+000 0.000000e+000 1.877818e-001 1.473547e-002
7 0.000000e+000 0.000000e+000 0.000000e+000 0.000000e+000 1.516974e-002 3.003834e+000
8 0.000000e+000 0.000000e+000 0.000000e+000 0.000000e+000 0.000000e+000 0.000000e+000
9 0.000000e+000 0.000000e+000 0.000000e+000 0.000000e+000 4.644210e-001 6.411281e-003
10 0.000000e+000 0.000000e+000 0.000000e+000 0.000000e+000 1.000000e+000 0.000000e+000
END MODE DEFINITION
BEGIN MODE DEFINITION
PROJECT
Overhang Beam New Model-2nd-1024
ESTIMATOR
FDD
FREQUENCY [HZ]: MEAN / SDEV
4.248047e+001 0.000000e+000
DAMPING [%]: MEAN / SDEV
0.000000e+000 0.000000e+000
MODE SHAPE: NODE / X-ABS / X-ANG / Y-ABS / Y-ANG / Z-ABS / Z-ANG
1 0.000000e+000 0.000000e+000 0.000000e+000 0.000000e+000 0.000000e+000 0.000000e+000
2 0.000000e+000 0.000000e+000 0.000000e+000 0.000000e+000 0.000000e+000 0.000000e+000
3 0.000000e+000 0.000000e+000 0.000000e+000 0.000000e+000 9.916485e-001 3.130013e+000
4 0.000000e+000 0.000000e+000 0.000000e+000 0.000000e+000 6.370033e-001 3.135881e+000
5 0.000000e+000 0.000000e+000 0.000000e+000 0.000000e+000 2.821689e-001 -2.693381e-002
6 0.000000e+000 0.000000e+000 0.000000e+000 0.000000e+000 1.000000e+000 0.000000e+000

7 0.000000e+000 0.000000e+000 0.000000e+000 0.000000e+000 8.917115e-001 -1.055724e-002
8 0.000000e+000 0.000000e+000 0.000000e+000 0.000000e+000 0.000000e+000 0.000000e+000
9 0.000000e+000 0.000000e+000 0.000000e+000 0.000000e+000 1.760099e-001 2.069404e-002
10 0.000000e+000 0.000000e+000 0.000000e+000 0.000000e+000 6.608537e-001 -1.739391e-002
END MODE DEFINITION
BEGIN MODE DEFINITION
PROJECT
Overhang Beam New Model-2nd-1024
ESTIMATOR
FDD
FREQUENCY [HZ]: MEAN / SDEV
9.082032e+001 0.000000e+000
DAMPING [%]: MEAN / SDEV
0.000000e+000 0.000000e+000
MODE SHAPE: NODE / X-ABS / X-ANG / Y-ABS / Y-ANG / Z-ABS / Z-ANG
1 0.000000e+000 0.000000e+000 0.000000e+000 0.000000e+000 0.000000e+000 0.000000e+000
2 0.000000e+000 0.000000e+000 0.000000e+000 0.000000e+000 0.000000e+000 0.000000e+000
3 0.000000e+000 0.000000e+000 0.000000e+000 0.000000e+000 9.508846e-001 -1.146590e-002
4 0.000000e+000 0.000000e+000 0.000000e+000 0.000000e+000 3.695647e-001 -3.072144e+000
5 0.000000e+000 0.000000e+000 0.000000e+000 0.000000e+000 9.393813e-001 -3.108959e+000
6 0.000000e+000 0.000000e+000 0.000000e+000 0.000000e+000 5.661596e-002 2.486435e+000
7 0.000000e+000 0.000000e+000 0.000000e+000 0.000000e+000 1.000000e+000 0.000000e+000
8 0.000000e+000 0.000000e+000 0.000000e+000 0.000000e+000 0.000000e+000 0.000000e+000
9 0.000000e+000 0.000000e+000 0.000000e+000 0.000000e+000 2.970265e-001 -3.029940e+000
10 0.000000e+000 0.000000e+000 0.000000e+000 0.000000e+000 7.706211e-001 7.505986e-002
END MODE DEFINITION

Appendix -D: APDL Input file of created FE model imported by ANSYS software

```
/CWD,'C:\Users\SAAD AL-WAZNI\Desktop\Overhang'
/title, Modal Analysis of Overhang Beam
/PREP7
!!!!!!!!!!!!!!!!!  CREATING POINTS !!!!!!!!!!!!!!!!!
J=0
Z=0
Y=0
*DO,X,0,425,25
I=1+J
K,I,X,Y,Z
J=J+1
*ENDDO
I=19
X=455
K,I,X,Y,Z
J=0
Z=0
Y=0
*DO,X,480,630,25
I=20+J
K,I,X,Y,Z
J=J+1
*ENDDO
I=27
X=650
K,I,X,Y,Z
J=0
Z=0
Y=0
*DO,X,675,975,25
I=28+J
K,I,X,Y,Z
J=J+1
*ENDDO
I=41
X=1005
K,I,X,Y,Z
J=0
Z=0
Y=0
```

```
*DO,X,1030,1330,25
I=42+J
K,I,X,Y,Z
J=J+1
*ENDDO
I=55
X=1350
K,I,X,Y,Z
J=0
Z=0
Y=0
*DO,X,1375,1525,25
I=56+J
K,I,X,Y,Z
J=J+1
*ENDDO
I=63
X=1555
K,I,X,Y,Z
J=0
Z=0
Y=0
*DO,X,1580,2005,25
I=64+J
K,I,X,Y,Z
J=J+1
*ENDDO
!!!!!!!!!!!!!!!!  CREATING LINES !!!!!!!!!!!!!!!!!!!!
II=0
*DO,X,1,80,1
I=1+II
J=I+1
L,I,J
II=II+1
*ENDDO
!!!!!!!!!!!!!!!!!!!!!!!!!!!!!!!!!!!!!!!!!!!!!!!!!!!! DEFINE ELEMENT TYPE
ET,1,BEAM4
ET, 2, mass21, 0, 0, 0
!!!!!!!!!!!!!!!!!!!!DEFINE REAL MATERIAL
!*use,real-constant.txt
*use,real-constant2.txt
!R,1,360.000,108000.000,1080.000,6.000,60.000,0
!RMORE,0,4043.52,,,,0
!R,2,330.000,83187.500,990.000,6.000,55.000,0
!RMORE,0,3706.56,,,,0
```

```
!R,3,0.0000000,0.0000000,0.0000680,0.000000,0.0425,0.000000
!!!!!!!!!!!!!!!!!!!!!!!!!!!!!!!!!!!!!!!!!!!!!!!!!!!!!!!!
*use,Material-Type.txt
!MP,EX,1,2.0E5                          ! DEFINE MATERIAL PROPERTIES
!MP,PRXY,1,0.3
!MP,DENS,1,7.86E-9
!!!!!!!!!!!!!!!!!!!!!!!!!!!!!!!!!!!!!!!!!!!!!!!!!!!!!!!!
LESIZE,ALL,,,1                          !DEFINE MESH,ELEMENT,REAL,MATERIAL
!!!!!!!!!!!!!!!!!!! DEFINING REAL CONSTANT  !!!!!!!!!!!!
TYPE,1
REAL,1
MAT,1
I=0
J=0
II=0
*DO,X,1,36,1      !LOOP FOR ASSIGNING REAL FOR THE LARGER ELEMENTS
    SECTIONS IN RANGES 1-36
I=1+II
J=I+1
LMESH,I,J,25
II=II+1
*ENDDO
TYPE,1
REAL,2
MAT,1
I=37
J=38
LMESH,I,J,25          !ASSIGNING REAL FOR THE SMALLER SECTION ELEMENT
    37
TYPE,1
REAL,1
MAT,1
I=0
J=0
II=0
*DO,X,1,2,1             !LOOP FOR ASSIGNING REAL FOR THE LARGER SECTIONS
    ELEMENTS 38 & 39
I=38+II
J=I+1
LMESH,I,J,25
II=II+1
*ENDDO
TYPE,1
REAL,2
MAT,1
```

```
I=0
J=0
II=0
*DO,X,1,2,1            !LOOP FOR ASSIGNING REAL FOR THE SMALLER SECTIONS
    ELEMENTS 40 & 41
I=40+II
J=I+1
LMESH,I,J,25
II=II+1
*ENDDO
TYPE,1
REAL,1
MAT,1
I=0
J=0
II=0
*DO,X,1,2,1             !LOOP FOR ASSIGNING REAL FOR THE LARGER SECTIONS
    ELEMENTS 42 & 43
I=42+II
J=I+1
LMESH,I,J,25
II=II+1
*ENDDO
TYPE,1
REAL,2
MAT,1
I=44
J=45
LMESH,I,J,25          !ASSIGNING REAL FOR THE SMALLER SECTION ELEMENT
    44
TYPE,1
REAL,1
MAT,1
I=0
J=0
II=0
*DO,X,45,80,1     !LOOP FOR ASSIGNING REAL FOR THE LARGER ELEMENTS
    SECTIONS IN RANGES 45-80
I=45+II
J=I+1
LMESH,I,J,25
II=II+1
*ENDDO
!!!!!!!!!!!!!!!!!!!!!!!!!!!!!!!!!!!!!!!!!!!!!!!!!!!!!!!!!!!!!!!!!!!!!!!
```

```
!ET, 2, mass21, 0, 0, 0          ! Element Type, No. of ET, Element's Name, Keyopt(1),
    Keyopt(2), Keyopt(3), respectively.
!R,3,0,0,0.000068,0,0.0425,0 ! 3D Concentrated mass with rotary inertia,real const.=3,
    massX=0,massY=0.2 N/(mm/sec^2),massZ=0, Ixx=Iyy=Izz =0(N-
    mm^2)/(mm/sec^2),Respectively
!R, 3,0.000068                   ! 3D Concentrated mass without rotary inertia (Keyopt(3)=2 ,
    mass = 1.147E-4 N/(mm/sec^2).
!R, 3, 0.68, 0              ! 2D Concentrated mass/inertia (mass with rotary inertia) real data ,
    mass = 0.2 N/(mm/sec^2), Izz = 0.075 (N-mm^2)/(mm/sec^2)
TYPE, 2
REAL, 3
MAT,1
EN, 81, 1               ! Element Number 81 (mass/inertia) is at node 1
EN, 82, 9               ! Element Number 82 (mass/inertia) is at node 9
EN, 83, 19
EN, 84, 27
EN, 85, 33
EN, 86, 41
EN, 87, 49
EN, 88, 55
EN, 89, 63
EN, 90, 73
EN, 91, 81
!!!!!!!!!!!!!!!!!!!!!!!!!!!!!!!!!!!!!!!!!!!!!!!!!!!!!!
FINISH
!!!!!!!!!!!!!!!!!!!!!!!!!!!!!!!!!!!!!!!!!!!!!!!!!!!!!!!!!!!!
/SOLU
ANTYPE,2                                ! Modal analysis
MODOPT,LANB,4                           ! BLOCK LANCZOS, 4 modes
DMPRAT,0.02
MXPAND,4                                ! Expand 4 modes
!!!!!!!!!!!!!!!!!!!!!!!!!!!!!!!!!!!!!!!!!!!!!!!!!!!!!!!!!!!!
DK,19,UX,0
DK,19,UY,0
DK,19,UZ,0
!DK,19,ROTZ,0
DK,19,ROTX,0
!DK,63,UX,0
DK,63,UY,0
DK,63,UZ,0
!DK,63,ROTZ,0
!DK,63,ROTX,0
!!!!!!!!!!!!!!!!!!!!!!!!!!!!!!!!!!!!!!!!!!!!!!!!!!!!!!!!!
SOLVE
FINISH
```

```
/POST1                          ! List solutions
SET,LIST
SET,FIRST
PLDISP                          ! Display first mode shape
!ANMODE,10,0.5, ,0                    ! Animate mode shape
!!!!!!!!!!!!!!!!!!!!!!!!!!!!!!!!!!!!!!!!!!!!!!!!!!!!!!!!!!!!!!!!!!!!!!!!!!!!!!!!!!!!!!!!!!!!!!!!!!!!!!!!!!!!!!!!!!!!!!!!!!!!!!!!!!!
!!!!!!!!!!!!!!!FOLLOWING STEPS FOR PRINTING RESULTS IN SEPERATED FILE
    (*.DAT)!!!!!!!!!!!!
!!!!!!!!!!!!!!!!!!!!!!!!!!!!!!!!!!!!!!!!!!!!!!!!!!!!!!!!!!!!!!!!!!!!!!!!!!!!!!!!!!!!!!!!!!!!!!!!!!!!!!!!!!!!!!!!!!!!!!!!!!!!!!!!!!!
*GET,NUM_elements,ELEM,0,COUNT          !RETRIEVE NUMBERS OF
    ELEMENTS
*GET,NUM_nodes,NODE,0,COUNT                    !RETRIEVE NUMBERS OF
    NODES
!Form table for nodes:
*DIM,TABLE_nodes,ARRAY,NUM_nodes
*DIM,X_nodes,ARRAY,NUM_nodes
*DIM,Y_nodes,ARRAY,NUM_nodes
*DIM,Z_nodes,ARRAY,NUM_nodes
*GET,min_N_id,NODE,,NUM,MIN             !DETERMINING THE FIRST MIN
    VALUE OF NODES
*GET,max_N_id,NODE,,NUM,MAX                    !DETERMINING THE MAX
    VALUE OF NODES
!!!!!!!!!!!!!!!!LOOP FOR PRINTING THE SEQUENCE AND COORDINATES FOR
    EACH NODE!!!!!!!!!!!!!!!
!Loop over all NODEs betwewn min_N, max_N_id
    j=0
    *do,i,min_N_id, max_N_id
       *GET,SEL_status,NODE,i,NSEL          !DETERMINING RANKING OF
    EACH NODE
           !Add new node 'i' to the TABLE
           j=j+1
           TABLE_nodes(j)=i
           *GET, X_nodes(j), NODE, i, LOC, X
           *GET, Y_nodes(j), NODE, i, LOC, Y
           *GET, Z_nodes(j), NODE, i, LOC, Z

    *enddo
*do,i,1,1
*VWRITE,TABLE_nodes(i),X_nodes(i),Y_nodes(i),Z_nodes(i)
(F11.0,3E13.5)
*enddo
!!!!!!!!!!!!!!!!!!!!!!!!!!!!!!!!!!!!
*cfopen,Frequency,DAT
```

```
*GET,ALL_NUM_modes,ACTIVE,,SET,NSET
ARG4=3                                  !NUMBER OF MODES NEEDED
NUM_modes=%ARG4%
*dim,FREQ_modes,array,NUM_modes
*dim,MASS_modes,array,NUM_modes
*if,NUM_modes,LE,ALL_NUM_modes,THEN
!!!!!!!!!!!!Loop over all available modes....START
*do,i,1,NUM_modes
  SET,,i
  *GET,FREQ_modes(i),ACTIVE,,SET,FREQ   !Leave a Blank Space after the Entity of
    type (ACTIVE)
    !!!!!!!!!!!!!!!!!!!!!!!!!!!!!!!!!   MASS CALCULATIONS FOR EACH MODE
    !!!!!!!!!!!!!!!!!!!!!
   !!!Sorts nodal data according the MAX(abs(vect_SUM_u))
     !!!!!!!!.......NSORT, Item, Comp, ORDER, KABS, NUMB, SEL
    ORDER=0!....Sort into descending order.
    KABS=1 !....Sort according to absolu1te value.
    !NUMB....(defaults to all nodes) which should be sorted
    !SEL = ' '/SELECT.....Allows selection of nodes in the sorted field.
     NSORT, U, SUM, ORDER, KABS
     *GET, MAX_sumU, SORT, 0, MAX     ! *GET, Par, SORT, 0, Item1
     MASS_modes(i)=1/(MAX_sumU*MAX_sumU)
    !!!!or   ......*GET,NODE_NUM_max,NODE,,NUM,MAX      !   GET   MAX   NODE
    NUMBER
    !!!!!example:  Benchmark C2 Input Listing......vmc.dat
             !!!!!!!!!!!!  *GET,SYM,NODE,MAXN,S,Y       ! GET DESIRED SY STRESS
    VALUE
    !!!!!!!!!!!!!!!!!!!!!!!!!!!!!!!!!!!!!!!!!!!!!!
    field_4=i   !ModeNumber
!*VWRITE,'MODE No.=',field_4
!(A10,F10.0)
!!!!!!!!!!!!!!!!!!!!!!!!!!!!!!!! FREQUENCY AND MASS CALCULATIONS  !!!!!!!!!!!!!!!!
    field_1=FREQ_modes(i) ! Current mode frequency
    field_2=MASS_modes(i) ! Current mode mass
    *VWRITE,field_1
(F7.3)
*enddo
*else
*endif
*cfclos,Frequency,DAT
*UILIST,Frequency,DAT
!!!!!!!!!!!!!!!!!!!!!!!!!!!!!!!!!!!!!!!!!!!!!!!!!!!!!!!!!!!!!!!!!!!!!!!!!!!!!!!!!!!!!!!!!!!!!!!!!!!!
!!!!!!!!!!!!!!!FOLLOWING STEPS FOR PRINTING RESULTS IN SEPERATED FILE (*.
    TXT)!!!!!!!!!!!!!
!!!!!!!!!!!!!!!!!!!!!!!!!!!!!!!!!!!!!!!!!!!!!!!!!!!!!!!!!!!!!!!!!!!!!!!!!!!!!!!!!!!!!!!!!!!!!!!!!!!!
```

```
!*GET, NUM_elements, ELEM,0,COUNT          !RETRIEVE NUMBERS OF
    ELEMENTS
!*GET,NUM_nodes,NODE,0,COUNT                !RETRIEVE NUMBERS OF
    NODES
!Form table for nodes:
!*DIM,TABLE_nodes,ARRAY,NUM_nodes
!*DIM,X_nodes,ARRAY,NUM_nodes
!*DIM,Y_nodes,ARRAY,NUM_nodes
!*DIM,Z_nodes,ARRAY,NUM_nodes
!*GET,min_N_id,NODE,,NUM,MIN                !DETERMINING THE FIRST
    MIN VALUE OF NODES
!*GET,max_N_id,NODE,,NUM,MAX                !DETERMINING THE MAX
    VALUE OF NODES
!!!!!!!!!!!!!!!LOOP FOR PRINTING THE SEQUENCE AND COORDINATES FOR
    EACH NODE!!!!!!!!!!!!!!!!!
!Loop over all NODEs betwewn min_N, max_N_id
   ! j=0
  !*do,i,min_N_id, max_N_id          !LOOP FOR CREATING A VECTOR OF
    ALL NODES IN ORDER TO FIND THEIR DISP. LATER
  !*GET,SEL_status,NODE,i,NSEL       !DETERMINING RANKING OF EACH
    NODE
        !Add new node 'i' to the TABLE
     ! j=j+1
     ! TABLE_nodes(j)=i          !VECTOR (TABLE) CREATED CONTAINING
    ALL NODES
        ! *GET, X_nodes(j), NODE, i, LOC, X
        ! *GET, Y_nodes(j), NODE, i, LOC, Y
        ! *GET, Z_nodes(j), NODE, i, LOC, Z
 ! *enddo
!*do,i,1,1      !THIS LOOP JUST PRINT COORDINATES OF ALL NODES IF WE
    ACTIVATE THE ABOVE DISACTIVATED THREE (*GET) STEPS
!*VWRITE,TABLE_nodes(i),X_nodes(i),Y_nodes(i),Z_nodes(i)
!(F11.0,3E13.5)
!*enddo
!!!!!!!!!!!!!!!!!!!!!!!!!!!!!!!!!!
*cfopen,Displacement,DAT
*GET,ALL_NUM_modes,ACTIVE,,SET,NSET
ARG4=3                                  !NUMBER OF MODES NEEDED
NUM_modes=%ARG4%
!*dim,FREQ_modes,array,NUM_modes
!*dim,MASS_modes,array,NUM_modes
*if,NUM_modes,LE,ALL_NUM_modes,THEN
!!!!!!!!!!!!Loop over all available modes....START
*do,i,1,NUM_modes
 SET,,i
```

```
 ! *GET,FREQ_modes(i),ACTIVE,,SET,FREQ   !Leave a Blank Space after the Entity of
     type (ACTIVE)
!!!!!!!!!!!!  *GET,SYM,NODE,MAXN,S,Y       ! GET DESIRED SY STRESS VALUE
    !!!!!!!!!!!!!!!!!!!!!!!!!!!!!!!!!!!!!!!!!!!!
!    field_4=i   !ModeNumber
!*VWRITE,'MODE No.=',field_4
!(A10,F10.0)
!!!!!!!!!!!!!!!!!!!!!!!!!!!!  STEPS FOR CALCULATIONS AND PRINTING OF
     DISPLACEMENYS OF NODES!!!!!!!!!
!!!!!!!!!!!!!!!!!!!!!!!!!!!!!Loop over all NODEs which should be
     exported....START!!!!!!!!!!!!!!!!!
     *do,j,1,NUM_nodes
          *GET,Disp_X,NODE,TABLE_nodes(j),U,X     !*GET, Par, NODE, N, Item1,
     IT1NUM, Item2, IT2NUM
         *GET,Disp_Y,NODE,TABLE_nodes(j),U,Y
          *GET,Disp_Z,NODE,TABLE_nodes(j),U,Z
          *GET,Vector,NODE,TABLE_nodes(j),U,SUM
     node_NUM=TABLE_nodes(j)
       *VWRITE,Disp_X,Disp_Y,Disp_Z,Vector
       (3F10.6,F10.6)
   *enddo
*enddo
*else
*endif
*cfclos,Displacement,DAT
*UILIST,Displacement,DAT
```

Appendix -E: Output results file of the modal analysis of the FE model exported by ANSYS software

```
*****  INDEX OF DATA SETS ON RESULTS FILE OF ALL NATURAL FREQUENCIES *****
   SET   TIME/FREQ    LOAD STEP   SUBSTEP  CUMULATIVE
     1  7.7240            1         1         1
     2  18.379            1         2         2
     3  42.511            1         3         3
     4  86.223            1         4         4

*****  INDEX OF DATA SETS ON RESULTS FILE OF FIRST MODE SHAPE VECTORS  *****
  0.000000  0.000000  1.297790  1.297790
  0.000000  0.000000  0.000000  0.000000
  0.000000  0.000000 -1.621000  1.621000
  0.000000  0.000000 -3.234597  3.234597
  0.000000  0.000000 -4.833421  4.833421
  0.000000  0.000000 -6.410157  6.410157
  0.000000  0.000000 -7.957573  7.957573
  0.000000  0.000000 -9.468547  9.468547
  0.000000  0.000000-10.936091 10.936091
  0.000000  0.000000-12.353381 12.353381
  0.000000  0.000000-13.713802 13.713802
  0.000000  0.000000-15.011052 15.011052
  0.000000  0.000000-16.239089 16.239089
  0.000000  0.000000-17.392130 17.392130
  0.000000  0.000000-18.464667 18.464667
  0.000000  0.000000-19.451491 19.451491
  0.000000  0.000000-20.347709 20.347709
  0.000000  0.000000-21.148759 21.148759
  0.000000  0.000000-21.850471 21.850471
  0.000000  0.000000-22.449206 22.449206
  0.000000  0.000000-22.941747 22.941747
  0.000000  0.000000-23.325257 23.325257
  0.000000  0.000000-23.597293 23.597293
  0.000000  0.000000-23.755810 23.755810
  0.000000  0.000000-23.799216 23.799216
  0.000000  0.000000-23.726518 23.726518
  0.000000  0.000000-23.537179 23.537179
  0.000000  0.000000-23.231065 23.231065
  0.000000  0.000000-22.808449 22.808449
  0.000000  0.000000-22.269998 22.269998
  0.000000  0.000000-21.616815 21.616815
  0.000000  0.000000-20.850568 20.850568
  0.000000  0.000000-19.973336 19.973336
  0.000000  0.000000-18.987556 18.987556
  0.000000  0.000000-17.896007 17.896007
  0.000000  0.000000-16.701791 16.701791
  0.000000  0.000000-15.408317 15.408317
  0.000000  0.000000-14.019279 14.019279
  0.000000  0.000000-12.538666 12.538666
  0.000000  0.000000-10.970819 10.970819
  0.000000  0.000000 -9.320323  9.320323
  0.000000  0.000000 -7.591947  7.591947
  0.000000  0.000000 -5.790621  5.790621
  0.000000  0.000000 -3.921404  3.921404
  0.000000  0.000000 -1.989456  1.989456
  0.000000  0.000000  0.000000  0.000000
```

```
0.000000  0.000000  2.041755  2.041755
0.000000  0.000000  4.130806  4.130806
0.000000  0.000000  6.262237  6.262237
0.000000  0.000000  8.431201  8.431201
0.000000  0.000000 10.632961 10.632961
0.000000  0.000000 12.862923 12.862923
0.000000  0.000000 15.116673 15.116673
0.000000  0.000000 17.390021 17.390021
0.000000  0.000000 19.679064 19.679064
0.000000  0.000000 21.980341 21.980341
0.000000  0.000000 24.290766 24.290766
0.000000  0.000000 26.607628 26.607628
0.000000  0.000000 28.928633 28.928633
0.000000  0.000000 31.251942 31.251942
0.000000  0.000000 34.041098 34.041098
```

Biography

Saad Jabbar Abbas Al-Wazni 25.03.1975 in Najaf, Iraq, where he finished elementary school and high school. He enrolled on October 1993 at College of Engineering, University of Baghdad, then he moved to complete his study in the second year in 1995 at Faculty of Engineering, University of Kufa in Najaf city and the graduate on July 1997, defended the graduate project in the field of structural analysis of prestressed concrete bridge with grade of very good. After graduating, he enrolled on November 1997 at Building and Construction Engineering Department, University of Technology in Baghdad to finish High Diploma in science of civil engineering and the graduate on October 1998, defended the thesis in the civil engineering with grade of excellent. After that, he enrolled on November 1998 at Building and Construction Engineering Department, University of Technology in Baghdad to finish Master in science of bridges and highway engineering and the graduate on July 2001, defended the thesis in the field of structural analysis of concrete pavements on elastic foundations with grade of excellent. After gradu After graduating, he started working in the private company from Najaf, Iraq in which works as an engineer designer of structures. On September 2002 begins his government job at the Southern Cement State Company in Najaf as designer engineer for steel and concrete structures. On April 2006, moved its appointment to the Department of Civil Engineering in Faculty of Engineering in University of Kufa as assistant lecturer. Working in teaching at Department of Civil Engineering Faculty of Engineering involves theories and practical subjects in civil engineering. Also, he performed many tasks during teaching in the faculty such as; scientific responsible of several laboratories, member and assistant director of examining committee and scientific responsible of follow up the publishing papers of CE department staff. Saad Al-Wazni was author and co-author of several scientific and professional papers in the field of concrete and steel structures, which were published in magazines, professional journals, international conferences, and symposiums in Iraq, Serbia and abroad. In addition to teaching-scientific, Saad Al-Wazni engaged in many activities and professional works. As a designer participated in the drafting of several tens of conceptual designs, preliminary project, the main projects and expert opinions for projects such as houses, buildings, highways, public facilities, sport facilities, industrial buildings, industrial facilities, river bridge, all of which carried out in Iraq. In November 2010, he got scholarship and came Serbia in Belgrade to start Serbian language within international program of "World in Serbia". In November 2011, Saad Al-Wazni enrolled in the doctoral studies in Structural Engineering Department of Faculty of Civil Engineering at University of Belgrade in Serbia. He could speak three languages, Arabic, English and Serbian.
Married and father of four children.

Biogrfija autora

Saad Džabar Abbas Al-Wazni roden je 25.03.1975. godine u Nadžafu, Iraku, gde je završio osnovnu školu i gimnaziju. Upisao je, u oktobri 1993. godine, na Fakultetu tehničkih nauka Univerziteta u Bagdadu, a zatim se preselio, da završi studije, u drugoj godini 1995. godine na Fakultet tehničkih nauka Univerziteta u Kufi u Nadžafu gdje je i diplomirao u julu 1997. godine, odbranivši diplomski projekt iz oblasti strukturna analiza prednapregnutog betonskog mosta sa ocenom veoma dobar. Nakon diplomiranja upisao je, u novembri 1997. godine, Univerzitet za tehnologiju u Bagdadu gdje je diplomirao građevinarstvo u oktobru 1998. godine. Nakon toga, upisao je u novembri 1998. godine inženjerstvo, Universiti of Technologi u Bagdadu gdje je magistrirao inženjerstvo mostova i autoputeva i diplomirao u julu 2001. godine, odbranivši rad iz oblasti strukturne analize betoniranja na elastičnim temeljima sa ocenom odličan. Nakon diplomiranja, zapošljava se u privatnoj firmi iz Nadžafa, Irak u kojoj radi kao inženjer projektant konstrukcija. Septembra 2002. godine zapošljava se u državnoj firmi u Nadžafu kao dizajner inženjer za čelične i betonske konstrukcije. Aprila 2006. godine, imenovan je na Odeljenju za građevinarstvo Inženjerski fakulteta Univerziteta u Kufi kao asistent. Radi u nastavi na Građevinskom fakultetu tehničkih nauka na teorijskim i praktičnim predmetima u građevinarstvu. Isto tako, obavlja mnoge poslove tokom nastave na fakultetu, kao što su; vodi nekoliko laboratorija, član je i pomoćnik direktora istražnog komiteta i odgovoran je za praćenje i objavljivanje radova zaposlenih u CE odeljenju. Saad Al-Wazni je autor i koautor više naučnih i stručnih radova iz oblasti betonskih i čeličnih konstrukcija, koji su objavljeni u naučnim časopisima, stručnim časopisima, međunarodnim konferencijama, i simpozijuma u Iraku, Srbiji i inostranstvu. Pored nastavno-naučnog, Saad Al-Wazni bavi se mnogim aktivnostima u stručnim organizacijama. Kao dizajner učestvovao je u izradi nekoliko desetina idejnih rešenja, idejnog projekta, glavnih projekata i stručnih mišljenja za objekte kao što su kuće, zgrade, autoputeve, javni objekati, sportski objekati, industrijski objekati, mostovi preko reka u Iraku. U novembru 2010. godine, dobio je stipendiju i došao u Srbiju, Beograd, gde počinje učiti srpski jezik u okviru međunarodnog programa "Svet u Srbiji". U novembru 2011. godine, Saad Al-Wazni upisuje doktorski studij niskogradnje, odeljenje Građevinskog fakulteta Univerziteta u Beogradu, Srbija. Govori tri jezika, arapski, engleski i srpski.

Oženjen je i otac deteta.

1. Ауторство - Дозвољавате умножавање, дистрибуцију и јавно саопштавање дела, и прераде, ако се наведе име аутора на начин одређен од стране аутора или даваоца лиценце, чак и у комерцијалне сврхе. Ово је најслободнија од свих лиценци.

2. Ауторство – некомерцијално. Дозвољавате умножавање, дистрибуцију и јавно саопштавање дела, и прераде, ако се наведе име аутора на начин одређен од стране аутора или даваоца лиценце. Ова лиценца не дозвољава комерцијалну употребу дела.

3. Ауторство - некомерцијално – без прераде. Дозвољавате умножавање, дистрибуцију и јавно саопштавање дела, без промена, преобликовања или употребе дела у свом делу, ако се наведе име аутора на начин одређен од стране аутора или даваоца лиценце. Ова лиценца не дозвољава комерцијалну употребу дела. У односу на све остале лиценце, овом лиценцом се ограничава највећи обим права коришћења дела.

4. Ауторство - некомерцијално – делити под истим условима. Дозвољавате умножавање, дистрибуцију и јавно саопштавање дела, и прераде, ако се наведе име аутора на начин одређен од стране аутора или даваоца лиценце и ако се прерада дистрибуира под истом или сличном лиценцом. Ова лиценца не дозвољава комерцијалну употребу дела и прерада.

5. Ауторство – без прераде. Дозвољавате умножавање, дистрибуцију и јавно саопштавање дела, без промена, преобликовања или употребе дела у свом делу, ако се наведе име аутора на начин одређен од стране аутора или даваоца лиценце. Ова лиценца дозвољава комерцијалну употребу дела.

6. Ауторство - делити под истим условима. Дозвољавате умножавање, дистрибуцију и јавно саопштавање дела, и прераде, ако се наведе име аутора на начин одређен од стране аутора или даваоца лиценце и ако се прерада дистрибуира под истом или сличном лиценцом. Ова лиценца дозвољава комерцијалну употребу дела и прерада. Слична је софтверским лиценцама, односно лиценцама отвореног кода.

Copyright assignment

Прилог 1.

Изјава о ауторству

Потписани: Saad Al-Wazni
број уписа : 918/2011

Изјављујем

да је докторска дисертација под насловом

DETEKCIJA I LOKALIZACIJA OSTECENJA PRI MONITORINGU STANJA GRADEVINSKIH KONSTRUKCIJA

DAMAGE DETECTION AND LOCALIZATION FOR CIVIL STRUCTURAL HEALTH MONITORING

- резултат сопственог истраживачког рада,
- да предложена дисертација у целини ни у деловима није била предложена за добијање било које дипломе према студијским програмима других високошколских установа,
- да су резултати коректно наведени и
- да нисам кршио/ла ауторска права и користио интелектуалну својину других лица.

Потпис докторанда

У Београду, Јун 2016

Declaration of identity paper and electronic versions of doctoral thesis

Прилог 2.

Изјава о истоветности штампане и електронске верзије докторског рада

Име и презиме аутора:	Saad Al-Wazni
Број индекса:	918/2011
Студијски програм:	Gradevinarstvo
Наслов рада:	DETEKCIJA I LOKALIZACIJA OSTECENJA PRI MONITORINGU STANJA GRADEVINSKIH KONSTRUKCIJA (DAMAGE DETECTION AND LOCALIZATION FOR CIVIL STRUCTURAL HEALTH MONITORING)
Ментор:	Assoc. Prof. Dr. Zoran Miskovic

Потписани: Saad Al-Wazni

Изјављујем да је штампана верзија мог докторског рада истоветна електронској верзији коју сам предао за објављивање на порталу **Дигиталног репозиторијума Универзитета у Београду**.

Дозвољавам да се објаве моји лични подаци везани за добијање академског звања доктора наука, као што су име и презиме, година и место рођења и датум одбране рада.

Ови лични подаци могу се објавити на мрежним страницама дигиталне библиотеке, у електронском каталогу и у публикацијама Универзитета у Београду.

Потпис докторанда

У Београду, Јун 2016

Statement on the use

Прилог 3.

Изјава о коришћењу

Овлашћујем Универзитетску библиотеку „Светозар Марковић“ да у Дигитални репозиторијум Универзитета у Београду унесе моју докторску дисертацију под насловом:

DETEKCIJA I LOKALIZACIJA OSTECENJA PRI MONITORINGU STANJA GRADEVINSKIH KONSTRUKCIJA

DAMAGE DETECTION AND LOCALIZATION FOR CIVIL STRUCTURAL HEALTH MONITORING

која је моје ауторско дело.

Дисертацију са свим прилозима предао/ла сам у електронском формату погодном за трајно архивирање.

Моју докторску дисертацију похрањену у Дигитални репозиторијум Универзитета у Београду могу да користе сви који поштују одредбе садржане у одабраном типу лиценце Креативне заједнице (Creative Commons) за коју сам се одлучио/ла.

1. Ауторство

2. Ауторство - некомерцијално

3. Ауторство – некомерцијално – без прераде

4. Ауторство – некомерцијално – делити под истим условима

5. Ауторство – без прераде

6. Ауторство – делити под истим условима

(Молимо да заокружите само једну од шест понуђених лиценци, кратак опис лиценци дат је на полеђини листа).

Потпис докторанда

У Београду, Јун 2016